THE UNIVERSITY
of EDINBURGH

Present-day and future lightning, and its impact on tropospheric chemistry

Declan Luke Finney

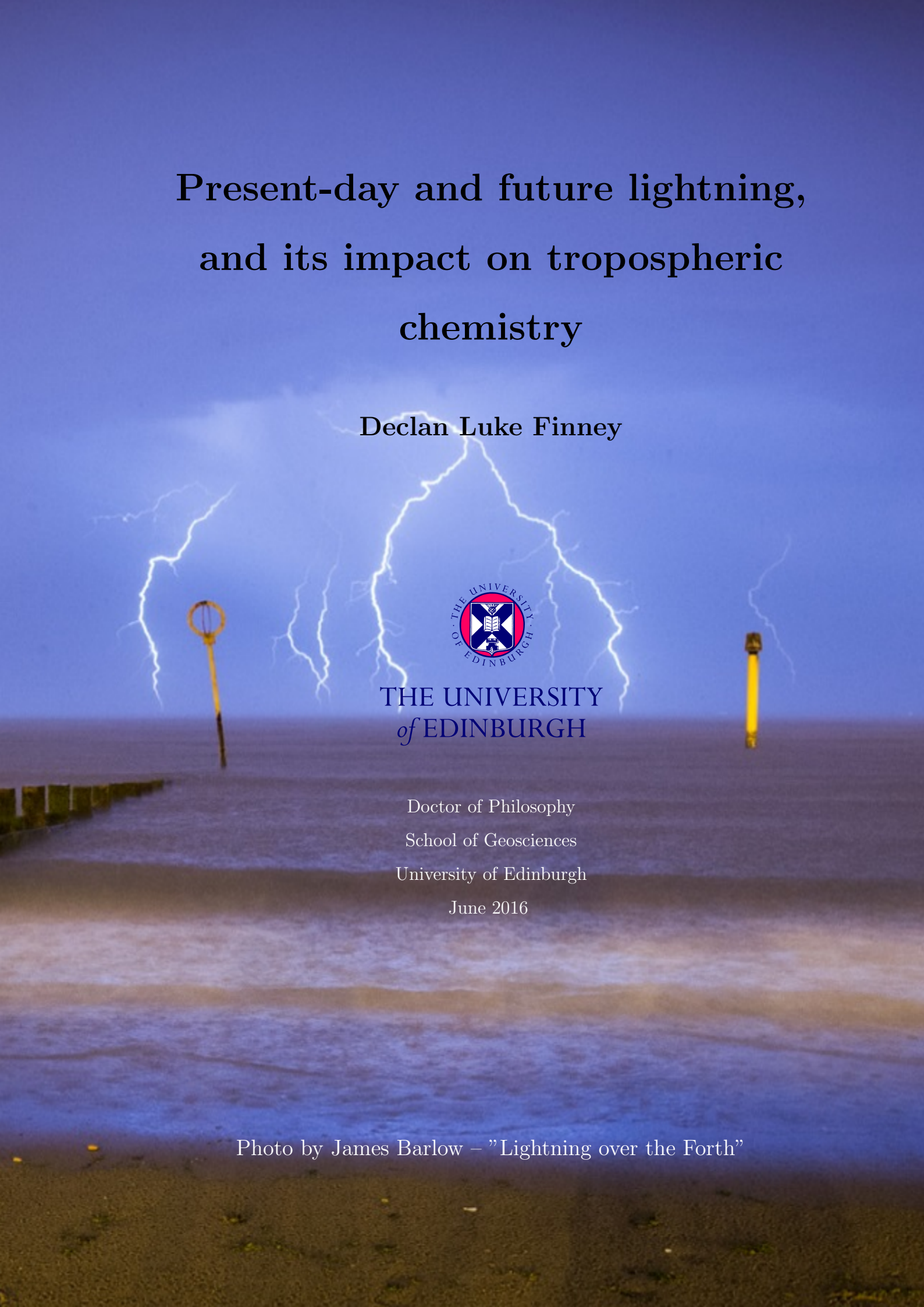

THE UNIVERSITY
of EDINBURGH

Doctor of Philosophy

School of Geosciences

University of Edinburgh

June 2016

Photo by James Barlow – "Lightning over the Forth"

Declaration

I declare that this thesis has been composed solely by myself and that it has not been submitted, either in whole or in part, in any previous application for a degree. Except where otherwise acknowledged, the work presented is entirely my own.

Declan Luke Finney

June 2016

Abstract

Lightning represents a key interaction with climate through its production of nitrogen oxides (NO_x) which lead to ozone production. These NO_x emissions are generally calculated interactively in chemistry-climate models but there has been little development of the representation of the lightning processes since the 1990s. In most models the parametrisation of lightning is based upon simulated cloud-top height. The aims of the thesis are: to explore existing schemes, and develop a new process-based scheme, to parametrise lightning; to use a new process-based lightning scheme to give insights regarding the role of lightning NO_x in tropospheric chemistry; and to use alternative lightning schemes to improve the understanding of the response of lightning to climate change, and the consequent impacts on tropospheric chemistry.

First, a new lightning parametrisation is developed using reanalysis data and satellite lightning observations which is based on upward cloud ice flux. This parametrisation is more closely linked to thunderstorm charging theory. It greatly improves the simulated zonal distribution of lightning compared to the cloud-top height approach, which overestimates lightning in the tropics. The new lightning scheme is then implemented in a chemistry-climate model, the UK Chemistry and Aerosol model (UKCA). It is evaluated against ozone sonde measurements with broad global coverage and improves the simulation of the annual cycle of upper tropospheric ozone concentration, compared to ozone simulated with the

cloud-top height approach. This improvement in simulated ozone is attributed to the change in ozone production associated with the improved zonal distribution of simulated lightning.

Subsequently, data from a chemistry-climate model intercomparison project (AC-CMIP) are used to study the state-of-the-art in lightning NO_x parametrisation along with its response to climate change. It is found that the models using the cloud-top height approach produce a very similar response of lightning NO_x to changes in global mean surface temperature of $+0.44 \pm 0.05\,\mathrm{TgN\,K^{-1}}$, for a baseline emission of $5\,\mathrm{TgN\,yr^{-1}}$. However, two models using two alternative lightning schemes produce a weaker and a negative response of lightning to climate change.

Finally, simulations in a future climate scenario for year 2100 in the UKCA model were performed with the cloud-top height and the ice flux parametrisations. The lightning response to climate change when using the cloud-top height scheme is in good agreement with the positive response found in the multi-model results of the cloud-top height approach. However, the new ice flux approach suggests that lightning will decrease in future. These opposing responses introduce large uncertainty into the projections of tropospheric ozone and methane lifetime in the future scenario. An analysis of the radiative forcing from these two species also shows the large uncertainty in the individual methane and ozone radiative forcings in the future. Due to the opposite effect that lightning NO_x has on methane (loss) and ozone (production) the net radiative forcing effect of lightning in present-day and future is found to be close to zero. However, there is a small positive feedback suggested by the results of the cloud-top height approach, whereas no feedback is evident with the ice flux approach.

These results show there are large and crucial uncertainties introduced by lightning parametrisation choice, not only in terms of the actual lightning distribution but also atmospheric composition and radiative forcing. The new

ice-based parametrisation developed here offers a good alternative to the widely-used approach and can be used in future to model lightning and develop the understanding of associated uncertainties.

Lay Summary

Thunderstorms occur in the troposphere – the lowermost layer of the atmosphere between the surface and approximately 15 kilometres. Lightning flashes form the gas nitric oxide. Reactions of nitric oxide with other gases leads to the production of ozone and to the destruction of methane. Ozone and methane are greenhouse gases which contribute to global warming. As the climate changes there may be an increase or decrease in lightning. Changes in the number of lightning flashes could in turn lead to more or less global warming through the interaction with ozone and methane.

In this thesis, computer models of the meteorology and chemistry in the atmosphere are used to better understand how lightning is affected by and affects the climate. The aims of the thesis are: to explore alternative methods to represent lightning in computer models, to use these alternative methods to give new insights regarding the role of lightning in the production of ozone and destruction of methane, and to use the alternative methods to improve the understanding of how lightning could be affected by, and affect, global warming.

To begin with, data based on weather observations are compared to observations of lightning in the tropics and subtropics. It is shown that intense movement of ice in clouds indicates regions where more lightning occurs. Such a relationship is consistent with past research which has shown that ice particles in thunderstorms

become charged and lead to lightning flashes. This work uses an ice-based method to estimate the location of lightning, which is shown to perform better than other methods. Most models use a method based on cloud height to predict lightning.

In the tropics, the ice-based approach estimates that there is less lightning than estimated by the cloud height approach. Such a finding is consistent with observations of lightning, and an atmospheric chemistry model is used to show that less lightning leads to less ozone production in the region. The reduced ozone also results in a better match to observations made of ozone in the tropics.

By applying the model to an example of a future climate where global warming has occurred, the response of lightning to climate change is determined. Both the ice-based and the cloud height approach show a general increase in lightning outside the tropics. However, within the tropics the cloud height approach predicts an increase in lightning, whilst the ice-based approach predicts a decrease. The cloud height approach would suggest that increased lightning leads to additional global warming which leads to increased lightning – a feedback. The ice-based approach, which better estimates present-day lightning, shows no such feedback under climate change. It is therefore important to consider whether the current methods for estimating future lightning and its impact on atmospheric chemistry should incorporate the ice-based approach.

Acknowledgements

A very big thank you to my supervisors, Ruth Doherty and Oliver Wild, who have given me the freedom to take a path through this PhD that I thought best, but who have also held me to account on every unjustified, terse or vague statement I have thrown at them. Thank you also to Alan Blyth and Hugh Pumphrey who have always been there to give great guidance. And thank you to my two PhD examiners, Bill Collins and Richard Essery, for their insightful critique which allowed me to develop my thesis even further. A Doctoral Training Grant from the Natural Environment Research Council has made the PhD possible.

Many scientists have given me ideas and helped me along the way so I thank the MacAQUE research group, folk at the UK Met Office and the ECMWF, Dave Plummer, Alex Archibald and the co-authors I have worked with on publications. I am grateful for data made available by the ECMWF and the TRMM team which have been integral to my research.

A big thanks to a few special people: Emma for showing me why Edinburgh would be an incredible place to do a PhD, and Oliver for being great company in treading the PhD path and always making me question the point of models. Thanks to Emma, Jamie and Claudia for giving comments on parts of this thesis, and James Barlow for the wonderful photo on the cover. Thank you to everyone in

the Crew attic and beyond for their friendship - Edinburgh has been a wonderful place to work because of you.

Keeping me sane over these years has been my Edinburgh housemates, undergrad friends, and fantastic family and friends in Essex. My mum, my dad, Woody and Chris Smith provide never-ending love and support which has been as invaluable during the PhD as ever. Finally, thank you to the most inspiring person in my life for bringing out all the creativity, love, life and happiness in me.

Contents

Chapter 1

Introduction

1.1 Motivation and research questions

Lightning interacts with with many parts of the Earth and atmosphere. As will be explained in this thesis, through its interactions, lightning represents a challenge to both our understanding of atmospheric physics and chemistry. Lightning is often researched with regard to the global electric circuit and as a natural wildfire ignition method. Another key research area, with respect to global lightning activity, is in the study of atmospheric chemistry. Nitrogen oxides (NO_x) produced by lightning flashes interacts with other chemical species to form ozone (O_3) in the troposphere. Tropospheric ozone is of interest in atmospheric chemistry as a greenhouse gas and as an air pollutant. Lightning has a role in both aspects but its principal effect is the production of ozone in upper troposphere, which is of particular importance to greenhouse gas radiative forcing. This is the main motivation driving studies of atmospheric composition within this thesis. A discussion and development of the physical representation of lightning in models

of atmospheric chemistry will provide a useful starting point of the research in thesis.

The aims of the thesis are given below, along with the main research chapters used to address the aims. The third aim is addressed by both of the final two research chapters, each using a different perspective.

1. To explore existing schemes, and develop a new process-based scheme, to parametrise lightning (Chapter 2)

2. To use a new process-based lightning scheme to give insights regarding the role of lightning NO_x in tropospheric chemistry (Chapter 3)

3. To use alternative lightning schemes to improve the understanding of the response of lightning to climate change, and the consequent impacts on tropospheric chemistry (Chapters 4 and 5)

The following sections introduce the physical processes driving lightning activity (Section 1.2) and discuss the measurement of lightning, including the main satellite instrument dataset used throughout the thesis (Section 1.3). Section 1.4 introduces the details of the production of nitrogen oxides from lightning, and the subsequent chemical processes. A general method for representing lightning in global models is then described (Section 1.5), and previous evaluation studies of lightning in chemistry-climate models are discussed (Section 1.6). Finally, Section 1.7 gives an introduction to previous studies regarding the response of lightning to climate change.

1.2 Dynamics, microphysics and electrification of a thunderstorm

A thunderstorm begins with convection, initiated by surface heating or topography, in unstable atmospheric conditions. The rising air parcels carry moisture up to the level of free convection where they can continue rising uninhibited. As the parcel cools, condensate forms and can freeze, with both effects resulting in latent heating of the air. The latent heating of air drives further convection to develop deep convective thunderstorms. Such storms can extend to the full height of the troposphere, and in vigorous cases overshoot the tropopause and extend into the lower stratosphere by several kilometres (Pan *et al.*, 2014). This is despite air above the tropopause having a higher potential temperature, and hence stable and convection inhibiting. Within the cloud, between isotherms of approximately 0 °C and -40 °C, the phase of cloud condensate can be mixed (Rosenfeld and Woodley, 2000). The mixed-phase region is comprised of small ice crystals, larger ice particles called graupel, and supercooled water droplets.

Ice particles are generated in storms by a variety of mechanisms. As well as freezing by homogeneous (without condensation nuclei) and heterogeneous (onto condensation nuclei) mechanisms, ice particles are generated through secondary processes such as the Hallet-Mossop process (Latham *et al.*, 2004). The Hallet-Mossop process is a result of splinters of ice being expelled when riming occurs - freezing of supercooled water onto an already frozen ice particle. The ice splinters can then go on to generate ice particles through heterogeneous freezing in collisions with other water droplets. Riming is also the mechanism by which graupel grows in size. As graupel from the top of the cloud falls through the mixed-phase region, supercooled droplets freeze (rime) to the particles. This releases latent energy and can further drive the convection. In intense storms, graupel can go through the cycle of falling, riming and be lifted within updraughts many times

thereby growing larger and larger before eventually being overcome by gravity and falling as hail.

The collision of smaller rising ice particles and falling graupel, and the transfer of ions between them, is the basis for the accepted theory for thunderstorm charging, the Non-Inductive Charging Mechanism (Reynolds *et al.*, 1957). It is still an active area of research to establish how charge is transferred between the particle types (Dash *et al.*, 2001; Ávila *et al.*, 2013) but several laboratory experiments have demonstrated that ice particles do transfer charge, as reviewed by Saunders (2008). The experiments also demonstrate that the sign of charge transfer is dependent on temperature and water vapour content which results in different charge centres forming in different parts of the thundercloud (Figure 1.1).

An example of an experimental study by Jayaratne *et al.* (1983) showing the temperature dependence of charge transfer to graupel, for a given liquid water content, is shown in Figure 1.1A. These show that, for temperatures colder than approximately -20°C graupel becomes negatively charged, whereas for warmer temperatures it becomes positively charged. The rising ice crystals will gain the opposite charge of graupel during the collision. This temperature dependence can be used to explain the typical tripole charge structure of thunderstorms, illustrated in Figure 1.1B as a small positive charge below a large negative charge below another large positive charge. The critical temperature for a shift in the sign of charge transferred varies with water vapour content as well as impurities in the ice particles (Jayaratne *et al.*, 1983; Saunders, 2008). Charge separation within the cloud provides a means to generate an electric field from which lightning can form. The electric field that forms from the processes described, holds the potential energy which is discharged when a lightning flash occurs.

It is worth noting that the charging of a cloud is not the whole picture of the processes leading to a lightning flash. Electric field measurements of storms

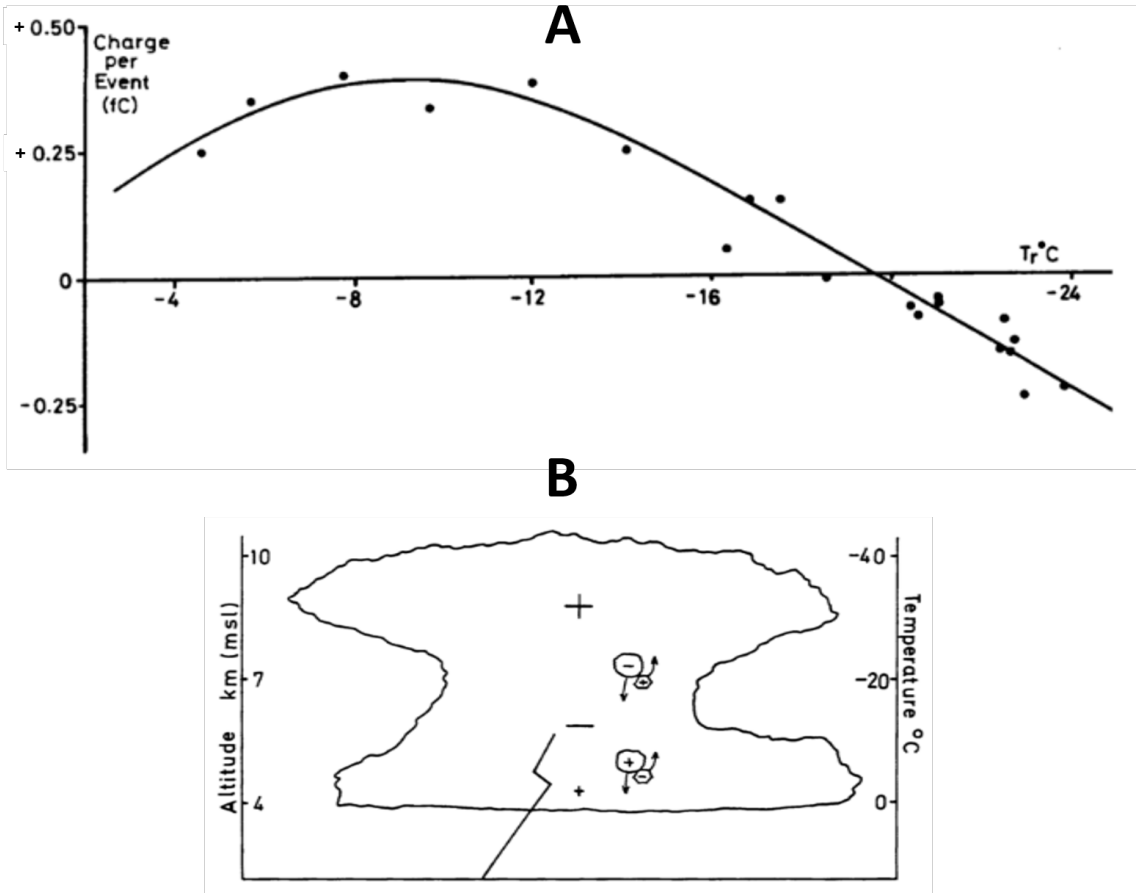

Figure 1.1: Experimental results and their relation to thunderstorm charging taken from a review of thunderstorm charging processes by Saunders (2008). A) The temperature-dependency of charge transfer to a graupel particle from ice crystal collisions from a laboratory experiment (Jayaratne *et al.*, 1983). B) A diagram of charge transfer between graupel and ice crystals, and the consequent charge structure in an idealised thunderstorm.

suggests that the magnitude of the field is an order of magnitude less than that needed for classic dielectric breakdown, i.e. for the attractive force between charges to overcome the electrical resistance of the atmosphere (Solomon *et al.*, 2001). Another branch of research explores how lightning is initiated within these lower electric fields (Gurevich and Karashtin, 2013; Owens *et al.*, 2014). This aspect of lightning, whilst potentially important, is not yet implemented in chemistry-climate models and would be difficult at this time to reliably develop. As such, it is not considered in any further detail in this thesis, with focus instead being on the Non-Inductive Charging Theory as the primary control on the formation of lightning.

1.3 Lightning observational data

There are three distinct data types currently available to measure lightning activity. These are: human-observed thunderstorm activity (Changnon and Changnon, 2001), detection of electromagnetic disturbances between 3 Hz–300 MHz (Rakov, 2013; Nag *et al.*, 2015), and visual detection by satellite imaging (Cecil *et al.*, 2014; Nag *et al.*, 2015). Human-observed thunderstorm activity is provided by meteorological records generally as the number of days where thunder was heard at a weather station. Electromagnetic disturbances are detected by ground-based instruments which work together in a network to pin-point the time and location of disturbances made by lightning up to distances of tens to thousands of kilometres, depending on the frequency band used. Higher frequency electromagnetic waves attenuate quicker as they propagate over the Earth's surface so each detection system has a limit based on the frequency it measures. Satellite instrument data uses a charge-coupled device (CCD) to observe flashes in the visible part of the electromagnetic spectrum.

Satellite instrument measurements of lightning will be the main source of observations in this thesis. The satellite based measurement method can provide long-term (over a decade) of relatively accurate and homogeneous detection efficiency spatially. While the data is not continuous, it can be averaged over longer time periods to attain useful climatological information.

Human-observed records provide little accuracy regarding lightning location, frequency and time, and also have great uncertainty associated with local topography and weather conditions. There is still some use for such data as it is the key data source when studying past conditions prior to the 1990s (Changnon and Changnon, 2001; Pinto *et al.*, 2013). I will not use this data due to its shortcomings and because the thesis aims to study present-day conditions for which more accurate data is available. Electromagnetic detection provides useful data for present-day. However, such measurements are predominantly useful over regional scales as variation in detection efficiency is complex, depending on the position of the lightning within the network and over time as detectors are added and removed. Due to the inhomogeneous detection efficiency, this dataset will also not be used for my analysis.

In summary, satellite instrument measurement of lightning has been chosen as the main data source for the thesis as it provides greater accuracy than meteorological records of thunderstorm days and has less variation in detection efficiency over such large regions than ground-based detection systems. Section 1.3.1 introduces the satellite lightning detection systems and Section 1.3.2 provides an overview of general features in the climatology of lightning as observed by satellite instruments.

1.3.1 Method and uncertainties of satellite instrument observation

Satellite-based measurements of lightning to date have been made by instruments aboard low-earth orbit satellites (Cecil *et al.*, 2014). There are planned lightning measurements from geostationary satellites over the Americas with the Geostationary Lightning Mapper (Goodman *et al.*, 2013) and Europe with the Meteosat Third Generation-Lightning Imager. However, for the observational datasets discussed here the methods and uncertainties are related to low earth orbit satellite characteristics.

The Lightning Imaging Sensor (LIS) is the main data source used to represent lightning observations in this thesis (Boccippio *et al.*, 2002). It was on board the Tropical Rainfall Measuring Mission (TRMM) satellite in a low earth orbit with an inclination of 35° between January 1998 and April 2015. It orbited the earth several times each day scanning the surface at different locations between ±38° latitude for approximately 90 seconds at a time. Over the course of 99 days the instrument will have sampled the diurnal cycle of all locations within its range twice (Cecil *et al.*, 2014). Using the climatologies and smoothed products described by Cecil *et al.* (2014) helps to address uncertainties associated with the LIS measurements but it is still important to bear in mind that the instrument is not observing all locations at all times. An example of LIS tracks and measurements over the course of its last day of measuring is shown in Figure 1.2.

The predecessor to LIS, the Optical Transient Detector (OTD) (Christian *et al.*, 2003), had a range of ±75° latitude and a longer viewing time for each location of ∼3 min. The OTD produced measurements from May 1995 to March 2000. The OTD instrument extends the time period of the LIS data and can be used to extend the coverage of a lightning climatology to cover all global locations where

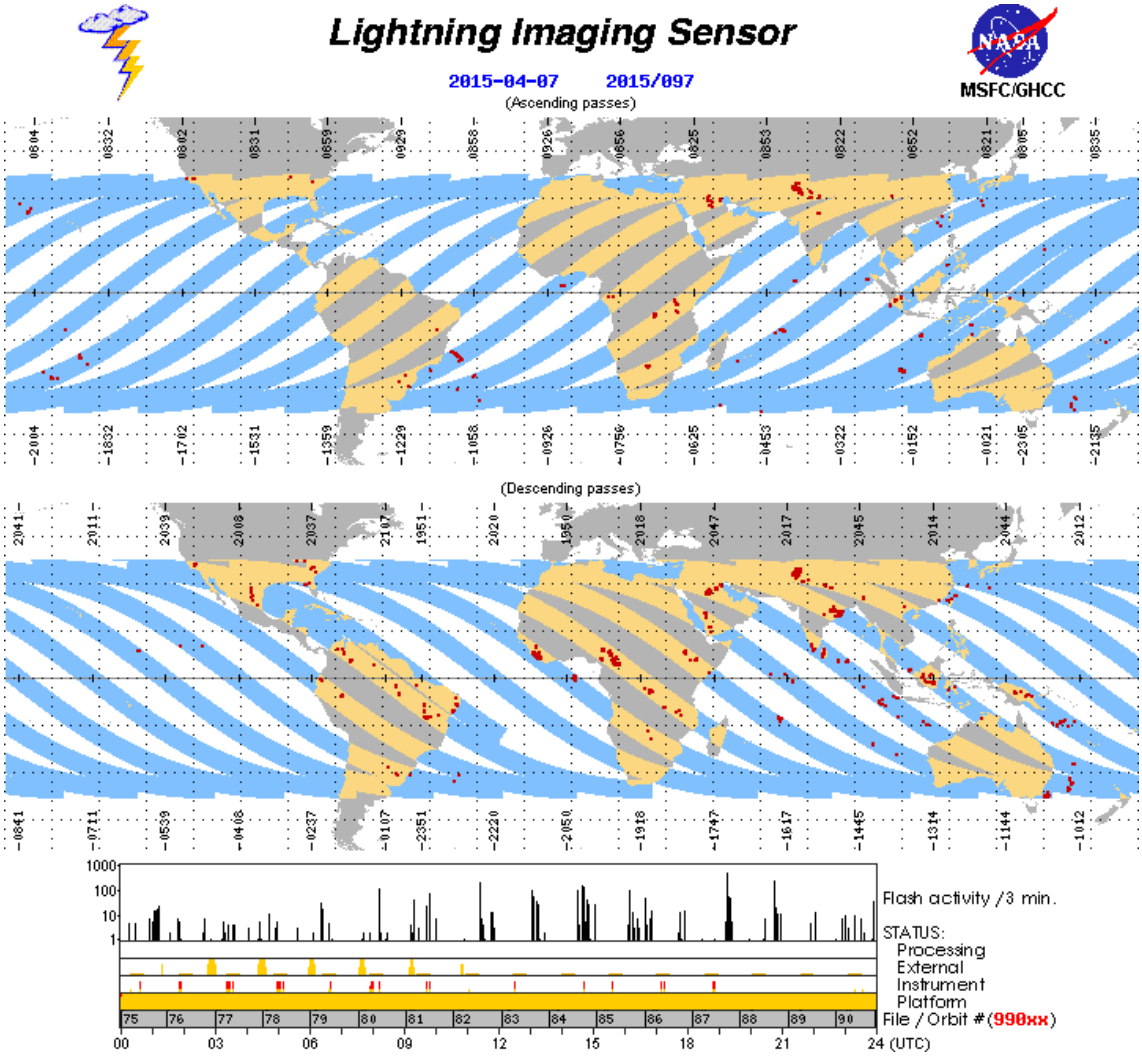

Figure 1.2: Quality controlled measurements made by LIS on 7th April 2015 (Downloaded from http://thunder.msfc.nasa.gov/lisib/lisbrowsecal on 16/03/2016). Blue/orange regions show the viewing regions of the instrument over ocean/land. Grey/white regions are unobserved on this day. Red dots show the flash measurements, with the time series of measurements shown in the bottom panel.

substantial lightning activity occurs. All locations in the long term climatologies have been sampled for 100s of hours.

The LIS and OTD instruments used a CCD to image the surface. They then applied 4 stages of filtering to discern lightning flashes as described by Christian *et al.* (2003). This includes the removal of the background scene and spectral filtering to the atomic oxygen emission wavelength of 777.4 nm, which further helps to separate flashes from the background cloud.

Bitzer *et al.* (2016) used a ground-based network to estimate an upper limit on the detection efficiency of LIS. Using the assumption that the two networks combined detect all occurrences of lightning, they find the detection efficiency of LIS has an upper limit of 96.8%. Two key sources of error are present in the measurements: 1) the diurnal variability in detection efficiency, and 2) difficulty in measuring within the South Atlantic Anomaly (SAA). These are described in detail below.

First, the instrument had its highest detection efficiency at night since the flashes are more easily discerned from the dark background image. Boccippio *et al.* (2002) estimated that the detection efficiency of LIS ranged from 69% at midday to 88% at midnight, and the detection efficiency of OTD between 38 % at midday to 49 % at midnight. These detection efficiencies were used by Cecil *et al.* (2014) to account for diurnal variability in detection when forming the LIS/OTD lightning climatology products.

Second, the SAA is a region over the South Atlantic and parts of South America where the LIS and OTD instruments experience a greater intensity of radiation. The increased radiation is a result of a weaker magnetic field in the region, which allows energetic space particles to reach closer to the Earth's surface. The measurements affected by disturbances were filtered from the data products

though this results in less viewing time over the SAA region and as such reduced confidence in the observation estimates.

1.3.2 A global lightning climatology from LIS and OTD satellite observations

The measurements made by the two satellite instruments, LIS and OTD, have been combined by Cecil *et al.* (2014) to form monthly climatologies of lightning activity between $\pm 75^\circ$ latitude. As already discussed, many uncertainties in measurements have been accounted for in the products through either quality control of which measurements to include or applying adjustments according to quantified detection efficiencies. To form the climatology product, measurements are totalled within daily, $0.5^\circ \times 0.5^\circ$ grid boxes. Then spatial and temporal smoothing is applied to remove noise. Spatial smoothing is applied using a $2.5^\circ \times 2.5^\circ$ boxcar moving average and temporal smoothing is applied using a 31-day boxcar moving average. The final dataset is the High Resolution Monthly Climatology (HRMC) product.

The seasonally averaged spatial distributions of the HRMC product are shown in Figure 1.3. Generally, flash rates are much lower over the oceans than over land, and flash rates are higher in the tropics - reducing substantially towards the poles. These features are also apparent in observations made by ground-based networks (Said *et al.*, 2013; Virts *et al.*, 2013). Some features in the ground-based observations can be different such as which continents in the tropics have the greatest flash rates. In the case of LIS/OTD data this is Africa, but in the case of the World Wide Lightning Location Network (WWLLN) data the lightning peaks are larger over North and South America (Virts *et al.*, 2013). However, there are fewer ground-based measurement stations in Africa and this leads to a reduced detection efficiency in this region (Hutchins *et al.*, 2012). The LIS/OTD

climatology has much less variation in detection efficiency (with the exception of the SAA) and therefore provides the more robust climatology product.

Figure 1.3 demonstrates that lightning occurs year-round in some locations in the tropics such as Central Africa and Indonesia. However, there are very large seasonal peaks in the subtropics and mid-latitudes. These peaks can be related to the monsoon seasons as in the case of India (MAM and JJA), or the greater surface heating and atmospheric instability in mid-latitudes in the summer months. During the course of the thesis, evaluation of the simulated lightning will consider the key regional features discussed here including the annual cycles and their regional variation.

Recent publications have explored the satellite lightning climatology in greater depth. For example, Cecil *et al.* (2015) considered how the frequency of thunderstorms in each location viewed by LIS contributes to the annual flash rate. They found that subtropical locations such as Argentina, the US and Pakistan exhibit much higher 'conditional' mean flash rates than their annual mean flash rate suggests, i.e. there are relatively fewer occurrences of thunderstorms, but they have higher flash rates than in other locations. Furthermore, using measurements from 1998-2013, a new very high resolution (0.1° x 0.1°) data product using LIS has now been developed (Albrecht *et al.*, 2016). This exhibits the same large-scale spatial features presented in Figure 1.3 along with features associated with the much greater detail. Albrecht *et al.* (2016) identifies the location with the most intense lightning activity, within the LIS viewing range, to be Lake Maracaibo, Venezuela. This lake is surrounded by mountains which, along with lake and sea breezes, drives the convective activity in the region. Albrecht *et al.* (2016) finds that many of the principal lightning hotspots are located near mountain ranges and lakes.

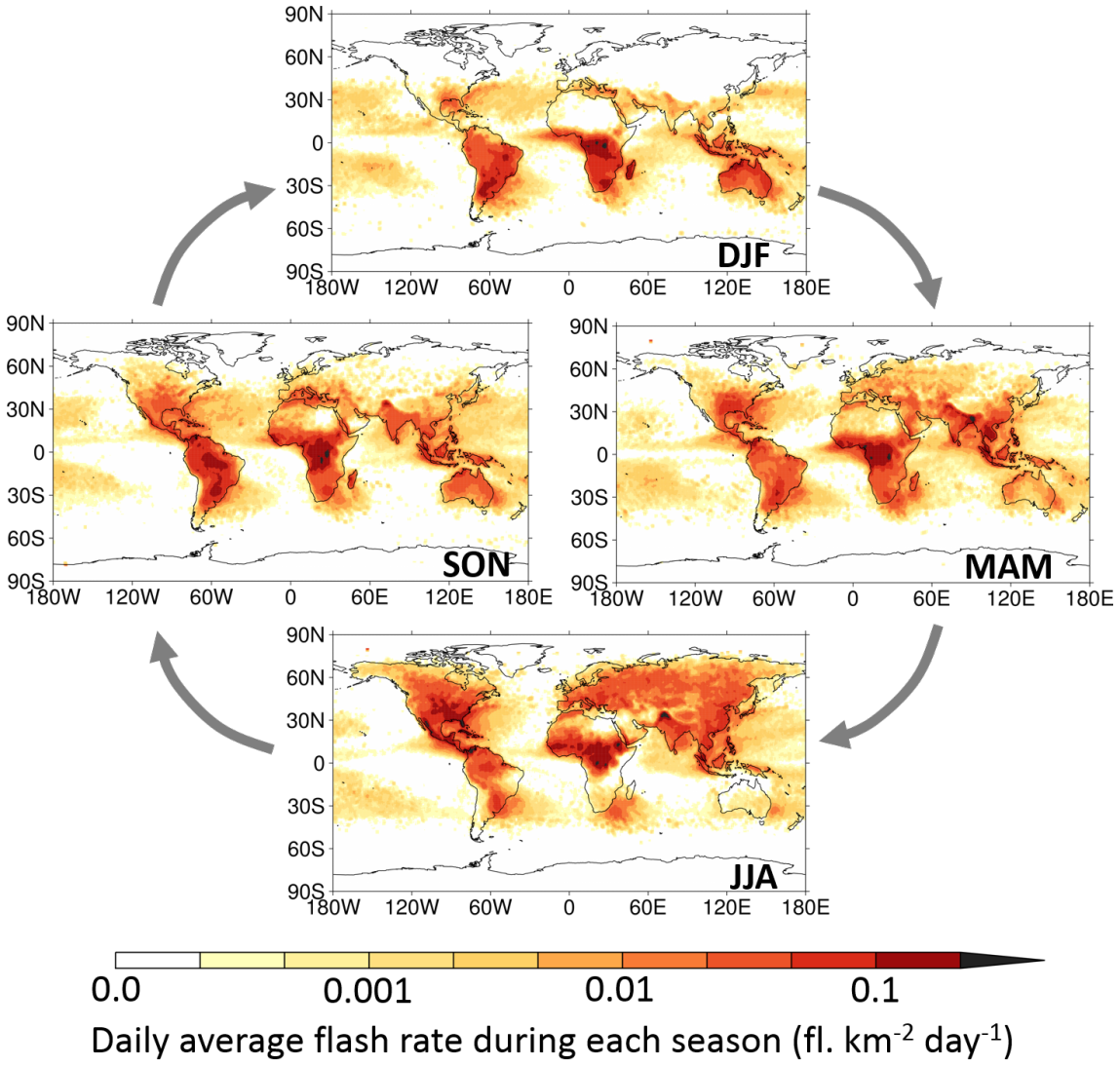

Figure 1.3: A seasonal climatology of lightning produced from the combined satellite High Resolution Monthly Climatology (HRMC) product of Cecil *et al.* (2014) using LIS and OTD measurements over the period May 1995 and December 2011.

1.4 Lightning and chemistry

A principal aim of this thesis is to improve the understanding of how the lightning source of NO impacts tropospheric chemistry, in present-day and in the future. Lightning NO emissions are not the only, nor the largest, source of NO in the atmosphere, however, lightning is the principal source of NO in the middle and upper troposphere where the only other source of NO is from aircraft. Furthermore, as a natural NO source which responds to climate change, and which affects the composition of greenhouse gases such as ozone and methane, lightning may represent a climate feedback. Due to its effect on chemical composition, lightning is represented in atmospheric chemistry models. All atmospheric chemistry models simulate the relevant chemistry and physical processes controlling atmospheric composition. However, meteorological processes may be represented using either: pre-defined offline meteorology from a general circulation model (GCM) or reanalysis (as in a Chemistry Transport Model (CTM)), or meteorology simulated online using a GCM coupled to a CTM (as in a Chemistry-Climate Model (CCM)).

Definition: Reanalysis data. "Estimates of historical atmospheric or oceanographic quantities, such as temperature, wind or currents. The datasets are produced by processing past meteorological or oceanographic observational data using a single version of a state-of-the-art weather forecasting or ocean circulation model with data assimilation techniques" (based upon Planton, 2013).

The following sections describe: the chemical mechanism of NO production by lightning and estimates of the amount of lightning NO produced (Section 1.4.1), and the chemical reactions of NO affecting tropospheric composition and past research regarding the impact of lightning on tropospheric chemistry (Section 1.4.2).

1.4.1 NO emission from lightning

For a fraction of a second, a lightning spark heats the air to temperatures over five times that of the surface of the sun. Molecular bonds of nitrogen and oxygen are broken. In another fraction of a second, the air rapidly cools and the free atoms react to form new compounds. NO is one of the predominant trace gas products as found in the thermal equilibrium modelling of Chameides (1986). This is then rapidly oxidised, by peroxy radicals (OH or HO_2) or ozone, to nitrogen dioxide (NO_2) to form an equilibrium NO_x (NO + NO_2) level.

A literature review of 39 studies between 1976 and 2007 by Schumann and Huntrieser (2007) reported a mean estimate of 250 mol NO_x per flash with an uncertainty range of 33-660 mol NO_x per flash. A selection of more recent studies using theoretical considerations or aircraft measurements, some in combination with satellite or model data, have provided estimates with a range of 31-700 mol NO_x per flash thereby providing little modification to the review uncertainty range (Huntrieser *et al.*, 2008; Cooray *et al.*, 2009; Huntrieser *et al.*, 2009; Bucsela *et al.*, 2010; Ott *et al.*, 2010; Huntrieser *et al.*, 2011; Miyazaki *et al.*, 2014; Pollack *et al.*, 2016).

Laboratory experiments provide a means to more accurately measure NO production of an electrical discharge. However, extrapolation of the discharge produced in the laboratory to a realistic lightning flash is required. A recent theoretical study by Cooray *et al.* (2009) has developed the theory underlying NO production, and compared their theoretical assertions to existing laboratory results. They conclude that extrapolation of laboratory results can be made more robust through the use of the measured current as well as energy. In addition, Cooray *et al.* (2009) consider how the NO production would vary at different stages of a lightning flash, and conclude that the previously ignored, slower discharge processes occurring at the beginning and end of a lightning flash are the main source of

NO production. Following their line of reasoning, Cooray *et al.* (2009) conclude that the global average NO production per lightning flash is 90 mol NO_x. This estimate is based on a combination of theory and available laboratory results, but one key assumption is a typical flash length of 45 km. The flash length cannot be well-constrained on the global scale, however, this study does provide a useful development on previous laboratory-based estimates considered in the Schumann and Huntrieser (2007) review.

A satellite study by Beirle *et al.* (2010) found that observed column NO_2 was unrelated to flash density, and estimated that LNO_x production rates were generally far lower than expected based on literature estimates such as that of Schumann and Huntrieser (2007). They commented that there is large variability in emissions per flash but that their results may have been biased through sampling of weaker flash rates. The satellite-based (SCIAMACHY) measurements of NO_2 used were taken at 10am local time and many (56%) of their cases were over the ocean. Higher lightning activity occurs over land and much of that activity occurs in the afternoon or evening (Albrecht *et al.*, 2016). The under-sampling of these times and locations is a source of potential bias in the findings of Beirle *et al.* (2010).

Martin *et al.* (2007) used the GEOS-Chem CTM to constrain the magnitude of the global source of lightning NO_x (LNO_x) to the observations of column NO_2 and other species measured upon satellites such as SCIAMACHY. They found that a lightning source was necessary and was best represented by a global source of 4-8 TgN yr^{-1}. Assuming 44 flashes s^{-1} (Christian *et al.*, 2003) (from now on flash is denoted as fl.), their top-down estimate is within the range of the review by Schumann and Huntrieser (2007) (Note that later in the thesis 46 flashes s^{-1} is referenced from Cecil *et al.* (2014) which is an estimate made since the Martin *et al.* (2007) study). One recent study used data assimilation of multiple satellite-based measurements of NO_2, O_3, HNO_3 and CO into the

CHASER CTM (Miyazaki *et al.*, 2014). They determined the NO_x production rate of lightning was 310 mol NO_x per flash with the uncertainty derived from sensitivty tests being $\pm$70 mol NO_x per flash. This estimate is also within the review range of Schumann and Huntrieser (2007). However, both of these last two methods of using satellite data include an assumption of a flash rate distribution based on the Price and Rind (1992) scheme, a scheme which will be discussed further in Section 1.5.

The most recent contribution to LNO_x estimates is an extensive aircraft campaign over the central and southern US which has been used to estimate the LNO_x production in that region (Pollack *et al.*, 2016). The study found that there was 117-332 mol NO_x produced per flash with the range including both variability between storms and uncertainty in the NO_x production estimate.

Globally, Schumann and Huntrieser (2007) report lightning to emit 5 TgN yr^{-1} with an uncertainty range of 2–8 TgN yr^{-1}. A 5 Tg NO_x source makes up approximately 10 % of total global NO_x emission which includes natural and anthropogenic sources such as fossil fuel burning, biomass burning, soil release and aviation (Schumann and Huntrieser, 2007). However, assuming a constant NO emission rate for each lightning flash is an over-simplification. For instance, Huntrieser *et al.* (2008) found that lightning in tropical storms may produce less NO than subtropical storms. Beirle *et al.* (2010) reported that their results were consistent with the result of Huntrieser *et al.* (2008). Emissions have been found to vary with energy, peak current, atmospheric pressure and flash length (Schumann and Huntrieser, 2007; Cooray *et al.*, 2009). Whilst the consequences for NO emission have not yet been explored, several studies have shown, with different datasets, that flashes over the ocean can be more energetic, have higher peak currents and be larger and brighter than flashes over land (Fullerkrug *et al.*, 2002; Hutchins *et al.*, 2013; Peterson and Liu, 2013; Said *et al.*, 2013; Beirle *et al.*, 2014). For the research in this thesis, a constant NO production per flash

is assumed, as causes of variability are not yet understood sufficiently well to parametrise in a CCM.

1.4.2 The role of NO in tropospheric chemistry

The NO emitted by lightning, along with other sources of NO, enter the NO_x cycle whereby NO is oxidised to NO_2 and then photolysed back to NO (Figure 1.4A). The NO_x cycling ends when NO_2 reacts with a hydroperoxy radical (OH) to form nitric acid (HNO_3) which can then be wet or dry deposited. In the cycling stage, NO can be oxidised to NO_2 by either ozone or peroxy radicals (HO_2 or RO_2). The balance between NO oxidation by ozone and by peroxy radicals will depend on the concentrations of the various species. Any oxidation by peroxy radicals leads to an increase in net ozone production from NO emissions through the mechanism illustrated in Figure 1.4B.

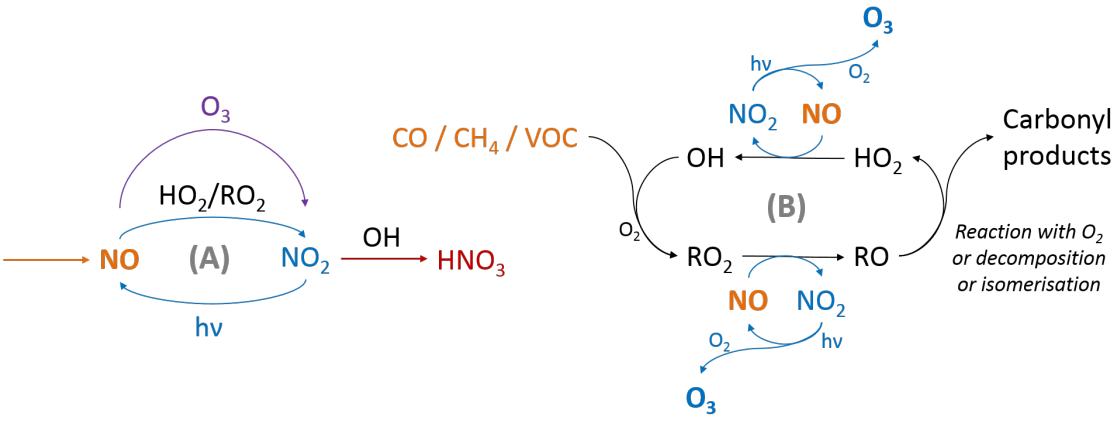

Figure 1.4: NO_x cycling and formation of ozone from NO. A) The oxidation, photolysis and loss in the NO_x cycle. B) Production of ozone from NO. RO_2 represents any organic peroxy radical. In orange are emitted species, in blue are the reactions leading to ozone production from NO, in red is the loss reaction for NO_x, and in purple is the loss of ozone through reaction with NO.

Figure 1.4B shows that, given a sufficient supply of methane (CH_4), carbon

monoxide (CO) or Volatile Organic Compounds (VOCs), the HO_x (OH and HO_2) cycle is driven in such a way to compliment the catalytic production of ozone by NO_x. As OH is produced from the oxidation of NO, additional OH is available to oxidise methane, CO or VOCs to form RO_2, which can then oxidise NO, and its products then react to form HO_2 again. Limitations on this process are the availability of VOCs to be oxidised by OH, the availability of light to photolyse NO_2, and the loss of NO_2 through reaction with OH to form nitric acid. The other main source of tropospheric ozone is through stratosphere to troposphere transport during tropopause folding events, typically occurring in mid-latitude cyclones but which can also occur during deep convective storms (Pan *et al.*, 2014).

The production of tropospheric ozone is balanced by: photolysis to O(1D) then reacting with water (Equation 1.1), direct loss through reaction with HO_x (Equations 1.2 and 1.3), dry deposition of ozone, and by troposphere to stratosphere transport of ozone in convective storms overshooting the tropopause (Huntrieser *et al.*, 2016). The chemical loss reactions above are given by:

$$O(^1D) + H_2O \rightarrow 2OH \tag{1.1}$$

$$O_3 + HO_2 \rightarrow OH + 2O_2 \tag{1.2}$$

$$O_3 + OH \rightarrow HO_2 + O_2 \tag{1.3}$$

By the chemical mechanism illustrated in Figure 1.4, lightning impacts the relatively short-lived greenhouse gas, ozone. The lifetime of ozone can vary from hours to months depending on the chemical environment, making it relatively difficult to model, yet it is estimated to have an important radiative forcing effect in present-day compared to the pre-industrial period (Myhre *et al.*, 2013, Fig. 8.15). As well as impacting ozone, lightning NO_x modifies the OH concentration

through oxidation of NO by peroxy radicals. OH is an important oxidation component of the troposphere which in turn is the key loss reaction for methane. Through its formation of OH, LNO_x acts to reduce the lifetime of methane. Methane, like ozone, is estimated to have a large radiative forcing effect (Myhre *et al.*, 2013).

Definition: Radiative forcing: "The change in net downward radiative flux at the tropopause after allowing for stratospheric temperatures to readjust to radiative equilibrium, while holding surface and tropospheric temperatures and state variables such as water vapor and cloud cover fixed at the unperturbed values" (Myhre *et al.*, 2013).

Lacis *et al.* (1990) showed that ozone produced in the upper troposphere had the greatest global warming potential of ozone produced anywhere in the troposphere or stratosphere, due to the region having the greatest difference in temperature to the surface. Several studies have estimated lightning's role in affecting radiative fluxes and forcing through its ozone production (Toumi *et al.*, 1996; Dahlmann *et al.*, 2011; Liaskos *et al.*, 2015). Dahlmann *et al.* (2011) attributed ozone radiative forcing to its various sources and found that LNO_x had a 5 times higher ozone production efficiency than surface sources of NO_x, and that the ozone produced had the highest radiative efficiency because it occurs at lower latitudes and higher altitudes. Liaskos *et al.* (2015) performed simulations of zero lightning emissions and with emissions increased from 124 to 492 mol NO_x per flash. This factor of four increase in emissions (i.e., using the value of 492 compared to 124), is within the uncertainty of NO_x production per flash (Section 1.4.1), enhances ozone by 60%, and increases the mean net radiative flux at the tropopause attributable to lightning-produced ozone by a factor of three. The flux attributable to lightning-produced ozone was calculated as the difference between the simulations with lightning NO_x and a simulation with no lightning NO_x. None of the above studies calculated the corresponding radiative cooling resulting from

lightning NO_x through its impact on methane. Wild *et al.* (2001) showed that the time-integrated radiative forcing from a pulse of lightning NO_x is negative, because the radiative cooling of methane dominates over the short-term warming of ozone.

Due its variable lifetime, ozone concentration both responds to local conditions and is transported substantial distances, but is not well-mixed like many other greenhouse gases. As such, ozone exhibits substantial spatial and temporal variability. Using several ozone tracers, Grewe (2007) modelled the natural and anthropogenic emission sources of NO, and reported the NO source contribution to zonal and vertical ozone distributions. Lightning was shown to impact ozone throughout the troposphere by at least 10% and was the largest source in the southern hemisphere and tropics with up to 40% contribution. Murray *et al.* (2013) found that imposing the observed interannual variability (IAV) in lightning improved the modelling of tropical ozone IAV. They also found that lightning IAV was a more important driver than biomass burning IAV for IAV of ozone, even though the IAV of biomass burning is greater than that of lightning.

As mentioned above, the lifetime of ozone can be sufficiently long that transport of ozone and its precursors play a significant role in its distribution (Grewe *et al.*, 2002). Due to the role of lightning emissions influencing ozone concentrations in the troposphere, dynamical effects are important in redistributing ozone produced by LNO_x not only around the troposphere but into the stratosphere (Grewe *et al.*, 2002; Banerjee *et al.*, 2014). Substantial dynamical transport of lightning NO_x emissions and associated ozone was found by Grewe *et al.* (2002) who estimated that around 10% of ozone and 50% of NO_x in the lowermost stratosphere in the northern hemisphere was of tropical lightning origin. Banerjee *et al.* (2014) also concluded that ozone produced by LNO_x was transported into the stratosphere, finding that increased LNO_x emissions in future contributed to a 6.4% increase

in stratosphere-troposphere exchange (STE) due to the transport of ozone from the tropical upper troposphere into the lower stratosphere.

The abundant evidence in the literature of the effect of lightning on ozone, in particular, on ozone in the region in which it acts as a strong greenhouse gas, has been presented. This demonstrates the importance of including LNO_x emissions in CCMs and understanding the uncertainties associated with the simulated LNO_x source.

1.5 Lightning parametrisation

Sections 1.2 – 1.4 described the observations and scientific understanding of how lightning behaves in the environment. There are large uncertainties in the measurement and modelling of lightning at many stages in the process. However, lightning is a key component of atmospheric chemistry and, through impacts on ozone and methane, it also has a radiative forcing effect. The inclusion of lightning emissions in CCMs and CTMs is essential.

One method to represent lightning in CCMs might be to produce an NO emission distribution based on a lightning climatology (Section 1.3.2). In the early stages of development of the LNO_x emission source in atmospheric chemistry models, such a method was used. However, this method is generally no longer used since LNO_x will not necessarily coincide with simulated convective events, and the transport and chemical reactions will not align. Furthermore, for climate simulations other than present-day there are no such observations to provide an emission distribution. Following these lines of reasoning, it is important to simulate lightning, and hence LNO_x, interactively based on convective activity in the model.

To model such small-scale processes, approximations must be used since the spatial and temporal resolution of GCMs are generally insufficient to capture the process. In the case of lightning, the scales of the convective and microphysical processes driving the thunderstorms vary on the order of metres to kilometres. Global models generally use a much coarser resolution on the order of 100s of kilometres. A parametrisation is the term used for the large-scale approximation of a sub-grid process and it is a modelling method that aims to represent the general features of the parametrised process on the scales that the model is considering.

Figure 1.5 demonstrates the different stages of a generic lightning NO emission parametrisation which are described in further detail along with variations in the parametrisation method in Sections 1.5.1–1.5.3.

1.5.1 Horizontal flash distribution

Of all the components of the lightning emission parametrisation, the lightning flash distribution (Part 1 in Figure 1.5) is the component being most focused upon within this thesis. The flash distribution is the first stage of the parametrisation, with input meteorology from reanalysis or a GCM applied to empirical lightning relationships to establish the flash rate in each model grid cell. Lightning flashes are three dimensional in nature. It is not currently possible to measure their 3D distribution on a global scale. It is, however, possible to measure the global and large-scale *horizontal* distribution of flash rate in each grid cell column with satellites (Section 1.3.1). Even though these measurements also have uncertainty associated with them, they are much better constrained than the LNO_x emission distributions. Therefore, the horizontal distribution of lightning flash rate is the most testable component of the parametrisation.

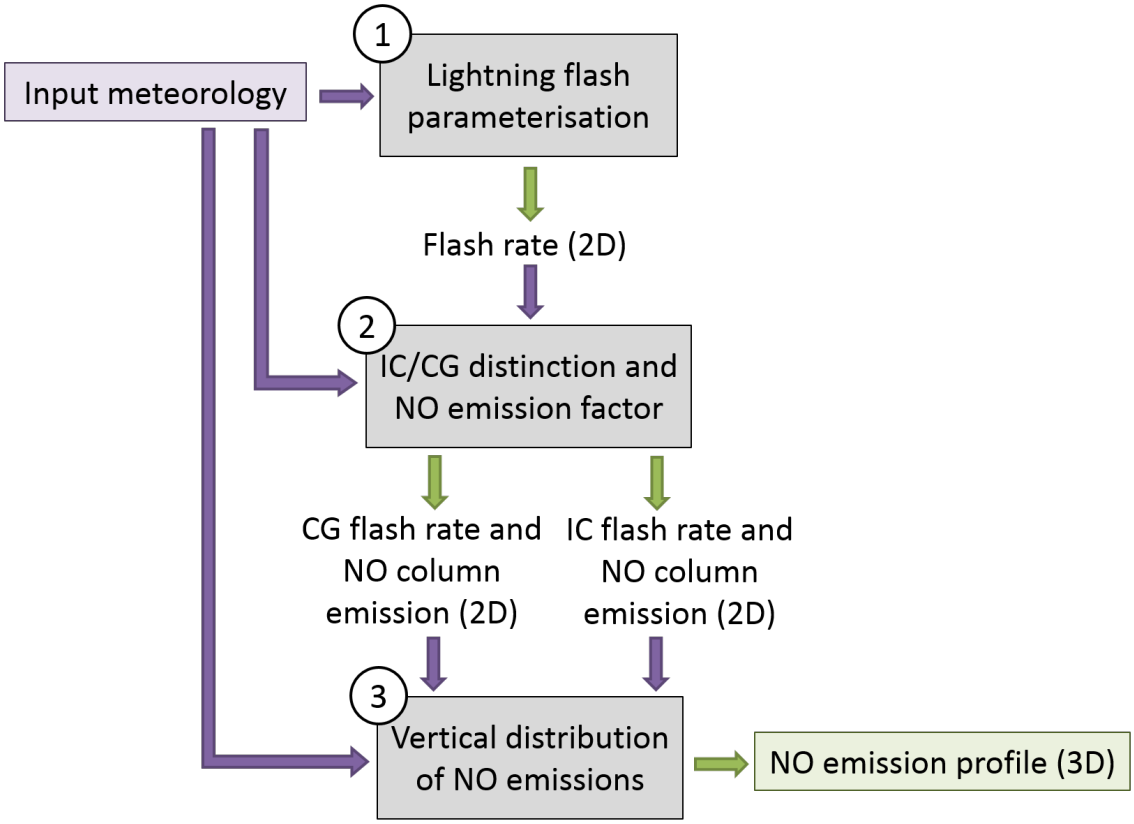

Figure 1.5: The generic form of lightning emission parametrisation as typically used in chemistry-climate and chemistry-transport models. The parametrisation would be calculated in each time step with new meteorology. Purple is used to indicate inputs to parts of the parametrisation, and green is used to indicate outputs. A distinction is often made between two types of lightning flash, cloud-to-ground (CG) and intra-cloud (IC). This distinction is discussed further in Section 1.5.2.

There have been many studies attempting to develop empirical relationships to parametrise lightning (Price and Rind, 1992; Grewe *et al.*, 2001; Meijer *et al.*, 2001; Allen and Pickering, 2002; Deierling *et al.*, 2008; Yoshida *et al.*, 2009; Romps *et al.*, 2014; Basarab *et al.*, 2015). The parametrisations from these studies are all broadly related to components of the non-inductive charging theory described in Section 1.2. Mostly the studies use input meteorological variables that are convection-based such as updraught velocity, updraught mass flux or Convective Available Potential Energy (CAPE) (Price and Rind, 1992; Grewe

et al., 2001; Allen and Pickering, 2002; Romps *et al.*, 2014). More recently, one study attempted to develop relationships between lightning and convective and ice-based variables to link more closely to the charging theory (Deierling *et al.*, 2008). In addition, a relationship between lightning and aerosols has been found which represents the indirect effect of aerosol on lightning through the control of aerosol on microphysical properties of clouds and radiation heating the surface (Altaratz *et al.*, 2010; Murray, 2016). So far these relationships using alternative variables have not been incorporated into large-scale CCMs.

By far the most commonly used parametrisation was developed by Price and Rind (1992) which uses cloud-top height as the input variable. The parametrisation is made up of two power-law relationships, one for continents and one for oceans. The continental relationship is based on storm measurements made at three locations in the US (Williams, 1985). The oceanic lightning relationship was formed by modifying the continental lightning relationship using the relationship between cloud-top height and maximum updraught velocity in oceanic and continental storms. The modification accounts for a shallower gradient between oceanic updraught velocity and cloud-top height. The two datasets and the parametrisations are shown in Figure 1.6. The adjustment over the ocean critically depends on the assumption that the relationship between maximum updraught velocity and flash rate (which they establish through combining the relationships for F_c and w_c in Figure 1.6) is independent of location. Price and Rind (1992) apply these relationships to International Satellite Cloud Climatology Project (ISCCP) data of cloud top heights. They show that globally the parametrisation is similar to global measurements of lightning made by a satellite instrument in 1977–1978.

Several studies since Price and Rind (1992) have looked to further develop understanding of the relationship between cloud height and lightning. Ushio *et al.* (2001) used coincident measurements of lightning and cloud-top height made upon

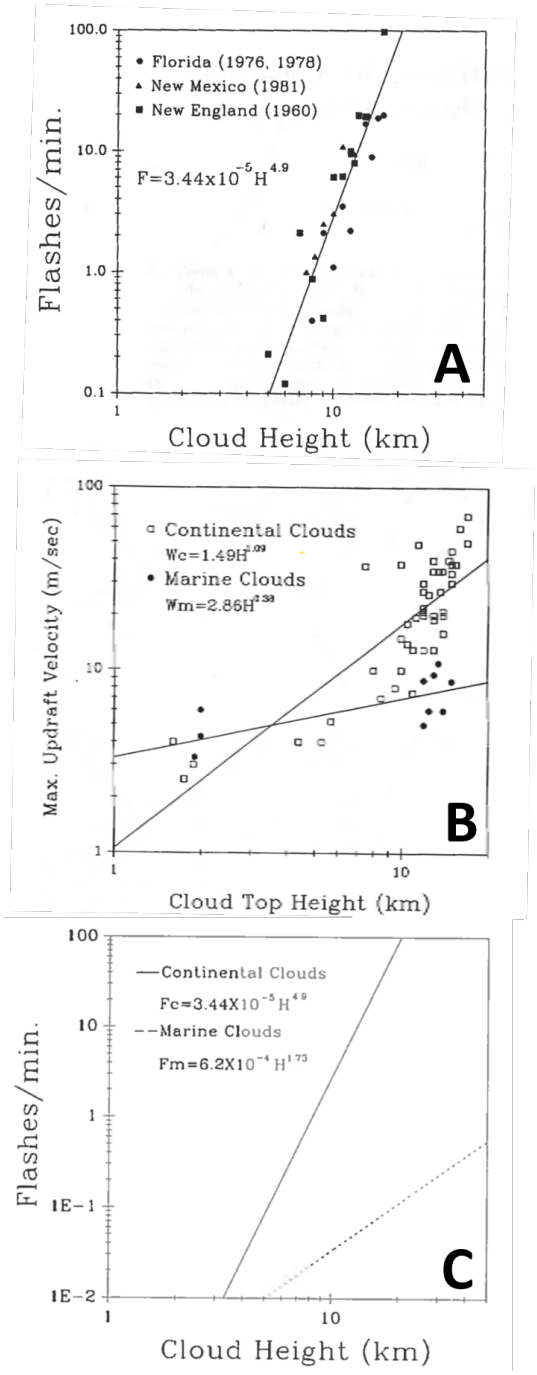

Figure 1.6: Three panels from Price and Rind (1992) to demonstrate the development of the widely-used cloud-top height parametrisation. A) The relationship between flash rate and cloud-top height in measurements of storms in the US. B) Relationships between maximum updraught velocity from literature separated into continental and oceanic measurements. C) The Price and Rind (1992) lightning parametrisation relationships.

the TRMM satellite to calculate power-law relationships. They found that the relationship is non-linear but has high variance and best fits vary with location and season. The parametrisation of Price and Rind (1992) was originally inspired by the research of Vonnegut (1963) who developed a theoretical model relating electrical power to storm geometry. As already stated, Price and Rind (1992) made assumptions regarding the application of relationships over the ocean, which Boccippio (2001) proposed are inconsistent with the original theory of Vonnegut (1963). Using revised formulations, Boccippio (2001) find that the original theory of Vonnegut (1963) is, to first order, consistent with satellite-based observations. Finally, Yoshida *et al.* (2009) used coincident measurements of cold cloud depth and flash rate of individual convective clouds from TRMM to show that a fifth-power relationship between these variables exists which is regionally independent (although the coefficient of the relationship is regionally dependent). To my knowledge the results of these studies have not been implemented in the lightning parametrisations of any CCMs. The aim of this thesis is to explore the use of an ice-based parametrisation based on the non-inductive charging theory (Chapter 2). A standard implementation of the Price and Rind (1992) parametrisation is used for comparison with this new scheme. However, the considerations above (e.g. used of cold cloud depth) could be used to improve the application of the cloud-top height based schemes in future.

1.5.2 Horizontal column NO emission distribution

From the flash distribution, a column NO emission distribution is determined by a simple method which considers each flash to have the same emission characteristics (Part 2 in Figure 1.5). This may be as simple as defining a parameter for the NO emission per flash based on studies discussed in Section 1.4.1 which use laboratory, aircraft measurements or theoretical considerations to

make estimates of production. There is much uncertainty in these estimates as each measurement method has its own advantages and disadvantages.

Whilst it is currently difficult to incorporate into CCMs, it is thought that flash energy, flash length or peak current may affect how much NO is produced by each flash (Cooray *et al.*, 2009). Therefore, this step in a parametrisation should include modelling of a variable NO production per flash depending on some or all of the three above characteristics of flashes. That would then modify the total NO emission by lightning. Simulating such fine detail is beyond the capability of CCMs at present. In some cases, two parameters have been used in CCMs to represent this level of complexity. For instance, in the UK Chemistry and Aerosol model (UKCA), a parameter for the energy per flash is multiplied by the NO production per Joule to derive the LNO_x production. This is equivalent to the single parameter method, since the product of the two parameters gives a single parameter for NO production per flash. However, there may in future be the potential to replace the energy per flash parameter with a calculation of the energy per flash dependent on the simulated meteorology.

One common differentiation made between flashes is to estimate how many are between the cloud and ground (CG) and how many occur within the cloud (intra-cloud, IC). This is done using a relationship between the cold cloud depth and the ratio of IC to CG (Price and Rind, 1993). The cold cloud depth may be modelled or determined using an empirical relationship of the variation of cold cloud depth with latitude from the same paper by Price and Rind (1993). With this method there are more IC flashes than CG, as has been found in multiple studies presented in the review by Schumann and Huntrieser (2007). The differentiation made is that the two flash types may produce different amounts of NO emissions or emit NO in different parts of the troposphere. The ratio of NO production by IC to CG flashes has been estimated to vary between 0.1-1 (Schumann and Huntrieser, 2007), but more recent estimates suggest that the ratio is likely to be much closer

to 1.0 (Ridley *et al.*, 2005; Cooray *et al.*, 2009; Ott *et al.*, 2010). I use a ratio of 1.0 in this thesis to correspond with these recent findings.

1.5.3 Vertical distribution of column NO emissions

A key feature of lightning emission is its three dimensional nature. Emissions occur throughout the tropospheric column, thereby requiring a vertical aspect to LNO_x parametrisation (Part 3 in Figure 1.5). A method to distribute column NO emissions to different altitudes uses prescribed percentages of emissions for each vertical cell, up to the model diagnosed cloud top.

A widely-used prescribed LNO_x vertical profile is from a study by Pickering *et al.* (1998). The study used a cloud-resolving model to estimate the distribution of emissions vertically following convective transport. Such a method is used in order to account for the transport that CTMs/CCMs are unable to reproduce due to the small spatial and temporal scales over which it occurs. In the study by Pickering *et al.* (1998), for a selection of observed storms, lightning NO_x emissions were initialised using the Price and Rind (1992) parametrisation, along with consideration of typical vertical distributions of lightning channels, and with NO production along the vertical extent of lightning flashes proportional to air density. The cloud-resolving model simulated NO_x transport, but not chemistry, on a 10 second time-scale and 1 km spatial resolution for each storm. After a few hours of simulation, the resulting domain-average lightning NO_x distribution was proposed as a useful distribution to be used in CTMS and CCMs. The authors note the uncertainty resulting from not allowing NO_x to be oxidised to other nitrogen compounds along with transport. However, they suggest that at the low altitudes of a convective storm there would be only small UV fluxes thereby slowing oxidation reactions, and at higher altitudes the lifetime of NO_x is on the

order of days and therefore there would not be substantial loss of NO_x over the course of a few hours.

Many aspects of the Pickering *et al.* (1998) study have since been improved upon in a study by Ott *et al.* (2010). In this latter study a 3D, instead of 2D, cloud-resolving model was used to determine vertical LNO_x profiles. Therefore, winds could be fully resolved. Furthermore, in the Ott *et al.* (2010) study, the initial distribution of lightning included greater detail through the use of observations of the vertical distribution of lightning. A CTM was also used with a three minute resolution to apply ozone photochemistry to the lightning NO_x. Studying the lightning NO_x distribution formed with and without chemistry, Ott *et al.* (2010) reported that NO_x was reduced by 5 and 20-33 % in two of the storms they considered. The large variation in oxidation occurring across the two storms highlights the sub-timestep chemical processes as a current uncertainty in the representation of LNO_x in CCMs. A key difference between the Pickering *et al.* (1998) and Ott *et al.* (2010) vertical profiles is that much less NO emission is placed at the surface by the Ott *et al.* (2010) profiles, as can be seen in Figure 1.7.

Other vertical LNO_x emission approaches use an initial lightning NO_x vertical distribution that is either uniform or with emissions distributed proportional to air density (Goldenbaum and Dickerson, 1993; Stockwell *et al.*, 1999; Jourdain and Hauglustaine, 2001). The updraughts and downdraughts in the CTM or CCM can then be used to re-distribute emissions resulting from simulated convection before applying the chemistry scheme. Such alternative approaches require: A) the time and spatial resolution of the model to be sufficiently small to resolve the convective processes that occur during emission, or B) the convective parametrisation used to distribute NO emissions in a way that produces a similar final LNO_x distribution to the work of Ott *et al.* (2010). If either case A or B is satisfied then the initial lightning NO_x emission profiles will be more consistent with the dynamics simulated in the underlying atmospheric model. However, since the common

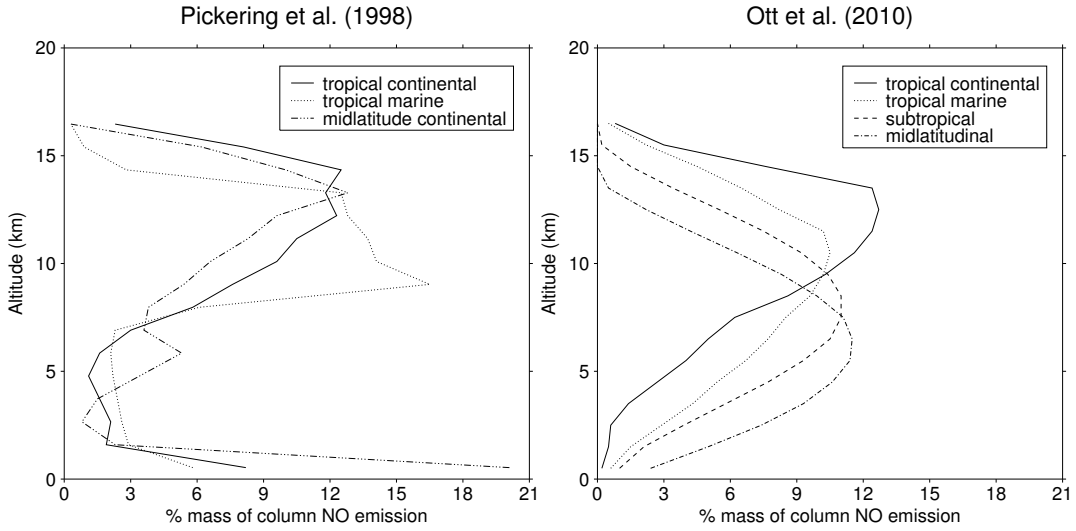

Figure 1.7: Prescribed vertical profiles, plotted from Pickering *et al.* (1998) and Ott *et al.* (2010), to be applied in different zonal bands to distribute column NO emission vertically in models. Note that the Pickering distribution has been scaled from a 16 km top to a 17 km top to correspond to the Ott distributions.

approach in CTMs/CCMs is to use prescribed vertical LNO_x profiles, this is the method chosen for use in this thesis. The most recent vertical profiles of Ott *et al.* (2010) will be used. The Ott *et al.* (2010) distributions assume an IC/CG ratio of 1.0. For consistency, and as already stated, the same ratio of unity is used in this thesis.

1.6 Past evaluation studies of lightning parametrisations

A selection of studies have included evaluation of different lightning parametrisations. These studies span from storm to regional to global scales.

The cloud-top height based lightning parametrisation (Price and Rind, 1992) has

been evaluated in more studies than any other parametrisation due to its wide usage in CTMs/CCMs. Meijer *et al.* (2001) and Allen and Pickering (2002) both found that the cloud-top height approach was less able to reproduce the observed lightning distributions than the parametrisations developed in those studies based on convective precipitation and on updraught mass flux, respectively. Allen and Pickering (2002) note that the fifth power dependence of the Price and Rind (1992) relationship is extremely sensitive to model biases in cloud-top height calculation. Using the Weather Research and Forecasting (WRF) model to reproduce two US storms, Barthe *et al.* (2010) found the Price and Rind (1992) parametrisation to be less reliable for a weaker storm and less robust in general because of its dependence on horizontal resolution. However, using a global CCM, Tost *et al.* (2007) found that the Price and Rind (1992) scheme was the most robust parametrisation, of those they tested, to the use of different convective schemes, although they noted the cloud-top height approach is only indirectly linked to the cloud electrification process.

Wong *et al.* (2013) examined in detail the use of the cloud-top height approach in a cloud-resolving model and found that some biases in simulated flash rate are associated with biases in simulated precipitation or convection. However, even once those biases were considered, Wong *et al.* (2013) concluded that the cloud-top height approach was not able to reproduce the observed frequency distribution of lightning flash rates. Flash rate frequency distributions are an under-researched metric of lightning compared to metrics based on averaging which, in particular, do not capture information regarding high-end extreme lightning flash rates.

Of the meteorological variables considered by Meijer *et al.* (2001), a lightning parametrisation based on a linear relationship with convective precipitation was found to best match lightning observations over Europe. The results of Meijer *et al.* (2001) are based upon meteorological variables provided by the European Centre for Medium-Range Forecasting (ECMWF) model, and compared to

ground-based lightning observations over Europe. Meijer *et al.* (2001) found that total cloud ice column was much less able to reproduce the observed lightning activity than their precipitation-based scheme. To my knowledge the precipitation-based lightning parametrisation of Meijer *et al.* (2001) has not been evaluated in any other studies.

A fitted polynomial relationship of updraught mass flux against lightning was determined to be a better lightning parametrisation that the cloud-top height approach, in a study by Allen and Pickering (2002). Allen and Pickering (2002) used convective fields from the Goddard Earth Observing System Data Assimilation System (GEOS DAS) and lightning observations over the US from the National Lightning Detection Network (NLDN) in a comparison study. Their analysis included comparison of the parametrisations to OTD global measurements of the spatial distribution of lightning flash rates, and ground-based measurements of the frequency distribution of lightning flash rates in 4 locations in the US. They found that fitted polynomial relationships of updraught mass flux performed better than their fitted polynomial relationships of convective precipitation, as well as the cloud-top height approach, in estimating the spatial and temporal distributions of lightning. The polynomial relationships of Allen and Pickering (2002) using updraught mass flux and convective precipitation have been evaluated in the studies by Tost *et al.* (2007) and Murray *et al.* (2012). Compared to other parametrisations, Tost *et al.* (2007) found that the updraught mass flux scheme of Allen and Pickering (2002), as well another updraught mass flux-based scheme (Grewe *et al.*, 2001), was sensitive to the choice of convective scheme. Tost *et al.* (2007) found that the precipitation-based scheme of Allen and Pickering (2002) was able to produce reasonable annual averages of lightning flash rate if the precipitation distribution was reproduced with the convective scheme. However, the temporal variability of lightning was poorly captured by the precipitation-based approach. Murray *et al.* (2012) evaluated the spatial

distribution of lightning produced by the cloud-top height scheme and the two Allen and Pickering (2002) schemes against the LIS/OTD lightning climatology. They found that while none of the parametrisations performed strongly, the Allen and Pickering (2002) schemes dramatically overestimated tropical marine lightning activity. The overestimation of lightning in the tropical Pacific by the polynomial relationships of Allen and Pickering (2002) seems to be the case across the majority of evaluations.

Barthe *et al.* (2010) used the Weather Research and Forecasting (WRF) model to reproduce two US storms, and compared the simulated lightning of six lightning parametrisations in the literature to observations. Barthe *et al.* (2010) had very mixed results concluding that the different parmetrisations each had faults but suggested that maximum updraught velocity would serve as a good proxy for the severe storm. Regarding ice-based parametrisations, Barthe *et al.* (2010) found that temporal development of storm flash rate was well produced, but not the magnitude.

In addition to evaluating lightning schemes against observations of flash rate, Meijer *et al.* (2001) compared the cloud-top height approach and linear convective precipitation approach, as well as two vertical LNO_x distributions, to aircraft chemistry observations over Europe. They found that all parametrisations underestimated the NO concentrations but attributed this to their coarse CTM resolution. In addition, Meijer *et al.* (2001) found that the Pickering *et al.* (1998) prescribed vertical NO distribution (with the convective precipitation flash rate parametrisation) resulted in a better match with regards to NO measurements taken during a set of aircraft campaigns, when compared to an alternative vertical distribution method. The alternative method placed CG emissions between the surface and the -15°C isotherm, and IC emissions between the -15°C isotherm and cloud top.

Allen and Pickering (2002) used a box model to study the impact on ozone production efficiency of differences in flash frequency distribution. They found that the cloud-top height approach, which has lower extremes and more mid-range flash rates, has a higher ozone production efficiency than when using frequency distributions based on observations of lightning.

Tost *et al.* (2007) looked at the average NO_x vertical emission profiles when a prescribed vertical LNO_x profile was applied between cloud base and cloud top. They found that, due to the differences in convective schemes, even with exactly the same lightning parametrisation there could be large differences in the vertical LNO_x profile. The updraught mass flux approaches were found to be more sensitive to varying the convective scheme than the cloud-top height or convective precipitation approaches.

The convective schemes of ECMWF model (Tiedtke, 1989) and UK Met Office Unified Model (UM) (Walters *et al.*, 2014) which are used in this thesis are based upon a mass flux approach which uses specific criteria to determine a single cloud type for each model grid cell. Cloud types are shallow, mid and deep convective. The criteria for cloud selection is based upon the stability and updraught velocity in the vertical column as found by computing the ascent of a surface air parcel. For deep convective clouds, both schemes determine updraught mass flux at the cloud base by using convective available potential energy (CAPE) closure based on Fritsch and Chappell (1980). This assumes that CAPE is removed over a defined timescale, which is nominally one hour for both the UM and ECMWF model. Updraught mass flux in the rest of the column uses the cloud base mass flux, and entrainment and detrainment rates. In chapter 2, the detrainment rate in the top part of the cloud from the ECMWF model is used. The ECMWF calculates this from the decrease in vertical velocity which arises due to negative buoyancy at the top of the cloud. Given the main focus of this thesis is the inclusion of cloud ice in a parameterisation, it is useful to have two similar convective schemes so

that differences in the behaviour of an ice-based lightning parameterisation can be more closely linked to differences in the representation of cloud ice in the two models. The cloud schemes of the ECMWF and UM are described in chapters 2 and 3, respectively. An indication of differences in the results that would arise with different convective schemes can be gained from studies such as Tost *et al.* (2007), which includes similar convective schemes to that of the ECMWF model and the UM.

Following a variety of evaluation methods, several lightning parametrisations have been proposed as performing reasonably well. Unfortunately, there is little agreement on the best parametrisation to use. In addition, the best parametrisation appears likely to depend on the convective parametrisation used by the underlying meteorology (Tost *et al.*, 2007). The cloud-top height approach does produce relatively good results across several of the evaluations. However, several papers note deficiencies with the approach, such a high sensitivity to biases in simulated cloud-top height due to the fifth power relationship, and only an indirect link with charging theory. Many CTMs and CCMs employ the cloud-top height approach, although based on the evaluations discussed here, the choice of lightning parametrisation remains an unresolved issue. This will be a key topic of research in this thesis.

1.7 Climate change and lightning

Since lightning is a meteorological phenomenon, it is inherently connected to the climate. It is possible that as the climate changes and the drivers of lightning generation change then the lightning activity will also change (Williams, 2005). Such responses to climate change are as relevant for the past as for the future. However, for this thesis the focus is on the response of lightning to future climate

change. An aim will also be to understand how changes to the LNO_x source influences key atmospheric constituents such as ozone.

On the whole, observations over large regions have not been taken for a long enough time period to comment on a long-term climate trend in lightning activity. Over the period 1995-2010, Cecil *et al.* (2014) reports that measurements of lightning by the LIS and OTD show no significant trend. However, this result is based on monthly mean values, whilst some current research looking at trends in the instantaneous measurements from LIS suggests there are negative trends in many parts of the tropics (Albrecht *et al.*, 2011). Furthermore, some studies of the trends in lightning have found significant regional trends across several decades in the number of thunderstorm days recorded by weather stations (Changnon and Changnon, 2001; Pinto *et al.*, 2013). Changnon and Changnon (2001) used data from US weather stations over the period 1896-1995 and Pinto *et al.* (2013) used data for three Brazilian cities over the period 1951-2009. Changnon and Changnon (2001) found that different parts of the US exhibited different trends in thunderstorm days over the period, with the west and south-central regions showing a significant positive trend and the eastern US showing a significant negative trend. Several US regions showed no significant trend. Pinto *et al.* (2013) found that two out of the three Brazilian cities showed significant positive trends in thunderstorms days. These findings suggest that there are some regional long-term trends in, and possibly a climate change affect on, thunderstorms but it is unclear if there is a long-term trend in global lightning activity.

Studies have also compared lightning observations over large regions to El Nino events (Williams, 2005; Satori *et al.*, 2009). The studies find that in general lightning activity increases during an El Nino event but that lightning can decrease in some regions such as the Pacific ocean. In addition, Doherty *et al.* (2006) reported a decrease in tropospheric column-average NO_x over Indonesia and South America during simulated El Nino events, due to suppressed convection, and

therefore lightning in these regions. Although the response of lightning to an El Nino event may not be the same as a response to climate change, the results above do at least provide a useful perspective regarding the lightning response to internal climate variability.

Through lack of sufficient observations, GCMs are the main source of estimates for the response of lightning and lightning NO_x emissions to climate change. A metric widely reported is the percentage change in global flashes or LNO_x, per degree change in global mean surface temperature. Schumann and Huntrieser (2007) reviews the reporting of these values in the literature. For 18 GCM studies between 1994 and 2006 there is a range in estimates from 4-60 $\% K^{-1}$ with a median of 15 $\% K^{-1}$. Additional studies since 2007 have a range of 5.5-16 $\% K^{-1}$ (Zeng *et al.*, 2008; Jiang and Liao, 2013; Banerjee *et al.*, 2014). This metric provides a useful means to compare the response of lightning across different models and parametrisations.

The majority of the above estimates are based on models using the cloud-top height approach. In contrast, a reduction in lightning in year 2030 is simulated by Jacobson and Streets (2009), who used an ice-based parametrisation. They find that decreasing ice content in convective clouds leads to decreased lightning. Such a parametrisation provides a closer link to the non-inductive charging theory than the cloud-top height approach. However, the temperature changes which the study considered are small and not necessarily relevant to the larger temperature changes expected to occur over the 21^{st} century. There remains a gap in understanding of the climate change impact on lightning, especially regarding the lightning parametrisation uncertainty. I will look to address this in Chapters 4 and 5.

1.8 Outline of research chapters

The main research chapters of this thesis are presented in the style of scientific journal articles. Where chapters have been published, a preamble will provide a link to the published paper and describe the relative contributions of myself and co-authors. Chapters 2 to 5 address the research aims of the thesis. Chapter 6 provides a summary and discussion of the main conclusions, along with limitations of the research and ideas for future research.

Chapter 2 - Using cloud ice flux to parametrise large-scale lightning.

Aim: To explore existing schemes, and develop a new process-based scheme, to parametrise lightning

Lightning data from the LIS satellite instrument are compared to convective and ice variables in the ERA-Interim reanalysis dataset of the European Centre for Medium-range Weather Forecasting for a single year. A relationship is developed for use in parametrising lightning based on the upward cloud ice flux. Temporal and spatial distributions of lightning simulated by this parametrisation are evaluated, along with other parametrisations in the literature, against five years of LIS data. The new process-based parametrisation based on upward ice flux (hereafter the ice flux approach) simulates more realistic spatial and temporal distributions of lightning than the existing parametrisations evaluated, most notably it is more realistic than the cloud-top height approach. And in particular, the ice flux approach simulates a more realistic zonal-average lightning distribution.

Chapter 3 - The impact of lightning on tropospheric ozone chemistry using a new global lightning parametrisation.

Aim: To use a new process-based lightning scheme to give insights regarding the role of lightning NO_x *in tropospheric chemistry*

The lightning parametrisation, developed in Chapter 2, is applied globally within the UK Chemistry and Aerosol model (UKCA). The ice flux and cloud-top height approaches of parametrising lightning are evaluated against the LIS/OTD climatology of lightning. The lightning distributions are used in the model to produce LNO_x emissions and simulate the impact upon tropospheric ozone chemistry. Ozone distributions arising from the two lightning schemes and from a simulation with no LNO_x emissions, are evaluated against satellite instrument and sonde measurements of ozone. Through a more realistic zonal distribution of lightning, the ice flux approach highlights the biases in upper tropospheric ozone resulting from overestimation of tropical lightning with the cloud-top height approach. The effect of the different lightning parametrisations on ozone chemistry are presented as well as an analysis of the impact of differences in the flash rate frequency distribution on ozone production. With the frequency distribution analysis it is found that, whilst higher flash rates lead to more ozone production, each flash has a lower ozone production efficiency than for lower flash rates.

Chapter 4 - Response of lightning NO_x **emissions and ozone production to climate change: Insights from the Atmospheric Chemistry and Climate Model Intercomparison Project**.

Aim: To use alternative lightning schemes to improve the understanding of the response of lightning to climate change, and the consequent impacts on tropospheric chemistry (a multi-model perspective)

Using time slice experiments of historical, present-day and future scenarios made by state-of-the-art CCMs in the Atmospheric Chemistry and Climate Model

Intercomparison Project (ACCMIP), two key aspects of LNO_x are explored. First, the response of lightning to climate change by CCMs with different interactive lightning parametrisations is presented. In this analysis, it is shown that different lightning parametrisations can simulate opposing responses to climate change, but in all cases the response is linear. Second, the ozone production efficiency of LNO_x is compared to other emission sources involved in ozone production. The LNO_x source is found to be much more efficient at producing ozone than surface NO_x sources, but that the ozone production efficiency from LNO_x varies greatly across different CCMs.

Chapter 5 - An uncertain future for lightning and the consequences for the atmospheric composition and radiative forcing.

Aim: To use alternative lightning schemes to improve the understanding of the response of lightning to climate change, and the consequent impacts on tropospheric chemistry (a process-based perspective)

Using the same CCM and two lightning parametrisations as in Chapter 3, a future climate scenario for the year 2100 is simulated. The response of lightning to climate change simulated by the ice flux approach is compared to that simulated by the cloud-top height approach. The responses to climate change simulated by the two schemes are opposing, as found for the different lightning schemes in Chapter 4 described above. The negative response of the ice flux scheme is due to reduced cloud ice and updraught mass fluxes in the tropical regions, whilst the positive response of the cloud-top height scheme is a result of a global deepening of clouds. The impact of the responses from each lightning scheme on tropospheric chemistry is analysed. As greenhouse gases, the changes in methane and tropospheric ozone have a radiative forcing effect. The radiative forcing effect resulting from LNO_x simulated by each of the two lightning parametrisations is determined. The radiative forcing results suggest that whilst the cloud-top height

based approach may simulate a small positive feedback, the ice flux approach simulates no such feedback.

Chapter 2

Using cloud ice flux to parametrise large-scale lightning

This chapter has been published in the open-access journal Atmospheric Chemistry and Physics (ACP), in collaboration with my PhD supervisors: Dr Ruth Doherty, Dr Oliver Wild, Dr Hugh Punphrey and Prof Alan Blyth. An additional co-author on the publication was Dr Heidi Huntreiser. The paper is available online from the ACP website (http://www.atmos-chem-phys.net/14/12665/2014/acp-14-12665-2014.html). I did the analysis and wrote the initial draft. My supervisors and other co-authors provided feedback before the manuscript was submitted for publication.

Finney, D. L., Doherty, R. M., Wild, O., Huntrieser, H., Pumphrey, H. C., and Blyth, A. M. (2014) Using cloud ice flux to parametrise large-scale lightning, Atmospheric Chemistry and Physics, **14**, 12665-12682, doi:10.5194/acp-14-12665-2014.

2.1 Introduction

Lightning is always occurring somewhere on Earth with an average of 46 flashes every second (Cecil *et al.*, 2014). Every flash has enormous quantities of energy and can extend over tens of km which allows for the dissociation of nitrogen (N_2) and oxygen (O_2) molecules in the air. The dissociation products combine to form reactive nitric oxide (NO) which quickly oxidises to NO_2, and an equilibrium between NO and NO_2 is reached, together they are known as NO_x, as discussed in Section 1.4. Air is predominantly detrained in the upper anvil levels of a thunderstorm thereby providing the principal natural source of these ozone precursors to the middle and upper troposphere (Grewe, 2007). In total, lightning is estimated to contribute approximately 10 % of the global NO_x source (Schumann and Huntrieser, 2007). Lightning has a large spatial variability as well as a seasonal cycle and interannual variability. As an important but highly variable source of NO_x driven by meteorological processes, both chemistry transport models and coupled chemistry–climate models require parametrisations of lightning (Section 1.5).

The first stage of a parametrisation is to estimate the large-scale distribution of flashes. Previous investigations have found several empirical relationships between lightning and convective variables including relationships based on cloud-top height (Price and Rind, 1992), updraught mass flux (Grewe *et al.*, 2001; Allen and Pickering, 2002) and convective precipitation (Meijer *et al.*, 2001; Allen and Pickering, 2002). The cloud-top height parametrisation is the most widely, almost universally, used but this is not considered ideal because it lacks a direct, physical link with the charging mechanism and because it has a fifth-power relationship for land which introduces large errors for any model bias in cloud-top height (Allen and Pickering, 2002; Tost *et al.*, 2007).

Satellite observations of lightning have enabled useful testing of the ability of

parametrisations to reproduce the large-scale distribution (e.g. Tost *et al.*, 2007). The Lightning Imaging Sensor (LIS) has good quality measurements of lightning for over a decade which allow model comparison over longer climatological periods. These most recent satellite observations lie between ±38° latitude. Bond *et al.* (2002) estimate that 76–85 % of all global lightning occurs within this region. Therefore, there is scope for using several years of observations to look at how well the parametrisations match the various statistical features of a lightning climatology. How the parametrisations differ with respect to their input variables, functional form and their strengths and weaknesses may guide development of new parametrisations.

Atmospheric reanalysis data (defined in Section 1.4) provide the closest representation of global meteorological conditions maintaining a spatially complete and coherent record. These type of data are used to drive chemistry transport and nudge global climate models towards real conditions. By using reanalysis data offline several parametrisations can be directly compared to the lightning observations.

As well as large-scale data enabling a top-down approach to evaluation and development, much work has been done with storm-scale models and field campaigns which offer insight for bottom-up development. Charge separation is necessary for the production of lightning in thunderstorms and occurs via the non-inductive charging mechanism (Reynolds *et al.*, 1957; Latham *et al.*, 2004)(Section 1.2). This postulates that light ice crystals in clouds that rise on convective updraughts collide with heavier, falling graupel and in doing so the two particle types become oppositely charged. The result is net accumulation of opposite charge in different parts of the thundercloud. This has been shown to be a realistic theory through a combination of laboratory, field measurement and satellite studies (Williams, 1989; Blyth *et al.*, 2001; Petersen *et al.*, 2005; Saunders, 2008; Deierling *et al.*, 2008; Liu *et al.*, 2012).

Global climate models are still at the early stages of representing large-scale distributions of ice in clouds. However, development is on-going with satellite and field measurements helping to form a picture of the current distributions of cloud ice (Waliser *et al.*, 2009; Stith *et al.*, 2014). The objective of this chapter is to test the usefulness of the current state of cloud ice modelling within a lightning parametrisation. It introduces a parametrisation that is more physically based and tests it against existing parametrisations.

The next two sections describe the data and existing parametrisations to be evaluated. Section 2.4 explains the development of a simple cloud-ice-based parametrisation. Section 2.5 evaluates the climatological performance of all the parametrisations. This is followed by a discussion and conclusions.

2.2 Data description

2.2.1 ECMWF ERA-Interim

The European Centre for Medium-Range Weather Forecasting (ECMWF) provides the ERA-Interim global atmospheric reanalysis data product (Dee *et al.*, 2011). ERA-Interim spans from 1989 to near present. The dynamical core is based on a T255 spectral grid which can be interpolated to a regular 0.75 ° lat–lon grid. In the vertical, a hybrid sigma-pressure grid is used with 60 levels up to 0.1 hPa. Some variables, such as updraught mass flux, are only archived as forecast data on 6 and 12 h steps initialised at 00:00 and 12:00 UT. While analyses exist for some other variables used here, such as temperature, only the forecast type is used to maintain consistency. There is also a distinction between accumulated (e.g. updraught mass flux) and instantaneous (e.g. temperature) variables. The accumulated variables have been divided by 6 h to obtain an average over the

period and are used in combination with the instantaneous variables at the end of the 6 h period - a necessary approximation given the output data available.

A selection of variables have been used as input to lightning parametrisations: surface pressure, temperature, cloud cover, specific cloud ice water content, convective precipitation, updraught mass flux and updraught detrainment rate. Processing of the raw data allowed the formation of 6-hourly data for cloud-top height, cold cloud depth, convective precipitation, updraught mass flux at 440 hPa and upward cloud ice flux at 440 hPa on a 0.75 ° regular grid. The use of each of these variables are explained in Sections 2.3 and 2.4.

Cloud-top height was taken as the highest level containing a non-zero updraught detrainment rate. This definition follows that used in the TM5 model which also uses ECMWF reanalysis data (P. Le Sager, 2012, personal communication). The cold cloud depth was calculated as the difference between cloud-top height and the interpolated height of the 0 °C isotherm. Updraught mass flux was interpolated to the 440 hPa level (typically about 6 km and −25 °C), as were cloud cover and specific cloud ice water content, which are used along with the updraught mass flux to calculate the upward cloud ice flux at 440 hPa as described in Section 2.4.

The cloud parametrisation in the ECMWF model version used for ERA-Interim is based on Tiedtke (1993) with moisture-related prognostic variables for humidity, cloud condensate and fractional cloud cover. Sources and sinks describe the major generation and destruction processes of cloud and precipitation including direct detrainment from parametrised convection. The phase of the cloud condensate is diagnosed according to a temperature-dependent function with all liquid phase for temperatures warmer than 0 °C, an increasing fraction of ice in the mixed-phase temperature region between 0 °C and −23 °C and all ice phase for temperatures colder than −23 °C. The parametrisation of convection is based on Tiedtke (1989) and detrains directly into the prognostic humidity, condensate and fractional

cloud cover variables following the same temperature-dependent phase function as above, and provides a direct link between the convection and stratiform cloud schemes.

State-of-the-art reanalysis data are the best input available over regions as large as the tropics/subtropics and for the range of input parametrisations needed to evaluate model performance. However, several known issues exist with the data that will affect the performance of parametrisations during the evaluation regardless of the correctness of their relationship with lightning. Broadly, it can be assumed that where observations are less dense there will be less accuracy, e.g. over Africa and the oceans.

Dee *et al.* (2011) provide an in-depth evaluation of ERA-Interim with respect to observations and improvements upon its predecessor, ERA-40. Several improvements, with reference to International Satellite Cloud Climatology Project (ISCCP) observations, have been made to the representation of clouds. Those relevant here are improved tropical cloud cover resulting from an improved hydrological cycle and the introduction of ice supersaturation which delays the formation of ice clouds (Tompkins *et al.*, 2007), and from improved deep convective triggering and a new boundary-layer scheme. There are few other studies directly evaluating the cloud properties as observations of clouds have their own large uncertainties. However, Schreier *et al.* (2014) and Ahlgrimm and Köhler (2010) have studied trade cumulus clouds represented in ERA-Interim. These are not directly related to deep convective clouds but at least can hint at some of the differences between the reanalysis and observations. A main finding was that the population of trade cumulus is over-estimated while the cloud fraction was under-estimated by ERA-Interim. Meanwhile, the cloud top was biased high by about 500 m.

Much more research has been done on the evaluation of precipitation. Dee *et al.* (2011) found that both the mean daily precipitation rate, compared to the Global

Precipitation Climatology Project (GPCP), and the mean total column water vapour, compared to microwave imager satellite retrievals, have improved from ERA-40 to ERA-Interim. There are still biases remaining over the tropical oceans, specifically around the western Pacific and Southeast Asia where the precipitation rate is up to $5\,\mathrm{mm\,day^{-1}}$ greater in some parts. The time series of precipitation rate over total land performs well whilst during the 2007–2011 period there is an over-estimation by approximately $0.4\,\mathrm{mm\,day^{-1}}$ over total ocean when compared to GPCP. Many independent studies have looked at precipitation compared to observations and other reanalysis sets (Kim *et al.*, 2013; Peña-Arancibia *et al.*, 2013; Pfeifroth *et al.*, 2013; Zhang *et al.*, 2013; Lin *et al.*, 2014). Generally, ERA-Interim was found to perform well. Most notably though was further confirmation of biases in Southeast Asia (Kim *et al.*, 2013), and the over-estimation of small and medium precipitation but under-estimation of high amounts compared to rain gauge data in the tropical Pacific (Pfeifroth *et al.*, 2013) and to the Tropical Rainfall Measuring Mission (TRMM) satellite in the tropics (Kim *et al.*, 2013).

While the errors in variables such as updraught mass flux remain unknown, it is assumed that ERA-Interim has remaining problems with the hydrological cycle over the western Pacific and Southeast Asia and that this is likely to affect all input variables. This will be considered when drawing conclusions from the evaluation.

2.2.2 Lightning Imaging Sensor

The LIS was a lightning detection instrument aboard the TRMM satellite (Boccippio *et al.*, 2002; Cecil *et al.*, 2014)(Section 1.3.1). Measurements were taken between 1998 and 2015 but the satellite received an orbit boost in 2001 which resulted in a larger field of view and slightly longer sampling duration. Lightning was detected by pulses of illumination in the 777.4 nm atomic oxygen multiplet above background levels. TRMM was in a low earth orbit, with coverage

between ±38° latitude and viewed each surface location for ∼90 s with more time spent viewing the edges of its latitudinal coverage. Over the course of 99 days, LIS sampled the full diurnal cycle twice for each location (Cecil *et al.*, 2014). Its spatial resolution was approximately 5 km. Detection efficiency ranged between 69 % at local time noon to 88 % at midnight (Cecil *et al.*, 2014). The Optical Transient Detector (OTD) was a similar instrument which is also obsolete but provided a broader latitudinal coverage of ±75° until 2000 (Christian *et al.*, 2003). OTD is not heavily used in this chapter but it contributes to the product used to determine the total global flash rate. As with all low-orbit satellites, the accuracy of OTD and LIS reduced within the South Atlantic anomaly (SAA) which reduces the robustness of the evaluation within this region. This point is elaborated upon in the discussion.

Several products have been produced by the NASA Marshall Space Flight Center lightning team using LIS data which are described fully in Cecil *et al.* (2014). The LIS–OTD low-resolution full climatology (LRFC) total flash count is used here to scale all lightning models to the same global annual total. The main product, used throughout this paper, is the LIS–OTD low-resolution monthly time series (LRMTS). The LRMTS provides one flash rate density per month on a 2.5° regular lat–lon grid for every month from May 1995 to present; post-2000 it contains data from the LIS instrument only.

It is useful to determine the number of years necessary to produce a lightning climatology. Using 10 years (2002–2011) of LRMTS data as the true climatology, different numbers of years are compared to determine their ability in representing that true 10 year climatology. Figure 2.1 shows some example plots from the approach with the 10 year average annual total spatial distribution with differences to the 5-year (2007–2011) and 2-year (2010–2011) sets, along with standard deviations for the three cases. It demonstrates that using 2-year averages would not be appropriate for evaluating this climatological period of lightning in

terms of the spatial distribution or the interannual variability, but that 5 years is representative.

For each set of years, significance tests were applied to each grid cell of average annual total spatial distribution as compared to the decade to determine which grid cell estimates diverged from the decadal climatology. An additional comparison was made using the spatial distribution of the standard deviation of annual totals to ensure there were no grid cells where the spread of annual totals was being over-estimated or under-estimated. It was found that a 5-year set was needed to satisfy these tests. Hence, the years 2007–2011 have been chosen to evaluate the lightning parametrisations in Section 2.5.

A lightning parametrisation based on upward ice flux is developed using the LRMTS product in Section 2.4. To reduce the bias that may occur by using the same data for development and evaluation, a year within 2002–2006 was chosen to develop the parametrisation which was most different from the 5-year evaluation set. The LRMTS average annual total spatial distribution was calculated for the 5-year climatology and each individual year. The sum of the absolute differences between the 5-year climatology and any given year was used as a metric for the difference. The equation for this metric is

$$d_{\text{year}} = \frac{1}{A} \sum_{i=\text{cells}} a_i |f_{i,\text{year}} - f_{i,5}|, \tag{2.1}$$

where d is the total area-averaged, absolute difference in flash density between the annual mean of any year in the range 2002–2006 and the climatological mean of the 5 years, 2007–2011. On the right of the equation, A is the total area, i loops over spatial grid cells, a is the area of a grid cell and f is the flash rate density. The difference, d_{year}, was greatest for 2002.

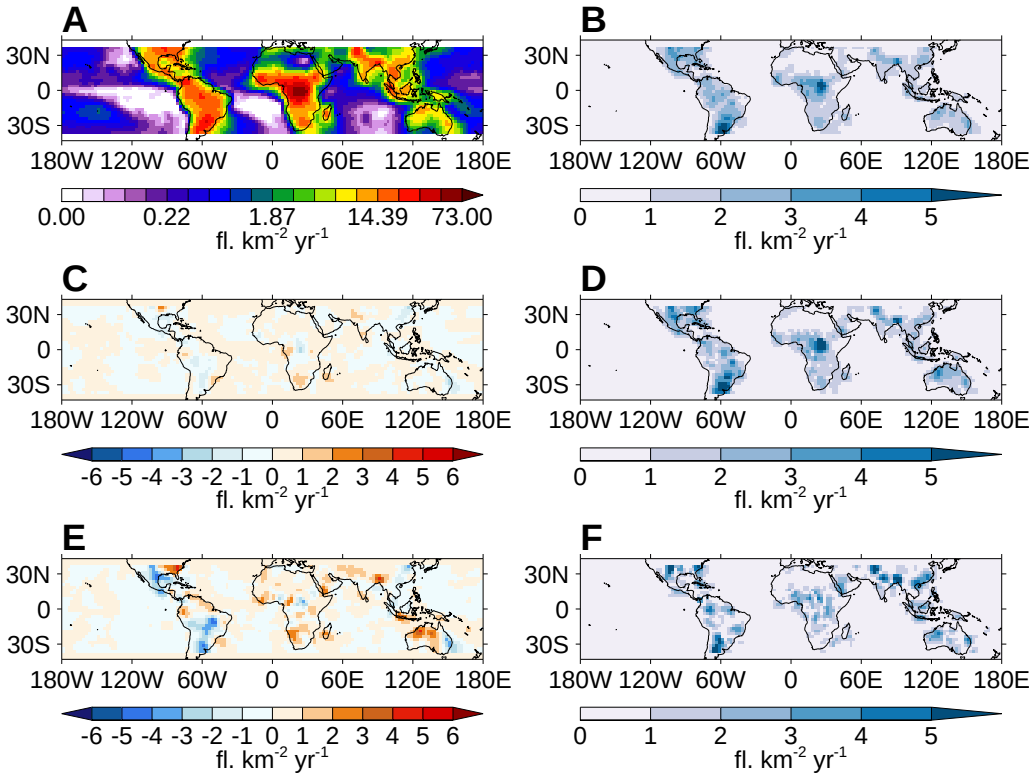

Figure 2.1: Average annual total LIS flash density spatial distributions of **(A)** the 10 year climatology (2002–2011) and differences between the **(C)** 10 year and 5 year (2007–2011) and **(E)** 10 year and 2 year (2010–2011) climatologies. **(B)**, **(D)** and **(F)** show the standard deviations of annual LIS totals for each of the 10 year, 5 year, and 2 year climatologies, respectively.

2.3 Existing parametrisations

Four existing parametrisations have been chosen for testing with ERA-Interim data. These chosen parametrisations include the commonly used cloud-top height scheme, along with three others which use different input variables and functional forms. Previous evaluation studies of these lightning parametrisations are described in Section 1.6.

Lightning flashes can be classified in different ways and in chemistry models they are typically separated into cloud-to-ground and intra-cloud types as these have different emissions. Some of the parametrisations have been developed to calculate total flashes and some to calculate cloud-to-ground flashes. The LIS satellite instrument measures total flashes, it does not discriminate between flash types and therefore, where necessary, parametrisation outputs for cloud-to-ground flashes are adjusted to represent total flashes by dividing by the proportion of total flashes that are cloud-to-ground, p. The ratio is determined by a fourth-order polynomial based on cold cloud depth as found by Price and Rind (1993):

$$p = \frac{1}{64.09 - 36.54D + 7.493D^2 - 0.648D^3 + 0.021D^4}, \tag{2.2}$$

where D is the depth of cloud above 0 °C. In addition, a minimum depth of 5.5 km is required for any flashes to occur (Price and Rind, 1993).

This approach is required to make like-for-like comparisons of parametrisations and is important for their use in estimating lightning emissions. However, it will introduce the error associated with determining cold cloud depth into parametrisations which include the use of Equation (2.2).

Some parametrisations include scaling equations to account for different model spatial resolutions. However, it is found here that none of these scalings produce

the correct magnitude for the total global flash rate as estimated by LIS. This problem has been raised in other studies. In particular, Tost *et al.* (2007) shows that scaling factors can vary by three orders of magnitude depending on the input from different convective schemes. Here, the same convective scheme is used throughout so variation between parametrisations is partly due to the use of different input variables and partly because the parametrisations were developed using different scales and regions. In this chapter, the global flash rate has been calculated from the LIS LRFC product to be $44\,\mathrm{fl.\,s^{-1}}$ (fl. is used throughout to abbreviate flashes). Only the average global annual total of the 5-year climatology for each parametrisation has been scaled. Spatial, seasonal and interannual distributions are produced using the parametrisations. On this basis, the additional global annual total scaling factors are 0.05, 1.39, 0.32 and 0.70 for the cloud-top height, updraught mass flux, convective precipitation (polynomial) and convective precipitation (linear) parametrisations of Section 2.3.1–2.3.4, respectively, and 1.09 for the new cloud ice flux scheme of Section 2.4. These additional scaling factors are smaller, and in the case of the cloud-top height parametrisation much smaller, than previously stated scalings (Tost *et al.*, 2007; Murray *et al.*, 2012). Much of this is expected to be related to a greater spatial resolution than those used in Tost *et al.* (2007) and Murray *et al.* (2012), and the 6-hour temporal resolution that this chapter is based upon. The increase of 9 % needed for the newly developed parametrisation is due to the combination of the use of different years for forming and evaluating the parametrisation, and the fitting of a parametrisation over anything less than the full globe is likely to mean that it does not predict exactly the same LIS–OTD global magnitude. Lightning scalings need to be more frequently discussed in future studies so that a clear picture of their dependencies can emerge.

In the title to each subsection a label is shown which is used to refer to the

parametrisation throughout the paper. For example the following cloud-top height-based parametrisation will be referred to as CTH.

2.3.1 Cloud-top height (CTH)

A commonly used proxy for lightning flash density is cloud-top height as proposed by Price and Rind (1992). Price and Rind built on theories developed by Vonnegut (1963) and Williams (1985) using storm measurements and satellite data to form the following parametrisation:

$$F_{\mathrm{l}} = 3.44 \times 10^{-5} H^{4.9} \tag{2.3}$$

$$F_{\mathrm{o}} = 6.2 \times 10^{-4} H^{1.73}, \tag{2.4}$$

where F is the total flash frequency (fl. min^{-1}), H is the cloud-top height (km) and subscripts l and o are for land and ocean, respectively. The separation between land and ocean is used to incorporate the difference in updraught velocity over the two surface types. In cases of a cloud depth less than 5 km the flash value was set to zero. The use of 5 km is based on the range of data used to develop the relationship in Price and Rind (1992). Note that Price and Rind (1994) developed an equation to translate the above equations to varying model resolutions. The equation used to calculate the scaling factor is

$$C = 0.97241 e^{0.048203R}, \tag{2.5}$$

where R is the product of longitude and latitude resolution (degrees^2) and C is a multiplication factor applied to Equations (2.3) and (2.4). In this chapter the scaling factor is applied to the initial flash estimates on the regular 0.75 ° grid. The scaling factor used is 0.9992. While this scaling has been included for consistency with the parametrisation, it is clear that at resolutions used in this

chapter and higher resolutions the scaling has very little impact. As discussed above, an additional scaling factor of 0.05 was applied to match the LIS global total flash rate.

2.3.2 Updraught mass flux (MFLUX)

A parametrisation based on updraught mass flux at $\sim 440\,\mathrm{hPa}$ was obtained by Allen and Pickering (2002). The choice of 440 hPa is based upon definitions of deep convective clouds in the International Satellite Cloud Climatology Project (ISCCP) (Rossow *et al.*, 1996). In this parametrisation no distinction is made between land and ocean locations. The equation is

$$F = \frac{\Delta x \Delta y}{A}(a + bM + cM^2 + dM^3 + eM^4), \tag{2.6}$$

where F is the flash frequency of cloud-to-ground flashes (fl. min^{-1}), M is the updraught mass flux at 440 hPa ($\mathrm{kg\,m^{-2}\,min^{-1}}$), $\Delta x\,\Delta y$ is the area of a grid cell and A is the area of a $2.0\,^\circ \times 2.5\,^\circ$ box centred at $30\,^\circ$ N. The polynomial coefficients a–e have the respective values of -2.34×10^{-2}, 3.08×10^{-1}, -7.19×10^{-1}, 5.23×10^{-1} and -3.71×10^{-2}.

Equation (2.6) only estimates cloud-to-ground flashes and is therefore divided by p in Equation (2.2). Following the condition on Equation (2.2), cases where the depth is less than 5.5 km are set to zero. The use of areas in this equation is again an approach to account for varying horizontal resolutions. As with the cloud-top height parametrisation, the scaling grid-box area is based on that of a regular $0.75\,^\circ$ grid. Limitations exist on the values of mass flux such that $0 < M < 9.6\,\mathrm{kg\,m^{-2}\,min^{-1}}$; all values outside this range are set to their nearest acceptable value in the range.

2.3.3 Convective precipitation (polynomial) (CPPOLY)

A parametrization based on convective precipitation is also presented by Allen and Pickering (2002). There are separate polynomial expansions for land and ocean,

$$F_i = \frac{\Delta x \Delta y}{A}(a_i + b_i P + c_i P^2 + d_i P^3 + e_i P^4), \tag{2.7}$$

where F is the flash frequency of cloud-to-ground flashes ($\mathrm{fl.\,min^{-1}}$), P_i is the daily grid cell convective precipitation ($\mathrm{mm\,day^{-1}}$) during the time step for grid cell type i: $i = \mathrm{l}$ for land and $i = \mathrm{o}$ for ocean. The polynomial coefficients a_l–e_l have the respective values of 3.75×10^{-2}, -4.76×10^{-2}, 5.41×10^{-3}, 3.21×10^{-4} and -2.93×10^{-6}. The polynomial coefficients a_o–e_o have the respective values of 5.23×10^{-2}, -4.80×10^{-2}, 5.45×10^{-3}, 3.68×10^{-5} and -2.42×10^{-7}.

Equation (2.7) only estimates cloud-to-ground flashes and is therefore divided by p in Equation (2.2). Following the condition on Equation (2.2), cases where the depth is less than 5.5 km are set to zero. The use of area is the same as for Equation (2.6). Limitations exist on the values of convective precipitation such that $7 < P < 90\,\mathrm{mm\,day^{-1}}$; all values outside this range are set to their nearest acceptable value in the range.

2.3.4 Convective precipitation (linear) (CPLIN)

An alternative parametrisation based on convective precipitation which uses a linear relationship is proposed by Meijer *et al.* (2001):

$$\overline{F} = 14\,700\mathrm{cp} + 1.7, \tag{2.8}$$

where $\overline{F}$ is the mean number of flashes and cp is the convective precipitation (m). Under this scheme ocean flashes are 10 times less than calculated by Equation (2.8) based on findings that convection over oceans is 10 times less efficient at generating lightning (Levy II *et al.*, 1996; Boersma *et al.*, 2005). Equation (2.8) only estimates cloud-to-ground flashes and is therefore divided by p in Equation (2.2).

2.4 A new ice-flux-based parametrisation (ICEFLUX)

The non-inductive charging mechanism is widely accepted as the primary means for charge separation and therefore lightning generation (Barthe and Pinty, 2007; Saunders, 2008). However, only indirectly related convective characteristics have so far been introduced into large-scale lightning parametrisations. Improved representation of cloud ice in models now allows the implementation of another aspect of the theory, the upward flux of ice crystals. Deierling *et al.* (2008) have shown that the upward ice flux displays a strong linear correlation with lightning flashes in 11 observed US storms.

The direct implementation of the fitted equation in Deierling *et al.* (2008) for non-precipitating ice (i.e. upward ice crystal) mass flux above $-5\,^{\circ}\mathrm{C}$ ($\mathrm{kg\,s^{-1}}$) was explored but it was found that anomalously high flash densities would be estimated along mid-latitude storm tracks. The bias not only could be due to underlying meteorology but also may be attributable to the form of the ice flux variable. In this chapter, the cloud fraction in the grid cell is used to propose an alternative measure of ice flux in storms which is related to the intensity of the flux ($\mathrm{kg\,m^{-2}\,s^{-1}}$) as opposed to the mass of ice alone.

There have been past comparisons of the ECMWF ice water content product to satellite measurements of cloud ice content (Li *et al.*, 2007; Waliser *et al.*, 2009; Wu *et al.*, 2009; Delanoë *et al.*, 2011). They show that while the ice content may be under-estimated, there is at least good spatial agreement between ECMWF and the satellite measurements. The ERA-Interim specific cloud ice water content product is an estimate of the non-precipitating ice (i.e. suspended ice crystals) in the grid cell. ERA-Interim also contains updraught mass flux and fractional cloud cover.

As with the parametrisations of Allen and Pickering (2002) and as defined by the International Satellite Cloud Climatology Project (Rossow *et al.*, 1996), the 440 hPa level is used as a pressure level representative of fluxes in deep convective clouds. An estimate for upward cloud ice flux at 440 hPa, ϕ_{ice} ($\text{kg}_{\text{ice}}\,\text{m}^{-2}_{\text{cloud}}\,\text{s}^{-1}$), for each 6-hourly time step has been calculated using the following equation:

$$\phi_{\text{ice}} = \frac{q \times \Phi_{\text{mass}}}{c}, \tag{2.9}$$

where q is specific cloud ice water content at 440 hPa ($\text{kg}_{\text{ice}}\,\text{kg}^{-1}_{\text{air}}$), Φ_{mass} is the updraught mass flux at 440 hPa ($\text{kg}_{\text{air}}\,\text{m}^{-2}_{\text{cell}}\,\text{s}^{-1}$) and c is the fractional cloud cover at 440 hPa ($\text{m}^2_{\text{cloud}}\,\text{m}^{-2}_{\text{cell}}$). Upward ice flux was set to zero for instances where $c < 0.01\,\text{m}^2_{\text{cloud}}\text{m}^{-2}_{\text{cell}}$. The relationship between this newly formed variable and lightning is explored below.

2.4.1 The upward ice flux–lightning relationship

To develop a relationship between lightning and upward ice flux, the ice flux produced using Equation (2.9) is compared to the lightning flash density of the LRMTS product. As described in Section 2.2.2, the year 2002 has been chosen as the training year as it is most different in terms of the spatial distribution to

the lightning climatology of years used in later sections. To compare to LRMTS, upward ice flux values between ±38° latitude were averaged to monthly values and interpolated to the LIS grid. A scatter plot of all monthly cell values is shown in Figure 2.2A and B for land and ocean regimes, respectively.

Lower levels of lightning over ocean have been attributed to weaker updraught strengths within ocean storms (Xu and Zipser, 2012). Many parametrisations are unable to predict these lower oceanic levels of lightning. Likewise, it is necessary to separate ocean and land regimes in the ICEFLUX parametrisation since ocean flash densities for a given upward ice flux were $\sim \frac{1}{7}$ of the land flash densities, as can be seen in Figure 2.2. This difference between land and ocean regimes is not quite as large but is of the same order of magnitude as the differences in existing parametrisations. The equations of the best fit lines in Figure 2.2A and B are

$$f_{\mathrm{l}} = 6.58 \times 10^{-7} \phi_{\mathrm{ice}} \tag{2.10}$$

$$f_{\mathrm{o}} = 9.08 \times 10^{-8} \phi_{\mathrm{ice}}, \tag{2.11}$$

where f_{l} and f_{o} are the flash density ($\mathrm{fl.\,m^{-2}_{cell}\,s^{-1}}$) of land and ocean, respectively.

The best fit equations use only one parameter, the slope of the regression. Other fits were tested including a two-parameter linear fit, polynomial fits and power fits. The single- and two-parameter linear fits produced the best results. The intercepts from the two-parameter linear fit for both land and ocean were small and positive. A positive intercept within the modelling environment results in erroneous flashes in time steps which contain no upward ice flux. Since the intercepts are small, there is little change to the fit if only a single-parameter fit is used. Furthermore, an intercept at the origin remains consistent with the non-inductive charging mechanism as charging would not be expected in cases of zero upward ice flux. These are the justifications for the single-parameter linear functional form.

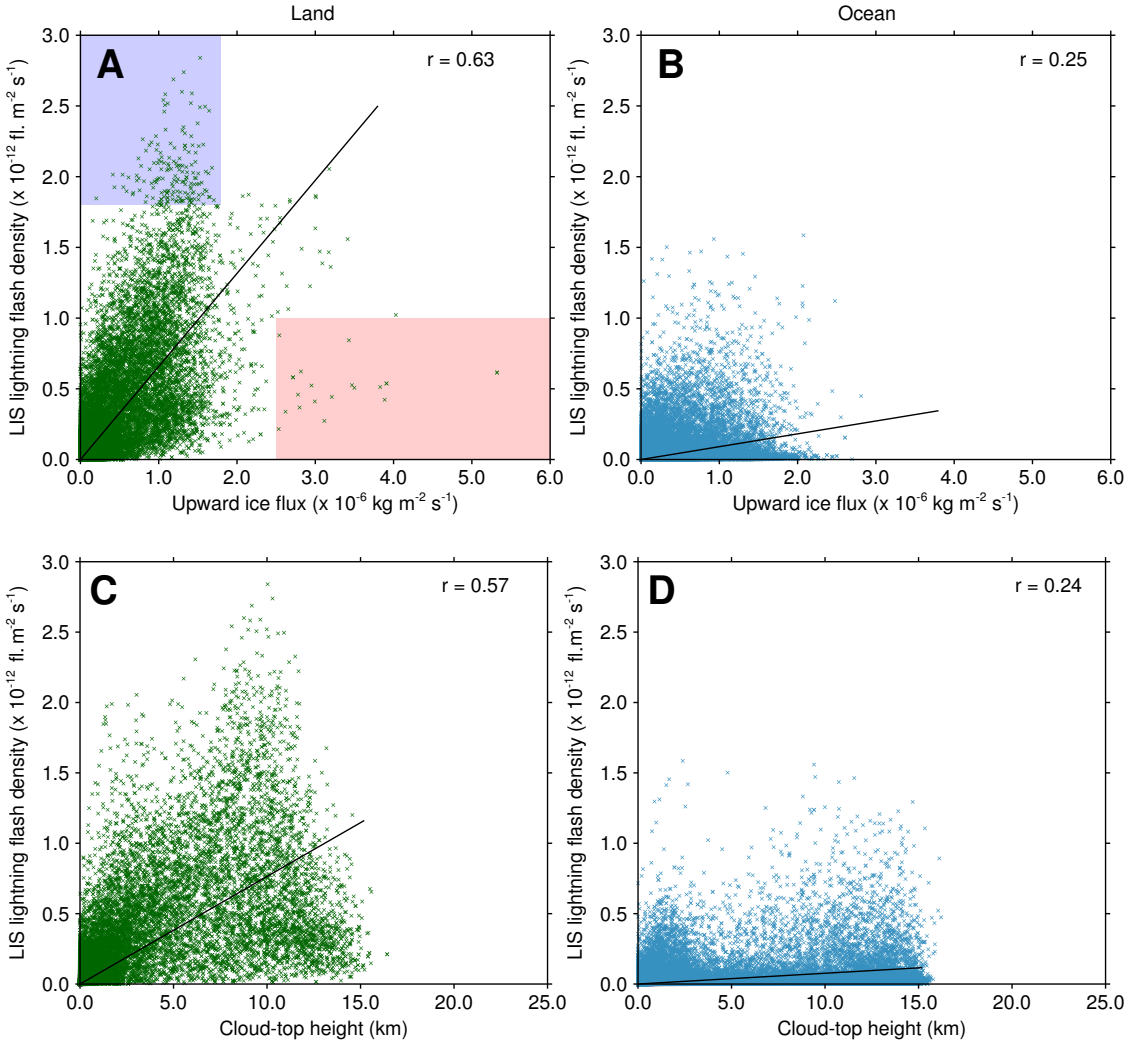

Figure 2.2: Scatter plots of upward ice flux at 440 hPa formed from ERA-Interim reanalysis against LIS flash density. Shown in **(A)** are land grid cells and **(B)** are ocean grid cells. Also shown is the cloud-top height formed from ERA-Interim reanalysis against LIS flash density over **(C)** land and **(D)** ocean. Each point represents the monthly average of each variable for a grid cell in the range $\pm 38^{\circ}$ latitude. The scatter points highlighted in **(A)** are used in Figure 2.3 for studying under-estimation (light blue) and over-estimation (light red) of this regression. All scatter points, even within the highlighted regions, were used to create the linear regression.

2.4.2 Application of the ICEFLUX relationship

Clearly there are shortcomings of the upward ice flux relationship when applied over such a large region. The correlation over the ocean is poor, $r = 0.25$, but this was also found when comparing cloud-top height against flash density, shown in Figure 2.2D. The land correlation is stronger at $r = 0.63$ but there are persistent deviations from the best fit. ERA-Interim reanalysis data, while being the best spatially complete representation of reality, are not equivalent to observations. Where observations are sparse, as over Africa and the oceans, there could be large errors. It does, however, offer a bridge between observation and modelling studies, providing the opportunity to compare model behaviour to measurements of lightning. While the correlation is only 0.06 greater than the cloud-top height variable, the use of upward ice flux is also a step towards a more physically based lightning parametrisation. This is also a step towards the possible future inclusion of a downward graupel flux, the other component of ice collisions and charging theory (Section 1.2), offering potential improvements in lightning estimation.

The regions and months for which continental lightning would have a large under-estimation (points with $f > 1.8 \times 10^{-12}\,\mathrm{fl.\,m^{-2}_{cell}\,s^{-1}}$, $\phi < 1.8 \times 10^{-6}\,\mathrm{kg_{ice}\,m^{-2}_{cloud}\,s^{-1}}$) or over-estimation ($f < 1.0 \times 10^{-12}\,\mathrm{fl.\,m^{-2}_{cell}\,s^{-1}}$, $\phi > 2.5 \times 10^{-6}\,\mathrm{kg_{ice}\,m^{-2}_{cloud}\,s^{-1}}$) are shown in Figure 2.3. These regions are highlighted in Figure 2.2 as light blue and red, respectively. There are large portions of Central Africa and northwest India where flashes will be under-estimated, a problem found in other studies (Tost *et al.*, 2007). To explain flash density differences between continental regions, Williams and Sátori (2004) explore a novel concept by describing meteorology in the Amazon as more oceanic in nature than that in Africa. This may suggest that fits of continental lightning are an average of different convective regimes with Central Africa representing the continental extreme thereby explaining its under-estimation in the continental fit.

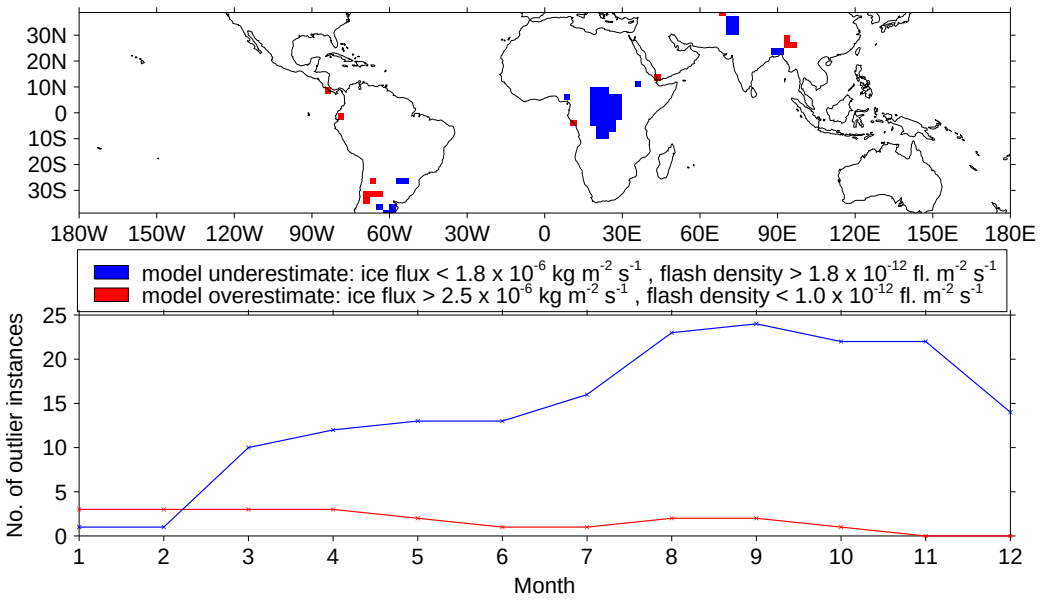

Figure 2.3: Continental regions that would be under- or over-estimated with the proposed ice flux parametrisation. Under-estimation in blue and over-estimation in red. Any coloured cell in the figure contains at least one month of large under- or over-estimation. Shown at the bottom is the number of cells of under- or over-estimation in each month. Under- and over-estimation are defined as scatter points in Figure 2.2 in the axis ranges of y axis $> 1.8 \times 10^{-12}$ fl. $\mathrm{m}_{\mathrm{cell}}^{-2}\,\mathrm{s}^{-1}$, x axis $< 1.0 \times 10^{-6}\,\mathrm{kg}_{\mathrm{ice}}\,\mathrm{m}_{\mathrm{cloud}}^{-2}\,\mathrm{s}^{-1}$ and y axis $< 1.8 \times 10^{-12}$ fl. $\mathrm{m}_{\mathrm{cell}}^{-2}\,\mathrm{s}^{-1}$, x axis $> 2.5 \times 10^{-6}\,\mathrm{kg}_{\mathrm{ice}}\,\mathrm{m}_{\mathrm{cloud}}^{-2}\,\mathrm{s}^{-1}$, respectively. The scatter points used to produce this plot are highlighted as the light-coloured regions in Figure 2.2.

In addition to the full-region scatter plot in Figure 2.2, relationships have been found for each grid cell individually using the twelve monthly data points. This uses the same data points but splits them so that each grid cell can be studied separately. Gradients and significance for the under-estimated portion of Central Africa are shown in Figure 2.4. Only 3 grid cells out of 32 corresponding to the Central African blue region in Figure 2.3 do not have significant correlation between flash density and upward ice flux. As demonstrated in Figure 2.4, the reason for under-estimation of the overall fit in Central Africa is not because a linear model does not apply but because the gradient is steeper, and the relationship between upward cloud ice and lightning is stronger. Gradients are up to three times greater than the full-region relationship in Equation (2.10). This could be accounted for using regional gradient lookup tables but the focus of this chapter is to explore a process-based parametrisation that is globally applicable. A lookup table would not allow consistent study of time periods with meteorology that is substantially different than present-day conditions.

Figure 2.3 shows adjacent grid cells with over-estimation and under-estimation in northeast India which suggest a lightning peak in that area that is misplaced to the east. There is some over-estimation near the southern Andes and under-estimation in Argentina and southern Brazil. This is a region where LIS has lower accuracy due to the SAA which makes it difficult to draw significant conclusions about the region (Section 1.3.1). Figure 2.3 also shows which months contain model over- and under-estimation of flash density. The under-estimation occurs throughout the year but with the least in January and February and the highest levels between August and November. Over-estimation of lightning occurs over much fewer regions and decreases gradually through the year.

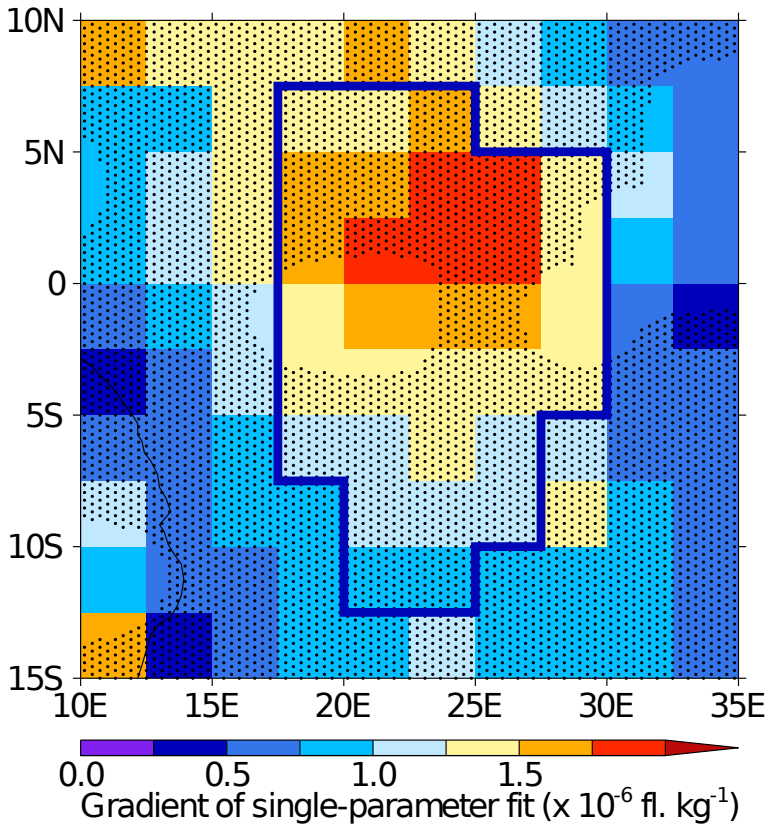

Figure 2.4: The gradients from single-parameter fitting of individual grid cells in Central Africa. The stippling shows grid cells with correlations significant at the 95 % level. Grid cell fits are made using the 12 monthly points for the cell in the year 2002. The solid blue line outlines the model under-estimated cells from the blue region in Figure 2.4.

2.4.3 Robustness on the 6-hourly timescale

Due to the temporal resolution of LIS data products it has been most appropriate to develop the ICEFLUX parametrisation using monthly data. However, in chemistry transport and chemistry–climate models the temporal resolution is of the order of an hour. To check that the parametrisation behaves reasonably when applied at these temporal scales, 6-hourly ECMWF data are used. A histogram of 6-hourly flash densities in the year 2011 using the five parametrisations is shown in Figure 2.5. All the tested parametrisations had approximately 95 % of instances less than $0.075\,\mathrm{fl.\,km^{-2}\,6\,h^{-1}}$.

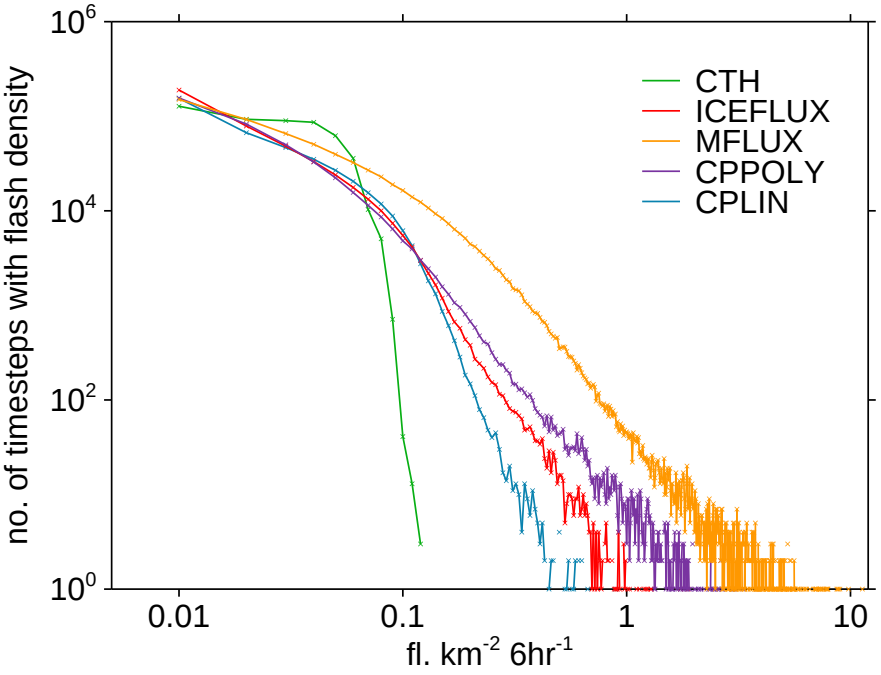

Figure 2.5: Histograms of 6-hourly flash density in the year 2011 for each parametrisation. Bin size is $0.02\,\mathrm{fl.\,km^{-2}\,6\,h^{-1}}$. The total number of time steps represented by each curve is the same. Grid cells from the full global region are used ($\pm 90^\circ$ latitude).

Wong *et al.* (2013) used hourly values from Earth Networks Total Lightning Network observations and shows that the CTH parametrisation produces fewer low and high flash frequencies compared to the observations. In another study for the US by Allen and Pickering (2002), National Lightning Detection Network and Long Range Flash Network observations at four locations for June 1997 were used to compare CTH, MFLUX and CPPOLY estimates of lightning. They found that CTH did not pick out the variability in flash rates as the model did not accurately represent the variability in cloud-top height. MFLUX and CPPOLY generally produced much more realistic distributions than CTH but at one location (Carlsbad, New Mexico) the instances of high flash rates are greatly under-estimated. This was attributed to the inability of the model to represent the North American monsoon.

Problems with the CTH frequency distribution are possibly a result of modelled convection or representation of cloud-top height within models, opposed to a failure of the relationship of the cloud-top height to lightning. A smaller-scale study measuring frequency distributions of cloud-top height and lightning would be required for confirmation. Given that this is a further study to find discrepancies in the lightning frequency distribution of the cloud-top height parametrisation, it may be important to determine how this affects the chemistry associated with lightning emissions.

In Figure 2.5 ICEFLUX is qualitatively more similar to MFLUX and CPPOLY than CTH but gives fewer high flash densities. Given that it lies between existing parametrisations and has a similar distribution, ICEFLUX is considered appropriate to apply at 6-hourly timescales.

2.5 Evaluation of the large-scale lightning parametrisations

The years 2007–2011 have been chosen to evaluate the performance of five different lightning parametrisations against LIS observations. As explained in Section 2.2.2, these five years provide a good estimate of the lightning climatology within the tropics and subtropics. There is a small ($+1.0 \times 10^{-5}\,\mathrm{fl.\,km^{-2}\,day^{-1}}$), significant ($p = 0.02$) trend in the deseasonalised, monthly climatological global annual total LIS flashes over the 5 years. The trend is at least an order of magnitude smaller than the statistics used here so the findings are considered to represent lightning behaviour independent of climate change. However, that is not to say that the small trend found over this short time period describes any long-term trends in lightning activity.

The parametrisations have been applied to the 6-hourly, 0.75 ° resolution ERA-Interim data to estimate flash density. For comparison to LIS measurements the parametrisation flash density is then averaged to monthly values, re-gridded to the 2.5 ° LIS grid, scaled to the same global total and the LIS viewing region of ±38° latitude selected.

The climatological average annual total flash density for the observations and parametrisations is shown in Figure 2.6. These results show that all parametrisations under-estimate flash density over Central Africa compared to LIS satellite measurements, suggesting that either an important component of lightning generation is missing from all parametrisations or the underlying meteorology data are biasing the results of parametrisations. In addition, the ocean flash density distribution of all parametrisations is focused heavily along the Inter-Tropical Convergence Zone, whereas LIS measurements do not show such a focus. Given that the ICEFLUX scheme has been developed here using separate ocean and

land equations, and scaled to the global total, one might expect the ocean and land total flashes to be the same as in the observations. However, since the fitted relationships (Figures 2.2A and B) are not perfect it can be expected that the land-ocean ratio in observations will not be perfectly captured. Indeed, it appears the ICEFLUX is broadly overestimating oceanic lightning flash rate in this region. This is in contrast to the CTH scheme which greatly underestimates ocean lightning activity.

The zonal and meridional average distributions are shown in Figure 2.7 to demonstrate that there are significant changes in the zonal distribution and ratios of lightning in the tropical chimneys. ICEFLUX has greatly improved on the ratio of tropical to subtropical lightning compared to the parametrisations, as can be seen in the zonal mean plot. The meridional mean plot highlights the under-estimation in Africa (0–30° E) and the over-estimation over the Americas (60–90° W) and Asia (90–120° E) of all parametrisations. ICEFLUX has made definite improvements within the latter two regions. Table 2.1 shows the spatial correlations and errors of average annual total between LIS measurements and each of the five parametrisations. By far the best spatial correlation with the LIS measurements over this period is with ICEFLUX, $r = 0.77$. The ICEFLUX parametrisation also shows the lowest RMSE of 4.65 which is almost half of the RMSE of CTH at 8.61.

CTH shows very large flash densities over northern South America and Southeast Asia while having low flash densities in most subtropical locations. ICEFLUX is spread much more evenly zonally and meridionally (Figure 2.7). MFLUX has a very different distribution to the other schemes. It shows high flash densities in southern South America and lower values elsewhere. Out of all the parametrisations it best estimates the activity in the southern US. This is to be expected as the parametrisation was developed using US data. As the only parametrisation not to distinguish between ocean and land it is unsurprising to

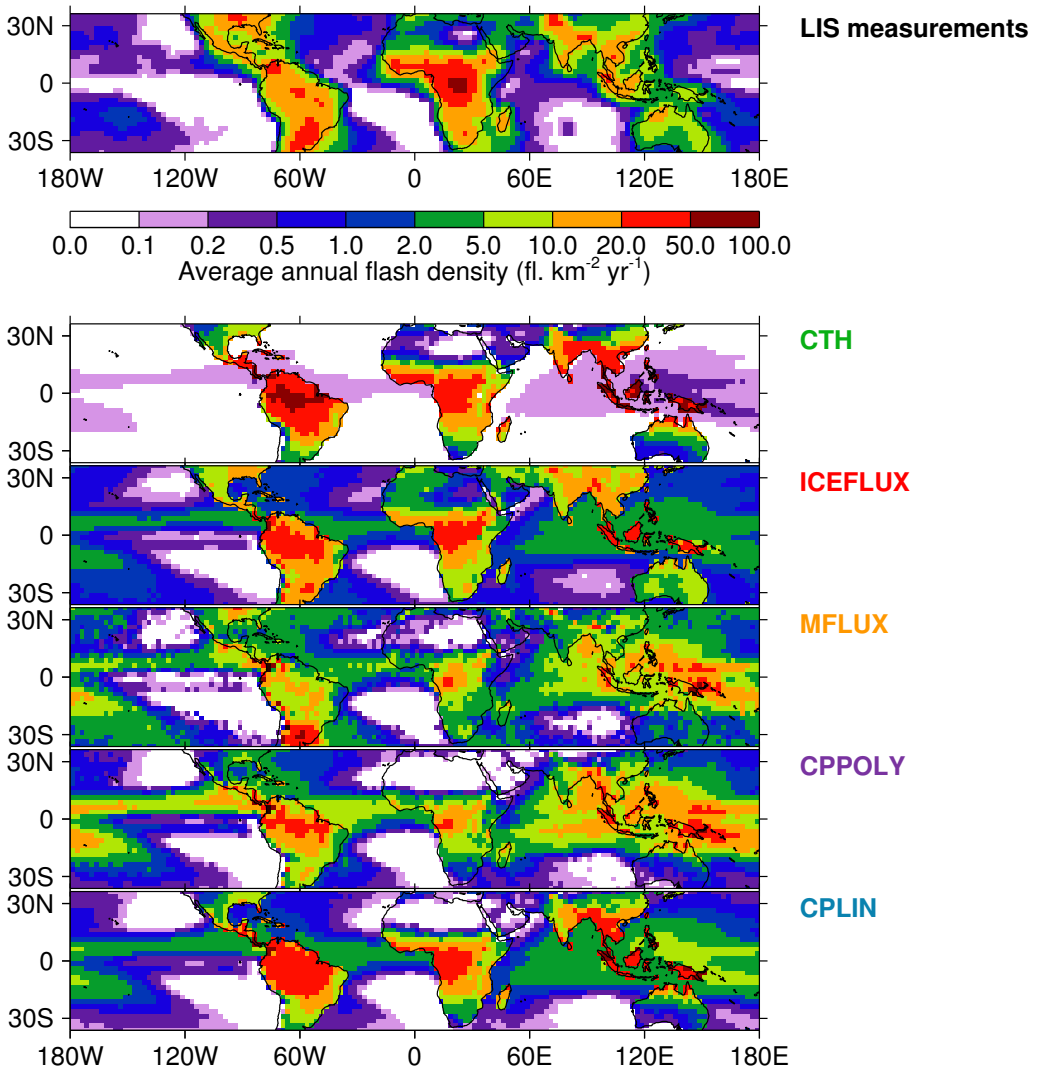

Figure 2.6: Five-year climatological annual total flash density (2007–2011). Results are shown for the LIS measurements and the five parametrisations.

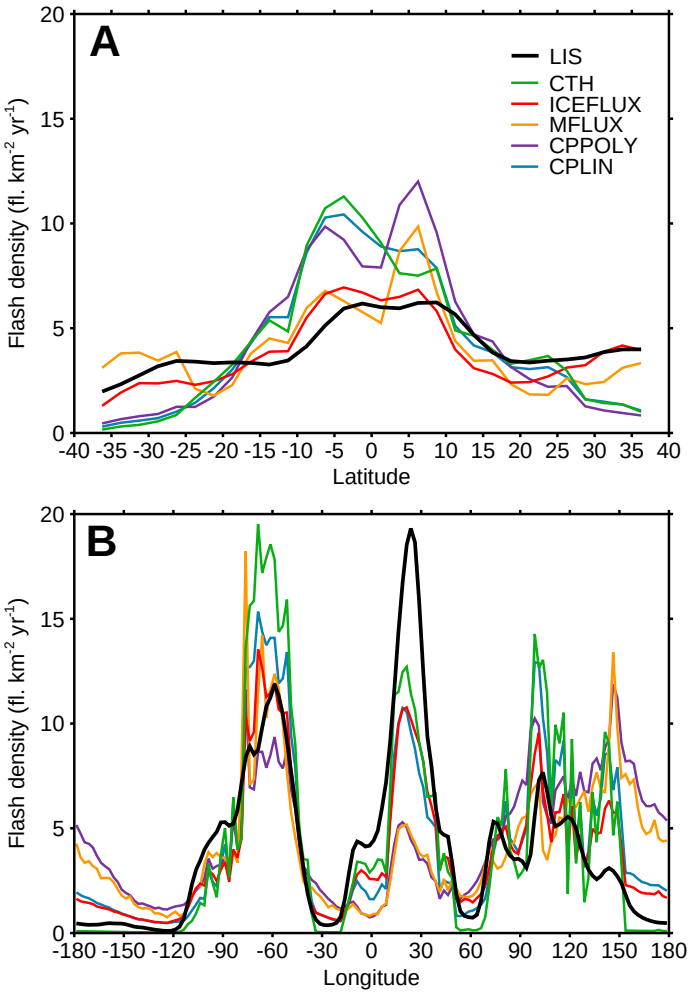

Figure 2.7: Five-year climatological **(A)** zonal and **(B)** meridional average flash density distribution (2007–2011). The meridional average is only taken within the LIS viewing region of $\pm 38^{\circ}$ latitude. Results are shown for the LIS measurements and the five parametrisations.

Table 2.1: Statistics of annual total spatial distribution, peak timing and interseasonal and interannual spatial distributions. For the spatial distributions, the correlation (r) and root mean square error (RMSE) are given.

Parametrisation	Annual total		Annual peak month		Seasonal variation		Interannual variation	
	r	RMSE ($\mathrm{fl.\,km^{-2}\,yr^{-1}}$)	Mean bias (month)	Mean absolute bias (month)	r	RMSE ($\mathrm{fl.\,km^{-2}\,day^{-1}}$)	r	RMSE ($\mathrm{fl.\,km^{-2}\,day^{-1}}$)
CTH	0.62	9.10	0.09	1.63	0.70	0.03	0.38	0.56
ICEFLUX	0.77	4.53	0.24	1.62	0.78	0.02	0.47	0.41
MFLUX	0.36	8.46	0.18	1.74	0.32	0.05	0.20	1.30
CPPOLY	0.37	7.74	0.14	1.71	0.38	0.04	0.09	0.95
CPLIN	0.62	7.13	0.13	1.65	0.69	0.03	0.34	0.52

see the over-estimation in the ocean. CPPOLY also shows very high ocean flash densities. CPLIN is qualitatively similar to CTH but with a smaller land–ocean contrast.

CTH has a reasonable correlation with the LIS observations but large errors, while CPLIN shows a similar correlation but reduced errors. MFLUX and CPPOLY have very poor spatial correlations with LIS. ICEFLUX has a good correlation and low errors.

Figure 2.8 shows the climatological annual cycle over the northern and southern tropical and subtropical regions. In both hemispheres, a delay of the peak month by $\sim$ 1 month for all parametrisations can be seen. Statistics regarding timing of the peak month in each grid cell are shown in Table 2.1. The statistics give a more precise measure of the delay by finding the difference in peak month for each grid cell in the LIS viewing region. They show that on average the peak month in each grid cell is shifted by 0.16 of a month, with the parametrisations ranging in their delay from 0.09 to 0.24 of a month. The average absolute difference has been calculated as it will better represent the total bias in the distribution of peak month. It shows that ICEFLUX performs best and MFLUX the worst for this metric. Interestingly with ICEFLUX there is a larger average delay in peak month but lower overall error in peak month compared to the other parametrisations.

As well as the delay of the peak month, Figure 2.8 shows there are biases in the magnitude. In the Southern Hemisphere all parametrisations except ICEFLUX over-estimate the magnitude of flashes. In the Northern Hemisphere the magnitude is well produced by CTH, CPPOLY and CPLIN and under-estimated by ICEFLUX and MFLUX. An inspection of the spatial distributions for July has shown that CTH, CPPOLY and CPLIN achieve the correct Northern Hemisphere flash density magnitude although large over-estimation occurs over India and Southeast Asia and under-estimation occurs in other areas. ICEFLUX

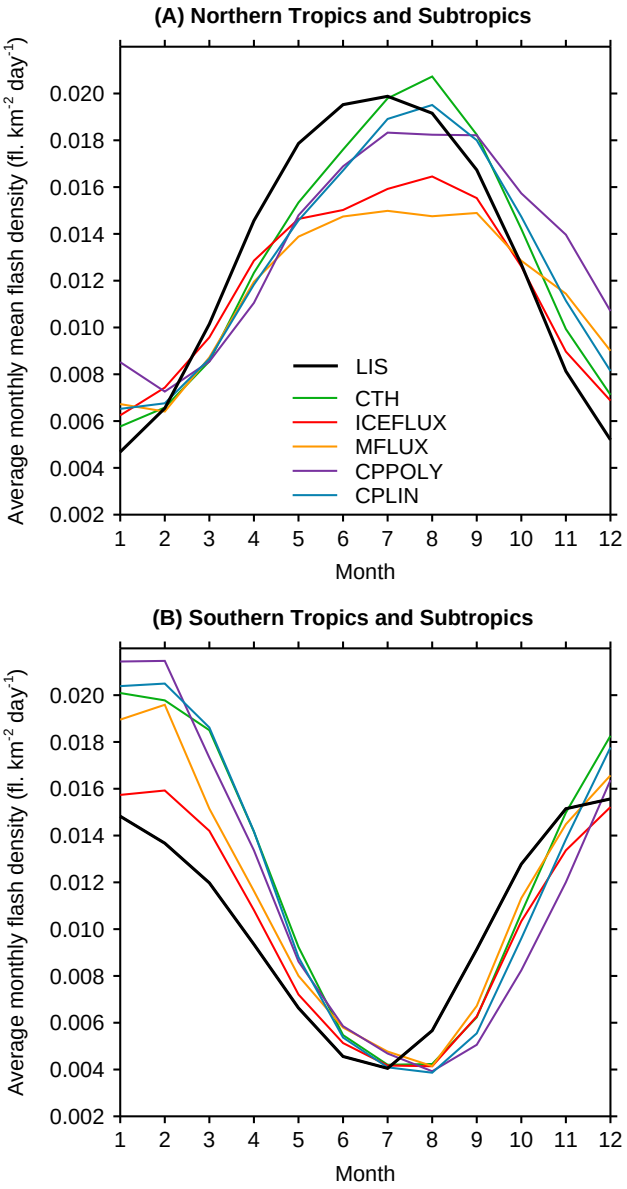

Figure 2.8: Five-year climatological annual cycle of flash density for 2007–2011 for **(a)**, the northern region (0 ° –38 ° N) and **(b)**, the southern region (38 ° S–0 °). Results are shown for the LIS measurements and the five parametrisations.

does not contain the same over-estimation but does under-estimate lightning activity in West Africa, leading to the overall under-estimation in the Northern Hemisphere peak. Another important issue is that none of the parametrisations establish the difference in total lightning between the Northern and Southern hemispheres seen in LIS measurements.

Figure 2.9 depicts the climatological seasonal peak-to-peak difference (difference of the minimum monthly value and the maximum monthly value during a year), and correlations and RMSEs are given in Table 2.1. This metric brings together the spatial and temporal variation in lightning; moreover, it highlights where inter-seasonal variation is large and therefore areas which can be dominant regions of lightning activity, even if they are not so prominent when considering yearly totals alone. The notable features in the observations that differ from the annual total plots are the low seasonal variation at the Central African location of maximum annual total and increased importance of northern India and North America.

CTH and ICEFLUX provide a reasonable distribution around Central Africa but have large biases elsewhere particularly in Asia and the US. ICEFLUX also under-estimates the seasonal variation in West Africa. Ocean seasonal variations are under-estimated by CTH and over-estimated by ICEFLUX. MFLUX and CPPOLY both produce too much inter-seasonal variation over the oceans. MFLUX over-estimates the seasonal variation in South America. CPLIN, as with other metrics, is qualitatively similar to CTH. The correlations and errors have the same ranking of ability as for the annual totals, with ICEFLUX consistently performing well.

Figure 2.10 shows the average change in lightning activity between consecutive years during the 5-year sample, and correlations and errors are given in Table 2.1. This metric is used to study the interannual peak-to-peak difference of the

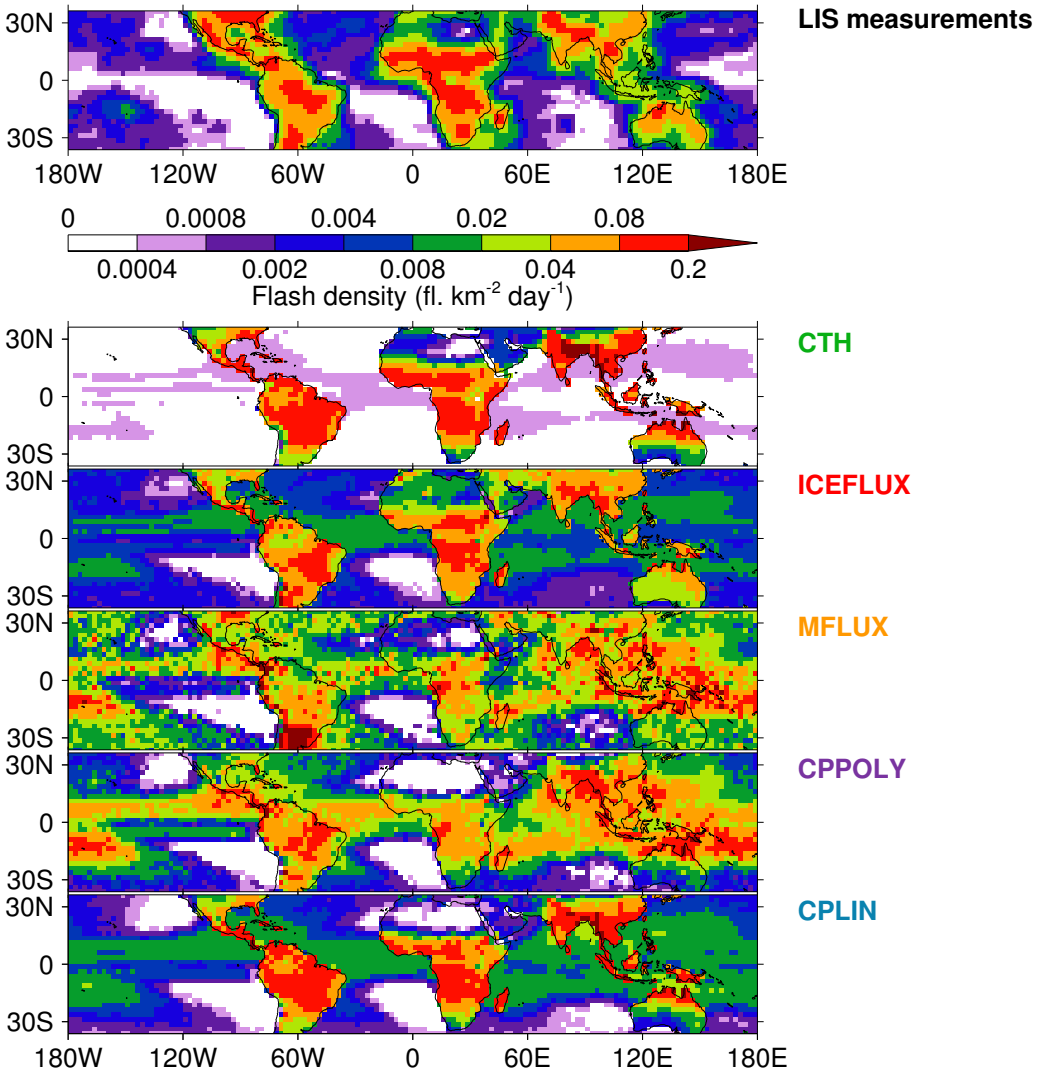

Figure 2.9: Five-year climatological seasonal peak-to-peak difference spatial distribution of flash density for 2007–2011. The seasonal peak-to-peak difference is the difference between the minimum monthly value and the maximum monthly value. Results are shown for the LIS measurements and the five parametrisations.

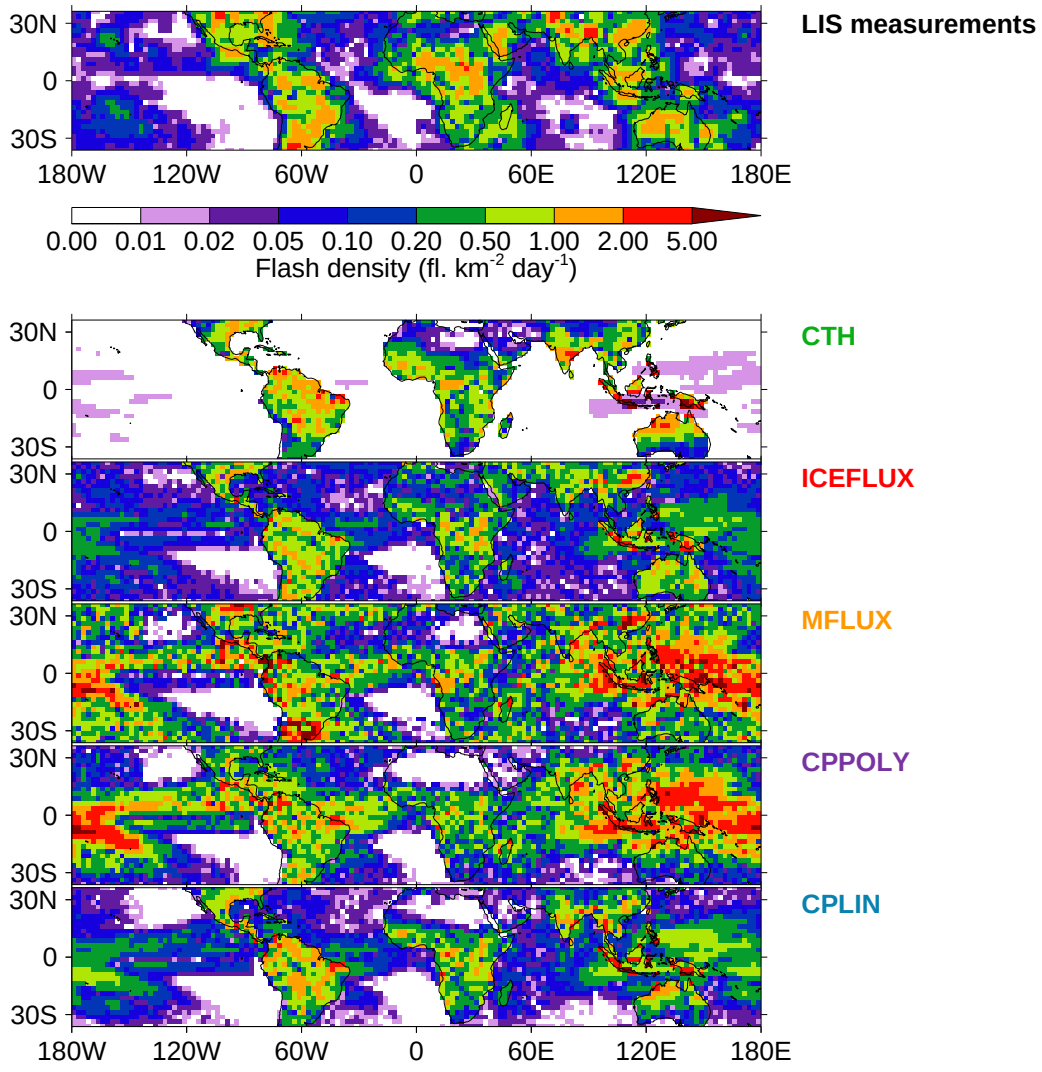

Figure 2.10: Five year climatological interannual peak-to-peak difference spatial distribution of flash density for 2007–2011. The interannual peak-to-peak difference has been calculated as the average difference between consecutive years over the five year period. Results are shown for the LIS measurements and the five parametrisations.

parametrisations and LIS measurements. Unlike other results so far, the spatial distribution is more heterogeneous with large differences in interannual variation between neighbouring cells. For example, the interannual variation in Central African grid cells differs by over an order of magnitude even though all cells display the same high annual total flash density. The ocean, unsurprisingly, shows lower interannual change compared to the land. The northeast and northwest of India are the two regions that stand out as having the greatest interannual variation which is expected to be related to monsoonal variability. Cecil *et al.* (2014) discussed lightning activity in northeast India in depth as it contains the greatest monthly flash density measured by LIS. The study of Cecil *et al.* (2014) and this chapter both support the significance of India with respect to the interannual and seasonal peak-to-peak differences of global lightning distributions.

All schemes have a low correlation of interannual peak-to-peak difference with the LIS measurements and fail to pick out northern India as having the greatest variation. Instead the parametrisations find that Southeast Asia has the greatest variation. Out of all the lightning statistics studied, the interannual peak-to-peak difference is the least well simulated across all parametrisations. This will be in part due to the underlying meteorology. Despite these difficulties ICEFLUX has made some improvement on the abilities of the other schemes in its ability to simulate interannual peak-to-peak difference of lightning flash density.

2.6 Discussion

This chapter compares one new and four existing lightning parametrisations using 6-hourly meteorological data. Other studies have compared some of the same existing parametrisations used here (Section 1.6). Tost *et al.* (2007) and Murray *et al.* (2012) give correlations for CTH, MFLUX and CPPOLY and reach the same

conclusions as in this study. CTH has a reasonable correlation whereas MFLUX and CPPOLY have poor correlations, with CPPOLY slightly better. Barthe *et al.* (2010) compared CTH, two updraught-based parametrisations and three ice and ice-flux-based parametrisations in cloud-resolving model simulations for two storms of different types. Most parametrisations had some success for particular storms and particular features with none standing out above the rest as best overall. This is contrary to our larger-scale findings which suggest that an ice-flux-based parametrisation successfully captures many large-scale features compared to the parametrisations based only on convective characteristics. A difference between the two studies is the nature of the upward ice flux variable; an intensive property was used in our case, whilst an extensive property was used in the case of Barthe *et al.* (2010), i.e. mass per area per time was used in our case opposed to only mass per time. The use of areal density provides a better measure of intensity of ice movement in the grid cell, whereas mass alone would have high values even if there is a high amount of cloud ice in a grid cell but rising slowly. As discussed in Section 2.4, this appears to be an important choice when including ice flux into the modelling environment.

By looking at several years of lightning satellite measurements this study has been able to quantify the annual total, seasonal and interannual behaviour of lightning across the tropics and subtropics. In line with other studies, Central Africa stands out as the most important feature with the greatest annual total lightning flashes. However, when considering seasonal and interannual spatial distributions the subtropics are just as important. India shows the greatest seasonal and interannual variation. There is substantial evidence linking these variations in lightning activity to monsoon seasons (Kumar and Kamra, 2012; Pawar *et al.*, 2012; Chaudhuri and Middey, 2013; Penki and Kamra, 2013). The ability of models to represent the monsoon as well as the links between the monsoon and lightning is important to consider when studying lightning in India.

In some of the parametrisations, most notably CTH, there is a clear bias towards the tropics which is not evident in the LIS measurements. While a significant portion of global lightning activity occurs in the tropics, demonstrated by the global annual peak located on the equator, the next most active regions are in the subtropics. CTH exhibits this tropical bias due to its foundation in cloud-top height which is limited by tropopause height, since tropopause height reduces away from the equator. ICEFLUX goes a long way to addressing this issue with the incorporation of updraught mass flux. Updraught mass flux on its own is typically not enough to provide a robust parametrisation – at least not with the formulation here. An alternative parametrisation by Grewe *et al.* (2001) exists which incorporates updraught mass flux into Equation 2.3. It was tested by Tost *et al.* (2007) and performed similarly to the other existing parametrisations being evaluated in this chapter.

To aid in understanding the sensitivities of the ICEFLUX parametrisation, some additional relationships using different independent variables have been found using the same approach as for Figure 2.2. These used the same LIS data but compared against (1) updraught mass flux only at 440 hPa, (2) upward cloud ice flux but at 540 hPa and (3) upward cloud ice flux at 340 hPa. The correlations over land were found to be 0.51, 0.47 and 0.65, respectively. Correlations over ocean varied by no more than 0.03. This suggests that the upward cloud ice variable significantly improves upon the correlation of updraught mass flux alone over land. The sensitivity to pressure is also demonstrated with higher pressures reducing the correlation but lower pressures maintaining a similar level of correlation. The gradients found for the 340 hPa level are $7.33 \times 10^{-7}\,\mathrm{fl.\,m^{-2}_{cell}/kg_{ice}\,m^{-2}_{cloud}}$ over land and $1.30 \times 10^{-7}\,\mathrm{fl.\,m^{-2}_{cell}/kg_{ice}\,m^{-2}_{cloud}}$ over ocean. These are similar to those at the 440 hPa level though larger. The gradients for the 540 hPa level are larger again which suggests the 440 hPa level gradients are sitting close to a minima in the gradient values. The significance of such a minima is not obvious and further

investigation at this point does not seem necessary since only slight gains can be made by arbitrarily optimising the pressure level.

A long standing problem when parametrising lightning has been over-estimation in the Amazon Basin and under-estimation in Central Africa. Complicating the study of this problem and evaluation of parametrisations in South America is the SAA which reduces the accuracy of LIS. So whilst this chapter has found that the ICEFLUX parametrisation reduces the Amazon bias, though not solving it, a robust conclusion cannot be drawn about lightning in the region. Regarding Central Africa, the good correlation but higher sensitivity to ice flux than elsewhere suggests additional factors are involved in the charging process. It is hoped that through presenting the results, they act as extra information to inform possible future satellite-based studies using the upcoming GOES-R and Meteosat Third Generation lightning detectors. These detectors, by operating continuously over the Americas and Europe and Africa on a geostationary satellite unaffected by the SAA, will provide a new and more robust perspective on lightning activity in these regions.

Error characteristics in both seasonal variation and annual total appear to depend very much on the functional form of the parametrisation. The power law form of CTH leads to large errors where biases in lightning flashes exist as demonstrated by it having the largest errors in the annual total spatial distribution. The polynomial forms of CPPOLY and MFLUX display less coherence between neighbouring grid cells, especially in the seasonal peak-to-peak difference plots, compared to the linear forms of CPLIN and ICEFLUX. The effect of functional form on errors is worth remembering when applying a parametrisation, which may have been developed for a specific region, on the global scale.

All the parametrisations have an average delay across all the grid cells in the seasonal peak of approximately 3–7 days. This may be a consequence

of inaccuracies in the reanalysis data, or the smoothing and averaging of LIS measurements which uses a 99 day and $7.5° \times 7.5°$ boxcar moving average (Cecil *et al.*, 2014). It could also be related to the occurrence of lightning in relation to other features of storms. It has been discussed in some papers that lightning peak months precede the rainfall peak months in monsoonal regions (Chaudhuri and Middey, 2013; Penki and Kamra, 2013). This may be relevant to variables such as convective rain and cloud-top height; however, one would expect the use of upward ice flux to begin to correct the delay. On the contrary, the ICEFLUX parametrisation shows the greatest delay bias although the lowest absolute bias. This suggests it could be an issue with the input meteorology or the need for an extension of the model to include a graupel flux, as in Deierling *et al.* (2008), to fully account for the seasonal cycle. Cloud resolving models would provide an appropriate means of testing the importance of graupel and other features of ice-based parametrisations as they include more explicit representations of cloud parameters. They can also be used in combination with field measurements to study the applicability of the ICEFLUX parametrisation on smaller scales which is vital in determining how widely the parametrisation can be used.

One other factor that may be important for explaining the variance in flash frequency density is geographical differences in flash characteristics. Recent research using a variety of data types has demonstrated different characteristics between land and ocean flashes such that ocean flashes are more energetic, powerful or longer (Hutchins *et al.*, 2013; Said *et al.*, 2013; Peterson and Liu, 2013; Beirle *et al.*, 2014). If this is the case then using the charging theory alone may not account for locations where there are fewer, more energetic flashes as opposed to more, less energetic flashes. The characteristics of lightning may also hold important information regarding the variance in emissions from lightning. Future development of lightning parametrisations should consider if flash characteristics contribute to observed lightning distributions.

2.7 Conclusions

A large-scale lightning parametrisation based on upward ice flux at 440 hPa (ICEFLUX) closely connected with the non-inductive charging mechanism has been developed here. While its development highlighted the challenge of forming a parametrisation for lightning over large scales, it showed no weaknesses that are not already inherent in existing parametrisations and which are, in part, due to the modelled input meteorology especially over Southeast Asia and the western Pacific. Its evaluation compared to satellite observations demonstrated several improvements on existing parametrisations regarding the large-scale spatial features of lightning in the tropics and subtropics. Under-estimation of Central African lightning remains but it has usefully been shown that linear relationships apply in this region; however, the flash rate here is highly sensitive to the upward ice flux compared to the rest of the tropics and subtropics.

The evaluation applied five different lightning parametrisations to the ECMWF ERA-Interim reanalysis, four well known and one newly developed, and compared their 5-year climatologies to Lightning Imaging Sensor (LIS) satellite measurements for the same period. The new ICEFLUX parametrisation showed the highest correlation and lowest bias for the spatial distributions of three properties: average annual total lightning density, and average seasonal and interannual peak-to-peak differences. It also represented well the annual cycle of lightning in the southern tropics and subtropics but under-estimated it in the northern tropics and subtropics principally due to a low bias in West Africa.

The Price and Rind (1992) parametrisation based on cloud-top height (CTH) had reasonable correlations with the spatial distributions and the least delay in the annual peak. However, it showed large biases in the zonal average distribution of lightning. The large biases were attributed to functional form which exacerbates any regional biases in the parametrisation.

The convective precipitation-based linear parametrisation (CPLIN) of Meijer *et al.* (2001) was qualitatively similar to CTH for all studied metrics. Two polynomial parametrisations based on convective precipitation (CPPOLY) and updraught mass flux (MFLUX) by Allen and Pickering (2002) were tested but found to perform poorly for the metrics and ERA-Interim meteorological input used here.

The simple ICEFLUX parametrisation more closely linked to the charging theory has been developed which now requires testing online in chemistry transport models to ensure its applicability for simulating NO emissions. The sensitivity of the chemistry to the different lightning features discussed in this chapter such as the seasonal variation will also be studied in Chapter 3. Results obtained indicate the potential of the parametrisation but rely on the convective scheme used in the ECMWF model. Therefore, use of the parametrisation by different modelling groups and other evaluation studies is needed to confirm the merits presented here. While individual chemistry–climate models are needed to confirm the wider use of the parametrisation, the conclusions presented here are directly applicable to chemistry transport model simulations performed using ERA-Interim meteorological input.

The upward ice flux parametrisation is presented as a means to explore the importance of cloud ice while models are still in the process of improving their cloud ice schemes. In future field campaigns it would be helpful to estimate the areal coverage of the storm along with the ice flow rate which can then be combined to give ice flux in units of $\mathrm{kg_{ice}\,m^{-2}_{cloud}\,s^{-1}}$. This may aid the formation of a global parametrisation based on storm observation data rather than reanalysis data as was necessary in this chapter. Even with this reanalysis approach, good improvements are made on the existing parametrisations compared here. Furthermore, there may be an opportunity in the future, as models of cloud ice

develop, where a downward graupel flux can be combined with the upward ice flux to represent both aspects of the non-inductive charging mechanism.

Chapter 3

The impact of lightning on tropospheric ozone chemistry using a new global lightning parametrisation

This chapter has been published as an open-access publication in Atmospheric Chemistry and Physics (ACP) in collaboration with: Dr Ruth Doherty, Dr Oliver Wild and Dr Luke Abraham. The paper is available online from the ACP website (http://www.atmos-chem-phys.net/16/7507/2016/acp-16-7507-2016.html). I did the analysis and wrote the initial draft. My supervisors and other co-authors provided feedback before the manuscript was submitted for publication. Dr Luke Abraham also provided technical assistance in the setup of the chemistry-climate model. In addition, Dr Paul Young provided processed sonde and satellite measurements of ozone. For the comparison of simulated ozone to sonde measurements I interpolated the model data to the same locations as sonde

measurements. For the comparison of simulated ozone to sonde measurements I used the NCEP tropopause climatology to mask the model data.

Finney, D. L., Doherty, R. M., Wild, O., and Abraham, N. L. (2016) The impact of lightning on tropospheric ozone chemistry using a new global lightning parametrisation, Atmospheric Chemistry and Physics, **16**, 7507-7522, doi:10.5194/acp-16-7507-2016.

3.1 Introduction

Lightning is a key source of nitric oxide (NO) in the troposphere. It is estimated to constitute around 10% of the global annual NO source (Schumann and Huntrieser, 2007). However, lightning has particular importance because it is the major source of NO directly in the free troposphere. The oxidation of NO forms NO_2 and the sum of these is referred to as NO_x. In the middle and upper troposphere NO_x has a longer lifetime and a disproportionately larger impact on tropospheric chemistry than emissions from the surface.

Through oxidation, NO is rapidly converted to NO_2 until an equilibrium is reached. NO_2 photolyses and forms atomic oxygen which reacts with an oxygen molecule to produce ozone, O_3 (Figure 1.4B). As a source of atomic oxygen, NO_2 is often considered together with O_3 as odd oxygen, O_x. Ozone acts as a greenhouse gas in the atmosphere and is most potent in the upper troposphere where temperature differences between the atmosphere and ground are greatest (Lacis *et al.*, 1990; Dahlmann *et al.*, 2011). Understanding lightning NO production and ozone formation in this region is important for determining changes in radiative flux resulting from changes in ozone (Liaskos *et al.*, 2015)(Section 1.4.2).

As reported by Lamarque *et al.* (2013), the parametrisation of lightning in

chemistry transport and chemistry-climate models (CCMs) most often uses simulated cloud-top height to determine the flash rate as presented by Price and Rind (1992). However, this and other existing approaches have been shown to lead to large errors in the distribution of flashes compared to lightning observations (Tost *et al.*, 2007). Several studies have shown that the global magnitude of lightning NO_x emissions is an important contributor to ozone and other trace gases especially in the upper tropical troposphere (Labrador *et al.*, 2005; Wild, 2007; Liaskos *et al.*, 2015). Each of these studies uses a single horizontal distribution of lightning so the impact of varying the lightning emission distribution is unknown. Murray *et al.* (2012, 2013) have shown that constraining simulated lightning to satellite observations results in a shift of activity from the tropics to extratropics, and that this constraint improves the representation of the ozone tropospheric column and its interannual variability. In Chapter 2, it was shown using reanalysis data that a similar shift in activity away from the tropics occurred when a more physically based parametrisation based on ice flux was applied.

The above studies and also that of Grewe *et al.* (2001) find that the largest impact of lightning emissions on trace gases occurs in the tropical upper troposphere. This is a particularly important region because it is the region of most efficient ozone production (Dahlmann *et al.*, 2011). Understanding how the magnitude of lightning flash rate or concentration of emissions affects ozone production is an ongoing area of research, and so far has focussed on individual storms or small regions (Allen and Pickering, 2002; DeCaria *et al.*, 2005; Apel *et al.*, 2015). DeCaria *et al.* (2005) found that whilst there was little ozone enhancement at the time of the storm, there was much more ozone production downstream in the following days. They found a clear positive relationship between downstream ozone production and lightning NO_x concentration which was linear up to ~ 300 pptv but resulted in smaller ozone increases for NO_x increases above this concentration. Increasing ozone production downstream with more NO_x was also

found by Apel *et al.* (2015). Allen and Pickering (2002) specifically explored the role of the flash frequency distribution on ozone production using a box model. They found that the cloud-top height scheme produces a high frequency of low flash rates which are unrealistic compared to the observed flash rate distribution. This results in lower NO_x concentrations and greater ozone production efficiency with the cloud-top height scheme. Differences in the frequency distribution between lightning parametrisations were also found across the broader region of the tropics and subtropics in Chapter 2. The importance of differences in flash rate frequency distributions to ozone production over the global domain remains unknown.

In this chapter, the lightning parametrisation developed in Chapter 2 which uses upward cloud ice flux at 440 hPa is implemented within the United Kingdom Chemistry and Aerosols model (UKCA). This parametrisation is closely linked to the Non-Inductive Charging Mechanism of thunderstorms (Reynolds *et al.*, 1957)(Section 1.2) and was shown to perform well against existing parametrisations when applied to reanalysis data (Chapter 2). Here the effect of the cloud-top height and ice flux parametrisations on tropospheric chemistry is quantified using a CCM, focussing especially on the location and frequency distributions. Section 3.2 describes the model and observational data used in the study. Section 3.3 compares the simulated lightning and ozone concentrations to observations. Section 3.4 analyses the ozone chemistry through use of O_x budgets. Section 3.5 then considers the differences in zonal and altitudinal distributions of chemical O_x production and ozone concentrations simulated for the different lightning schemes. Section 3.6 provides a novel approach to studying the effects of flash frequency distribution on ozone. Section 3.7 presents the conclusions.

3.2 Model and data description

3.2.1 Climate-chemistry model

The model used is the UK Chemistry and Aerosols model (UKCA) coupled to the atmosphere-only version of the UK Met Office Unified Model version 8.4. The atmosphere component is the Global Atmosphere 4.0 (GA4.0) as described by Walters *et al.* (2014). Tropospheric and stratospheric chemistry are modelled, although the focus of this chapter is the troposphere. The UKCA tropospheric scheme is described and evaluated by O'Connor *et al.* (2014) and the stratospheric scheme by Morgenstern *et al.* (2009). This combined *CheST* chemistry scheme has been used by Banerjee *et al.* (2014) in an earlier configuration of the Unified Model. There are 75 species with 285 reactions considering the oxidation of methane, ethane, propane, and isoprene. Isoprene oxidation is included using the Mainz Isoprene Mechanism of Pöschl *et al.* (2000). Squire *et al.* (2015) gives a more detailed discussion of the isoprene scheme used here.

The model is run at horizontal resolution N96 (1.875° longitude by 1.25° latitude). The vertical dimension has 85 terrain-following hybrid-height levels distributed from the surface to 85 km. The resolution is highest in the troposphere and lower stratosphere, with 65 levels up to $\sim$30 km. The model time step is 20 minutes with chemistry calculated on a 1 hour time step. The exception to this is for data used in section 3.6 where it was required that chemical reactions accurately coincide with time of emission and hence where the chemical time step was set to 20 minutes. The coupling is one-directional, applied only from the atmosphere to the chemistry scheme. This is so that the meteorology remains the same for all variations of the lightning scheme, and hence, differences in chemistry are solely due to differences in lightning NO_x.

The cloud parametrisation (Walters *et al.*, 2014) uses the Met Office Unified Model's prognostic cloud fraction and prognostic condensate (PC2) scheme (Wilson *et al.*, 2008a,b) along with modifications to the cloud erosion parametrisation described by Morcrette (2012). PC2 uses prognostic variables for water vapour, liquid and ice mixing ratios as well as for liquid, ice and total cloud fraction. The cloud ice variable includes snow, pristine ice and riming particles. Cloud fields can be modified by shortwave and longwave radiation, boundary layer processes, convection, precipitation, small-scale mixing, advection and pressure changes due to large-scale vertical motion. The convection scheme calculates increments to the prognostic liquid and ice water contents by detraining condensate from the convective plume, whilst the cloud fractions are updated using the non-uniform forcing method of Bushell *et al.* (2003).

Evaluation of the distribution of cloud depths and heights simulated by the Unified Model has been performed in the literature. For example, Klein *et al.* (2013) conclude that across a range of models, the most recent models improve the representation of clouds. They find that HadGEM2-A, a predecessor of the model used in this chapter, simulates cloud fractions of high and deep clouds in good agreement with the International Satellite Cloud Climatology Project (ISCCP) climatology. In addition, Hardiman *et al.* (2015) studied a version of the Unified Model which used the same cloud and convective parametrisations as used here. They found that over the tropical Pacific warm pool that high cloud of 10-16 km occurred too often compared to measurements by the CALIPSO satellite. This will bias a lightning parametrisation based on cloud-top height, over this region. Cloud ice content and updraught mass flux, which are used in the ice flux based lightning parametrisation presented in this chapter, are not well constrained by observations and represent an uncertainty in the simulated

lightning. However, these variables are fundamental components of the Non-Inductive Charging Mechanism and therefore it is appropriate to consider a parametrisation which includes such aspects.

Simulations for this chapter were set up as a time-slice experiment using sea surface temperature and sea ice climatologies based on 1995-2004 analyses Reynolds *et al.* (2007), and emissions and background lower boundary GHG concentrations, including methane, are representative of the year 2000. A one year spin-up for each run was discarded and the following year used for analysis.

3.2.2 Lightning NO emission schemes

The flash rate in the lightning scheme in UKCA is based on cloud-top height by Price and Rind (1992, 1993), with energy per flash and NO emission per joule as parameters drawn from Schumann and Huntrieser (2007). The equations used to parametrise lightning, as in Chapter 2, are:

$$F_{\mathrm{l}} = 3.44 \times 10^{-5} H^{4.9} \tag{3.1}$$

$$F_{\mathrm{o}} = 6.2 \times 10^{-4} H^{1.73}, \tag{3.2}$$

where F is the total flash frequency (fl. min^{-1}), H is the cloud-top height (km) and subscripts l and o are for land and ocean, respectively (Price and Rind, 1992). A resolution scaling factor, as suggested by Price and Rind (1994), is used although it is small and equal to 1.09. An area scaling factor is also applied to each grid cell, which consists of the area of the cell divided by the area of a cell at 30° latitude.

This lightning NO_x scheme has been modified to have equal energy per cloud-to-ground and cloud-to-cloud flash based on recent literature (Ridley *et al.*,

2005; Cooray *et al.*, 2009; Ott *et al.*, 2010). The energy of each flash is 1.2 GJ and NO production is 12.6×10^{16} NO molecules J^{-1}. These correspond to 250 mol(NO) fl.$^{-1}$ which is within the estimate of emission in the review by Schumann and Huntrieser (2007). It also ensures that changes in flash rate produce a proportional change in emission independent of location since different locations can have different proportions of cloud-to-ground and cloud-to-cloud flashes. As a consequence, the distinction between cloud-to-ground and cloud-to-cloud has no effect on the distribution or magnitude of lightning NO_x emissions in this chapter. The vertical emission distribution has been altered to use the recent prescribed distributions of Ott *et al.* (2010)(Section 1.5.3, Figure 1.7) and applied between the surface and cloud top. Whilst the Ott *et al.* (2010) approach is used for both lightning parametrisations, the resulting average global vertical distribution can vary because the two parametrisations distribute emissions in cells with different cloud top heights. This simulation with the cloud-top height approach will be referred to as CTH.

Two alternative simulations are also used within this chapter: 1) lightning emissions set to zero (ZERO), and 2) using the flash rate parametrisation in Chapter 2 (ICEFLUX). As in Chapter 2, the flash rate equations used are:

$$f_{\mathrm{l}} = 6.58 \times 10^{-7} \phi_{\mathrm{ice}} \tag{3.3}$$

$$f_{\mathrm{o}} = 9.08 \times 10^{-8} \phi_{\mathrm{ice}}, \tag{3.4}$$

where f_{l} and f_{o} are the flash density (fl. $\mathrm{m}^{-2}\,\mathrm{s}^{-1}$) of land and ocean, respectively. ϕ_{ice} is the upward ice flux at 440 hPa and is formed using the following equation:

$$\phi_{\mathrm{ice}} = \frac{q \times \Phi_{\mathrm{mass}}}{c}, \tag{3.5}$$

where q is specific cloud ice water content at 440 hPa ($\mathrm{kg\,kg}^{-1}$), Φ is the updraught mass flux at 440 hPa ($\mathrm{kg\,m}^{-2}\,\mathrm{s}^{-1}$) and c is the fractional cloud cover at 440 hPa

($m^2\,m^{-2}$). Upward ice flux was set to zero for instances where $c < 0.01\,m^2m^{-2}$. Where no convective cloud top is diagnosed, the flash rate is set to zero.

Both the CTH and ICEFLUX parametrisations when implemented in UKCA produce flash rates corresponding to global annual NO emissions within the range estimated by Schumann and Huntrieser (2007) of 2-8 $TgN\,yr^{-1}$. However, for this chapter I choose to have the same flash rate and global annual NO_x emissions for both schemes. A scaling factor was used for each parametrisation that results in the satellite estimated flash rate of $46\,fl.\,s^{-1}$, as given by Cecil *et al.* (2014). The flash rate scaling factors needed for implementation in UKCA were 1.57 for the Price and Rind (1992) scheme and 1.11 for the ICEFLUX scheme. The factor applied to the ice flux parametrisation is similar to that used in Chapter 2, which used a scaling of 1.09. This is some evidence for the parametrisation's robustness since Chapter 2 is based upon reanalysis data, however, the scaling may vary in other models. Given that each parametrisation produces the same number of flashes each year and each flash has the same energy, a single value for NO production can be used. As stated above, a value of 12.6×10^{16} NO molecules J^{-1} was used for both schemes which results in a total annual emission of 5 $TgN\,yr^{-1}$.

3.2.3 Lightning observations

The global lightning flash rate observations used are a combined climatology product of satellite observations from the Optical Transient Detector (OTD) and the Lightning Imaging Sensor (LIS) (Section 1.3.2). The OTD observed between ±75° latitude from 1995-2000 while LIS observed between ±38° from 2001-2015 and a slightly narrower latitude range between 1998-2001. The satellites were low earth-orbit satellites so did not observe everywhere simultaneously. LIS, for example, took around 99 days to twice sample the full diurnal cycle at each location on the globe. The specific product used here is referred to as the High

Resolution Monthly Climatology (HRMC) which provides 12 monthly values on a 0.5° horizontal resolution made up of all the measurements of OTD and LIS between May 1995 - December 2011. Cecil *et al.* (2014) provides a detailed description of the product using data for 1995-2010, which had been extended to 2011 when data was obtained for this chapter. The LIS/OTD climatology product was regridded to the resolution of the model (1.875° longitude by 1.25° latitude) for comparison.

3.2.4 Ozone column and sonde observations

Two forms of ozone observations are used to compare and validate the model and lightning schemes. Firstly, a monthly climatology of tropospheric ozone column between ±60° latitude, inferred by the difference between two satellite instrument datasets (Ziemke *et al.*, 2011). These are the total column ozone estimated by the Ozone Monitoring Instrument (OMI) and the stratospheric column ozone estimated by the Microwave Limb Sounder (MLS). The climatology uses data covering October 2004 to December 2010. The production of the tropospheric column ozone climatology by Ziemke *et al.* (2011) uses the NCEP tropopause climatology so, for the purposes of evaluation, simulated ozone in this chapter is masked using the same tropopause. In Section 3.3.2, the simulated annual mean ozone column is regridded to the MLS/OMI grid of 5° by 5° and compared directly to the satellite climatology without sampling along the satellite track.

In an evaluation against ozone sondes with broad coverage across the globe, the MLS/OMI product generally simulated the annual cycle well (Ziemke *et al.*, 2011). The annual mean tropospheric column ozone mixing ratio of the MLS/OMI product was found to have a root mean square error (RMSE) of 5.0 ppbv, and a correlation of 0.83, compared to all sonde measurements. The RMSE was lower

and correlation higher (3.18 ppbv and 0.94) for sonde locations within the latitude range 25° S to 50° N.

Secondly, ozone sonde observations averaged into 4 latitude bands were used. The ozone sonde measurements are from the dataset described by Logan (1999) (representative of 1980–1993) and from sites described by Thompson (2003) for which the data has since been extended to be representative of 1997–2011. The data consists of 48 stations, with 5, 15, 10 and 18 stations in the southern extratropics (90S-30S), southern tropics (30S-Equator), northern tropics (Equator-30N) and northern extratropics (30N-90N) respectively. In Section 3.3.2, the simulated annual ozone cycle is interpolated to the locations and pressure of the sonde measurements. The average of the interpolated points is then compared to the annual cycle of the sonde climatology without processing to sample the specific year or time of the sonde measurements. Both of these observational ozone datasets are the same as used in the Atmospheric Chemistry and Climate Model Intercomparison Project (ACCMIP) study by Young *et al.* (2013).

3.3 Comparison to observations

3.3.1 Global annual spatial and temporal lightning distributions

Using the combined OTD/LIS climatology allows extension of the evaluation made in Chapter 2 which was over a smaller region. Figure 3.1 shows the satellite annual flash rate climatology alongside the annual flash rate estimated by UKCA using CTH and ICEFLUX. The annual flash rate simulated by UKCA is broadly representative of the decade around the year 2000 as it uses SST and

sea ice climatologies for that period. A spatial correlation of 0.78 between the flash rate climatology estimated by ICEFLUX and the satellite climatology is an improvement upon the correlation of flash rates estimated by CTH which is 0.65. Furthermore, the root mean square error (RMSE) of the ICEFLUX climatology to the satellite data of 3.7 fl. $km^{-2}\,yr^{-1}$ is favourably reduced compared to the 6.0 fl. $km^{-2}\,yr^{-1}$ RMSE of the CTH climatology.

These results are similar to those found in Chapter 2 where offline ERA-Interim meteorology was used as the input to the parametrisation. Neither approach for simulating lightning achieves the observed ocean to land contrast despite using separate equations, and neither displays the large peak flash rate in central Africa. The ICEFLUX approach over the ocean provides a contrast to the CTH approach by being an overestimate instead of an underestimate compared to the satellite lightning observations. While not achieving the magnitude of the observed Central African peak the ICEFLUX scheme does yield closer agreement over the American and Asian tropical regions.

Figure 3.2 shows comparisons of the monthly mean flash rates for 4 latitude bands. The focus on the HRMC mean as this provides the highest resolution data. The range provided by the low resolution monthly climatology (LRMTS) product is referred to where appropriate to place the single year simulation results in context. The monthly mean of the LRMTS product can differ from the HRMC product because it is produced at a coarser resolution and undergoes a 99-day boxcar temporal smoothing instead of the 31-day boxcar temporal smoothing of the HRMC product. Therefore the comparison also provides an indication of how this difference in smoothing window influences the estimated lightning activity.

The ICEFLUX approach simulates lightning well in the extratropics with good temporal correlations with the LIS/OTD HRMC product in both hemispheres. The correlation of CTH with LIS/OTD is higher in the southern extratropics but

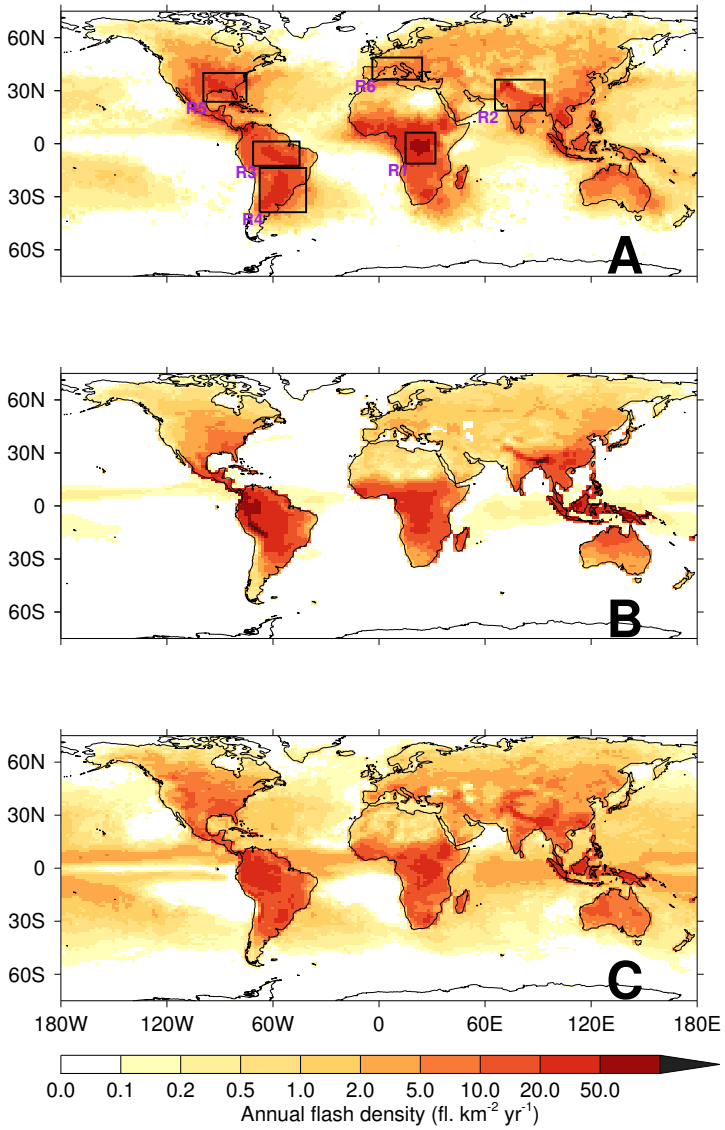

Figure 3.1: Annual flash rates from (A) a combined climatology from LIS/OTD satellite observations spanning 1995-2011, (B) the CTH scheme using the year 2000 of UKCA output and (C) the ICEFLUX scheme using the year 2000 of UKCA output. The horizontal resolution of the climatology product has been degraded to match that of the model which is 1.875° longitude by 1.25° latitude. Boxes for the regions R1–R6 correspond to regions of interest for which the annual cycles are shown in Figure 3.3.

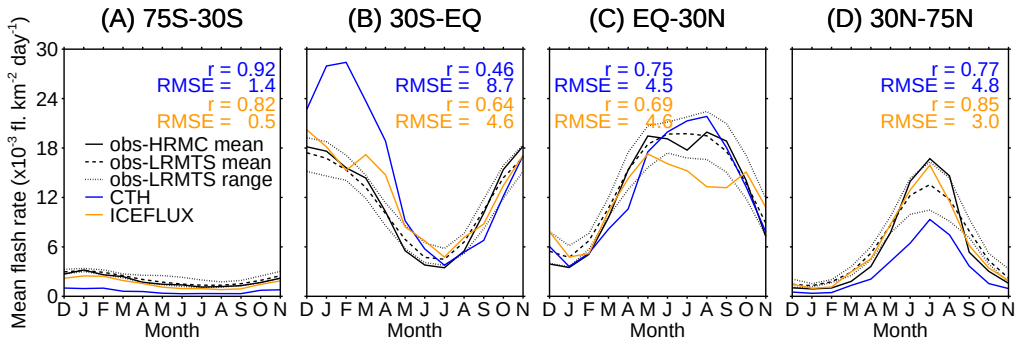

Figure 3.2: Mean monthly flash rate averaged over four latitudinal bands for the two different schemes for 2000 and two LIS/OTD climatology products spanning 1995-2011. HRMC is the high resolution monthly climatology and LRMTS is the low resolution monthly time series as used in Chapter 2. The LRMTS product range is the highest and lowest values for each month based on individual year data. For the extratropical locations 4 years provide the mean and range of the LRMTS product based on OTD data, whereas there are 17 years in the tropics based on OTD and LIS data. The simulated values use one year of UKCA model output. Also given are the temporal correlations (r) between the CTH scheme (blue) and LIS/OTD HRMC mean and between ICEFLUX (orange) and LIS/OTD HRMC mean. The corresponding root mean square errors (RMSE) are given in units of $10^{-3}\,\mathrm{fl.\,km^{-2}yr^{-1}}$.

this improvement compared to ICEFLUX is contrasted by much larger absolute errors. Correlations for both approaches are lowest in the southern tropics.

Figure 3.2B shows that CTH has very large root mean square errors during December to April in the southern tropics. A more detailed analysis (not shown) suggests that these errors are due to overestimation over South America. In the northern tropics the temporal correlation with the LIS/OTD HRMC product suggests CTH performs slightly better than the ICEFLUX approach, although Figure 3.2C shows that the CTH approach is not capturing the double peak characteristic of this latitude band. The ICEFLUX approach appears to simulate a double peak but it does not achieve the timing, which leads to a poor correlation.

However, since the double peak does not appear in the mean of the LRMTS product, its significance is unclear. The CTH scheme has simulated lightning within the range of the LRMTS whilst the ICEFLUX scheme has underestimated the summertime lightning in this latitude band. In the northern tropics, the more detailed analysis found that both schemes failed to match the observed magnitude of the August peak of Central America and the Southern US, nor the duration of the lightning peak over Northern Africa which lasts from June to September. The delay in the lightning peak that was apparent in annual cycles shown in Chapter 2 over the tropics and subtropics is not so apparent here although there may be some delay in the southern tropics. The underestimation of ICEFLUX in the northern tropics and overestimation of CTH in the southern tropics found in Chapter 2 is also found here.

Overall, the ICEFLUX approach reduces the errors in the annual cycles of lightning. This scheme improves the correlation between simulated and observed lightning compared to CTH scheme in the northern extratropics and southern tropics. It has a lower correlation in the northern tropics, where both approaches for simulating lightning have difficulties, and in the southern extratropics, where the magnitude of the bias is much reduced compared to the CTH approach.

To further understand how the schemes perform on a regional scale, the annual cycles of the simulated and observed lightning, for a selection of key regions, are shown in Figure 3.3. A box showing each region is plotted on Figure 3.1A. The regions of Figure 3.3 include many of the peak areas of lightning shown in Figure 3.1A or, in the case of Europe, are an area in which a higher density of measurement studies are undertaken including using ground-based lightning detectors.

Figure 3.3A shows the Central African peak lightning region where both parametrisations successfully simulate the observed peak months of lightning in

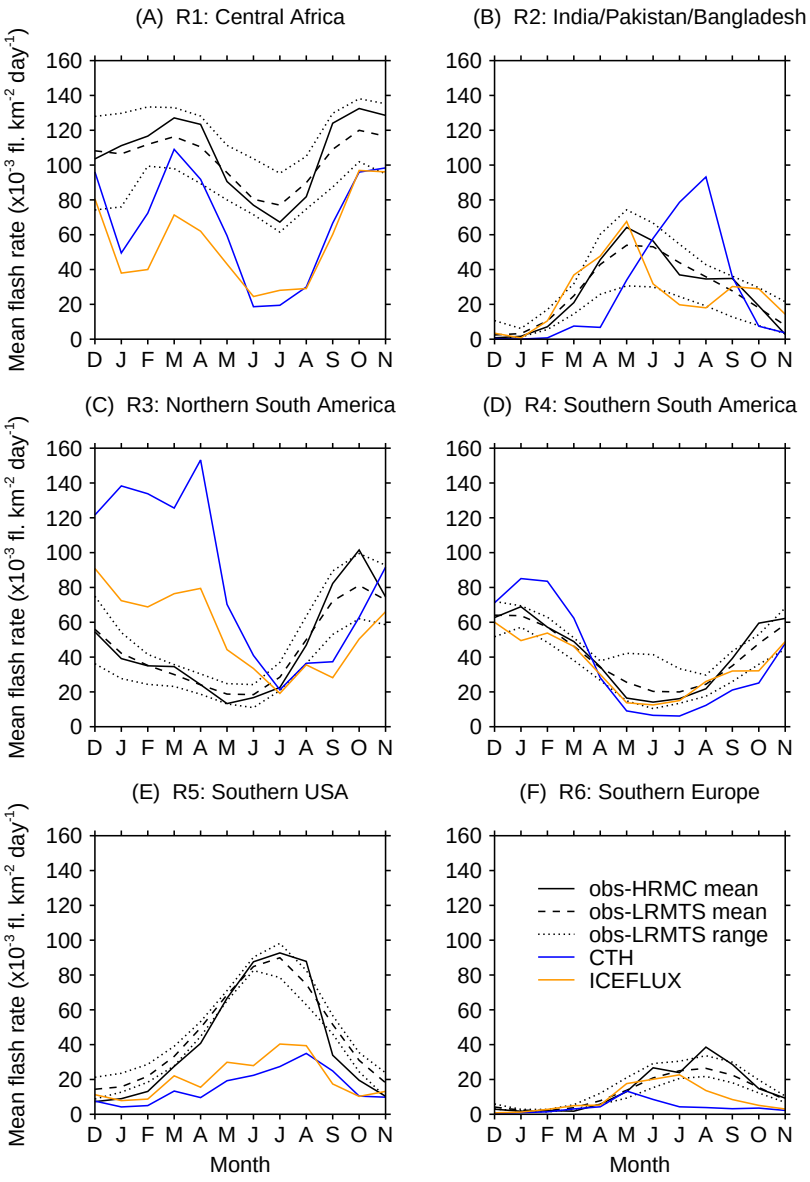

Figure 3.3: Mean monthly flash rate averaged over six regions (R1–R6) for the two different schemes for year 2000 and the LIS/OTD climatology products spanning 1995-2011. Means and ranges of the LRMTS products in D-F use 4 years of data as parts of these regions lie outside the LIS range and therefore rely on OTD data only. Lines represent the lightning simulated using the CTH approach (blue) and the ICEFLUX approach (orange), and the LIS/OTD observed climatology (black). Regions R1-R6 are shown as boxes on Figure 3.1.

the LIS/OTD data. For the most part, both parametrisations produce similar flash rates. However the simulated flash rates generally underestimate lightning compared to the observations. Interestingly, the ICEFLUX approach has a greater underestimation of the observed Spring lightning peak compared to the CTH approach. This suggests that the input meteorology for the ICEFLUX scheme over the Central African region is less well simulated during this season, or that the ICEFLUX scheme does not capture some necessary aspect of thunderstorm activity during the season. Over the Indian region (Figure 3.3B), the two schemes substantially differ in their flash estimates. The ICEFLUX scheme achieves a much more realistic annual cycle than the CTH scheme. This suggests that aspects of charging during the Indian monsoon seasons may not be captured by the cloud-top height approach. Two regions in South America are shown in Figure 3.3 C and D. Both schemes capture the southern South American annual cycle of lightning flash rates well but both perform poorly in the northern region (the ICEFLUX approach results in a much lower bias). Biomass burning aerosols could be a key control on lightning activity in the region, as was shown by (Altaratz *et al.*, 2010). The flash rate peak in the southern USA region is greatly underestimated by both schemes (Figure 3.3). The lack of difference between the two schemes suggests that it may not be the best study region for distinguishing which is a more successful parametrisation. Finally, over the southern European region, both schemes show an underestimation of flash rates compared to LIS/OTD, although the bias is less in the case of the ICEFLUX approach. The August peak in this region is not captured by either approach, which may relate to lightning activity over the Mediterranean Sea, given that both schemes also underestimate the annual flash rate over the Mediterranean Sea as shown in Figure 3.1.

The analysis of the annual cycle of flash rates in some key regions has shown that the ICEFLUX scheme is similar to or improves upon the simulated annual

cycle by the CTH scheme when compared to the LIS/OTD satellite climatology. The exception is for the Central African peak in Spring. Any future studies of the Central African region could explore this difference further. Neither parametrisation captures the magnitude of flash rates over the southern USA or southern European regions. The high density of measurements in these regions it should be possible to study why this underestimation occurs in future studies. Finally, one of the greatest sources of bias in the flash rate estimates by the CTH scheme are over northern South America. The ICEFLUX scheme reduces this bias but still does not capture the annual cycle. In southern South America both parametrisations reproduce the observed annual cycle of lightning. Therefore, I suggest that field campaigns comparing the southern and northern regions of South America would be particularly useful in improving the understanding of lightning processes and finding reasons for large-scale biases in models.

3.3.2 Global annual spatial and temporal ozone distributions

Ozone has an average lifetime in the troposphere of a few weeks and can be transported long distances during that time. It can therefore be challenging to identify the sources of measured ozone but two types of measurements are used here to analyse how lightning emissions influence ozone distribution. Satellite column ozone measurements provide estimates of effect on the annual horizontal distribution of ozone whilst ozone sonde measurements demonstrate the altitudinal effect of lightning emissions on monthly varying ozone.

Comparisons with the MLS/OMI tropospheric column ozone climatology are made using Pearson correlations, RMSE and mean bias assessments. The model ozone is masked to the troposphere by applying the NCEP tropopause climatology to each month and regridding to the 5° by 5° horizontal resolution of the

MLS/OMI climatology. Table 3.1 gives the annual results for the three simulations using CTH, ICEFLUX and ZERO lightning.

Table 3.1: Spatial comparisons of correlation, errors and bias of annual tropospheric ozone column between model runs and the MLS/OMI satellite climatology product over the range ±60°. Adjusted root mean square error (RMSE) refers to the RMSE following the subtraction of the mean bias from the field.

Run	r	RMSE (DU)	Mean bias (DU)	adjusted RMSE (DU)
CTH	0.82	5.5	-2.8	4.1
ICEFLUX	0.84	5.7	-3.2	3.9
ZERO	0.83	10.7	-7.4	4.6

The inclusion of lightning emissions from either scheme has a large effect on the amount of ozone in the column as shown by the reduced mean bias and RMSE compared to the ZERO simulation, however, there is little difference between the two lightning schemes. There is a slightly larger mean bias with the ICEFLUX approach. To analyse the error in distribution without the bias present, an adjustment is made by subtracting the mean biases from the respective simulated ozone column distributions. Once this adjustment is made the ICEFLUX approach shows a slightly lower RMSE than the CTH approach (Table 3.1).

Figure 3.4 uses sonde measurements averaged over four latitudinal bands and taken at three pressure levels. The temporal correlations and mean biases of the model monthly means, interpolated to the same pressure and locations, against the sonde observations are shown.

Both lightning schemes show a reduction in mean bias compared to the ZERO run throughout all latitude bands and altitudes (Figure 3.4). The greatest impact of lightning is on the tropical, middle and upper troposphere. In these locations

the ozone concentration simulated by the ICEFLUX scheme has a much better temporal correlation with sonde measurements than that simulated by the CTH scheme. The ICEFLUX approach has a larger bias than the CTH approach which is discussed further in the following paragraph.

Figure 3.5 shows the monthly ozone comparisons between sonde measurements and the model at 250 hPa and 500 hPa for the northern and southern tropics. It is clear that in the middle and upper troposphere the lightning scheme is important in achieving a reasonable magnitude of ozone. Both schemes still show an underestimate compared to observations all year round in the southern tropics and during spring in the northern tropics, but are within the variability of sonde measurements. Other aspects of simulated ozone chemistry or uncertainty in total global lightning emissions, which is ±3 TgN on the 5 TgN used here, may contribute to this bias.

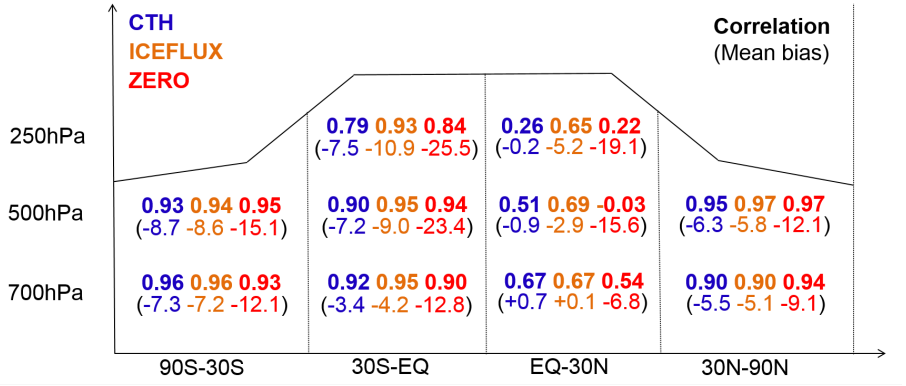

Figure 3.4: Temporal correlations and mean biases of the annual cycle of modelled ozone in UKCA over the year 2000 compared to a climatology of ozone sonde measurements averaged over 1980-1993 and 1997-2011. The simulated ozone data was interpolated to the location and pressure level of the sonde measurements. The sonde and modelled ozone were then averaged into 4 latitude bands which correspond to the bands used in Figure 3.2.

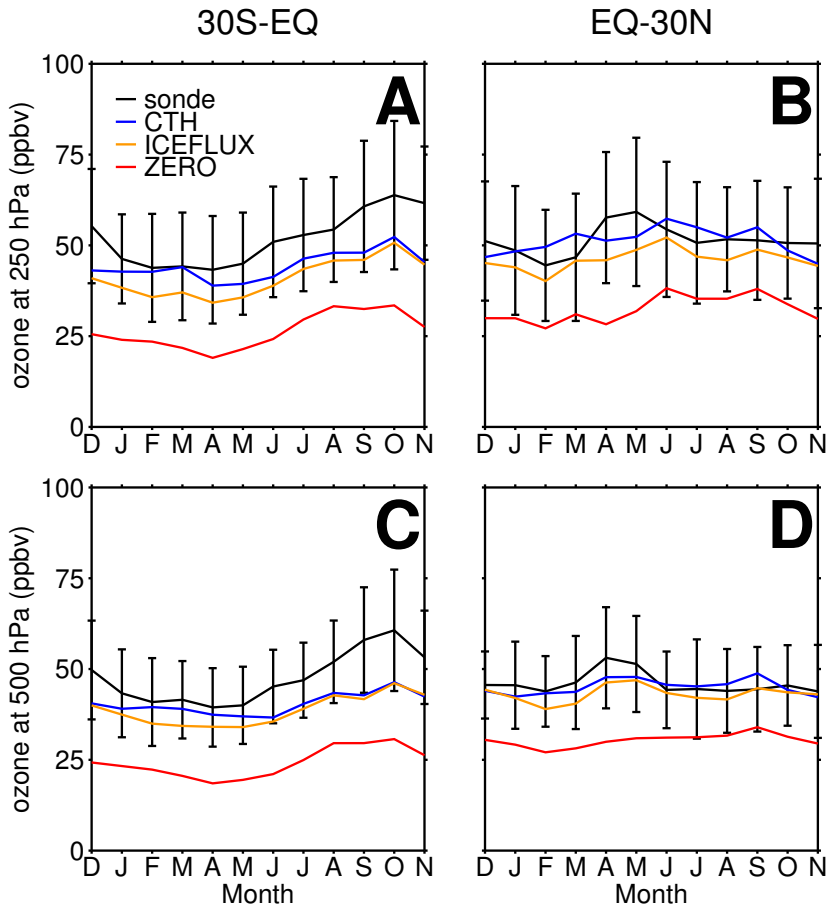

Figure 3.5: Middle and upper tropospheric UKCA simulated ozone concentration for the year 2000 compared to a climatology of sonde measurements averaged over 1980-1993 and 1997-2011. These cycles correspond to the 500 hPa and 250 hPa correlations for 30S-EQ and EQ-30N in Figure 3.4. The vertical black bars show the average interannual standard deviation for each group of stations.

In Wild (2007) and Liaskos *et al.* (2015) the ozone burden and mean tropospheric column ozone respectively, scaled approximately linearly with increases in lightning emissions. Using the mean bias data in Table 3.1, the mean increase in ozone column associated with each TgN emission from lightning can be calculated. The average mean bias in ozone column of the ICEFLUX and CTH simulations is -3.0 DU, where as the mean bias of the ZERO simulation is -7.4 DU. Therefore, 5 TgN of lightning emissions has increased the mean ozone column by, on average, 4.4 DU. If the effect of emissions is assumed to be linear, these biases imply that the mean global effect of lightning on ozone column is 0.9 DU TgN^{-1}. Changing lightning emissions to 8 TgN could increase the ozone column by 2.7 DU and result in a bias of less than 1 DU. Such bias potentially introduced by the uncertainty in total emissions or other aspects of the model is much greater than the difference in mean bias between the two lightning schemes given in Table 3.1. Therefore, the small difference in mean bias between the two lightning schemes does not necessarily imply greater accuracy, instead the correlation values between the model and sonde data (Figure 3.4) provide a more useful evaluation of parametrisation success.

In Figure 3.5 some features of the results from the simulations with lightning emissions stand out as being different from that in the ZERO run. These features occur as ozone peaks in April in the northern tropics (most notably at 500 hPa)(Figure 3.5D) and in October in the southern tropics (most notably at 250 hPa)(Figure 3.5A). The northern tropics peak in ozone improves the comparison to sondes at 500 hPa, if slightly underestimated. However, the 250 hPa April peak in Figure 3.5B does not appear in any of the model simulations. Potentially, the modelled advection is not transporting the lightning NO_x emissions or ozone produced to high enough altitudes. An anomalous southern tropical peak in March in Figures 3.5A and C, particularly shown by CTH, is not shown in the

sonde measurements, but this corresponds to a month where the CTH scheme especially is overestimating lightning, as seen in Figure 3.2. The ICEFLUX scheme is a much closer match to the lightning activity in the southern tropics in March and correspondingly the modelled ozone is less anomalous compared to the ozone sonde measurements in that month. The well modelled lightning activity in the southern tropics in October (Figure 3.2C) results in a correctly matched peak in the ozone sonde measurements at both pressure levels which does not occur in the ZERO run. From these comparisons to ozone sondes I conclude that the lightning emissions have impacts in particular months which include the months of peak ozone. Figure 3.2 shows that these are not necessarily the month of highest lightning activity in the region, but instead as the lightning activity builds in the region. It may be of particular use for field campaigns studying the chemical impact of lightning to focus on these months and, as discussed in Section 3.3.1, South America could provide a useful region in which to develop understanding of lightning activity and therefore also its impacts on tropospheric chemistry.

3.4 The influence of lightning on the global annual O_x budget

The O_x budget considers the production and loss of odd oxygen in the troposphere. Several studies have used O_x budgets to study tropospheric ozone (Stevenson *et al.*, 2006; Wu *et al.*, 2007; Young *et al.*, 2013; Banerjee *et al.*, 2014). Here, the O_x approach has particular use because it responds more directly to the emission of NO than O_3 which may form in outflows of storms and take several days to fully convert between O_x species (Apel *et al.*, 2015).

There are different definitions of O_x family species and here a broad definition is used that includes O_3, O(1D), O(3P), NO_2 and several NO_y species (Wu *et al.*,

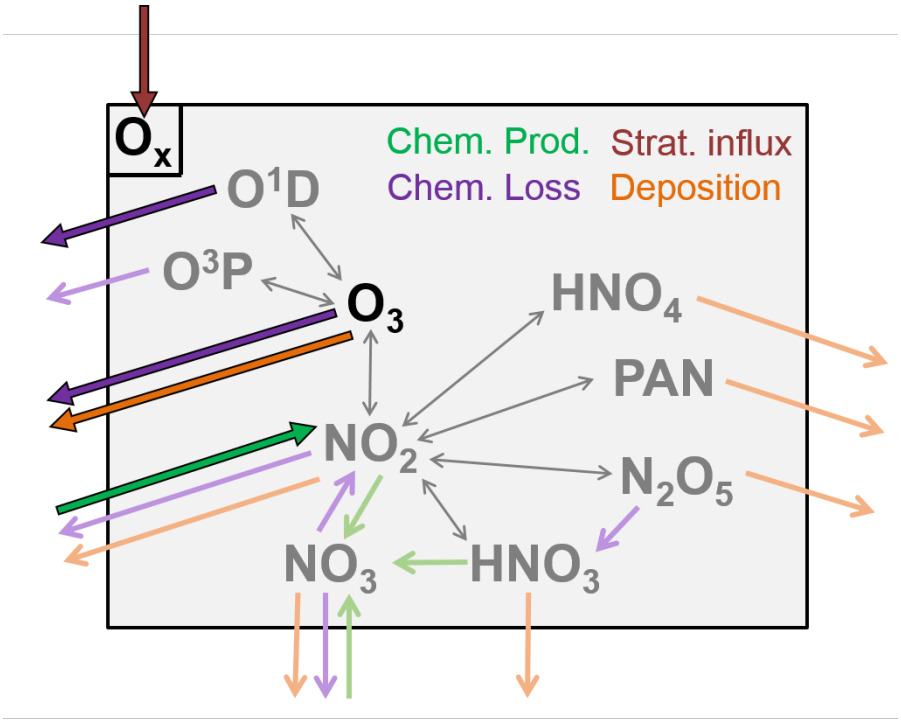

Figure 3.6: The UKCA definition of O_x species and the O_x budget. Major contributors are shown in bright colours and black outlines, minor contributors in pale colours. Grey arrows are reactions between O_x species and therefore result in no production or loss. The stratospheric influx is not determined for individual species. Instead the total O_x influx is inferred to balance the production and loss terms. The burden and stratospheric influx of O_x are dominated by the burden and stratospheric influx of O_3.

2007). The O_x species and the different terms of the budget are illustrated in Figure 3.6. Of particular relevance to this chapter is the chemical production of O_x, the majority of which occurs through oxidation of NO to NO_2 by peroxy radicals. The ozone burden is considered along with the budget terms as it is the key species of interest and it makes up the majority of the O_x burden.

The global annual O_x budgets for CTH, ICEFLUX and ZERO are given in Table 3.2. These budget terms are for the troposphere. Here, the tropopause is defined at each model time step using a combined isentropic-dynamical approach based

Table 3.2: Global annual tropospheric O_x budget terms for the year 2000 for three different simulations: CTH, ICEFLUX and ZERO. All terms in Tg yr^{-1} except Burden which is in Tg and lifetime which is in days. The percentage difference with respect to the CTH budget is shown in brackets. In addition to the tropospheric budget terms, the whole atmospheric ozone burden is also included. Stratospheric influx is inferred to complete the O_x budget through balancing the chemical loss and production and deposition.

	CTH	ICEFLUX	ZERO
Chem. prod.	4472	4443 (-1%)	3638 (-19%)
Chem. loss	3848	3821 (-1%)	3115 (-19%)
Net chem. prod.	624	622 (0%)	522 (-16%)
Deposition	1006	1006 (0%)	899 (-11%)
Strat. influx*	382	384 (0%)	376 (-2%)
Trop. O_3 burden	267	261 (-2%)	205 (-23%)
Whole atm. O_3 burden	3253	3240	3162
τ_{O_3}	19.8	19.5 (-2%)	18.4 (-7%)

on temperature lapse rate and potential vorticity (Hoerling *et al.*, 1993). Clearly, the ZERO simulation demonstrates the large control that lightning has on these budget terms with changes of around 20% in the ozone burden and chemical production and losses when lightning NO_x emissions are removed (Table 3.2). The O_x budget for the ZERO simulation shows that through reduced ozone production, there is reduced ozone burden and therefore chemical losses and deposition fluxes are reduced. The lifetime of ozone is given by the burden divided by the losses. Since the burden decreases more than the losses, the ozone lifetime reduces overall, although to a lesser extent than the burden and loss terms individually.

There is uncertainty in the global lightning NO_x source of 2-8 TgN emissions (Schumann and Huntrieser, 2007), and there will be an associated uncertainty in

the O_x budgets. Using no lightning (ZERO) corresponds to a reduction of 5 TgN emissions over the year - less than the range of uncertainty in LNO_x. Therefore large changes in O_x budget terms can be expected within the uncertainty range of the global lightning NO_x emission total. In contrast, it would seem that for constant emissions of 5 TgN and a reasonable change in the flash rate distribution by using the ICEFLUX approach instead of the CTH approach, there are only small differences in the global O_x budget terms. The largest differences between the O_x budgets of the ICEFLUX and CTH approaches are in the ozone burden and lifetime but these are only 2 %.

The O_x budget discussed so far represents the troposphere, but if the whole atmospheric ozone burden is considered (Table 3.2) then it is apparent that there is also a reduction in ozone in stratosphere which must be due to changes in the troposphere-stratosphere exchange of ozone. Previous studies have also found that ozone produced from lightning is transported into the lower stratosphere (Grewe *et al.*, 2002; Banerjee *et al.*, 2014). In this chapter, I quantify the different transport between the two lightning schemes by considering differences in whole atmospheric ozone burden against differences in tropospheric ozone burden. The whole atmospheric ozone burden simulated with the ICEFLUX approach is 13 Tg less than that simulated by the CTH approach. Given that the tropospheric ozone burden simulated by the ICEFLUX approach is only 6 Tg less than that of the CTH approach, this means that the majority of the difference in ozone burden ($\sim$55%) occurs in the stratosphere. On the other hand, the whole atmospheric ozone burden simulated in the ZERO run was 91 Tg less than that of the CTH approach. The tropospheric ozone burden was 62 Tg less so accounts for around two thirds of the total difference in this case. The ICEFLUX approach has resulted in less lightning emissions in the upper tropical troposphere and therefore less ozone is available in the region to be transported into the stratosphere. Such a change in the lightning distribution, whilst maintaining the same level

of total emissions, results in reduced net ozone production but much, and even the majority, of this reduction in ozone can occur in lower stratospheric ozone.

3.5 Differences in the zonal-altitudinal distributions of O_x and O_3 between the two lightning schemes

In the previous section, it was demonstrated that the global tropospheric O_x budget is affected principally by the magnitude of emissions and not the location of emissions. This was achieved by using the same total emissions but different distributions of lightning in the CTH and ICEFLUX approaches (Figure 3.1), which simulate little difference in the global O_x budget terms. This section now considers changes in the zonal and altitudinal location of O_x chemistry and ozone concentration as a result of changes in the lightning emission distribution. The zonal-altitudinal net chemical O_x production, as well as its components of gross production and loss, are shown in Figure 3.7A-C for the CTH scheme as well as changes as a result of using ICEFLUX instead of CTH in Figure 3.7D-F.

The difference in net O_x production when using the ICEFLUX scheme compared to the CTH scheme is dominated by the change in gross production (Figure 3.7D and E). Figure 3.7E shows a shift away from the tropical upper troposphere to the middle troposphere and the subtropics. There is over a 10% reduction in the upper troposphere net production and 100% changes in the subtropics (Figure 3.7D). However, the high subtropical percentage change is principally due to small net production in these regions. The changes in O_x production result as a shift in emissions which happens by: 1) reduced and more realistic lightning in the tropics (see Figure 3.8), and 2) decoupling of the vertical and

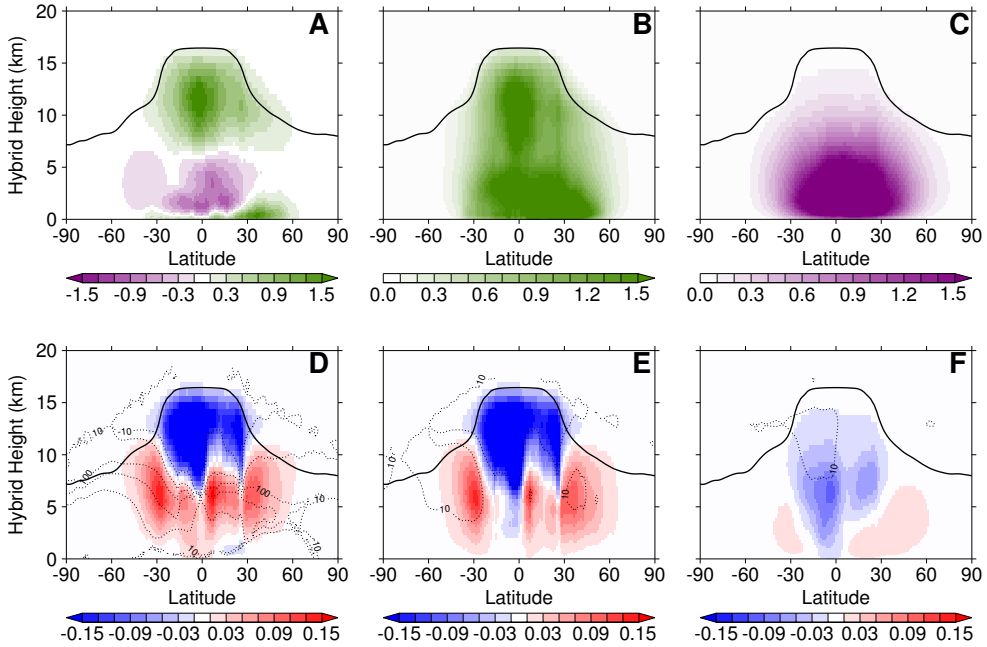

Figure 3.7: Annual total zonal-altitudinal distributions of O_x reaction fluxes for CTH for the year 2000. These fluxes are A) Net production, B) gross production, and C) gross loss of O_x. The respective differences between simulations using the ICEFLUX scheme and the CTH scheme are shown in D-F. All units are Tg(O_3). Values are annual and meridional totals. The solid line is the annual mean tropopause and dashed lines contour 10% and 100% changes. The O_x fluxes were masked with the model tropopause every time step.

horizontal emissions distributions by not using cloud-top in both aspects (as is the case in CTH). As described in section 3.2.2, the column LNO_x is distributed up to the cloud-top, and this is how a coupling exists between the horizontal LNO_x distribution simulated by the CTH approach and the height that LNO_x emissions reach. This means that, by basing the horizontal lightning distribution on cloud-top height and then distributing emissions to cloud top, LNO_x is most effectively distributed to higher altitudes. Hence, a lightning parametrisation for which the horizontal distribution is different to that of cloud-top height will, to some extent, naturally distribute emissions at lower altitudes. This is demonstrated best in Figure 3.7E which shows gross production in the northern tropics. Whilst both lightning schemes have similar total lightning at these latitudes (shown in Figure 3.8), and therefore similar column O_x production, the gross O_x production occurs less in the upper troposphere and more in the middle troposphere when using the ICEFLUX scheme.

Results with the ICEFLUX approach are consistent with observations of the zonal distribution of lightning, i.e. that there is less lightning in the tropics than estimated by CTH here. The results are also consistent with current understanding that the most intense lightning flash rates do not always occur in the highest clouds. I would therefore suggest that the change to the net O_x production using the ICEFLUX approach is a more realistic representation of the distribution of production than with the CTH approach. The improved sonde correlations presented in section 3.3.2 support this conclusion.

Whilst O_x gross production changes, mainly representing oxidation of NO to NO_2 by peroxy radicals, show a close resemblance to the lightning NO emissions changes, they are only part of the picture with regard to changes in the distribution of ozone. This is because the lifetime of ozone is much longer than the timescales for NO forming an equilibrium with NO_2. Furthermore, ozone precursors are transported downwind of convection, and into the stratosphere by

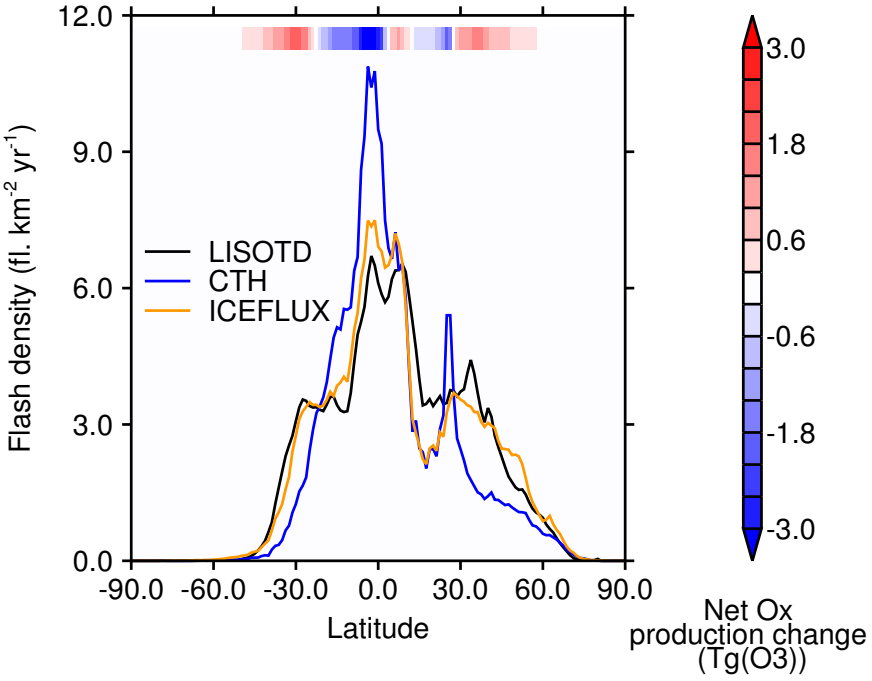

Figure 3.8: Zonal mean lightning flash rate from the LIS/OTD climatology and as modelled by CTH and ICEFLUX. The zonal changes in net tropospheric column O_x production (ICEFLUX-CTH) are shown by the colour bar. The units of O_x are expressed as a mass of ozone.

means of overshooting convection, before they form ozone. The difference in O_x production (Figure 3.7) between the two lightning schemes influences not only ozone locally but also downwind where ozone is transported to. Additionally, the differences in Ox production in the stratosphere due to differences between the two schemes will influence the ozone distribution. The differences in stratospheric O_x production of Figure 3.7 have been masked out to focus on the troposphere. These stratospheric differences will be much smaller than differences in the upper troposphere since the upper troposphere is where the majority of LNO_x is formed and where O_x production is most efficient. As in the troposphere, stratospheric O_x production and loss, and the balance of the two, will depend on the chemical environment.

Figure 3.9 presents the percentage changes in ozone distribution as a result of using the ICEFLUX scheme instead of the CTH scheme. There is reduced tropical upper tropospheric ozone of up to 10% (Figure 3.9) due to reduced NO emission in that region. This results in less ozone transported into the lower stratosphere under the ICEFLUX scheme compared to the CTH scheme. The lower stratospheric ozone may also be lower due to less NO_x being available for transport, and therefore reduced chemical production in the stratosphere. Whilst ozone is lower in most of the lower stratosphere in the simulation with ICEFLUX the percentage changes are largest (up to 5%) nearer to the tropopause.

In the middle and lower tropical troposphere there is also a reduction in ozone concentration (Figure 3.9) despite increased net O_x production (Figure 3.7D). This is because there is less ozone produced in the upper troposphere, and therefore there are lower ozone concentrations in the air transported within the vertical circulation in the tropics. In the southern tropics, the net O_x production increase is due to reduced O_x loss as a result of lower ozone concentrations in the region. Note that both schemes experience the same meteorology because the chemistry is not coupled. The percentage changes in ozone in the northern tropics

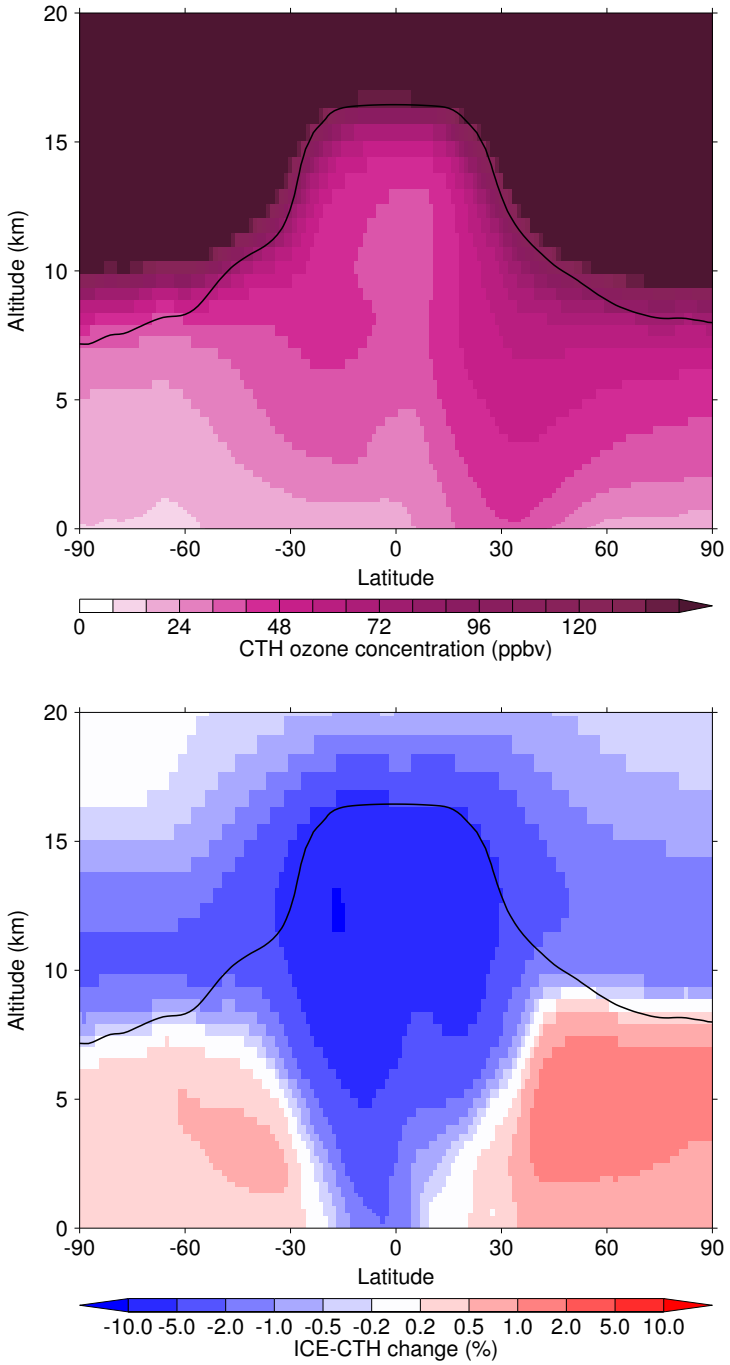

Figure 3.9: Annual mean distribution of ozone concentration modelled using the CTH approach, and the percentage difference between ICEFLUX and CTH simulated ozone concentration. The solid line shows the mean annual tropopause as diagnosed using the modelled meteorology.

are less than in the southern tropics (Figure 3.9). This is likely to be in part due to offsetting through increased lightning emissions in the northern tropical middle troposphere. Finally, the increased lightning emissions in the subtropics with the ICEFLUX compared to the CTH scheme results in small changes in ozone throughout the extratropics.

It is worth noting that OH concentrations (not shown) respond in a similar manner to ozone concentration with the change from the CTH to the ICEFLUX scheme. These changes are more localised to emission changes but are still apparent in the lower stratosphere and extratropics. A change from the CTH to ICEFLUX scheme results in only small changes in the methane lifetime as a result of the changes in OH. Hence, in this setup it is not expected that ozone changes would be greatly modified with the use of interactive methane.

Liaskos *et al.* (2015) identified that even with the same total global emissions, the magnitude and distribution of radiative forcing resulting from lightning emissions is dependent on the method for distributing the emissions horizontally and vertically. The changes in zonal-altitudinal distribution discussed in this section show that these changes could be expected as a result of changes in ozone in the upper troposphere.

3.6 Frequency distributions of lightning and associated O_x production

Lightning is a highly dynamic process. This section presents analysis of the frequency distribution of flash rates as a means to study the finer scale effects.

The CTH scheme simulates extremely low flash rates over the ocean. For

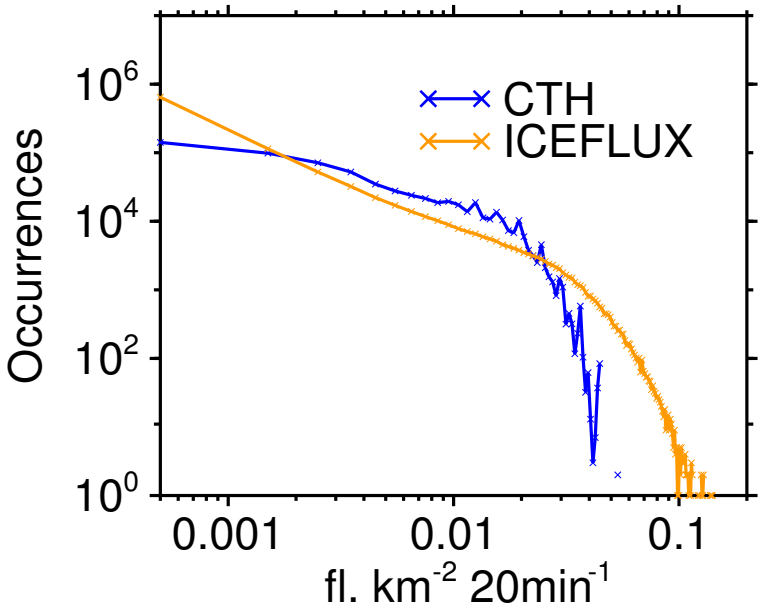

Figure 3.10: Frequency distribution of continental lightning flash rates using all time steps, for one month (September 2000) as modelled by the CTH and ICEFLUX schemes. The binsize used is 0.001 fl. $\mathrm{km}^{-2}20\mathrm{min}^{-1}$ with crosses placed at the centre value of each bin.

instance, the maximum September oceanic flash rate using CTH was 1.1×10^{-4} fl. $\mathrm{km}^{-2}\,20\mathrm{min}^{-1}$ where as using ICEFLUX the maximum was over 100 times greater. This difference is not surprising given the difference in annual oceanic lightning activity shown in Figure 3.1. CTH tends to underestimate ocean lightning compared to satellite observations. The focus here will be on continental lightning. Other studies of frequency distribution in the literature have also focussed on continental locations so this work can be more directly compared to those.

Figure 3.10 shows the hourly continental flash rate frequency distribution for one model month (September). September was chosen as a month with a reasonable balance of lightning activity between the hemispheres and where total lightning activity, and therefore emissions, was similar for the two lightning schemes.

When compared to the frequency distribution simulated by ICEFLUX, CTH has lower maximum flash rates, fewer occurrences of low flash rates and more occurrences of mid-range flash rates (Figure 3.10). Other studies have drawn similar conclusions regarding the frequency distributions of CTH when comparing to other parametrisations and lightning observations (Allen and Pickering, 2002; Wong *et al.*, 2013). The ICEFLUX approach produces a similar distribution to that produced by the same scheme applied in Chapter 2. In that chapter (Figure 2.5), the ICEFLUX frequency distribution had a fairly average distribution compared to four other lightning parametrisations with slightly more occurrences of low flash rates.

In Figure 3.10, the CTH frequency distribution displays some unusual periodic characteristics in the occurrence rate, most notably towards high flash frequencies. These features are also apparent in the cloud-resolving simulations presented in Wong *et al.* (2013). I suggest here that these features may arise due to discretised nature of the cloud-top height input variable.

The importance of the global flash rate frequency distribution to atmospheric chemistry frequency distributions is currently unknown but simplified model studies have suggested some key features:

- Compared to a set of observations over the US, a simulation using the CTH approach led to a greater ozone production efficiency due to the non-linear nature of ozone production and NO_x (Allen and Pickering, 2002).

- Total ozone production increased approximately linearly up to 300 pptv of lightning NO_x and then increased at a slower rate beyond that. This may be due to the ozone production approaching the maximum possible for the given altitude, solar zenith angle and HO_x concentration (DeCaria *et al.*, 2005).

In the following analysis, O_x production rather than ozone production is considered because it exhibits a more immediate response to NO emission. This is important given the difficulty and errors associated with tracking ozone production associated with each emission source in a global model. However, there are some comparable results which I will compare to the previous findings above, as well as new insights into the consequences of different frequency distributions and lightning parametrisations.

Figure 3.11 presents two metrics of the gross column chemical O_x production resulting from continental lightning in each of the frequency bins of Figure 3.10. The metrics are: A) the mean column O_x production, and B) the mean O_x production per flash. Each flash corresponds to 250 mol(NO) emission so the O_x production per mole of emission can easily be inferred from the O_x production per flash. O_x production resulting from lightning is calculated as the difference between the model run with lightning and the model run with no lightning, using the grid cells from the no lightning run that correspond to the cells used in each bin for the relevant lightning parametrisation. This means that this work is focussing on the *initial* O_x production occurring in the 20 minute time step in which emissions are produced. Where grid cells are close to other grid cells containing lightning there will be some cross-transport of LNO_x and associated O_x production. However, for the average over all grid cells containing lightning this is likely to be small. The initial O_x production described above has been calculated to be approximately 15% of total O_x production associated with lightning for both parametrisations. The calculation was made as the difference between the total O_x production resulting from lightning in the sampled grid cells and the total O_x production resulting from lightning over the whole globe in all time steps. The remaining 85% of production must occur after the initial time step and be a result of advected emissions or changes to the large-scale distributions of constituents such as ozone or OH as discussed in section 3.5.

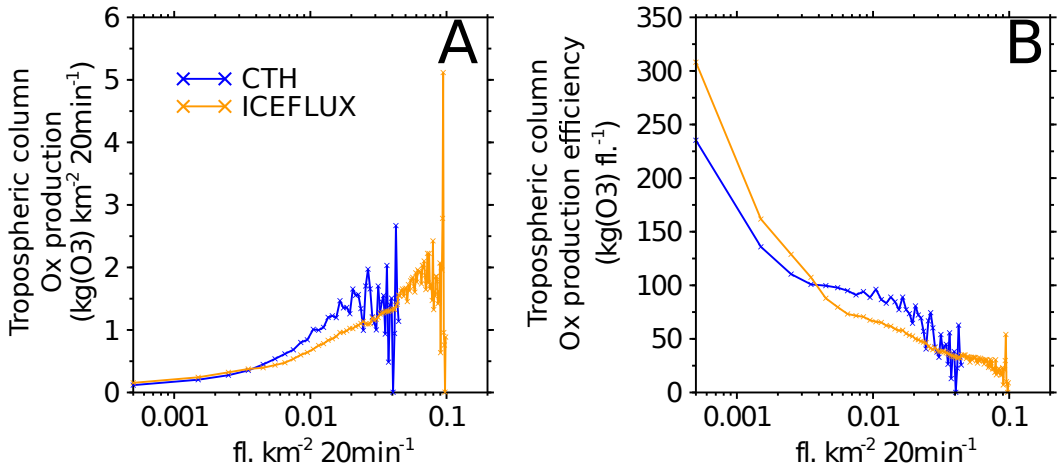

Figure 3.11: Two metrics of initial gross column O_x production as a result of continental lightning simulated by the CTH and ICEFLUX schemes. The cells used in each bin correspond to those used in Figure 3.10. The metrics are A) mean column O_x production in each bin, and B) mean column O_x production per flash in each bin. The O_x production resulting from lightning was determined by subtracting the column O_x production in the no lightning run from the each lightning parametrisation for the corresponding cells. To reduce noisiness, data is only plotted up to the highest bin of each parametrisation where there are at least two occurrences in Figure 3.10. The units of O_x are expressed as a mass of ozone.

The mean column O_x production in Figure 3.11A shows, as expected, that increasing flash rate (i.e. more NO emissions in a cell) results in increased column O_x production. The higher extreme flash rates of ICEFLUX compared to CTH result in greater column O_x productions as a result of individual occurrences. A linear increase in O_x production is apparent up to approximately $0.02\,\mathrm{fl.\,km^{-2}\,20min^{-1}}$ at which point the two schemes produce 1 to $1.5\,\mathrm{kg\,km^{-2}\,20min^{-1}}$ of O_x. Beyond this point, the O_x production simulated by the ICEFLUX approach increases still linearly but with a shallower gradient. The ICEFLUX scheme produces less O_x for a given flash rate than the CTH scheme at higher flash rates but more at lower flash rates (Figure 3.11A). This is due to emissions from high flash rates in ICEFLUX not necessarily being distributed to such high altitudes as with CTH. At the higher altitudes that emissions reach when using the CTH scheme, NO_x has a greater ozone production efficiency, as discussed in section 3.5. Conversely, in the ICEFLUX scheme, lower flash rates can occur in relatively deeper cloud so in these there can be greater O_x production efficiency compared to the CTH scheme because the CTH scheme will always place these low flash rates at lower altitudes. On larger scales, whilst high extreme flash rates produce more O_x, they occur relatively infrequently so do not greatly affect the global O_x budget.

Figure 3.11B shows the mean column O_x production per flash for each flash rate bin. It is derived by dividing the data in Figure 3.11A by the mid-point flash rate of each bin. Whilst Figure 3.11A shows that lower flash rates produce less O_x, they do produce O_x more efficiently than higher flash rates. Flash rates of $0.0005\,\mathrm{fl.\,km^{-2}\,20\,min^{-1}}$ produce ~ 10 times more O_x per flash than flash rates of $0.05\,\mathrm{fl.\,km^{-2}\,20min^{-1}}$. This suggests that as the NO increases, NO_x cycling and therefore ozone production decreases in efficiency. This is likely a result of peroxy radical availability and VOC abundance limiting the rate of NO_x cycling (Section 1.4.2). Evidence for such control of VOC precursors on ozone production in US thunderstorms has been presented by Barth *et al.* (2012).

ICEFLUX displays the greatest contrast in efficiency between high and low flash rates of the two parametrisations (Figure 3.11B). As with the column mean production, because the CTH scheme places the most emissions in the highest cloud tops it is more efficient at producing O_x at higher flash rates but the ICEFLUX scheme is more so at lower flash rates. Using the NO production per flash of 250 mol(NO) fl.$^{-1}$ stated in Section 3.2.2, the range of initial O_x production per mol of emission is 25 mol(O_x) mol^{-1}(NO) at low flash rates for ICEFLUX to less than 2 mol(O_x) mol^{-1}(NO) for the highest flash rates in the ICEFLUX scheme (Figure 3.11B).

In summary, and as found by Allen and Pickering (2002), O_x production becomes less efficient at higher flash rates. It is important to consider that, with the method used here, the higher flash rates are less efficient at the point of emission - the emissions may go on to produce O_x elsewhere following advection. Also, similarly to DeCaria *et al.* (2005), it is found that the mean column O_x production increases linearly up to a point, in this chapter 0.02 fl. km^{-2} 20min^{-1}, then increases at a slower, but still linear rate beyond that. New insights provided through the use of a global model are:

- Both lightning schemes produce about 15% of the O_x associated with lightning in the first 20 minutes after the time of emission

- For the CTH approach, oceanic flash rates are so low that associated O_x production at the time of emission is negligible for the global production

- Because CTH places the most emissions in the highest clouds (where ozone production efficiency is greater), more O_x is produced by the CTH scheme than ICEFLUX at high flash rates, but ICEFLUX produces more at low flash rates

- Initial O_x production per flash is approximately 10 times greater for low flash rates than high-end flash rates

These findings regarding the O_x production per flash provide a useful metric to evaluate lightning parametrisations with observations. Several differences between the CTH and ICEFLUX scheme suggest further study is needed to determine the true nature of O_x production. For instance, the almost negligible proportion of O_x production that will occur over the ocean when using the CTH scheme due to very low flash rates would benefit from oceanic measurements of ozone and NO_x in the vicinity of storms. This chapter has analysed the O_x production occurring in the first 20 minutes, but further O_x production can occur over longer time periods. An extension of the work here could be to run idealised experiments of pulse lightning emissions in a global model to see how the O_x and ozone production develop with time and hence, assess the lag between NO emission and ozone production.

3.7 Conclusions

A new lightning parametrisation based on upward cloud ice flux, developed in Chapter 2, has been implemented in a chemistry-climate model (UKCA) for the first time. It is a physically based parametrisation closely linked to the Non-Inductive Charging Mechanism of thunderstorms. The horizontal distribution and annual cycle of flash rates as calculated through the new ice flux approach and the commonly-used, cloud-top height approach were compared to the LIS/OTD satellite climatology. The ice flux approach is shown to generally improve upon the performance of the cloud-top height approach. Of particular importance is the realistic representation of the zonal distribution of lightning using the ice flux

approach, whereas the cloud-top height approach overestimates the amount of tropical lightning and underestimates extra-tropical lightning.

The ice flux approach greatly improves upon the cloud-top height approach in UKCA with regards to the temporal correlation to the observed annual cycle of ozone in the middle and upper tropical troposphere. Through considering a simulation without emissions and the simulated annual cycle of lightning, it is clear that the ice flux approach reduces the biases in ozone in months where the cloud-top height approach has the largest errors in simulating lightning.

The zonal flash rate distribution when using the ice flux approach instead of the cloud-top height approach results in a shift of O_x production away from the upper tropical troposphere. As a consequence there is a 5-10% reduction in upper tropical tropospheric ozone concentration along with smaller reductions in the lower stratosphere and small increases in the extratropical troposphere. These changes in ozone concentration are a result of the change in distribution of lightning emissions only, the total global emissions are the same for both schemes. I conclude that biases in zonal lightning distribution of the cloud-top height scheme increase ozone in the upper tropical troposphere and, as demonstrated by comparison to ozone sondes, this reduces the correlation to observations in ozone annual cycle in this region.

Analysis of the continental flash rate frequency distribution shows the cloud-top height approach has lower high-end extreme flash rates, more frequent mid-range flash rates and less frequent low-end flash rates, compared to the frequency distribution using the ice flux approach. Such features simulated by the cloud-top height approach have been found in comparisons to the observed frequency distribution over the US and this current evidence suggests such a frequency distribution is unrealistic. A novel analysis is applied to determine the impact of the differences in flash rate frequency distribution on the initial O_x production

resulting from lightning emissions. As expected, the higher the flash rate, the more O_x is initially produced. However, the O_x production efficiency reduces for higher flash rates; lower flash rates initially produce approximately 10 times as much O_x as higher flash rates. Further study is warranted to determine how emissions produce ozone downstream of a storm in complex chemistry models, but the result here is relevant to aircraft campaigns measuring NO_x and ozone near to the thunderstorms. It would be useful to study such measurements to determine if less intense storms exhibit such a difference in O_x production efficiency.

The global lightning parametrisation using upward cloud ice flux has proven to be robust at simulating present-day annual distributions of lightning and tropospheric ozone. The reduced ozone in the upper tropical troposphere could be important for the understanding of ozone radiative forcing. In addition, the differences in the frequency distribution when using different lightning schemes is shown to affect the chemical O_x production. The parametrisation is appropriate for testing in other chemistry transport and chemistry-climate models where it will be important to determine how the parametrisation behaves using different convective schemes. Furthermore, this new parametrisation offers an opportunity to diversify the estimates of the sensitivity of lightning to climate change which will be the focus of Chapter 5.

Chapter 4

Response of lightning NOx emissions and ozone production to climate change: Insights from the Atmospheric Chemistry and Climate Model Intercomparison Project

This chapter has been published as an open-access letter in Geophysical Research Letters (GRL) in collaboration with: Dr Ruth Doherty, Dr Oliver Wild, Dr Paul Young and Dr Adam Butler. The letter and supplementary material is available online from the GRL website (http://onlinelibrary.wiley.com/doi/10.1002/2016GL068825/full). The supplementary material has either been incorporated into the main text or added as supplementary material at the end of the chapter. I did the analysis and wrote

the initial draft. My supervisors and other co-authors provided feedback before the manuscript was submitted for publication. Dr Paul Young processed the raw ACCMIP data of emissions, surface temperature and ozone production to produce annual values for each time-slice and model. Dr Adam Butler advised on technical aspects of the statistical method.

Finney, D. L., Doherty R. M., Wild O., Young P. J., and Butler A. (2016), Response of lightning NOx emissions and ozone production to climate change: Insights from the Atmospheric Chemistry and Climate Model Intercomparison Project, Geophysical Research Letters, **43**, 5492?5500, doi:10.1002/2016GL068825.

4.1 Introduction

Lightning is the dominant source of nitric oxide in the upper troposphere. In this region of the atmosphere, nitrogen oxides (NO_x) are much more efficient at catalysing ozone production than surface emissions (Wild, 2007; Wu *et al.*, 2007; Dahlmann *et al.*, 2011). Lightning, driven by meteorological conditions, is expected to respond to any future changes in climate (Section 1.7). Understanding the sensitivity of this response is important for assessment of future ozone concentrations and associated radiative forcing. In addition, the radiative forcing from methane, which is indirectly influenced by NO_x through reactions with OH, is affected by changes in lightning (Section 1.4.2).

Observational studies suggest that warmer surface temperatures are correlated with increased lightning across diurnal to interannual timescales, although whether such a relationship also applies to longer term climate change remains uncertain (Williams, 2005). Estimates from chemistry-climate models suggest that lightning NO_x emissions will increase by 4-60% per degree increase in global

mean surface temperature (Schumann and Huntrieser, 2007). More recent estimates have been: $5.5\,\%\,K^{-1}$ (Zeng *et al.*, 2008), $10\,\%\,K^{-1}$ (Jiang and Liao, 2013) and $16\,\%\,K^{-1}$ (Banerjee *et al.*, 2014). The value for Jiang and Liao (2013) was calculated from the LNO_x change published and with a temperature change of 1.6 K over the period 2000-2050 (Hong Liao, pers. comm., 27 July 2015).

There is a gathering concensus on the sensitivity of lightning NO_x emissions to climate, but this may primarily be due to the similarity of lightning parametrisations used in most models. One isolated study using an alternative lightning parametrisation based on ice particle collisions (Jacobson and Streets, 2009) found that lightning NO_x emissions decreased as temperatures increased.

The approach used in most global scale models applies a relationship between cloud-top height and lightning (Price and Rind, 1992; Price *et al.*, 1997), as has been evaluated in Chapters 2 and 3. This cloud-top height relationship provides a reasonable proxy for lightning activity but has several limitations. These include a high sensitivity to any biases in modelled cloud-top height and a relatively indirect link to the underlying physical processes (Tost *et al.*, 2007; Wong *et al.*, 2013) (Section 1.6), which are described by the non-inductive charging theory of storms (Reynolds *et al.*, 1957) (Section 1.2). Other parametrisations, related to convection (e.g. Meijer *et al.*, 2001; Allen and Pickering, 2002; Grewe *et al.*, 2001; Romps *et al.*, 2014) or cloud ice (e.g. Deierling *et al.*, 2008; Jacobson and Streets, 2009; Basarab *et al.*, 2015, and Chapter 2), have been demonstrated successfully in individual studies but have yet to be widely adopted (Section 1.6). To date there has been little investigation into how these alternative approaches respond to climate change.

The recent Atmospheric Chemistry and Climate Model Intercomparison Project (ACCMIP) provides lightning NO_x emission (LNO_x) distributions from 12 models using three distinct interactive lightning parametrisations under past, present-day

Table 4.1: Time slice experiments used (X) in addition to a year 2000 baseline for each model. Models and time slice experiments used in the mixed model regression of ozone production in addition to the year 2000 baseline experiments are marked with *.

	1850	1980	2030 RCP2.6	2100 RCP2.6	2030 RCP4.5	2100 RCP4.5	2030 RCP6.0	2100 RCP6.0	2030 RCP8.5	2100 RCP8.5	Total
CESM-CAM-superfast*	X*	X*	X*	X*			X*	X*	X*	X*	8
CMAM*	X*	X*			X*	X*			X*	X*	6
EMAC	X	X			X	X				X	5
GFDL-AM3*	X*	X*	X*	X*	X*	X*	X*	X*	X*	X*	10
GISS-E2-R	X	X	X	X	X	X	X	X	X	X	10
HadGEM2	X	X		X		X				X	5
LMDzORINCA	X	X	X	X			X	X	X	X	8
MIROC-CHEM*	X	X	X*	X*			X*	X*	X*	X*	8
MOCAGE	X	X	X	X			X	X	X	X	8
NCAR-CAM3.5	X	X	X	X	X	X	X	X	X	X	10
STOC-HadAM3*	X*	X*	X*	X*					X*	X*	6
UM-CAM*	X*	X*	X*	X*	X*	X*			X*	X*	8
Total	12	12	9	10	6	7	7	7	10	12	92

and a range of future emission scenarios (Lamarque *et al.*, 2013). There are 92 relevant multi-year time slice experiments to compare to a multi-year baseline centered around the year 2000 (Table 4.1), allowing a more complete assessment of lightning sensitivity than has been possible in any previous study.

The availability of three distinct parametrisations allows an exploration of how the choice of parametrisation is important for the emission response to climate change. Ten of the models use the same lightning parametrisation based on cloud-top height (Price and Rind, 1992), and this allows for the the most rigorous assessment of the climate response of the cloud-top height approach to date. A subset of models, from which ozone production was archived, is then used to explore how these climate-driven changes in lightning NO_x emissions can influence global ozone production.

4.2 Statistical Methods

A linear regression assumes independence of data points. However, data produced using the same model share a dependence. To determine robust estimates of the standard errors of regression coefficients when using a multi-model dataset such as in this chapter, it is appropriate to use a linear mixed effect regression.

Linear mixed effect regressions are extensions of linear regression models which include random effects as well as fixed effects (Pinheiro and Bates, 2000; Bolker *et al.*, 2008). Fixed effects are either numeric or categorical variables for which interest lies in the specific effects of each category. Random effects are categorical variables for which the effects of each category can be regarded as being sampled from a larger population of possible categories, so that interest lies in variation between categories.

In the context of this chapter, the inclusion of 'model' as a random effect allows for differences in model configuration to be accounted for (through random effects) while estimating the role of explanatory variables (as fixed effects). Both applications of a linear mixed effect regression in this chapter use a random-slope regression which determines an individual slope and intercept, the random effect, for each model. The random slopes and intercepts are assumed to be correlated.

As with a simple linear regression, it is useful to calculate the variance explained by the regression model, the R^2 value. For linear mixed effect models two values of R^2 can be calculated: the *marginal* R^2, reflecting the proportion of the variance explained by fixed effects, and the *conditional* R^2, reflecting the variance explained by both fixed and random effects (Nakagawa and Schielzeth, 2013; Johnson, 2014). The marginal R^2 is an estimate of the predictive capability of the fixed effects, whereas the conditional R^2 represents the the variance explained in the dataset and models used in this chapter.

The linear mixed effect regressions were carried out using R, for which the statistical methods are described by Pinheiro and Bates (2000). The steps below describe the R packages and functions used to carry out the analysis:

1. From the package *lmerTest*, a linear mixed effect regression can be fitted using *lmer* where a correlated mixed-slope effect for LNOx with each chemistry-climate model (chemModel) is included with the term $(LNOx|chemModel)$.

2. The use of the function, *summary*, provides the details of the regression including coefficients, standard errors and p-values for each fixed effect. Random effect coefficients are displayed using the function, *ranef*.

3. Significance of the random effects can be determined with a likelihood ratio test provided by the function, *rand*.

4. The R package *MuMIn*, includes the function, *r.squaredGLMM*. The use of this function on the regressed fit implements the statistical analysis described by Nakagawa and Schielzeth (2013) and Johnson (2014) to determine the marginal and conditional R^2 of the linear mixed effect regression. In the case of a random-slope regression it is necessary to use version 1.10.0 or later of the *MuMIn* package, which includes the extension of Johnson (2014).

5. The *step* function can be used to perform the AIC stepwise selection process.

4.3 Response to Temperature

Generation of thunderstorms is only partly related to the surface temperature, and reflects local rather than global conditions. However, based on past studies (Section 1.7), surface temperature provides a simple proxy for changes in the atmosphere that affect lightning.

Figure 4.1A shows the relationship between total annual lightning NO_x emissions and global mean surface temperature. Each data point is from a single time slice experiment, averaged over multiple years as specified in Table 2 of Lamarque *et al.* (2013), where each year has identical anthropogenic and biomass burning emissions. The data used encompasses time slices of the present-day baseline, historical 1850 and 1980 simulations, and all future scenarios using the Representative Concentration Pathways (RCPs) produced by each model. A significant linear relationship between LNO_x and surface temperature is evident for each model. This is the first time enough comparable data have been produced from a range of models to allow robust conclusions regarding the form of the relationship.

Despite the clear conclusion that each model exhibits a linear relationship,

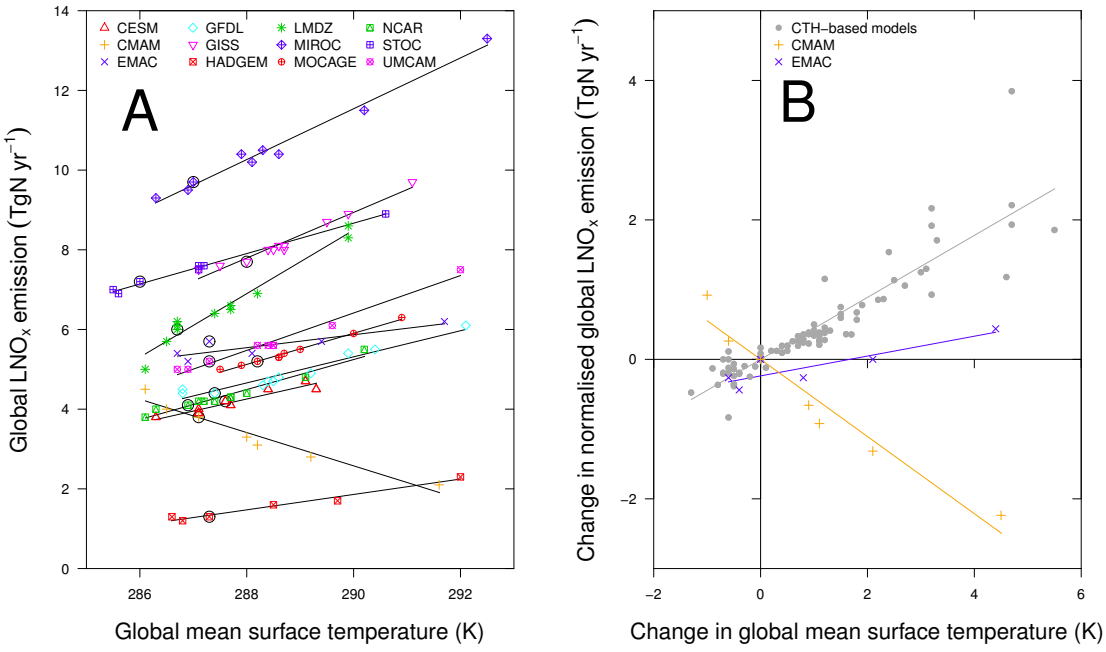

Figure 4.1: Total annual lightning NO_x emissions against global mean surface temperature for the ACCMIP models with interactive lightning schemes. Absolute global emissions and surface temperatures are shown in panel (A); changes in lightning NO_x emissions with respect to the year 2000 baseline, normalised to 5 TgN in year 2000, and grouped according to lightning parametrisation are shown in panel (B). Circled points in A are from the year 2000 baseline simulations.

Figure 4.1A shows a substantial spread between the models. Sources of inter-model spread include the magnitude of the baseline emissions, which vary from 1.3 to 9.7 $\mathrm{TgN\,yr^{-1}}$, and differences in the baseline mean surface temperature which ranges from 286.0 to 288.2 K (see circled points Figure 4.1A). These variations are removed by normalising the baseline lightning NO_x emissions in each model to 5 TgN and considering changes in temperature and lightning NO_x emissions relative to this baseline (Figure 4.1B). The choice of 5 TgN is based on the best estimate for present-day emissions (Schumann and Huntrieser, 2007).

Results from models using the cloud-top height approach are grouped together. These models show a consistent linear response of LNO_x to temperature once the differences in present-day surface temperature and global emission totals are adjusted for. A linear mixed effect regression on the data points simulated by models using the cloud-top height approach has been applied. Surface temperature is the regressed fixed effect, while random effects are a random intercept for each model and a random slope for the interaction between each model and the effect of surface temperature. All effects considered are significant at the 5% level and the regression model has a marginal R^2 of 0.82 and a conditional R^2 of 0.96.

A robust estimate of the lightning NO_x emission climate response of $0.44 \pm 0.05\,\mathrm{TgN\,K^{-1}}$ is found for models using the cloud-top height approach (individual model fits are provided in Table 4.8). This corresponds to $8.8 \pm 1.0\,\%\mathrm{(baseline)\,K^{-1}}$, where the uncertainty range represents one standard error. This is lower than the median determined by Schumann and Huntrieser (2007) but similar to recent estimates which have a range of 5.5-16 $\%\,\mathrm{K^{-1}}$ (Zeng *et al.*, 2008; Jiang and Liao, 2013; Banerjee *et al.*, 2014). Differences in the LNO_x response among models using the cloud-top height approach arise from differing responses to climate change from convective and microphysical schemes, the vertical resolution for resolving cloud-top height and structural differences in implementation

of the approach. Details of the lightning parametrisation used by each model are described in Table S2.

The ACCMIP data allow for a robust estimate of the sensitivity of the cloud-top height approach. However, the two ACCMIP models using alternative parametrisations provide rather different estimates. The EMAC model uses a combination of updraft mass flux within the cloud and cloud depth (Grewe *et al.*, 2001) and shows a much weaker sensitivity ($0.14\,\mathrm{TgN\,K^{-1}}$) than the cloud-top approach. The CMAM model uses a parametrisation based on updraft mass flux at 440 hPa (Allen and Pickering, 2002) and shows the opposite response of a reduction in $\mathrm{LNO_x}$ with increasing temperature ($-0.55\,\mathrm{Tg\,K^{-1}}$).

The various responses described above for each parametrisation fundamentally depend on the changes in convection simulated by the models. It is possible that these two models are anomalous in their responses to climate change for convection. Further investigation of convection in the different models or application of different parametrisations would be needed to establish this. However, it is unlikely that the models with different lightning parametrisations also have anomalous convection responses and therefore it is suggested that the lightning parametrisations are the source of the different responses seen. It is also possible that changes in cloud-top height differ somewhat from changes in the intensity of convective updrafts. Stevenson *et al.* (2005) and Banerjee *et al.* (2014) have found that in some locations the occurrence of deep convection decreases under climate change but that the depth increases. Findings here suggest that it is vital to determine whether the cloud-top height approach provides the most appropriate representation of lightning, or whether a greater diversity of lightning parametrisations is needed. Uncertainty remains as to whether lightning $\mathrm{NO_x}$ emissions will increase or decrease in future.

4.4 Spatial Variation of Response to Temperature

The impacts of LNO_x on atmospheric chemistry and radiative forcing are dependent on the spatial distribution of emissions as well as the global total (Liaskos *et al.*, 2015, and Chapter 3). I consider here the spatial distribution of LNO_x and change in LNO_x between present-day and future, and whether there is anomalous behaviour underlying the distributions. The results of MOCAGE have been excluded from analysis of the spatial distribution of changes because it displays anomalous wave-like features. Following advice from the model contact, Beatrice Josse, I have chosen to include the model in the analysis of annual LNO_x totals in previous section as these values have not been compromised.

Figure 4.2A-C shows the mean baseline (year 2000) distribution of lightning NO_x emissions from eight models using the cloud-top height approach for which spatial distributions of emissions are available, as well as from each of the models using alternative schemes. The emission distributions of all three approaches represent, to a reasonable extent, the climatological distribution of lightning flash rate provided by the Lightning Imaging Sensor and Optical Transient Detector (Cecil *et al.*, 2014). In particular, they show lightning NO_x emission peaks in tropical continental locations, and lower values towards the poles and over the oceans. The distributions of change in surface temperature (Figure S4.4) and precipitation (Figure S4.5) between the present-day and year 2100 using the RCP8.5 scenario are shown in supplementary material. CMAM and EMAC do not simulate anomalous temperature or precipitation changes compared to the other ACCMIP models. The robustness of these two models, which use alternative lightning parametrisations, among the other ACCMIP models regarding these three variables gives confidence that they are not outliers in terms of their broad representation of climate change.

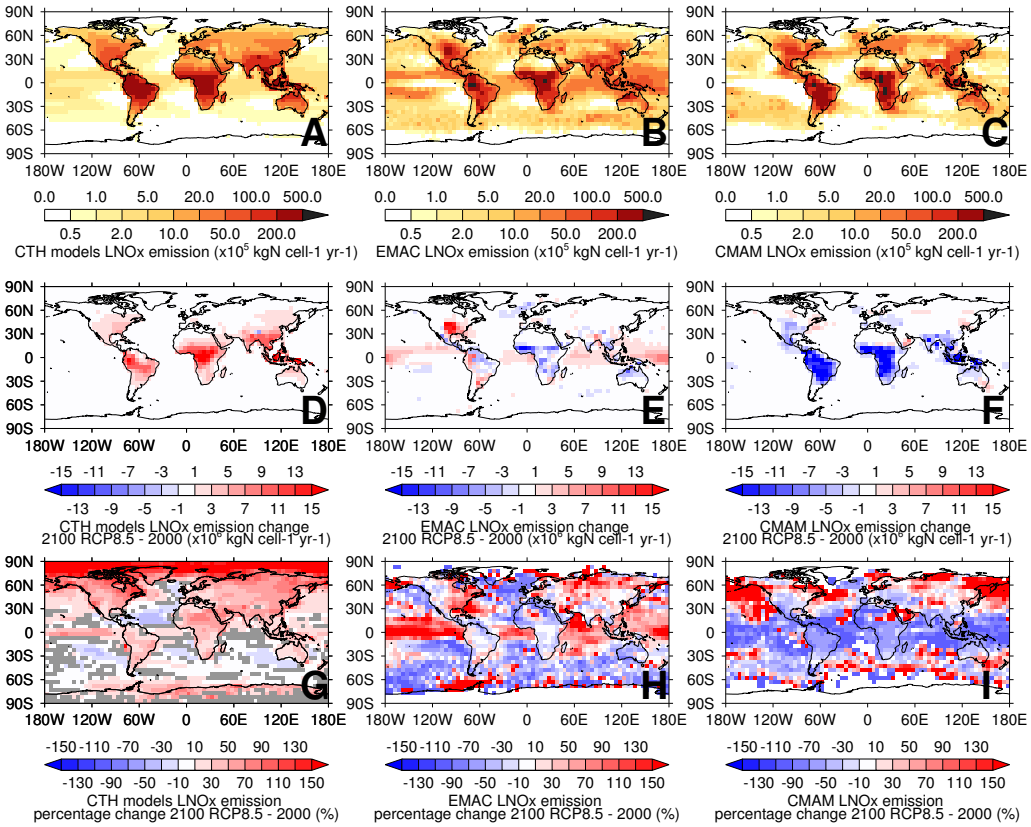

Figure 4.2: Annual vertically-integrated lightning NO_x emission distribution for the year 2000 baseline and absolute and percentage change with respect to RCP8.5 year 2100. Annual emissions for year 2000 baseline are normalised to 5 TgN for all models with the same normalisation factors applied to year 2100 RCP8.5 emissions. The number of model years contributing to the year 2100 time slice average are: CTH (79 years across 8 models), EMAC (9 years) and CMAM (10 years). The top row shows the baseline distributions for year 2000, the second row shows the absolute changes in distribution for the year 2100 RCP8.5 experiments, and the bottom row shows the equivalent percentage changes. The left column panels are the mean of eight models using the cloud-top height approach. The middle and right columns plots are the individual results for the EMAC and CMAM models, respectively. Mean values are calculated after scaling and regridding all models to a common resolution (5° x 5°). In (G) the greyed cells represent grid cells in which there is not at least five models that estimate the same sign of change.

Figures 4.2D-F show the absolute changes in lightning NO_x emissions between the present-day and year 2100 using the RCP8.5 scenario for each type of lightning parametrisation. As with the global total LNO_x changes in Figure 4.1, the three approaches represent largely positive (Figure 4.2D), mixed (Figure 4.2E) and largely negative changes (Figure 4.2F). From all three approaches, it is clear that changes in LNO_x under future climate change are non-uniform. The largest absolute changes typically occur where there are highest baseline lightning NO_x emissions and the sign of these changes are generally consistent with the sign of global total LNO_x changes found with each lightning parametrisation.

The percentage changes in lightning NO_x emissions between the present-day and year 2100 using the RCP8.5 scenario are shown in Figures 4.2G-I. The changes in the models using alternative schemes appear more noisy. This is partly due to averaging over a number of models that use CTH (Figure 4.2G), but even compared to individual model simulations of LNO_x based on cloud-top height the alternative schemes produce a more heterogeneous response (Figure S4.3). The cloud-top height will be partly limited by the tropopause which will vary smoothly and, therefore, may lead to smoothness in the simulated LNO_x distribution by models using the CTH approach.

Percentage changes between present-day and future are generally large over ocean as well as over land. Most of the globe experiences changes of >10%. While absolute changes in LNO_x are small away from dominant source regions, the percentage changes are larger away from high emission regions. Such large relative changes may be important in remote locations where there are few other sources of NO_x.

There is agreement between the different schemes on the sign of the change in some locations which can be seen in Figure 4.2 G-I. Mostly these are located in the mid-latitudes. Increases in LNO_x in the Northwest Atlantic and Pacific suggest

an increase in lightning activity within northern mid-latitude storms or a shift in location of the storm tracks. Decreases in the Southeast Pacific are consistent with significant drying reported in the IPCC AR5 report by Collins *et al.* (2013, Fig. 12.22). Collins *et al.* (2013) indicated significantly increased rainfall in Russia and eastern Canada in year 2100 under RCP8.5, corresponding to increases in LNO_x in Figures 4.2 G-I, thereby suggesting the changes in rainfall in these regions correspond to changes in the frequency or intensity of thunderstorms. There are many other locations where changes in lightning NO_x emissions do not correspond to similar changes in precipitation. The non-uniformity of these changes in lightning is an important argument for using interactive lightning schemes that are not constrained spatially by present-day observations.

4.5 Ozone Production

Ozone is sensitive to a large number of variables influenced by climate change and so it is difficult to attribute changes in ozone concentration directly to changes in lightning NO_x emissions. Changes in temperature, humidity, deposition, other ozone precursor emissions and stratosphere-troposphere exchange all contribute to changes in ozone (Fiore *et al.*, 2012; Doherty *et al.*, 2013; Young *et al.*, 2013) (Section 1.4.2). The most direct impact of lightning NO_x emissions on ozone is through chemical production. Based on model sensitivity studies, Wild (2007) found that an increase in LNO_x produced $\sim$3 times more global tropospheric ozone production per Tg(N) than an increase in surface NO_x emissions. Using alternative methods, Wu *et al.* (2007) and Dahlmann *et al.* (2011) found that LNO_x produced six and five times more ozone than surface NO_x, respectively. This disproportionately large effect is due to lightning NO_x emission in the middle and upper troposphere where temperatures are cooler, NO_x and ozone have longer lifetimes, and where ozone production efficiency is high.

Tropospheric ozone chemical production fluxes were archived from a subset of six models during ACCMIP. Relevant emission variables from all time slices and scenarios (Table 4.1) are used here to perform a linear mixed effect regression to describe global tropospheric ozone production. Fixed effects for lightning NO_x, surface NO_x, CO and NMVOC emissions and the methane tropospheric burden were included within the initial mixed effect regression, along with random effects for 'model' and for the interaction between 'model' and the effect of lightning. The surface NO_x variable includes NO_x emissions from aircraft but these are less than 2% of the total emissions and their effects are assumed to be small.

A stepwise selection process, based on the Akaike information criteria (AIC) (Burnham and Anderson, 2002), was used to identify whether the initial regression model could be simplified, and this led to NMVOC emissions and CO emissions being removed. The remaining explanatory variables all have significant coefficients with $p < 0.05$. The model has a *marginal* R^2 of 0.57 and a *conditional* R^2 of 0.99. An equation for the fitted linear model is given by:

$$\hat{P} = 104(\pm 37)E_{LNO_x} + 16.0(\pm 0.9)E_{surfNO_x} + 0.0793(\pm 0.0104)B_{CH_4} - 1.85(\pm 14.74) + U_{1,m}E_{LNO_x} + U_{2,m} \quad (4.1)$$

where $\hat{P}$ is the estimated global tropospheric ozone production ($\mathrm{mol}(O_3)\mathrm{yr}^{-1}$), E_{LNO_x} and E_{surfNO_x} are emissions of lightning NO_x and surface NO_x ($\mathrm{mol(N)yr}^{-1}$), and B_{CH_4} is methane tropospheric burden ($\mathrm{mol}(CH_4)$). Ranges given in Equation 4.1 are the standard errors associated with each coefficient. The random model slope, $U_{1,m}$, represents an adjustment to the fixed lightning effect, and the random model intercept, $U_{2,m}$, an adjustment to the regressed intercept, for each model, m. There are six models and therefore U_1 and U_2 are

each a vector of six values. The mean of the values of any random effect, U, is zero. The standard deviations of the values of $U_{1,m}$ and $U_{2,m}$ are 75 and 28, respectively.

The coefficients of Equation 4.1 represent the number of moles of ozone produced for each mole of the species, i.e., the ozone production efficiency (OPE). For example, the OPE associated with surface NO_x sources is 16 $\mathrm{mol}(O_3)\,\mathrm{mol}^{-1}(\mathrm{N})$. The underlying fixed LNO_x effect found in the regression is 6.5 times larger than that of surface NO_x sources, similar to that found by Wu *et al.* (2007) and Dahlmann *et al.* (2011), and representing a disproportionally larger efficiency of LNO_x in producing ozone.

It is important to consider the size of the emissions or burden in combination with regression coefficients to fully understand the context of the statistical regression results. By applying the regressed ozone production efficiencies of Equation 4.1 for E_{LNO_x} including the random slopes, E_{surfNO_x}, and B_{CH_4} to the emissions in each time slice experiment, a proportion of the estimated ozone production can be attributed to each of the individual effects. There are 50 time slice experiments used (summarized in Table 4.1). The mean and range for the three effects is: $E_{LNO_x}41\%(3-78\%)$, $E_{surfNO_x}38\%(12-68\%)$ and $B_{CH_4}21\%(9-51\%)$. These results show that the three effects, at least for the range of experiments in ACCMIP, produce similar amounts of ozone, with CH_4 generally producing less ozone and with a wider range of contributions to ozone production from LNO_x across the experiments.

4.6 Causes of Variability in Ozone Production Efficiency

The regression model described by Equation 4.1 provides a means to remove the estimated ozone production by species other than LNO_x and therefore study the production by LNO_x alone. In addition, the random slope values, $U_{1,m}$, determined in the regression can either be removed to see the estimated underlying ozone production from LNO_x across models, or included to see the estimated ozone production from LNO_x in each model. These components of ozone production are shown by the partial residuals of ozone production against LNO_x in Figures 4.3A and B.

The partial residual is the actual ozone production with the estimated ozone production of some terms in the regression removed. Figure 4.3A is the conditional partial residual of ozone production with respect to lightning NO_x emissions, ϵ_1, i.e., the general relationship across models given by the fixed effect of E_{LNO_x} in Equation 4.1 and described by Equation 4.2:

$$\epsilon_1 = \hat{P} - 16.0E_{surfNO_x} - 0.0793B_{CH_4} - 1.85 - U_{1,m}E_{LNO_x} - U_{2,m} \qquad (4.2)$$

Figure 4.3B shows the individual model relationships between ozone production and LNO_x, ϵ_2, i.e., the combination of the fixed effect, E_{LNO_x}, and individual random slopes, $U_{1,m}$. This partial residual residual is described by Equation 4.3:

$$\epsilon_2 = \hat{P} - 16.0E_{surfNO_x} - 0.0793B_{CH_4} - 1.85 - U_{2,m} \qquad (4.3)$$

These partial residuals demonstrate the effect of lightning NO_x emissions and clearly reveal the differences in OPE between the models.

The vertical distribution of LNO_x differs greatly between the models, as shown

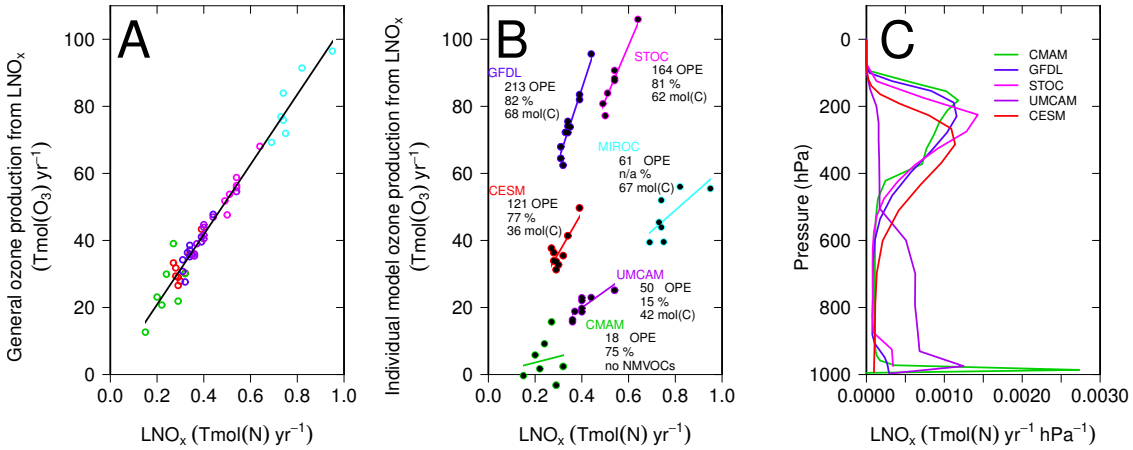

Figure 4.3: Tropospheric ozone production from lightning $\mathrm{NO_x}$ emissions and the role of NMVOC emissions and the vertical distribution of lightning $\mathrm{NO_x}$ emissions. A) "General ozone production from $\mathrm{LNO_x}$" is a partial residual with respect to $\mathrm{LNO_x}$ described by Equation 4.2. B) "Individual model ozone production from $\mathrm{LNO_x}$" is a partial residual with respect to $\mathrm{LNO_x}$ described by Equation 4.3. The text in B) for each model is, from top to bottom, the ozone production efficiency (OPE) from $\mathrm{LNO_x}$, the percentage of baseline lightning $\mathrm{NO_x}$ emissions in the middle and upper troposphere [500-100 hPa], and the mean NMVOC emissions. C) is the baseline global $\mathrm{LNO_x}$ vertical distribution. The MIROC model is not included in (C) because the emission distribution was not archived. For (C), values of pressure are based on a uniform 1000 hPa surface pressure and annual lightning $\mathrm{NO_x}$ emissions are normalised to 5 TgN.

in Figure 4.3C. Vertical distribution methods are based upon modelled updrafts, prescribed distributions (Pickering *et al.*, 1998; Ott *et al.*, 2010), or air density (Goldenbaum and Dickerson, 1993; Stockwell *et al.*, 1999; Jourdain and Hauglustaine, 2001). The LNO_x vertical distribution method used by each model in ACCMIP is given in Table S2.

The proportion of lightning NO_x emission in the middle and upper troposphere (500-100 hPa) and the gradient (OPE) for each individual model determined by the mixed effect regression are presented in Figure 4.3B. Although there are relatively few models, there is a direct relationship between the amount of ozone in the middle and upper troposphere and the OPE of lightning. An exception is the CMAM model which has a relatively weak relationship between ozone production and LNO_x and a low OPE. It would require a targeted study to identify the cause of this difference, but I note that CMAM does not include NMVOC chemistry, representing this instead through extra CO emissions. The majority of NMVOC emissions are in the form of biogenic emissions and are high over tropical rainforests where lightning activity is also high. It is possible that the combined emissions of NMVOC and LNO_x increase OPE in these regions through a greater radical pool. CMAM also has a different spatial distribution of the response of LNO_x to climate change compared to other models. Changes in regions of lower ozone production may contribute to a weaker relationship between ozone production and LNO_x.

The considerations above encourage further research to understand variability among models. LNO_x and OPE will have seasonal and regional responses to climate change which have not been investigated here. Furthermore, research into the effect on OPE of LNO_x being concentrated within convective outflow plumes would be valuable, given that this feature is not captured by the resolutions of ACCMIP models. Dedicated sensitivity simulations within a chemistry-climate model would allow quantification of the role of the vertical emission

distribution of lightning NO_x and the representation of NMVOCs on the OPE of LNO_x. This would permit these effects to be isolated and allow determination of the contribution of LNO_x differences to the inter-model variation of OPE in Figure 4.3B. The standard deviation of individual model estimates of OPE can be used as a proxy for the uncertainty on the fixed LNO_x effect discussed in Section 4.5, suggesting that the OPE of LNO_x is 6.5 $\pm$ 4.7 times that of surface NO_x sources.

4.7 Conclusions

The large dataset of model results archived for ACCMIP has allowed a rigorous analysis of the climate sensitivity of lightning NO_x emissions for models using the cloud-top height parametrisation of Price and Rind (1992). This parametrisation is widely used and performs very similarly across models with a positive linear response of $0.44 \pm 0.05\,\mathrm{TgN\,K^{-1}}$ for a baseline annual emission of 5 TgN. Two models using different parametrisations of lightning simulate a weaker and an opposite climate response of lightning NO_x emissions. Therefore, despite the important role that lightning NO_x emission plays in ozone chemistry, it is clear from the two ACCMIP models using alternative lightning schemes that there cannot be complete confidence in the magnitude or even sign of the lightning NO_x emission sensitivity to climate change. While there is agreement among the three parametrisations in a few locations regarding the projected spatial change of LNO_x in future, generally this is as uncertain as the global changes.

There is no indication that the models using alternative schemes are outliers in terms of their representation of surface temperature or precipitation change. I therefore conclude that the different responses of lightning to climate change are due to the use of different lightning parametrisations. Studies establishing

the climate sensitivity of multiple lightning parametrisations within the same model, as will be carried out in Chapter 5, are needed to confirm whether the results here solely reflect the different parametrisations. The cloud-top height approach has been well characterised in this chapter thereby providing a useful reference point in understanding the behaviour of alternative schemes. I therefore suggest that chemistry-climate modelling groups consider additional simulations with alternative lightning schemes, as a greater diversity of schemes would help advance understanding of uncertainties in the response of lightning NO_x to climate change and its subsequent effects on ozone.

Uncertainty in the climate response of lightning will undoubtedly lead to uncertainty in the changes in ozone production from LNO_x. The tropospheric ozone production from LNO_x and other sources has been quantified using the data from a selection of models in ACCMIP. The results suggest that lightning NO_x emissions are 6.5 ± 4.7 times more efficient than surface NO_x sources at producing ozone in the troposphere. The method for distributing emissions vertically as well as the treatment of emissions of NMVOCs appear to be responsible for at least some of this variability in ozone production efficiency from lightning. Therefore, direct determination of the role of the vertical LNO_x distribution for ozone production is necessary before a consistent approach among models can be developed.

4.8 Supplementary material

This supporting information provides additional figures and tables which show individual model analysis, including for models using the cloud-top height approach to parametrize lightning which are generally combined in the main text. Figures showing the distribution of surface temperature and precipitation change simulated by the models between year 2100 RCP8.5 and present-day is provided which is discussed in the main text regarding the robustness of these climate indicators across the models.

Table S4.1: Individual model normalisation factors for 5 TgN in year 2000 baseline emission, regressions of normalised change in LNO_x against change in global mean surface temperature, and the adjusted R^2 and p-values for the regressions

Model	Baseline emissions ($TgN\,yr^{-1}$)	Normalising factor	Gradient ($TgN\,yr^{-1}\,K^{-1}$)	Intercept ($TgN\,yr^{-1}$)	Adj R^2	p-value
CESM-CAM-superfast	4.2	1.19	0.36	-0.079	0.89	7.44e-05
CMAM	3.8	1.32	-0.55	-0.014	0.94	0.00021
EMAC	5.7	0.88	0.14	-0.237	0.72	0.02028
GFDL-AM3	4.4	1.14	0.37	0.071	0.93	9.37e-07
GISS-E2-R	7.7	0.65	0.37	0.060	0.96	5.99e-08
HadGEM2	1.3	3.85	0.74	0.147	0.96	0.00039
LMDzORINCA	6.0	0.83	0.66	-0.114	0.96	1.25e-07
MIROC-CHEM	9.7	0.52	0.33	-0.038	0.98	1.69e-07
MOCAGE	5.2	0.96	0.38	0.001	0.99	3.41e-08
NCAR-CAM3.5	4.1	1.22	0.46	-0.026	0.95	2.31e-07
STOC-HadAM3	7.2	0.69	0.27	-0.041	0.99	1.45e-06
UM-CAM	5.2	0.96	0.45	-0.051	0.98	2.85e-07

Table S4.2: Details of models and the lightning parametrisations used within this chapter (Lamarque *et al.*, 2013).

Model	Resolution (lat/lon/# levels), Top level	Lightning NO_x (horizontal distribution)	Lightning NO_x (vertical distribution)
CMAM	3.75/3.75/L71, 0.00081 hPa	Interactive, based on convective updraft mass flux (modified version of (Allen and Pickering, 2002))	65% of lightning NO_x into layers where the updraft detrains, 25% spread evenly over the depth of the convection (updraft mass flux > 0) and 10% is added to the bottom-most cloud layer(defined by having updraft mass flux > 0)
EMAC	T42/L90, 0.01 hPa	Interactive, updraft velocity as a measure of convective strength and associated cloud electrification with the flash frequency (Grewe *et al.*, 2001)	Prescribed distributions of Pickering *et al.* (1998)

Continued on next page

Table S4.2 – *Continued from previous page*

Model	Resolution (lat/lon/# levels), Top level	Lightning NO_x (horizontal distribution)	Lightning NO_x (vertical distribution)
GFDL-AM3	2/2.5/L48, 0.017 hPa	Interactive, based on models convection (Price *et al.*, 1997), scaled to produce $\sim 3-5$ TgN	Prescribed distributions of Pickering *et al.* (1998)
GISS-E2-R	2/2.5/L40, 0.14 hPa	Interactive, based on models convection (modified from Price *et al.* (1997))	Prescribed distributions of Pickering *et al.* (1998)
HadGEM2	1.24/1.87/L38, hPa	Interactive, based on models convection (Price and Rind, 1992)	As used by UM-CAM (Stockwell *et al.*, 1999)
LMDzORINCA	1.9/3.75/L19, hPa	Interactive, based on models convection (Price *et al.*, 1997)	Prescribed distributions of Pickering *et al.* (1998)

Continued on next page

Table S4.2 – *Continued from previous page*

Model	Resolution (lat/lon/# levels), Top level	Lightning NO_x (horizontal distribution)	Lightning NO_x (vertical distribution)
MIROC-CHEM	2.8/2.8/L80, 0.003 hPa	Interactive, based on models convection based on (Price and Rind, 1992)	Distributed by updrafts/downdrafts following an initially uniform vertical distribution leading to C-shape profiles as studied by Pickering *et al.* (1998)
MOCAGE	2.0/2.0/L47, 6.9 hPa	Climate sensitive (based on Price and Rind (1992) and Ridley *et al.* (2005))	

Continued on next page

Table S4.2 – *Continued from previous page*

Model	Resolution (lat/lon/# levels), Top level	Lightning NO_x (horizontal distribution)	Lightning NO_x (vertical distribution)
NCAR-CAM3.5	1.875/2.5/L26, 3.5 hPa	Interactive, based on models convection (Price *et al.*, 1997; Ridley *et al.*, 2005), scaled to produce $\sim 3-5$ TgN	A modified version of Pickering *et al.* (1998), to have a reduced proportion of the emissions emitted near the surface, similar to that used by DeCaria *et al.* (2005) (Emmons *et al.*, 2010; Lamarque *et al.*, 2012)
STOC-HadAM3	5.0/5.0/L19, 50 hPa	Interactive, based on models convection (Price and Rind, 1992; Price *et al.*, 1997)	Prescribed distributions of Pickering *et al.* (1998) scaled to the model cloud top

Continued on next page

Table S4.2 – *Continued from previous page*

Model	Resolution (lat/lon/# levels), Top level	Lightning NO_x (horizontal distribution)	Lightning NO_x (vertical distribution)
UM-CAM	2.5/3.75/L19, 4.6 hPa	Climate sensitive; based on parameterization from (Price *et al.*, 1997)	Distributed proportional to air density with intra-cloud emissions between 500 hPa and model cloud top, and cloud-to-ground between the surface and 500 hPa (Stockwell *et al.*, 1999)

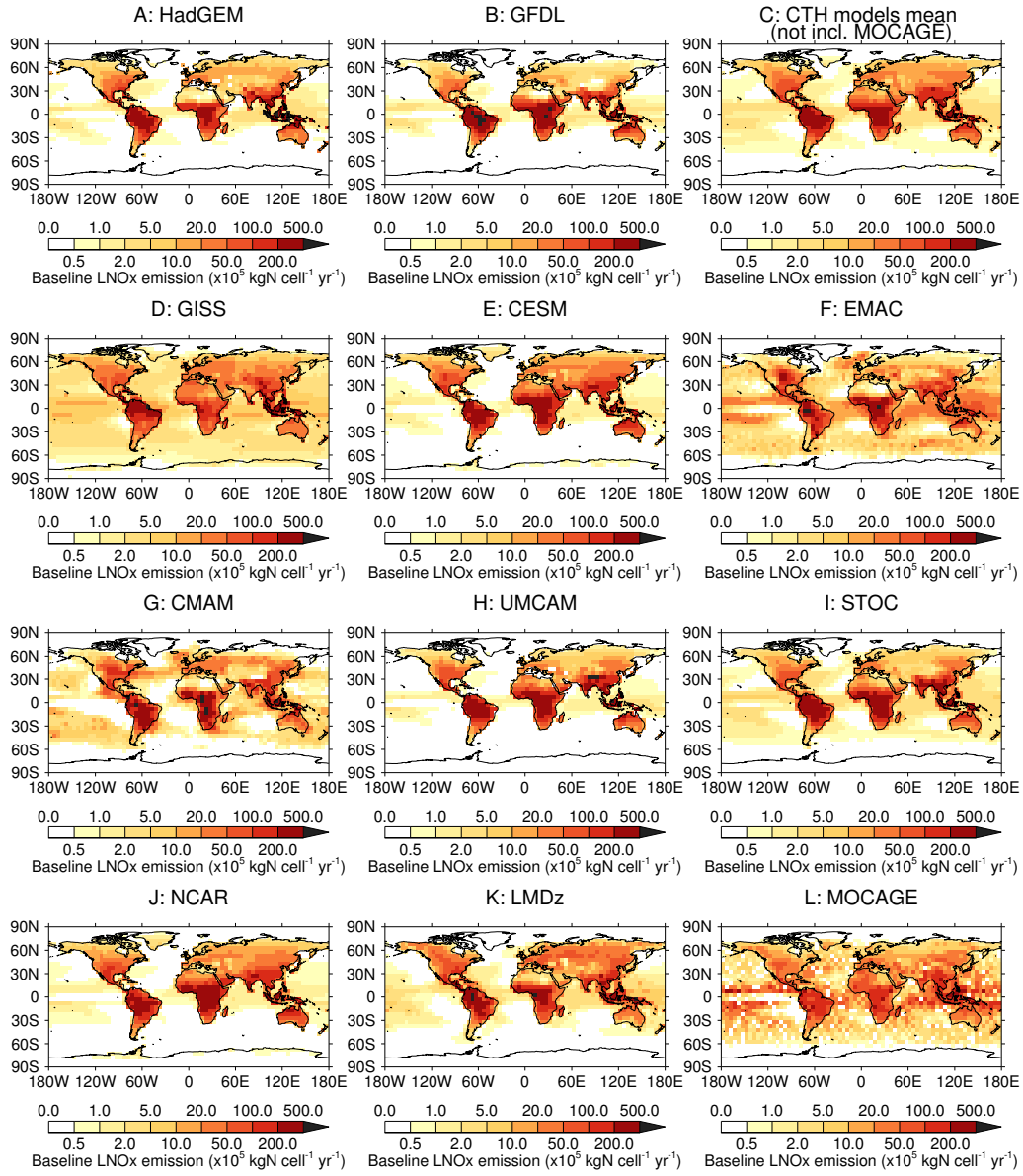

Figure S4.1: Year 2000 baseline $\mathrm{LNO_x}$ for each model regridded to a common resolution of 5° x 5° and normalised to 5 TgN emissions.

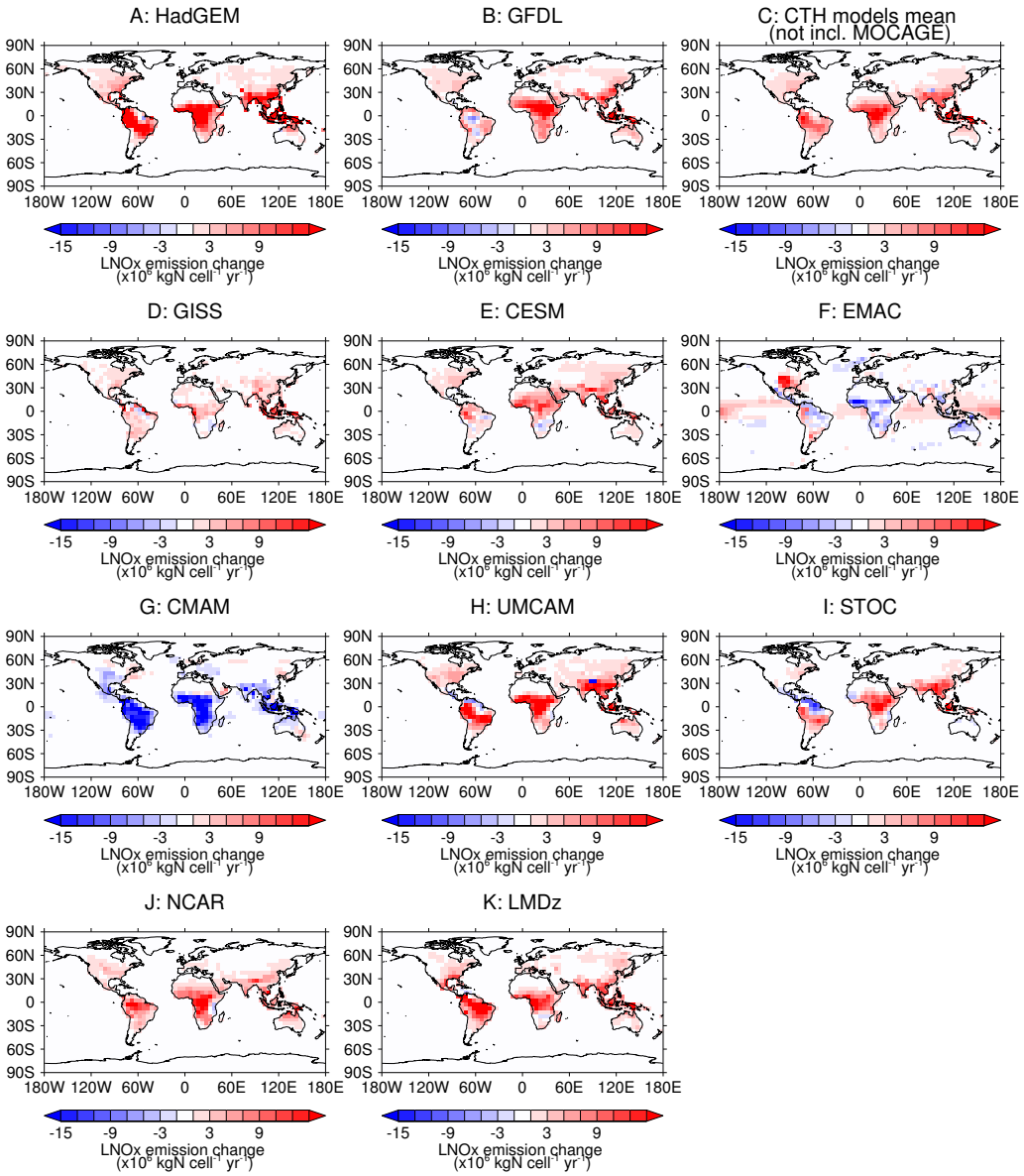

Figure S4.2: LNO_x absolute changes for each model and CTH model mean regridded to a common resolution of 5° x 5° and normalised to 5 TgN emissions in year 2000 baseline. MOCAGE is excluded for reasons stated in Section 4.4.

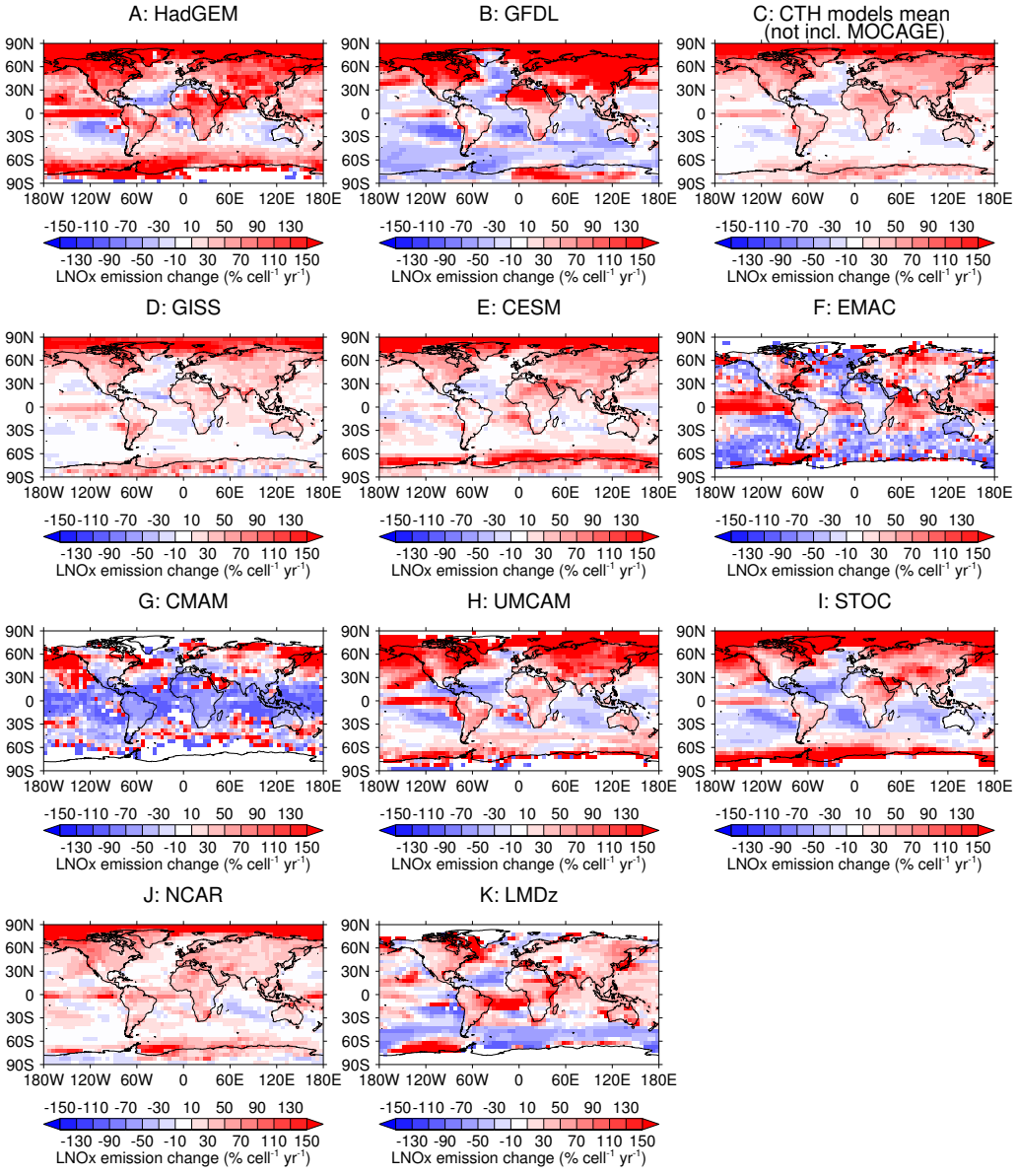

Figure S4.3: LNO_x percentage changes between year 2000 and year 2100 RCP8.5, for each model and the CTH model mean. Data is regridded to a common resolution of 5° x 5° and normalised to 5 TgN in year 2000 baseline. MOCAGE is excluded for reasons stated in Section 4.4.

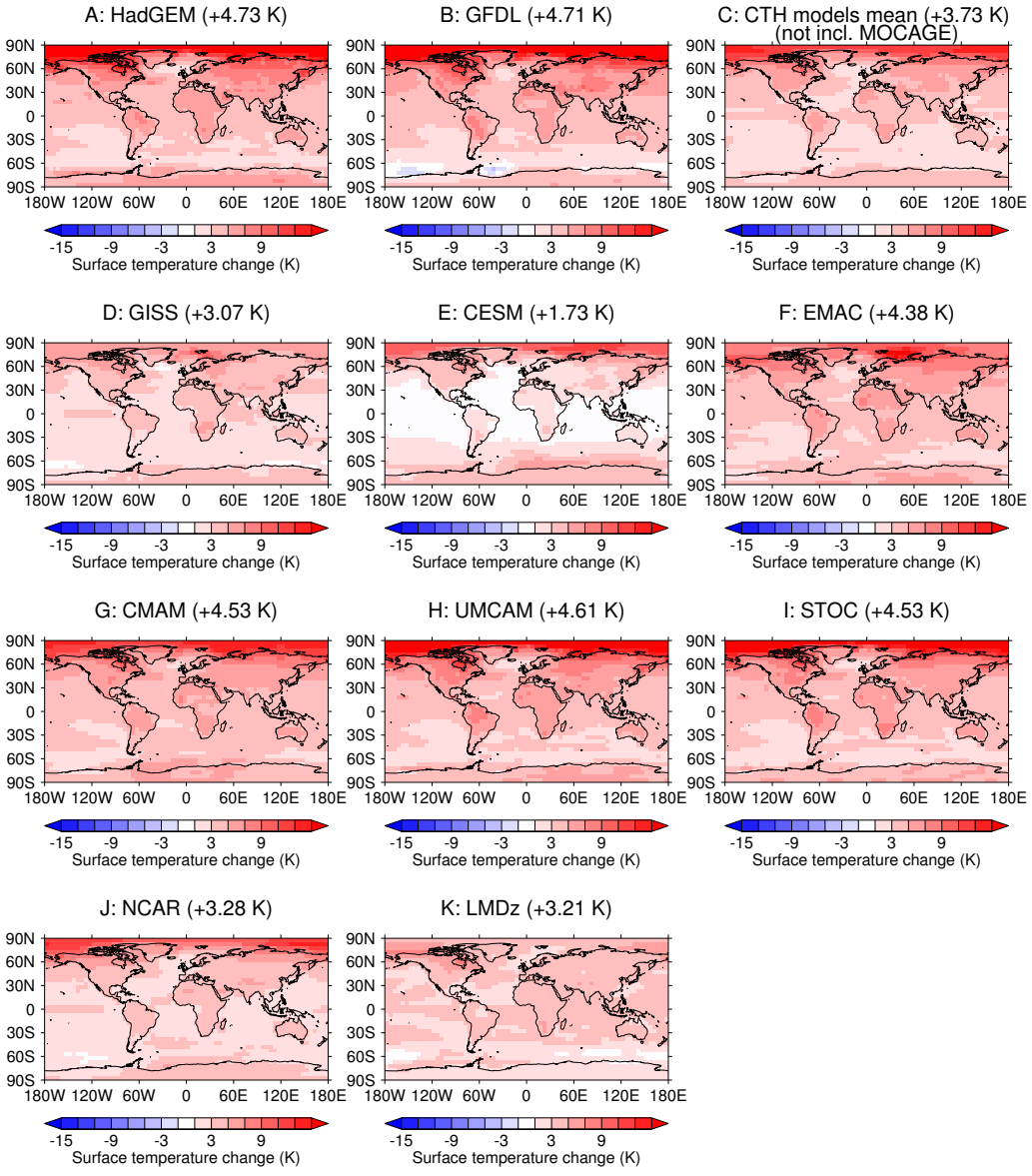

Figure S4.4: Surface temperature change between year 2000 and year 2100 RCP8.5, for each model and CTH model mean. Data regridded to a common resolution of 5° x 5°. Surface temperature is defined as the temperature of the lowest model level. Area-weighted global mean surface temperature change for each model is given in brackets. MOCAGE is excluded for reasons stated in Section 4.4.

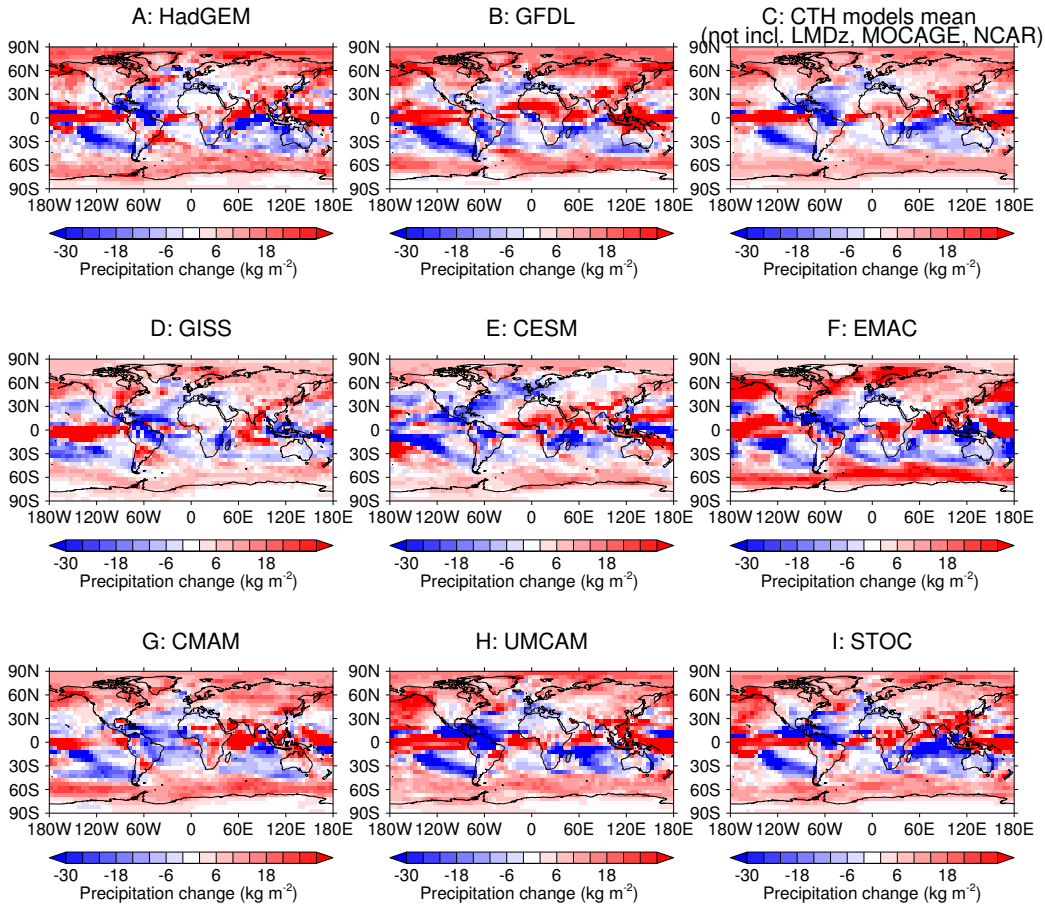

Figure S4.5: Precipitation change between year 2000 and year 2100 RCP8.5, for each model and CTH model mean. Data regridded to a common resolution of 5° x 5°. MOCAGE is excluded for reasons stated in Section 4.4, whilst precipitation data for the NCAR and LMDz models were not available.

Chapter 5

An uncertain future for lightning and the consequences for atmospheric composition and radiative forcing

This chapter has not yet been submitted for publication. I have carried out the analysis. Dr Oliver Wild provided the HTAP value of 0.95 for the ozone response to a methane change, given in Section 5.2.4.

A draft publication of this chapter, written by myself, is currently a work in progress. The draft publication has received feedback from co-authors: Dr Ruth Doherty, Dr Oliver Wild, Prof David Stevenson, Dr Ian Mackenzie, and Prof Alan Blyth.

5.1 Introduction

Changes in climate over the coming century are expected to alter atmospheric temperature, humidity, stability and dynamics (Collins *et al.*, 2013). The occurrence of lightning depends on all of these factors through their effect on the convection and ice particles which generate electrical charge in thunderstorms (Reynolds *et al.*, 1957) (Section 1.2). As an important source of NO_x (NO + NO_2), lightning needs to be represented interactively in chemistry-climate models (CCMs) to fully simulate the response of NO_x, and hence ozone, OH and methane lifetime, to climate change. Both ozone and methane are greenhouse gases meaning that changes in their concentrations can lead to a warming or cooling the atmosphere.

The distribution of lightning flash rates is determined interactively in CCMs based on the simulated meteorological variables (Section 1.5.1). Several studies have simulated lightning under future climate scenarios to estimate the response of lightning to climate change (Section 1.7). A comprehensive review by Schumann and Huntrieser (2007) reported a median estimate of a 15% increase in lightning NO_x emissions (LNO_x) per degree increase in global mean surface temperature, with more recent estimates in the range of 5-16 % (Zeng *et al.*, 2008; Jiang and Liao, 2013; Banerjee *et al.*, 2014, and Chapter 4). However, the majority of these models use the same lightning parametrisation based on cloud-top height.

In Chapter 4, I showed that models using alternative parametrisations to the cloud-top height approach project weaker or negative responses. In addition, Jacobson and Streets (2009) used an alternative parametrisation based on cloud ice fluxes and found a decrease in lightning as temperature increased, although only a small change in global mean surface temperature was examined due to the short time period considered. While the cloud-top height approach provides a reasonable estimate of the present-day lightning distribution, it is only indirectly

related to lightning generation following the non-inductive charging theory of thunderstorms (Reynolds *et al.*, 1957; Saunders, 2008), described in Section 1.2. This theory describes the transfer of charge during collision of small, rising ice crystals and larger, falling ice particles within thunderstorms, and provides a physical basis for parametrising lightning generation.

A global lightning parametrisation based on upward cloud ice flux at 440 hPa has been presented in Chapter 2. By using cloud ice flux, this parametrisation incorporates more aspects of the charging theory than the cloud-top height approach. Present-day lightning simulated using this ice flux approach has been compared to that simulated using the cloud-top height approach in a CCM (Chapter 3). The ice flux scheme was generally found to provide closer agreement than the cloud-top height scheme with the satellite-observed global lightning distribution. Through the corresponding changes in the lightning NO_x source, the annual cycle of ozone was improved compared to ozone sonde observations.

Numerous studies have shown the impact of changes in the lightning NO_x source on key tropospheric oxidants, ozone and OH, as well as methane lifetime. Murray *et al.* (2013) found that variations in the lightning NO_x source were more important than variations in biomass burning sources in determining the interannual variability of OH. Banerjee *et al.* (2014) found that under the RCP8.5 climate scenario, the tropospheric ozone burden increased by 33 Tg in the year 2100, due to an increase of 78 % in lightning NO_x. In addition, future increases in lightning NO_x due to climate change may result in enhanced OH in the tropical upper troposphere, decreasing methane lifetime by as much as 0.75 years or 10 % (Banerjee *et al.*, 2014). However, both of these studies use the cloud-top height approach. The uncertainty in future ozone and OH concentrations associated with the choice of lightning parametrisation is currently unknown.

Changes in the concentrations of ozone and methane exert a radiative forcing

on the atmosphere. Ozone produced by LNO_x has a higher radiative efficiency than that produced by other NO_x sources because it enhances ozone in low latitude, high altitude regions (Dahlmann *et al.*, 2011). In these regions the temperature contrast between the atmosphere and the surface is greatest thereby increasing the radiative forcing efficiency (Lacis *et al.*, 1990). Futhermore, Toumi *et al.* (1996) suggest that a positive feedback may exist between lightning and climate whereby lightning and LNO_x increase with increased surface temperature, producing more ozone which further warms the climate. They found using a global two-dimensional atmospheric model that following an increase in global surface temperature, lightning increased and the total ozone forcing from the temperature increase was $+0.1\,\mathrm{Wm^{-2}}$. However, lightning also generates a methane radiative forcing through changes to the OH concentration, with increases in NO_x emissions decreasing the methane forcing. Wild *et al.* (2001) found that this negative methane radiative forcing offsets the positive ozone forcing, resulting in a net integrated forcing over 50 years of $-2.8\,\mathrm{mW\,m^{-2}\,yr}$, based on a 0.5 TgN lightning NO_x perturbation over one year.

In this chapter, I use the two LNO_x parametrisations used in Chapter 3, to estimate the response of lightning activity to future climate change and the impact on atmospheric composition and radiative forcing. The cloud-top height and ice flux approaches for parametrising lightning are described in Section 5.2.2. Sections 5.2.3 and 5.2.4 describe the analysis methods used. The response of each LNO_x parametrisation to climate change is presented in Section 5.3, along with discussion of the changes in the driving meteorology in Sections 5.3.3 and 5.3.4 . The corresponding impacts on atmospheric composition and on radiative forcing are presented in Sections 5.4 and 5.5, respectively.

5.2 Model and methods

The UK Chemistry and Aerosols model (UKCA) coupled to the atmosphere-only version of the UK Met Office Unified Model version 8.4 is used for this chapter. The atmosphere component is the Global Atmosphere 4.0 (GA4.0) (Walters *et al.*, 2014). Both tropospheric and stratospheric chemistry processes are represented. The tropospheric scheme, most relevant to this chapter, is described and evaluated by O'Connor *et al.* (2014). There are 75 species with 285 reactions that include the oxidation of the hydrocarbons: methane, ethane, propane, and isoprene.

The model is run at horizontal resolution N96 (1.875° longitude by 1.25° latitude). The vertical dimension has 85 terrain-following hybrid-height levels between the surface and 85 km. The resolution is highest in the troposphere and lower stratosphere, with 65 levels below $\sim$30 km. The chemistry-climate coupling is one-directional, applied only from the atmosphere to the chemistry scheme, i.e. meteorological fields from the atmosphere component are applied to the chemistry scheme but ozone and aerosol fields in the radiative scheme are prescribed climatologies. Cloud processes and variables are identical to those described in Section 3.2.1, where additional details on the GA4.0 cloud parametrisation are provided.

5.2.1 Experimental set-up

In this chapter, seven experiments have been performed with different lightning schemes and representing either the year 2000 or the year 2100 under Representative Concentration Pathway 8.5 (RCP8.5). Each experiment is run for ten years and in all cases the chemistry scheme uses natural (including isoprene) and anthropogenic emissions, and Greenhouse Gas (GHG) concentrations, representative of the year 2000. GHG concentrations in the future scenario are altered in

Table 5.1: Experiment details and global annual LNO_x production. IFLUX and IFLUX390 experiments use sampling pressure levels of 440 hPa and 390 hPa, respectively.

Experiment	Lightning scheme	SSTs, sea ice and GHGs	LNO_x source ($TgN\,yr^{-1}$)
ZERO-2000	no LNO_x	2000	0.00
ZERO-2100	no LNO_x	2100	0.00
CTH-2000	Price and Rind (1992)	2000	4.91
CTH-2100	Price and Rind (1992)	2100	7.03
IFLUX-2000	Finney *et al.* (2014) (Ch. 2)	2000	4.96
IFLUX-2100	Finney *et al.* (2014) (Ch. 2)	2100	2.92
IFLUX390-2100	modified Finney *et al.* (2014)	2100	4.19

the radiative scheme in order to represent changes to the radiative properties of the atmosphere under RCP8.5. Methane mixing ratios in the chemistry model are fixed at present-day levels in all experiments using a prescribed lower boundary condition to avoid lengthy spin-up times. Sea surface temperatures (SSTs) and sea ice concentrations for present-day simulations are taken from decadal average climatologies based on 1995 - 2004 analyses (Reynolds *et al.*, 2007). For SSTs and sea ice in the future scenario, decadal average anomalies from the Coupled Model Intercomparison Project Phase 5 (CMIP5) HadGEM2-ES simulations for 1995 - 2005 and 2095 - 2105 were applied to the present-day SST and sea ice analysis fields. A summary of the lightning parametrisation and climate scenario used for each experiment is given in Table 5.1. There are three present-day simulations (for the two lightning schemes and a no lightning case). The two lightning schemes and the no lightning case are also applied to a future scenario, as well as a variation on the lightning scheme based on ice flux. All simulations within the same time period experience the same meteorology and consequently the same changes in surface temperature between the two time periods.

5.2.2 Lightning parametrisations

The cloud-top height (CTH) and ice flux (IFLUX) parametrisations described below determine the flash rate interactively from meteorology as simulated by the atmospheric model (GA4.0). The flash rate is used to determine the LNO_x emission per model grid cell. Each flash corresponds to a NO_x emission of approximately 250 mol(N), which is within the range of estimates of Schumann and Huntrieser (2007). The LNO_x is distributed vertically based upon the prescribed vertical profiles of Ott *et al.* (2010) (Figure 1.7) between the surface and the cloud top. Both schemes are normalised to give a global annual average of 46 flashes s^{-1} (or 1.5×10^9 flashes yr^{-1}) (Cecil *et al.*, 2014) (flashes denoted as fl. hereafter) in a one-year present-day simulation, using factors of 1.57 for the CTH scheme and 1.11 for the IFLUX scheme, as provided in Chapter 3. The same factors are used in the future climate change experiments but the global annual flash rate changes in response to the changing meteorology.

The widely-used parametrisation based on cloud-top height, which has also been used in Chapters 2–4, is described by Price and Rind (1992, 1993). The equations used to parametrise lightning are:

$$F_\mathrm{l} = 3.44 \times 10^{-5} H^{4.9} \tag{5.1}$$

$$F_\mathrm{o} = 6.2 \times 10^{-4} H^{1.73}, \tag{5.2}$$

where F is the total flash frequency (fl. min^{-1}), H is the convective cloud-top height (km) and subscripts l and o are for land and ocean, respectively. A resolution scaling factor is used, as suggested by Price and Rind (1994), but is small (1.09). An area scaling factor is also applied to each grid cell by normalising the area of the cell with the area of a cell at 30° latitude.

The parametrisation based on upward cloud ice flux is described in Chapter 2

and implemented in UKCA in Chapter 3. The equations used to parametrise lightning are:

$$f_{\mathrm{l}} = 6.58 \times 10^{-7} \phi_{\mathrm{ice}} \tag{5.3}$$

$$f_{\mathrm{o}} = 9.08 \times 10^{-8} \phi_{\mathrm{ice}}, \tag{5.4}$$

where f_{l} and f_{o} are the flash density (fl. $\mathrm{m}^{-2}\,\mathrm{s}^{-1}$) over land and ocean, respectively. ϕ_{ice} is the upward ice flux at 440 hPa and is calculated using the following equation:

$$\phi_{\mathrm{ice}} = \frac{q \times \Phi_{\mathrm{mass}}}{c}, \tag{5.5}$$

where q is specific cloud ice water content at 440 hPa ($\mathrm{kg\,kg}^{-1}$), Φ is the grid cell mean updraught mass flux at 440 hPa ($\mathrm{kg\,m}^{-2}\,\mathrm{s}^{-1}$) and c is the fractional cloud cover at 440 hPa ($\mathrm{m}^2\,\mathrm{m}^{-2}$). The flash rate is set to zero where $c < 0.01\,\mathrm{m}^2\mathrm{m}^{-2}$ or where no convective cloud top is diagnosed.

The choice of the 440 hPa pressure level is based upon the definition of deep convective clouds by the International Satellite Cloud Climatology Project (Rossow *et al.*, 1996). In Section 5.3.1, the choice of sampling pressure level is revisited in the context of climate change.

5.2.3 Lightning and atmospheric composition analysis

For each of the experiments, 10 years of simulation were averaged to form a decadal climatology (time-slice) for the meteorological and chemical variables used in this chapter. This permits investigation into the effect of changing climate independent of interannual variability.

To investigate finer temporal variability of lightning and its meteorological drivers, frequency distributions of lightning flash rate were studied for a single year using

the first simulated year of each experiment. There is some interannual variability of the frequency distribution but this variability is relatively small (not shown). Therefore analysis of the 1-year frequency distributions can be considered as broadly representative of the year 2000 and year 2100 time-slices.

Changes in climate have direct impacts on atmospheric composition which may mask the effects of changes in lightning alone. Therefore, to isolate the impacts of lightning on distributions of ozone and OH, I remove the effect of changes in atmospheric composition between the present-day and future using simulations with no lightning emissions (ZERO-2000 and ZERO-2100, Table 5.1).

5.2.4 Radiative forcing analysis

Lightning impacts radiative forcing through its effect on the concentrations of methane and tropospheric ozone (Section 5.1). LNO_x will also affect nitrate aerosol and other aerosols indirectly via changes in oxidants (Murray, 2016), but these effects are not simulated here. The lower boundary condition for methane used by the model chemistry scheme is prescribed in all present-day and future simulations as 1746 ppbv. This limits the changes in atmospheric composition to changes in short-lived species resulting from lightning NO_x emission changes and the direct impact of climate change. Only the lower boundary is constrained, but the global methane burden varies by less than 3% over all the simulations.

With a fixed lower boundary condition, the methane mixing ratio does not adjust to the oxidation rate as the OH concentration is modified by changes in climate and LNO_x. Therefore the feedback between methane and OH is not accounted for. However, the equilibrium methane mixing ratio can be calculated using the change in methane lifetime and a feedback factor which is typically around 1.3 in ACCMIP models (Stevenson *et al.*, 2013) with a range in the literature of

1.19 to 1.53 (Prather *et al.*, 2001; Stevenson *et al.*, 2013; Voulgarakis *et al.*, 2013; Banerjee *et al.*, 2014). I calculate the equilibrium methane mixing ratio for each experiment relative to the CTH-2000 experiment. This is then used to determine the methane radiative forcing (RF) following Myhre *et al.* (1998).

For ozone, the short-term radiative forcing is calculated using the differences in the annual mean spatial distribution of tropospheric ozone column between each experiment and CTH-2000. These differences are multiplied by the horizontal spatial distribution of the radiative forcing efficiency of ozone ($\mathrm{mW\,m^{-2}\,DU^{-1}}$), using an average derived from models contributing to ACCMIP (Stevenson *et al.*, 2013). The area-weighted mean over the distribution provides the global short-term ozone radiative forcing. As ozone is also influenced by changes in methane, there is an additional long-term ozone radiative forcing resulting from the equilibrium methane change. The tropospheric ozone response to a 20% reduction in methane from present-day levels across a range of models contributing to the Task Force on Hemispheric Transport of Air Pollution (TF-HTAP) studies is $0.95\pm0.25\,\mathrm{DU}$. This range is used to estimate the long-term ozone change associated with the inferred methane change, accounting for the non-linear response of ozone to methane changes following Wild *et al.* (2012). The long-term ozone RF is calculated from this change, and the combined long and short term ozone RFs provide the total ozone radiative forcing.

5.3 Changes in lightning between present-day and future

Figure 5.1 shows the simulated change in horizontal distribution of annual mean surface temperature and lightning flash rate between year 2000 and year 2100 under RCP8.5 for the two parametrisations. The changes in surface temperature

(Figure 5.1A) are broadly as expected, with generally increases across the globe and the strongest warming around the North Pole. The global mean increase in surface temperature is +4.87 K which is at the higher end of the warming simulated by the models in ACCMIP for year 2100 (Figure S4.4).

The two parametrisations simulate approximately the same global total flashes in present-day, although the simulated spatial distributions of flash rate do differ. The IFLUX scheme simulates less lightning in the tropics and more in the extratropics than the CTH approach (Figure 3.8). The lightning simulated using the IFLUX scheme was shown, in Section 3.3.1, to correlate well with a climatology of satellite observations, and generally improved upon lightning simulated with the CTH scheme.

The simulated changes in lightning flash rate between present-day and future differ greatly depending on the lightning parametrisation used. The CTH scheme in Figure 5.1B simulates an increase in magnitude of the global flash rate by 0.61×10^9 fl. yr^{-1} in future. Conversely, the IFLUX scheme simulates a global total decrease of 0.58×10^9 fl. yr^{-1} (Figure 5.1C). Changes in LNO_x are proportional to changes in flash rate as each flash produces 250 mol(NO) fl.$^{-1}$ (Section 5.2.2).

The change in horizontal distribution of lightning also differs between the two schemes. With the CTH approach, there are increases everywhere except over some tropical ocean locations and a few locations over land (Figure 5.1B). Changes are largest over tropical land where present-day flash rates are also much higher (Figure 3.1). The decrease in magnitude of the global total lightning simulated by the IFLUX approach stems from changes in the tropics (Figure 5.1C). The flash rate simulated by the IFLUX scheme generally increases in the extratropics, although there are some regions in the mid-latitudes where flash rate decreases such as in the Central USA (Figure 5.1C).

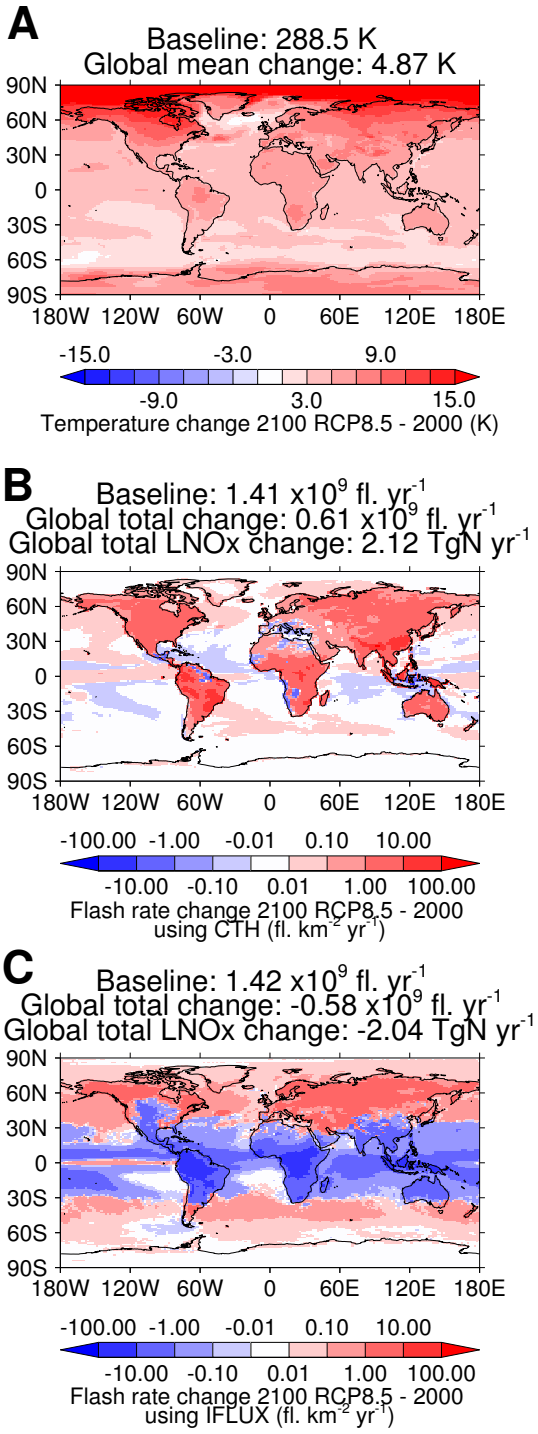

Figure 5.1: Spatial distributions of changes in surface temperature and lightning flash rate between year 2000 and year 2100 RCP8.5. A) is the change in annual mean surface temperature. B) and C) are the change in annual total lightning flashes as simulated by the CTH and IFLUX approaches, respectively. Annual means and annual totals are calculated as the average over the 10 years of simulation.

A decrease in tropical lightning flashes is consistent with some ongoing research regarding the trend observed by the Lightning Imaging Sensor (LIS) satellite instrument (Albrecht *et al.*, 2011) (Section 1.7). Albrecht *et al.* (2011) find that over 13 years of LIS measurements there is generally a decreasing trend in tropical flashes. Over such a short time period the relevance to climate change is uncertain but it does suggest that in a warming climate there may be changes to tropical dynamical and microphysical processes that decrease lightning flashes.

Results in Chapter 4 showed a significant linear response of LNO_x to global mean surface temperature in atmospheric chemistry models using the CTH lightning parametrisation as well as for two models using alternative parametrisations. In this chapter there is only one present-day and one future experiment which precludes the assessment of the relationship between lightning and global surface temperature. However, the CTH approach suggests a response of $0.44\,\mathrm{TgN\,K^{-1}}$ given a present-day emission of $\sim 5\,\mathrm{TgN}$. This is the same as the average value estimated in Chapter 4 of $0.44 \pm 0.05\,\mathrm{TgN\,K^{-1}}$, thereby providing confidence that the CTH scheme applied to the meteorology simulated with this CCM produces a similar climate response to other CCMs. Interestingly, the IFLUX approach simulates an opposite response of $-0.42\,\mathrm{TgN\,K^{-1}}$.

The next section will look to develop the estimate based on upward ice flux by considering the sensitivity to sampling pressure level used in the context of climate change. Section 5.3.2 will present the frequency distribution of lightning in present-day and future, followed by the frequency distributions of meteorological drivers of the simulated lightning in Section 5.3.3. Section 5.3.4 will analyse vertical distributions of meteorlogical drivers to place both the frequency distributions and sampling sensitivity experiment in context.

5.3.1 Sensitivity under climate change of the IFLUX parametrisation to pressure level sampling (IFLUX390)

The IFLUX parametrisation was developed using present-day observations and samples the upward cloud ice flux through the 440 hPa pressure level. This pressure level was chosen based on the definition of deep convective clouds by the International Satellite Cloud Climatology Project (Rossow *et al.*, 1996). The definition is based on present-day observations and the pressure level choice may not hold for a future climate in which the vertical structure, for example the vertical temperature profile, of the atmosphere could change.

A new pressure level for the future climate can be calculated and used in the year 2100 experiment. The following section describes the approach used to calculate a future pressure level which is suitable for the time-slice simulations used here. However, studies using transient simulations would need to generalise this approach, for which I provide a discussion in Section 5.7.

For this study, to calculate the new pressure level, two reference levels are defined, between which the future sampling pressure level will have the same relative position as the 440 hPa level does in the present-day climate. The basis for the reference levels will be atmospheric properties related to the thunderstorm charging process. A key feature is the region in which ice can form, i.e. regions where the temperature is less than 0°C. This isotherm will be used as a lower reference level. Two options for an appropriate upper reference level, shown in Figure 5.2A, are: the tropopause (as a soft limit on thunderstorm vertical development), or the -40°C level (as an approximate limit on the mixed phase region of clouds since at colder temperatures homogeneous freezing of all cloud droplets would be expected (Rosenfeld and Woodley, 2000)). Alternatively, an appropriate reference may be to sample at the same mean temperature level as

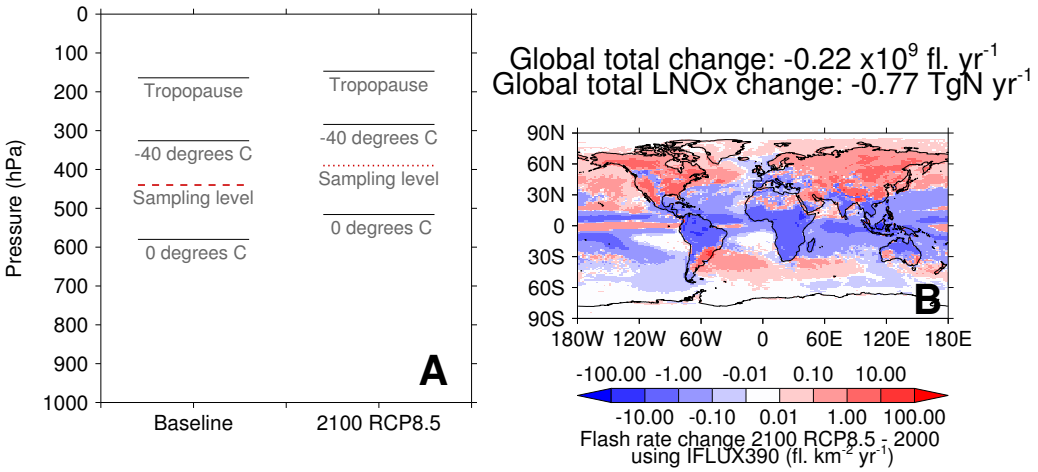

Figure 5.2: Global mean pressure levels used to determine the IFLUX sensitivity experiment and the lightning spatial change between year 2000 and year 2100 RCP8.5 using IFLUX390. A single year is used for the 2000s and 2100s in calculation of pressure levels.

the present-day temperature of the 440 hPa level to ensure that the same part of the charging region is sampled.

Consistent with the original parametrisation, a single pressure-level is chosen at which to sample the upward ice flux. This is done by considering the mean global pressure level associated with the isotherms and tropopause (as discussed above) in the first year of the simulation for the present-day decade compared to the first year of the future decade. Three cases have been considered: 1) where the relative position of the pressure-level is between 0°C and the tropopause, 2) where the relative position of the pressure-level is between 0°C and -40°C, and 3) whereby the global average temperature of the pressure-level (which is 250 K in present-day) is maintained in the year 2100.

All cases result in a pressure-level of approximately 390 hPa for year 2100 RCP8.5.

Hence, this pressure level will be used in an experiment for 2100 as an alternative to the 440 hPa level since it captures the new positions in the future atmosphere, of the key features discussed above.

This alternative experiment for year 2100 will use the same equations as IFLUX but with an input variable of upward cloud ice flux at 390 hPa (IFLUX390-2100, Table 5.1). Comparing the IFLUX390-2100 experiment to the IFLUX-2000 experiment (hereafter, the IFLUX390 variant), the simulated change in the horizontal distribution of lightning flash rate, when using the 390 hPa level in the future time period and the 440 hPa level in present-day, is shown in Figure 5.2B. The IFLUX390 variant results in a similar change in spatial distribution of lightning flash rate but a weaker response than the IFLUX approach, when compared to the IFLUX-2000 experiment (Figures 5.1C and 5.2B). When using the 390 hPa pressure level in the future climate, global total flash rate decreases by 0.22×10^9 fl. yr^{-1} between present-day and future, with a corresponding decrease in LNO_x. This is compared to a 0.58×10^9 fl. yr^{-1} decrease when using the 440 hPa pressure level. The lightning NO_x response relative to the change in global mean surface temperature is estimated to be - 0.15 TgN K^{-1}, compared to - 0.42 TgN K^{-1} using the 440 hPa level.

The results simulated with the IFLUX-2100 and IFLUX390-2100 represent two different methods for applying the ice flux based scheme in a future climate. Therefore, the results of these two schemes do not represent a range of uncertainty of lightning simulated using the ice flux based lightning parameterisation, but instead provide the sensitivity associated with the fixed pressure level against varying pressure level methods. It will be for further studies to determine uncertainty for each given method.

The use of 390 hPa to determine the response of lightning to future climate change produces results consistent with recent regional studies (Brooks, 2013; Romps

et al., 2014). Romps *et al.* (2014) used convective available potential energy and precipitation to parametrise lightning. They found that, for the models they considered, lightning was projected to increase over the US in the late 21^{st} century in response to climate change under RCP8.5, with a mean response of $+12\,\%\,K^{-1}$. The results using the 390 and 440 hPa pressure levels produce a change in lightning flash rate over the US, between present-day and future, of +3.4 and -1.1 $\%\,K^{-1}$, respectively . As for the IFLUX390 variant and the work of Romps *et al.* (2014), the CTH approach also simulates an increase in US lightning ($+14.2\,\%\,K^{-1}$). Brooks (2013) also proposed that changes in convective available potential energy could drive increased thunderstorms in the US. However, they suggested that drivers of change in thunderstorm activity in Europe may not be so simply linked to global warming. Uncertainty in the response of European lightning to climate change is also apparent in the results here; over continental Europe the estimated responses of lightning are -2.3, +9.4 and $+4.5\,\%\,K^{-1}$ using the IFLUX390 variant, and the IFLUX and CTH schemes, respectively. The global results here highlight that changes in extratropical locations such as the US may not be representative of the global total lightning changes which are largely driven by changes of meteorology in the tropics.

5.3.2 Future changes in lightning frequency distribution

The change in the mean state of lightning activity, as so far discussed, is useful for studying the change in the annual lightning NO_x source but does not provide information regarding changes in the frequency or intensity of flash rates. The frequency distributions of flash rates for a year of simulation in present-day and in future (Section 5.2.3), for each parametrisation, in the tropics (30S-30N) and extratropics, are shown in Figure 5.3. The total number for flashes over each region (tropics and extratropics) during the year are provided in Table 5.2, along

with the probability of lightning, based on hourly data. The probability increases if either lightning occurs in more grid cells or during more hours over the course of the year. A value of 1 would correspond to lightning occurring in every grid cell in every hour during the year.

The CTH approach exhibits periodic spikes in the distribution (Figure 5.3A and C). The cloud-top height variable is determined as the height of the centre of the model level in which the cloud top lies. This results in a limited set of possible cloud-top heights and therefore of possible flash rates within each grid cell. There are the same number of peaks as model levels in the range of the cloud-top height variable so it is inferred that this periodicity is an artefact of vertical discretisation of the cloud-top height variable. For the remainder of the study, the focus is on the general form of the distribution, ignoring the periodic features.

In the tropics, all future experiments simulate a reduction in the probability of lightning of between 6–20 % (Table 5.2). With the CTH scheme, even though there is a reduction in probability, there is a shift in the lightning frequency distribution to higher flash rates (Figure 5.3A). Overall, this shift to higher flash rates increases the total tropical flashes (Table 5.2). In contrast the IFLUX approach simulates a decrease in mid-range and high flash rates and therefore simulates a decrease in total tropical flashes. When using the 390 hPa pressure level in the future instead of the 440 hPa, there is little change in the frequency distribution compared to present-day. Therefore, total tropical flashes decrease by a similar proportion to the reduction in probability of lightning when using the 390 hPa level for the future climate. Overall, these results suggest that lightning will occur less often in the tropics in future, but that this may be accompanied by a shift in the frequency distribution to higher or lower flash rates depending on the lightning parametrisation used.

In the extratropics, all future experiments simulate an increase in total flashes,

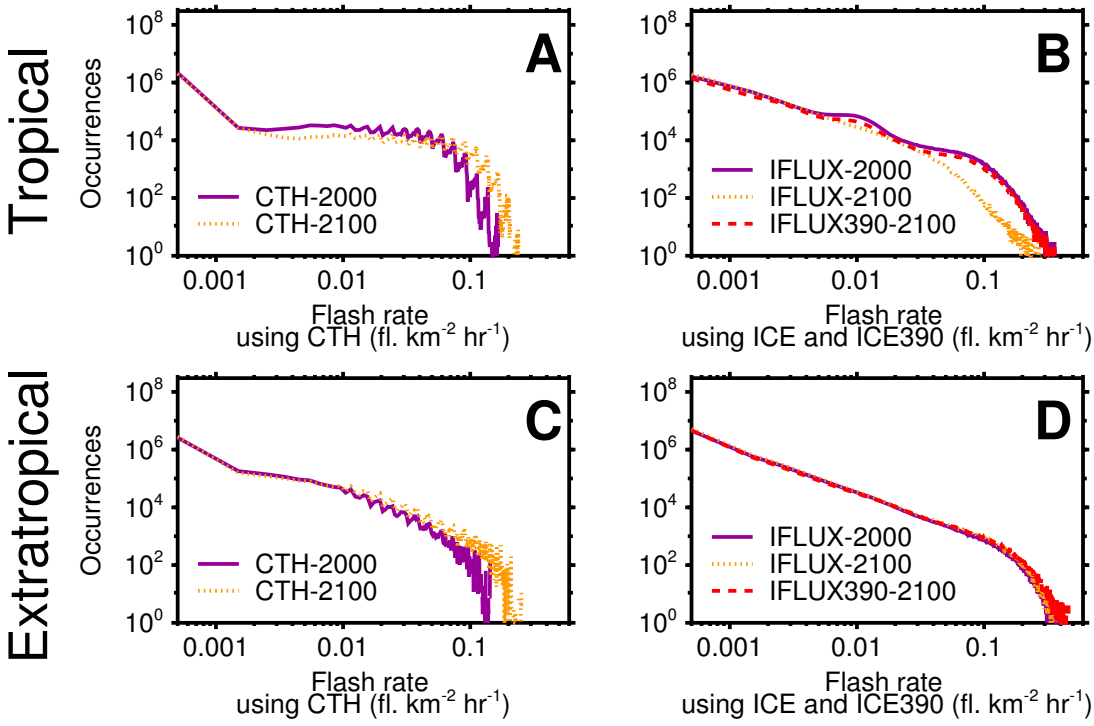

Figure 5.3: Tropical (30S-30N) and extratropical frequency distribution of lightning simulated by the CTH, IFLUX and IFLUX experiments, and for year 2000 and year 2100 RCP8.5 using instantaneous hourly values for all grid cells from the first year simulated in each respective experiment. Solid purple and dotted orange lines are results for the year 2000 and year 2100, respectively. Dashed red lines in (C) and (D) are the IFLUX390-2100 simulation.

Table 5.2: Total annual flashes and probability of lightning in the tropics and extratropics for each experiment. Percentage changes relative to 2000 for each approach are given in brackets. The probability metric represents the probability of lightning occurring in any given grid cell and hour over the course of the year.

Experiment	Tropics Total flashes ($\times 10^8$ fl. yr^{-1})	Tropics Probability of lightning	Extratropics Total flashes ($\times 10^8$ fl. yr^{-1})	Extratropics Probability of lightning
CTH-2000	10.9	0.056	3.07	0.021
CTH-2100	14.2 (+30.3%)	0.049 (-12.5%)	5.31 (+73.0%)	0.024 (+14.3%)
IFLUX-2000	9.29	0.059	4.87	0.036
IFLUX-2100	3.22 (-65.3%)	0.055 (-6.8%)	5.15 (+5.7%)	0.040 (+11.1%)
IFLUX390-2100	6.66 (-28.3%)	0.047 (-20.3%)	5.34 (+9.7%)	0.036 (+0.0%)

and either no change or an increase in the probability of lightning, compared to present-day. The frequency distribution of flash rates simulated with the ice flux based experiments, for both pressure levels, changes little. However, the CTH approach shows a greatly increased occurrence of high flash rates in the future climate which leads to the increase of 73 % in extratropical flashes.

Total extratropical flashes increase proportionally more than total tropical flashes within all future experiments. Although, in the case of the ice flux based experiments for both sampling pressure levels, this is because there is a decrease in tropical flashes but a small increase in extratropical flashes. Consequently the results here suggest that in future, extratropical lightning (primarily in the mid-latitudes) may play a more substantial role in the global lightning distribution.

5.3.3 Frequency distributions of meteorological drivers of future changes in simulated lightning

Differences in the projected changes in lightning between the lightning parametrisations arise through their use of different aspects of meteorology to parametrise lightning. In this section, I consider how the variables used by each parametrisation alter with climate change.

It is important to note that there will be uncertainty in the representation of the meteorological variables in both present-day and in their response to climate change. By presenting analysis of the meteorological drivers of the lightning parametrisations, it will be possible for further studies to consider how the parametrisations would behave if the driving meteorological variables are simulated respond differently to climate change.

Lightning simulated using the CTH approach is based on the cloud-top height

variable with a condition that the cloud depth must be greater than 5 km. The changes of the cloud-top height variable (not shown) are the main driver of changes in simulated lightning by the CTH approach. However, the cloud-base height must also play a role in the number of occurrences of lightning flashes as it is used to determine the cloud depth. In the tropics and for the 2100s (using the first year of simulations as discussed in Section 5.2.3), the mean height of the cloud-top, in grid cells where lightning is determined to occur, increases by 900 m compared to the 2000s, whilst the mean cloud-base height only increases by 40 m. This implies that in the tropics the clouds are deepening. In the extratropics, a deepening of thunderstorm clouds in the future is also found, where the mean cloud-top height increases by 680 m whilst the mean cloud-base height increases by only 300 m. The simulated future changes in cloud height are in combination with the projected decrease in the probability of lightning in the tropics and the increase in probability of lightning in the extratropics, discussed in Section 5.3.2. This implies that there are fewer but deeper clouds with lightning in the tropics, and more occurrences of, as well as deeper clouds with lightning in the extratropics.

Interpreting the future changes in lightning simulated by the IFLUX approach is more complex since three meteorological input variables are used to parametrise flash rate. The frequency distributions of specific cloud ice content, updraught mass flux and cloud fraction for instances where the IFLUX or IFLUX390 experiments have simulated lightning to occur are shown in Figure 5.4. In the tropics, the projected changes in lightning by the IFLUX approach are driven through reduced cloud ice content and reduced updraught mass flux. The projected changes in lightning by the IFLUX390 variant occur for similar reasons although the shift in Figure 5.4A to lower ice contents is less apparent. Instead the reduction in the probability of lightning, as discussed in Section 5.3.2, is the dominant cause of reduced lightning flashes in the tropical region when using the 390 hPa pressure level in the future simulation. In the extratropics, increases in

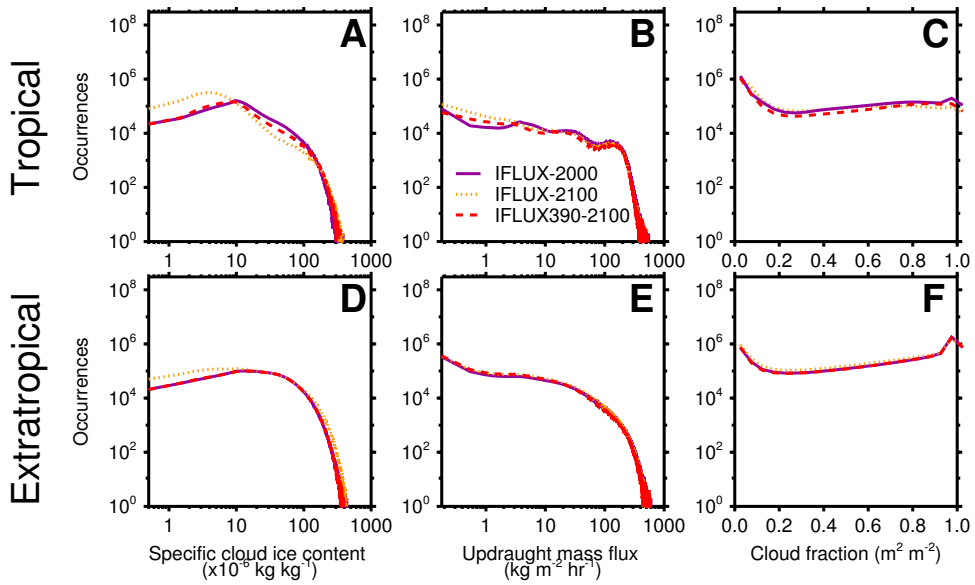

Figure 5.4: Frequency distributions in the tropics and extratropics for year 2000 and year 2100 RCP8.5 of: specific cloud ice content, updraught mass flux and cloud fraction, using only occurrences when lightning was deemed to occur. Purple solid and orange dotted lines are results using IFLUX for the year 2000 and year 2100, respectively. Red Dashed lines are results for year 2100 using IFLUX390. Results also use the first year of simulation for the two time periods as in Figure 5.3.

lightning are mainly due to increased probability of lightning once again, although when using the 440 hPa sampling level in the 2100s, the increased probability is mainly through more occurrences at low ice and high ice contents, with mid-range ice contents occurring to a similar extent in future as for present-day.

The shifts in ice content are principally decreases due to increased temperature, but some increases in ice may also occur due to increased moisture content in the atmosphere. Changes in updraught mass flux relate to the stability of the atmosphere. In this chapter, increased stability appears to occur most of all in the tropical region, since this region shows the largest reduction in updraught

mass flux. Increased tropical static stability can arise as a result of the decreased moist adiabatic lapse rate in a warmer atmosphere (Knutson and Manabe, 1995; Lu *et al.*, 2008). It has also been suggested by Held and Soden (2006) that the convective updraught mass flux would be expected to decrease in the tropics due to changes in the hydrological cycle under climate change - a feature that is apparent amongst simulations in the IPCC CMIP5 ensemble (Collins *et al.*, 2013). Furthermore, the results here are consistent with the mechanism proposed by Chou and Chen (2010) whereby a future increase in tropical tropopause height ($\sim$1 km in the simulations here, as shown in Figure 5.7), allows for deeper convection and stabilises the tropical atmosphere. Overall, Collins *et al.* (2013) highlight several mechanisms which contribute to reduced tropical ascent under climate change which supports the simulation of a reduction in updraught mass flux in this Chapter.

5.3.4 Annual average vertical distribution of meteorological variables driving lightning

Section 5.3.3 has described the input variables for the ice flux based experiments in the present-day and future climate. In this section, it is considered whether the pressure levels used have represented broader changes in the atmosphere through analysis of the annual mean vertical distributions of relevant meteorological variables.

Figure 5.5 shows the decadal average vertical distributions of cloud ice content, updraught mass flux in convective cloud, convective cloud fraction and bulk cloud fraction for the present-day and future time-slices. These are the variables which are sampled at the 390 and 440 hPa pressure levels for use within the IFLUX and IFLUX390 experiments. The grid cell mean updraught mass flux for use in the IFLUX parametrisation is formed by multiplying the updraught mass flux

in convective cloud by the convective cloud fraction. Examining the vertical distributions of these key variables provides further insights into the importance of the sampling pressure level (dashed lines) on the simulated lightning flash rate. It also enables links to be made between the meteorological drivers of the two lightning parametrisations.

In the tropics, cloud ice content (Figure 5.5A) reduces at most levels except where the cloud height increases, i.e. where the bulk cloud fraction increases at the lower pressures (Figure 5.5D). In Figures 5.5 B and C, the updraught mass flux and convective cloud fraction, above ∼900 hPa, generally decrease. The bulk cloud fraction (Figure 5.5D) generally decreases which acts to intensify the upward ice flux since the flux is occurring within a smaller region. However, the change in the cloud fraction is likely to be outweighed at most levels by the reduction in cloud ice content and updraught mass flux. Except where additional cloud occurs due to an increase in cloud height, most altitudes within the tropical region show a decrease in updraught mass flux and ice content suggesting the changes in lightning projected using the ice flux approach are capturing broader changes in dynamics and microphysics within the clouds.

In Section 5.3.2 it was shown that using both the 390 and 440 hPa pressure levels in the ice flux approach, there was only a small increase in extratropical lightning in future. When using the 440 hPa level for year 2100, this was due to an increase in lightning probability. When using the 390 hPa level for year 2100, the small increase is likely due to a slight increase in cloud ice content which is evident over pressures less than ∼450 hPa (Figure 5.5E).

Finally, in both the tropics and extratropics there is an increase in cloud fraction at higher levels (< 200 hPa) in 2100 (Figures 5.5D and H) which suggests an increase in the average cloud-top height, consistent with the mean cloud-top height results discussed in Section 5.3.3. Along with higher cloud in the future, there is a shift in

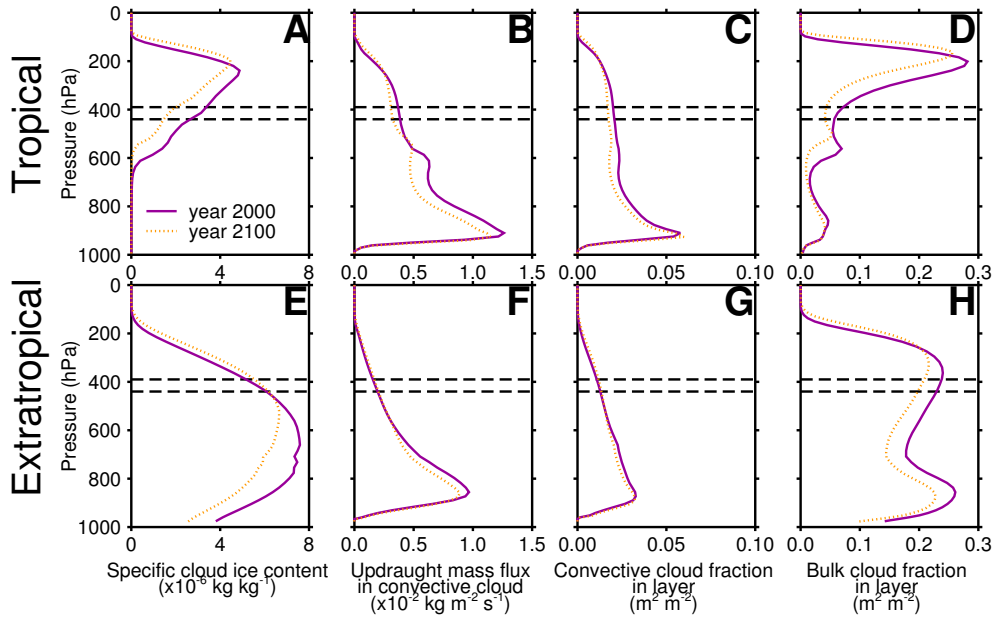

Figure 5.5: Vertical distributions, in the tropics and extratropics and for the 2000s and 2100s under RCP8.5, of the decadal climatology of: specific cloud ice content, updraught mass flux in convective cloud, convective cloud fraction and bulk cloud fraction. Values for the meteorological variables are taken at the sampling pressure level used in each experiment. Solid purple and dotted orange lines are results for the 2000s and 2100s, respectively. Dashed lines show the 440 and 390 hPa sampling levels used in the IFLUX and IFLUX390 experiments. Unlike the analysis for Figures 5.3 and 5.4, this figure includes all data for each variable, not only that where lightning is deemed to occur.

the vertical distribution of cloud ice content and updraught mass flux to higher levels. I therefore conclude that the higher level of 390 hPa has appropriately accounted for the shift in vertical distribution between present-day and future of the key meteorological variables in the charging process. Whilst the CTH approach has captured the increase in cloud-top height, it does not capture these key reductions of updraught mass fluxes and ice contents within the tropical convective clouds and therefore has simulated a different response of lightning to climate change than the ice flux based experiments.

5.4 Future atmospheric composition change driven by changes in lightning

The following sections describe the impacts of changes in lightning NO_x on tropospheric ozone, OH and methane lifetime.

5.4.1 Ozone

Both the global total and the spatial distribution of lightning and LNO_x simulated by the lightning parametrisations substantially change in the future (Section 5.3). These changes in LNO_x impact tropospheric ozone. Table 5.3 shows the tropospheric ozone burden and lifetime for each experiment described in Table 1. There is a small increase in total tropospheric air mass between the present-day and future scenarios of 0.7%. Such a change implies there could be a small increase in ozone burden and other tropospheric constituents, however, based on the results of Table 5.3, any increase is outweighed by the decreasing effects of both climate change and LNO_x.

Table 5.3: Tropospheric ozone burden, tropospheric ozone lifetime and methane lifetime of each experiment. Percentage changes relative to year 2000 for each approach are given in brackets. Radiative forcings (RF) for each future experiment with respect to the relative year 2000 experiment are also given. These are used to produce Figure 5.8. The net RF is the sum of the CH_4 RF and the net O_3 RF

Experiment	O_3 burden (Tg)	O_3 lifetime (days)	CH_4 lifetime (yrs)	CH_4 RF (mW m^{-2})	net O_3 RF (mW m^{-2})	net RF (mW m^{-2})
ZERO-2000	209	18.7	12.5			
ZERO-2100	191 (-9%)	15.5 (-17%)	9.9 (-21%)	-169.7	-140.5	-309.2
CTH-2000	271	20.1	9.9			
CTH-2100	266 (-2%)	16.9 (-16%)	7.5 (-24%)	-189.0	-95.0	-284.0
IFLUX-2000	266	19.8	9.9			
IFLUX-2100	223 (-16%)	16.1 (-19%)	8.8 (-11%)	-81.9	-228.7	-310.6
IFLUX390-2100	237 (-11%)	16.3 (-18%)	8.1 (-18%)	-135.0	-177.5	-312.6

The change in ozone between the ZERO-2000 and ZERO-2100 experiments represents the direct impact of climate change on tropospheric ozone independent of LNO_x. The direct climate change effect simulated with the present-day and future ZERO experiments is a reduction of tropospheric ozone burden and ozone lifetime. This direct climate change effect on tropospheric ozone will be through increases in atmospheric temperature and humidity (Jacob and Winner, 2009; Doherty *et al.*, 2013; Stevenson *et al.*, 2013). In particular, ozone in low NO_x regions will be reduced through increased loss of O(1D) by reaction with water vapour, as described in Section 1.4.2.

For experiments including LNO_x emissions, the change in ozone burden between present-day and future will be a combination of the change in LNO_x and the direct climate change effect described above. The CTH approach simulates a smaller reduction in the ozone burden between the present-day and future than the equivalent ZERO experiments. This is because the increased LNO_x response to climate change, simulated by the CTH scheme, offsets much of the reduction in ozone burden that would otherwise have occurred due to the direct climate change effect. The tropospheric ozone lifetime is much less affected because the smaller reduction in ozone burden that occurs in the CTH experiments is counteracted by a larger increase in chemical loss in the CTH experiments (not shown). The IFLUX approach, which simulates a decrease in future LNO_x, has the opposite effect of the CTH approach, with a greater decrease in tropospheric ozone burden and lifetime. Using the 390 hPa pressure level in the future leads to a smaller reduction in LNO_x than using the 440 hPa level, and therefore smaller decreases in ozone burden and lifetime.

For each of the seven experiments in Table 5.3, the tropospheric ozone burden is plotted in Figure 5.6 along with gross and net ozone production. Within each of the climate time-slices there is a linear response of all three variables to LNO_x. Linearity is also found in the response to LNO_x changes of methane lifetime and

other terms in the ozone budget (not shown). The results are consistent with the study by Wild (2007) who find approximate linearity in ozone burden in present-day in response to LNO_x changes over the range 0-7.5 $TgN\,yr^{-1}$.

Banerjee *et al.* (2014), who applied the CTH scheme in present-day and future climates, found that ozone production responded linearly, and ozone burden non-linearly, to LNO_x changes. However, as Banerjee *et al.* (2014) notes, these changes were across different climates in which meteorological factors can also influence the ozone burden. Figure 5.6 also shows the response of ozone production, loss and burden per $TgN\,yr^{-1}$ change in LNO_x. This was calculated for each experiment by dividing the difference of each variable with its value in the corresponding ZERO experiment by the total annual LNO_x emission. For the CTH approach, there is only a slight difference in gross ozone production efficiency (OPE) of LNO_x between the present-day and future time periods, whereas the net ozone production and ozone burden are substantially less affected by LNO_x in the future climate compared to present-day. These two findings are consistent with the findings of Banerjee *et al.* (2014), and suggest that some of the non-linearity seen across different climates in ozone burden changes, is due to a weaker effect of LNO_x in the future climate. However, the ice flux approach, using either pressure level in the future climate, produces larger changes in gross OPE and less change in the ozone burden than the CTH experiments. The most consistent response across experiments is a reduction of net OPE from LNO_x in the 2100s compared to present-day.

Figure 5.7 shows the percentage change between present-day and future in the zonal mean distribution of ozone mixing ratio resulting from the CTH and IFLUX lightning parametrisations and the IFLUX390 variant. The changes in ozone mixing ratio due to climate change (within the ZERO experiments) have been removed from the overall changes in ozone distributions to show the effect of LNO_x only. The general response across all three cases is consistent with the

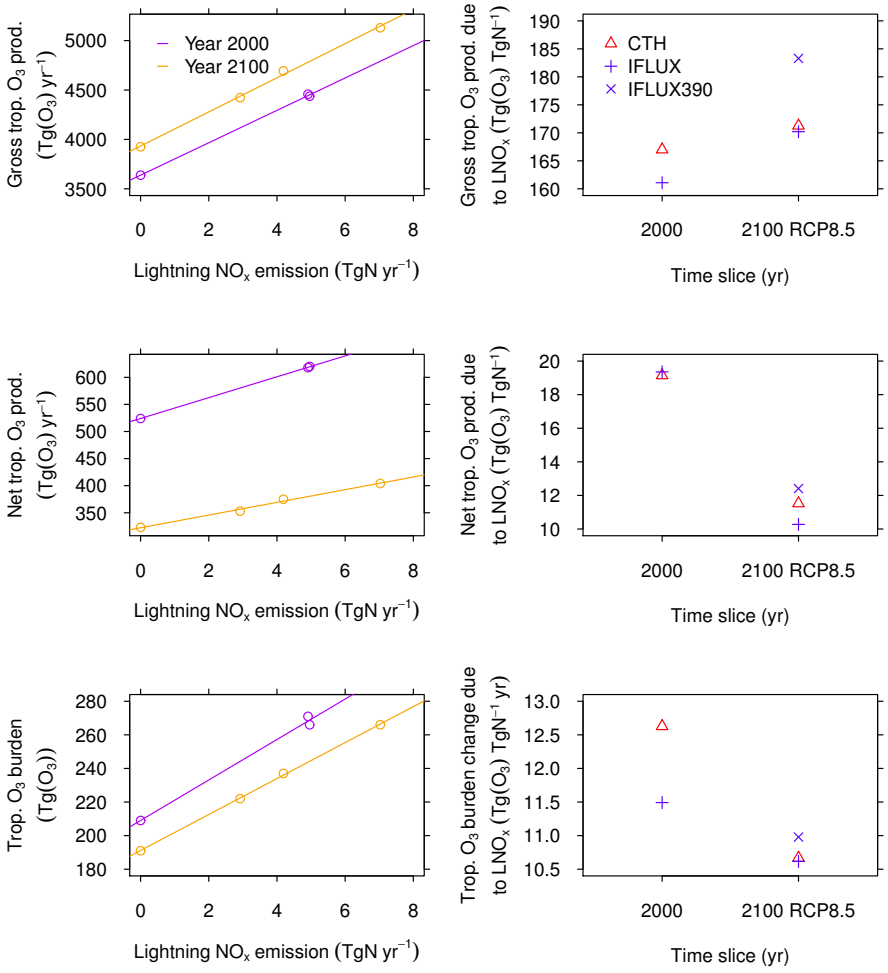

Figure 5.6: Gross and net tropospheric ozone production and tropospheric ozone burden change due to lightning $\mathrm{NO_x}$. The left column shows the raw values of ozone production and burden grouped into the present-day (purple) and the 2100s RCP8.5 (orange) experiments. The right column shows the ozone production efficiency and the change in ozone burden, per TgN change in lightning $\mathrm{NO_x}$ only. This change was calculated by subtracting the ozone production or burden in the ZERO experiment from the production or burden in the CTH/IFLUX/IFLUX390 experiment in the equivalent time-slice and dividing by the total $\mathrm{LNO_x}$ emissions in that experiment.

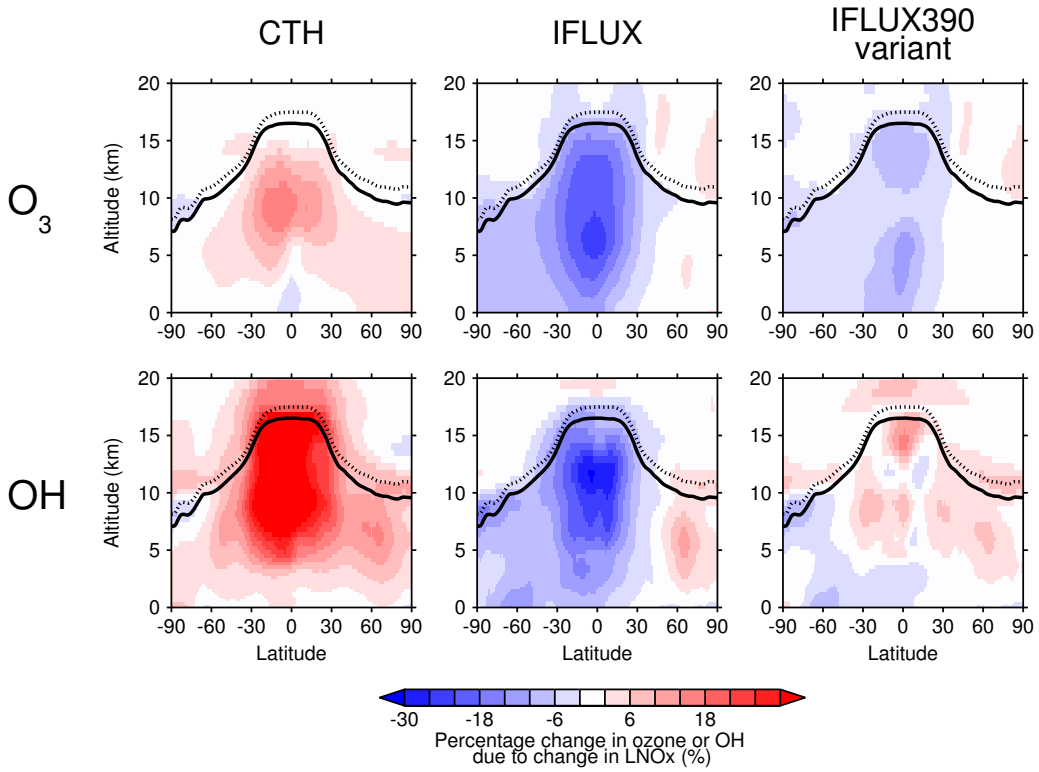

Figure 5.7: Zonal mean percentage change in ozone mixing ratio, and OH concentration, between the 2000s and 2100s under RCP8.5 for the CTH and IFLUX approaches and the IFLUX390 variant. The direct effect of climate changes has been removed by first subtracting the change in the ozone mixing ratio, and OH concentration, between the ZERO-2000 and ZERO-2100 experiments. The present-day (solid) and future (dotted) zonal annual mean tropopause are shown. The tropopause is determined using the combined isentropic-dynamical definition as described by (Hoerling *et al.*, 1993).

global ozone burden changes shown in Table 5.3. However, the distribution of change is markedly different for the CTH and IFLUX approaches. The CTH scheme simulates an increase in ozone with a maximum around the mid to upper troposphere, as a consequence of the shift to higher flash rates and therefore LNO_x emissions in the tropics under climate change, as shown by Figure 5.3A. The IFLUX scheme simulates more vertically spread changes throughout the tropical troposphere with a maximum in the mid troposphere. This is a consequence of a reduction in mid-range and high flash rates reducing lightning NO_x emissions throughout the whole troposphere. The change of ozone between present-day and future simulated using the IFLUX390 variant is similar to, but less than, that using the IFLUX approach. The largest percentage changes in ozone between present-day and future for all lightning schemes are located in the tropics, corresponding to the largest changes in LNO_x. However, the vertical location of changes in ozone are not fully co-located with changes in the NO_x emission source but are also affected by transport and chemical losses of ozone.

5.4.2 OH and Methane lifetime

OH is a key oxidant in the atmosphere and the main sink for methane in the troposphere, controlling the methane lifetime. As noted in Section 5.2.1, methane concentrations are constrained to present-day levels in the present-day and future simulations. Hence, the methane lifetime is affected only by changes in loss rate. The global methane lifetime for each experiment is given in Table 5.3 where additional methane loss mechanisms in the stratosphere, from tropospheric chlorine, and soil uptake are assumed fixed at values provided by Prather *et al.* (2012, their Table S1). An increase in OH, and decrease in methane lifetime, is expected due to increased water vapour in the future climate (Section 1.4.2), and this is apparent as a 21% reduction in methane lifetime in the ZERO experiments

(Table 5.3). The LNO_x source drives production of OH which also acts to decrease the methane lifetime (Figure 1.4). Therefore, changes in methane lifetime between present-day and future, for the experiments including LNO_x emissions, will be a combination of the climate change effect and the effect of LNO_x changes.

The experiment using the CTH lightning scheme simulates an increase of LNO_x in the 2100s, which leads to an increase in OH and therefore a greater reduction in methane lifetime occurs than from climate change alone. In contrast, the IFLUX scheme, and to a lesser extent the IFLUX390 variant, simulate a decrease in LNO_x in the future which offsets some of the reduction in methane lifetime seen in the climate change only (ZERO) experiments.

The changes in OH due to LNO_x changes between the present-day and future simulations are mainly located in the tropics (Figure 5.7). In the case of the CTH and IFLUX approaches, the percentage changes in OH are greater than 30% (positive and negative, respectively) in some locations, and consistent with changes in the methane lifetime discussed above. The IFLUX390 variant simulates a less coherent change across the tropics with much smaller percentage changes.

5.5 Radiative forcing driven by changes in lightning

The radiative forcing (RF) associated with the substantial changes in tropospheric ozone burden and methane lifetime described in Section 5.4 are now considered. In this chapter, methane concentration is not interactive and therefore the feedback on OH concentration and on the ozone burden is accounted for through feedback factors provided in literature, as described in Section 5.2.4. Typical factors are used to calculate RFs which are shown in Figure 5.8. In addition, uncertainty

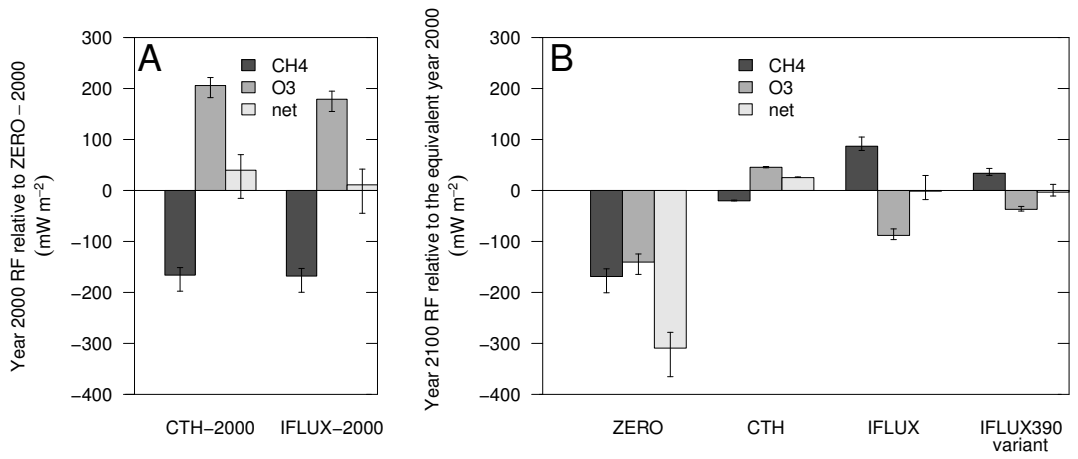

Figure 5.8: Radiative forcing (RF) of ozone, methane and the net forcing resulting from changes in lightning emissions and climate. Uncertainty bars are the RF estimated using two sets of parameters for a high and a low methane feedback as described in Section 5.2.4. A) shows the RF of $\mathrm{LNO_x}$ in present-day with respect to an atmosphere with no $\mathrm{LNO_x}$. B) shows, for each future experiment, the RF relative to its corresponding present-day experiment (in the case of the IFLUX390 variant this is IFLUX-2000). In addition, for the CTH, IFLUX and IFLUX390 RF values, the RF as a direct result of climate change given by the ZERO experiments has been removed so only the $\mathrm{LNO_x}$ effect is shown.

ranges in factors for the methane feedback and the ozone response are used to provide an estimate of the uncertainty in radiative forcing, and these are presented as error bars.

Figure 5.8A shows the radiative forcing of present-day $\mathrm{LNO_x}$ using the CTH and IFLUX approaches relative to the ZERO-2000 experiment which has no lightning $\mathrm{NO_x}$. With both approaches, it is clear that there is strong radiative warming from ozone produced by $\mathrm{LNO_x}$ but that this is counteracted by a strong radiative cooling resulting from reduced methane. The smaller ozone forcing simulated by the IFLUX scheme arises because less ozone is produced in the upper tropical troposphere than by the CTH scheme, and in this region ozone has its greatest radiative forcing efficiency. The net radiative forcing of $\mathrm{LNO_x}$ generated by the

CTH (39.8 mW m^{-2}) and by the IFLUX (11.1 mW m^{-2}) schemes are both positive. However, the uncertainty represented by the error bars spans zero, indicating that with a stronger methane feedback the net forcing could be zero or negative.

The radiative forcing due to methane and ozone for the future climate relative to present-day, based on the simulations without LNO_x (ZERO) is shown in Figure 5.8B. The direct effect of climate change on methane and ozone thus reduces the radiative forcing of both species, resulting in a strong net radiative cooling of -309 (-278 to -365) mW m^{-2} in the year 2100 under RCP8.5 from these two chemical species. For the remaining experiments depicted in Figure 5.8 this RF due directly to climate change is removed so that only the future RF from LNO_x is shown. The direct climate change RF in the ZERO experiments is different to that in the CTH and IFLUX experiments since background concentrations of ozone and OH vary. Therefore, a small direct climate change RF remains within the future RFs from LNO_x, but it is reasonable to associate this with the lightning NO_x emissions themselves.

Relative to the year 2000, changes in LNO_x projected with the CTH scheme for the 2100s represent a predominantly positive radiative forcing due to an increase in ozone burden. The RF uncertainty is small due to a small methane radiative forcing. The net RF from methane and ozone in 2100 relative to 2000 is 25.2 mW m^{-2} using this CTH scheme (Figure 5.8B). This implies that the CTH approach would induce a positive climate feedback overall as postulated by Toumi *et al.* (1996), given that it also simulates a positive response of lightning to increased surface temperatures. The IFLUX scheme and its IFLUX390 variant, relative to present-day, show approximately zero net forcing due to future climate change, but could have small positive or negative forcing depending on the size of the uncertainty in the methane feedback. The zero net forcing of these schemes is due to a balance of the RF arising from changes in ozone and methane. Because methane is a well-mixed GHG, whilst ozone is regionally variant, there may be

regional variation in the RF despite the global net forcing being close to zero. However, the global balance suggests that for the climate change scenario in 2100 investigated here, although lightning activity is affected by climate change, there is no lightning-climate feedback when using the IFLUX/IFLUX390 approach.

5.6 Conclusions

A lightning parametrisation based on upward cloud ice flux has been shown in a CCM, UKCA, to project a reduction in global total lightning in the 2100s in response to climate change under the RCP8.5 climate scenario. This reduction occurs through both reduced cloud ice and updraught mass flux in the tropics. The widely-used parametrisation based on cloud-top height (Price and Rind, 1992) exhibits a contrasting response of increased lightning in future due to a general deepening of convective clouds. Given the close link of the ice flux approach to thunderstorm charging theory, the difference in the simulated response of lightning between the parametrisations raises the question of whether the cloud-top height approach fully incorporates the necessary meteorological variables to simulate the response robustly. However, it is acknowledged that the changes to meteorological variables, such as cloud ice and updraught mass flux, driving the ice flux approach in future climates are also uncertain. As understanding of the response of convective and microphysical processes to climate change improves, projections made using lightning parametrisations should also become more robust. Based on the evidence presented here, and in Chapter 4, a diversity of parametrisations is currently necessary to capture the uncertainty in simulated lightning under climate change.

The simulated responses of global annual lightning NO_x emissions to global mean surface temperature change are $+0.44\,\mathrm{TgN\,K^{-1}}$ and -0.42 $\mathrm{TgN\,K^{-1}}$, given a

present-day source of ∼5 TgN, for the cloud-top height and ice flux approaches, respectively. A sensitivity study with the ice flux approach, adjusting the sampling pressure level in the future climate to reflect changes in atmospheric structure with climate change, provides a more robust estimate of the lightning-climate response for the ice flux approach of -0.15 $TgN\,K^{-1}$. The sensitivity study used here could be generalised with a time-varying pressure level thereby providing an appropriate lightning parametrisation for different models and climates. Such a generalisation has not been implemented in this chapter and would require evaluation against present-day observations.

Simulations with lightning switched off are used to show that climate change, primarily through changes in humidity, leads to a decreased tropospheric ozone burden and a decreased methane lifetime. The simulated changes in lightning NO_x due to climate change are shown to modify these underlying climate change effects on tropospheric ozone, OH and the methane lifetime. Increases in the global tropospheric ozone burden, due to a change in lightning simulated using the cloud-top height approach, offsets much of this reduction in tropospheric ozone due to climate change. In contrast, the reduction in lightning simulated by the ice flux approach, especially in the tropics, reinforces the climate change effect in tropospheric ozone burden. In addition, the enhanced lightning NO_x simulated with the cloud-top height approach reinforces the reductions in methane lifetime due to climate change, while the ice flux approach counteracts the climate change effect.

By using the simulated changes in ozone and calculating an equilibrium change in the methane mixing ratio, the radiative forcing of lightning NO_x in the present-day and future are estimated. It is found that the production of lightning NO_x in the present-day leads to large and opposing radiative forcings from ozone and methane. The net radiative forcing is close to zero but most likely small and positive. The simulated future change in lightning by the cloud-top height

approach results in a small net positive forcing in the year 2100 under RCP8.5 of 25.2 $\mathrm{mW\,m^{-2}}$. The individual forcings of ozone and methane due to future lightning changes simulated by the ice flux approach are large and opposite, thus cancelling to give a net radiative forcing in the year 2100 of approximately zero.

The choice of lightning parametrisation greatly affects the simulated changes in lightning associated with climate change. This has important consequences for our understanding of tropospheric ozone, OH and methane and their likely responses to climate change. This uncertainty in future atmospheric composition and radiative forcing is not captured by models which largely use the cloud-top height scheme for parametrising lightning. Further research using improved, more physical representations of lightning in models is needed to reduce these uncertainties and improve our understanding of future lightning, and lightning NO_x driven changes in atmospheric composition.

5.7 Supplementary text: Generalisation of the IFLUX390-2100 experiment

In this supplement, a generalisation of the changing pressure-level approach of the IFLUX390-2100 experiment is presented for possible use in further studies.

For different CCMs or different time periods the sampling pressure level would vary depending on the position of the pressure levels plotted in Figure 5.2A. It is beyond the scope of this chapter to implement and evaluate a generalisation of the variable sampling level, however, the following paragraph describes a method that further studies could use.

The relative position of the variable sampling level, based on the mean pressure of the 0°C isotherm and the tropopause, as described above, can be generalised using the following equations:

$$p_{sample}(t) = \bar{p}_{0C}(t) - K_{2000}(\bar{p}_{0C}(t) - \bar{p}_{trop}(t)) \tag{5.6}$$

$$\text{with } K_{2000} = \frac{\bar{p}_{0C}(year2000) - 440hPa}{\bar{p}_{0C}(year2000) - \bar{p}_{trop}(year2000)} \tag{5.7}$$

where p_{sample} is the pressure level at which to sample the upward cloud ice flux, t is the time period, K_{2000} is a constant determined from the present-day climate, $\bar{p}_{0C}$ is the simulated global mean pressure of the 0°C isotherm, and $\bar{p}_{trop}$ is the simulated global mean pressure of the tropopause. In the simulations made here, it has been calculated that $K_{2000} \simeq \frac{1}{3}$. Alternatively, the simulated global mean pressure of the -40°C isotherm could be used instead of $\bar{p}_{trop}$ in Equations 5.6 and 5.7.

Chapter 6

Conclusions

6.1 Summary

For some time scientists have been aware of the importance of lightning to atmospheric chemistry. Through the generation of lightning nitrogen oxides (NO_x) in the upper troposphere, there can be large impacts on tropospheric ozone and OH. The connection of lightning to atmospheric composition necessitates its inclusion in chemistry-climate models (CCMs). However, there remain large uncertainties regarding the representation of lightning in CCMs. Therefore the aims of this thesis have been to:

1. To explore existing schemes, and develop a new process-based scheme, to parametrise lightning

2. To use the new process-based lightning scheme to give insights regarding the role of lightning NO_x in tropospheric chemistry

3. To use alternative lightning schemes to improve the understanding of the

response of lightning to climate change, and the consequent impacts on tropospheric chemistry

The research carried out to achieve these aims has led to the advancement of scientific knowledge in several key areas.

It has been shown in Chapter 2 that cloud ice fluxes, fundamental to the non-inductive charging theory, can be used to simulate lightning activity globally. Several lightning parametrisations in the literature have been developed through explicit measurement of individual thunderstorms followed by application of the parametrisation on a larger scale. However, in this thesis a large-scale method has been adopted whereby reanalysis data is used to provide the best approximation of global meteorological conditions to compare to satellite lightning observations. As a result, a new global lightning parametrisation based on cloud ice flux has been constructed. A comparison of the new parametrisation to existing parametrisations, based on alternative meteorological variables, suggests that the novel process-based approach improves upon existing methods for parametrising lightning. In particular, the ice flux approach simulates a more realistic annual zonal mean distribution of lightning than the existing parametrisations, including that based on cloud-top height.

In chapters 3 and 4, the effect of lightning NO_x on atmospheric chemistry is studied using a range of lightning parametrisations and CCMs, including a detailed study with one CCM. The chapters provide a number of insights regarding the uncertainties and sources of bias within simulations of atmospheric composition associated with lightning parametrisation. First, in Chapter 3, the more realistic zonal lightning distribution simulated with the new ice flux approach compared to the widely-used cloud-top height approach, leads to reduced tropical ozone and improved correlation with ozone sonde measurements. Second, in Chapter 4, six models from a model intercomparison project are

shown to have large variation in the ozone production efficiency of lightning NO_x. Some evidence suggests that the source of variation could be in the method to distribute lightning NO_x vertically, or the representation of Non-Methane Volatile Organic Compounds (NMVOCs). These two insights provide modellers with new knowledge regarding the effect of lightning on simulated ozone and its uncertainties, when considering results across experiments. They also highlight areas of the parametrisation, such as the vertical distribution of lightning NO_x, which would benefit from further research in measurements campaigns.

Finally, in Chapters 4 and 5, the response of lightning and lightning NO_x to climate change was quantified using a range of lightning parametrisations and CCMs. Chapter 4 quantified the lightning NO_x response using 11 CCMs and 1 chemistry transport model (CTM) from a model intercomparison project with interactive lightning schemes: 10 models using the cloud-top height approach, 1 model using updraught mass flux and cloud depth, and 1 model using updraught mass flux 440 hPa. Once normalised to the same baseline emissions, the models using the cloud-top height approach demonstrated a consistent response to an increase in global mean surface temperature of $+0.44 \pm 0.05\,\mathrm{TgN\,K^{-1}}$. However, the other two schemes demonstrated a much weaker response and a negative response. These contradictory responses clearly show that there is large parametrisation uncertainty of the lightning response to climate change. The parametrisation uncertainty was further highlighted in Chapter 5, in which the cloud-top height approach and the ice flux approach are shown to have opposing responses to climate change. Study of the meteorology driving the ice flux scheme, highlights that, in the CCM used, cloud ice content and convective activity reduce in the tropics leading to a simulated reduction in lightning activity. The cloud-top height approach does not capture such a change in the conditions in convective clouds suggesting that the consistent response of models using the approach in Chapter 4 may not be as reliable as it seems.

6.2 Discussion of the main results

6.2.1 The parametrisation of lightning

Aim: To explore existing schemes, and develop a new process-based scheme, to parametrise lightning

The motivation for this work is based upon the lack of variation in lightning parametrisation choice amongst CCMs. Almost all models use a lightning scheme based on cloud-top height, which does not represent the underlying lightning generation processes of the non-inductive charging theory, as described in Section 1.2. In Chapter 2, meteorological reanalysis fields from the European Centre of Medium-range Weather Forecasting (ECMWF) ERA-Interim dataset together with lightning observation products of the Lightning Imaging Sensor (LIS) were used to develop and evaluate lightning parametrisations between $\pm 38^{\circ}$ latitude. The first part of the chapter used one year of data from 2002 to develop a possible new parametrisation for lightning using an upward ice flux variable derived from the reanalysis dataset. This lightning parametrisation is more closely linked to the non-inductive charging theory than the cloud-top height approach. The second part of the chapter used five years of data (2007-2011) to evaluate the new parametrisation and four existing parametrisations against the lightning observations, across a range of spatial and temporal metrics. The main results from Chapter 2 are:

- A new process-based lightning parametrisation was developed based on the upward cloud ice flux at 440 hPa.

- When compared to existing lightning parametrisations, the new parametrisation improves the correlation and reduces the errors, with respect to observations, regarding the spatial distribution of annual total lightning, as well as the seasonal and interannual variability of lightning.

- The cloud-top height based parametrisation showed large meridional and zonal biases in lightning flash rate, whilst the two parametrisations of Allen and Pickering (2002) showed large over-estimation of lightning flash rate over the tropical pacific.

- A clear improvement in the zonal mean distribution of lightning was demonstrated with the ice flux approach, with less overestimation in the tropics and underestimation in the subtropics than the cloud-top height approach.

There have been previous studies to relate cloud ice to lightning but the work of Chapter 2 provides the first large-scale evaluation of a lightning parametrisation based on cloud ice. Relationships between cloud ice properties and lightning have been found previously by Deierling *et al.* (2008) for individual US thunderstorms. However, the relationships have not been adopted on the larger-scale, and whilst the same relationships were explored in Chapter 2, they over-estimated lightning activity over midlatitude oceans. The reason for such over-estimation may be that the relationships consider bulk ice fluxes, and when this is applied to a grid cell the distinction between large synoptic storms and smaller-scale and more intense tropical thunderstorms may be lost. The ice flux parametrisation developed in Chapter 2 uses the ice flux per area of cloud, thereby capturing such differences in the intensity of ice flux.

To demonstrate that the ice flux approach could be applied to a CCM as well as reanalysis data, the first part of Chapter 3 implemented the new approach in the UK Chemistry and Aerosol (UKCA) model. Then the simulated lightning was

evaluated, along with that generated by the cloud-top height approach, against the LIS and Optical Transient Detector (OTD) combined lightning climatology. The relevant conclusions regarding CCM lightning parametrisations from Chapter 3 are:

- The ice flux approach shows a higher spatial correlation (r=0.78 vs r=0.65) and generally reduced biases than the conventional cloud-top height approach when compared to the combined LIS/OTD climatology between $\pm 75^{\circ}$ latitude.

- The ice flux approach is shown to represent the annual mean zonal distribution well over this broader evaluation region, and generally the biases in the annual cycle of lightning flash rate in different latitudinal bands are smaller with the ice flux approach than with the cloud-top height approach.

- In southern South America both parametrisations capture the annual cycle well, but both have large biases in northern South America, although these are less with the ice flux approach. The comparison of measurements in the two locations may offer new insight into lightning processes.

A range of existing lightning schemes, including the traditional cloud-top height approach, have been studied using reanalysis data and using the UKCA CCM (Chapters 2 and 3). The cloud-top height approach performs similarly across the two research chapters which consider offline and online meteorology. By considering both offline and online cases, the lightning schemes have been evaluated against the most complete representation of present-day observed meteorology (reanalysis), as well as within the physically consistent framework of a state-of-the-art CCM. A similar behaviour is also seen across the CTMs/CCMs simulating lightning using the cloud-top height approach in the Atmospheric Chemistry and Climate Model Intercomparison Project (ACCMIP) (Chapter 4).

However, this consistency across CTMs, CCMs and reanalysis using the cloud-top height scheme also includes consistently large biases involving the overestimation of lightning in northern South America and underestimation in the extratropics and over the ocean. The simulated lightning distributions of other existing parametrisations in Chapter 2 and 4, such as those of Allen and Pickering (2002), seem less consistent across CCMs and reanalysis. For instance, the Allen and Pickering (2002) lightning scheme based on updraught mass flux implemented in the CMAM model (Chapter 4) does not display the same tropical ocean biases in lightning as the same scheme using ECMWF reanalysis (Chapter 2). The new ice flux parametrisation, developed in Chapter 2, reduces many of the biases in flash rate associated with the cloud-top height approach and performs consistently across the study using reanalysis (Chapter 2) and using a CCM (Chapter 3).

6.2.2 The impact of lightning on tropospheric chemistry

Aim: To use a new process-based lightning scheme to give insights regarding the role of lightning NO_x in tropospheric chemistry

Chapter 3 continues with a comparison study of how the cloud-top height approach and the ice flux approach impact the simulation of tropospheric ozone chemistry within UKCA. First, simulated ozone is evaluated against satellite and sonde observations of ozone. Then, O_x (odd oxygen) production is used to understand the chemistry underlying ozone production as it represents the amount of NO_x cycling occurring. Analysis has been carried out of the impact of lightning NO_x on the global O_x budget and the distribution of O_x production. In addition, a finer-scale analysis has studied how O_x production is influenced by the frequency distribution of flash rates. The relevant conclusions regarding the impact of lightning on tropospheric chemistry from Chapter 3 are:

- An evaluation against satellite column ozone observations of the simulated ozone with different lightning schemes did not show a large difference between the schemes. However, an evaluation of the simulations against ozone sondes showed that the ice flux approach provided a better correlation with the observed annual ozone cycle, than the cloud-top height approach, in all latitude bands and pressure levels.

- It was shown that ozone simulated when using the ice flux approach had particularly higher correlations with observed tropical upper tropospheric ozone than the cloud-top height approach (e.g. r=0.93 vs r=0.79 in the southern tropical upper troposphere). Importantly, when using the ice flux scheme, lightning was reduced during key months when lightning was over-estimated by the cloud-top height scheme.

- An analysis of the effect of flash rate on O_x production occurring after the emission of lightning NO_x found that, whilst more O_x is produced with higher flash rates ($0.1\,\mathrm{fl.\,km^{-1}\,20min^{-1}}$), O_x is approximately ten times more efficiently produced at lower flash rates ($0.001\,\mathrm{fl.\,km^{-1}\,20min^{-1}}$). This is likely due to the availability of other ozone precursors not increasing in tandem with higher flash rates, therefore limiting the additional O_x production that is possible with each additional mole of NO_x produced.

The overestimation of tropical lightning activity by the CTH approach has been shown here to lead to biases in tropospheric ozone. Murray *et al.* (2012) also found that the cloud-top height scheme over-estimated tropical lightning. They used local scaling factors to better match lightning activity to observations, resulting in a reduction in tropical upper tropospheric ozone. Here, the ice flux parametrisation achieves the observed zonal distribution of lightning without the need for regional scaling factors. Therefore, it offers a robust means to improve the representation of tropospheric ozone whilst maintaining the direct link to simulated meteorology.

In order to understand how ozone chemistry associated with lightning varies across CCMs, in Chapter 4, a statistical regression of ozone production against the emissions of the ozone precursors is performed using data from six CCMs from ACCMIP which archived ozone budget terms. This statistical regression model allowed an ozone production efficiency for lightning NO_x to be determined in the context of other ozone precursors. In addition, an estimate for the ozone production efficiency for each atmospheric chemistry model was provided. The relevant conclusions regarding the impact of lightning on tropospheric chemistry from Chapter 4 are:

- The ozone production efficiency of lightning NO_x emissions across the six ACCMIP CCMs used was found to be 6.5±4.7 times larger than the ozone production efficiency of surface NO_x emissions.

- The vertical distribution methods of lightning NO_x and the representation of NMVOCs are highlighted as a possible causes of the large variability in ozone production efficiency from lightning NO_x amongst the models.

This range of the ozone production efficiency of lightning NO_x is consistent with previous estimates from individual CTM/CCM studies (Wild, 2007; Wu *et al.*, 2007; Dahlmann *et al.*, 2011). The research in Chapter 4, which encompasses a range of models with different lightning and chemistry schemes in a range of climate scenarios, has illustrated more robustly the large differences in ozone production efficiency from lightning NO_x across CCMs. Future studies should aim to identify and quantify the causes of the inter-model variability.

6.2.3 Interactions between lightning and climate change

Aim: To use alternative lightning schemes to improve the understanding of the response of lightning to climate change, and the consequent impacts on tropospheric chemistry

The relationship between LNO_x and global mean surface temperature is described in Chapter 4, based upon the data from the twelve CTMs/CCMs from ACCMIP with interactive lightning schemes. The data spans time slice experiments of historical, present-day and future scenarios. Simulated lightning NO_x emissions are approximately proportional to the lightning flash rate. The relevant conclusions regarding the response of lightning NO_x to climate change from Chapter 4 are:

- The ten CTMs/CCMs in ACCMIP using the cloud-top height approach were shown to simulate a consistent response of lightning to climate change. A regression of their response of lightning NO_x to a change in global mean surface temperature, across all time slice experiments, provided an estimate of $+0.44 \pm 0.05\,\mathrm{TgN\,K^{-1}}$ for a baseline emission of $5\,\mathrm{TgN\,yr^{-1}}$.

- A CCM using a parametrisation based on updraught mass flux and cloud depth simulated a small positive response of $+0.14\,\mathrm{TgN\,K^{-1}}$, whilst a CCM using a parametrisation based on updraught mass flux at 440 hPa simulated a contrasting response of -0.55 $\mathrm{TgN\,K^{-1}}$.

- The spatial distribution of the lightning response to climate change in all parametrisations showed regions of increases and decreases. There were some regions (mainly in the midlatitudes) where the parametrisations agreed on the sign of the lightning response. However, in the majority of regions, and particularly in tropical regions, the parametrisations were not in agreement on the sign of change. The lack of agreement in the tropics,

led to the contrasting global total lightning responses across models using different parametrisations.

Recent estimates by CCMs using the cloud-top height approach have been similar to that found here (Zeng *et al.*, 2008; Jiang and Liao, 2013; Banerjee *et al.*, 2014) and these are contrasted by the negative response found by Jacobson and Streets (2009) who used an ice-based parametrisation. The parametrisation of Jacobson and Streets (2009) is complex. For example it includes various sizes and types of hydrometeors. The complexity of the parametrisation means that many models may not explicitly simulate the variables needed to implement the scheme. Furthermore, the largest global mean temperature change explored by Jacobson and Streets (2009) was an increase of 0.14 K. This small change in temperature limits the applicability of the response to longer-term climate change. However, the contrasting response to many other parametrisations suggests that an ice-based parametrisation may incorporate meteorological changes important to lightning generation, not otherwise captured by lightning schemes.

In Chapter 5, the conventional cloud-top height approach and the new ice flux approach are used to simulate how lightning responds to climate change within the UKCA model. The detailed responses of both the lightning and meteorology are analysed. The radiative forcing of lightning NO_x, which results from its impact on atmospheric composition, is then calculated. The relevant conclusions regarding the response of lightning to climate change from Chapter 5 are:

- As with the ACCMIP model results, the cloud-top height approach using the UKCA model shows a response of $+0.44\,\mathrm{TgN\,K^{-1}}$ to a change in global mean surface temperature in the year 2100 under the RCP8.5 scenario.

- The ice flux approach shows a response of -0.42 $\mathrm{TgN\,K^{-1}}$; however, once an

adjustment is made to the sampling pressure level used, in order to better represent the future climate, the response is -0.15 $\mathrm{TgN\,K^{-1}}$.

- The contrasting global total response of the ice flux approach arises from a reduction of lightning in the tropics due to decreased cloud ice content and updraught mass flux.

- Both parametrisations exhibit an increase in the proportion of global lightning occurring in the extratropics in the future climate.

- The tropospheric ozone burden change due to lightning NO_x emissions is different in the present-day and future climates. By considering the changes in ozone production and ozone loss between present-day and a future scenario, it is shown that the net ozone production efficiency of lightning NO_x decreases with climate change.

- The opposite global responses of the two parametrisations to climate change result in opposite responses in tropospheric ozone, OH and methane lifetime.

- The radiative forcings arising from the two parametrisations for ozone and for methane act in opposite directions. However, for both parametrisations the net forcing is close to zero though is slightly positive in the case of the cloud-top height approach.

- The small positive net radiative forcing in the future for the cloud-top height approach suggests that there may be a small positive feedback given that the lightning simulated by the cloud-top height approach responds positively to increases in the global mean surface temperature. For the ice flux approach, the net forcing is approximately zero and therefore no feedback between lightning and climate would be expected.

The research in this thesis has provided a detailed account of our current understanding of the response of global lightning to climate change. This has involved a

study of many state-of-the-art CCMs and the new ice flux parametrisation. There is very little agreement across parametrisations even regarding the sign of the response, highlighting the large uncertainty in simulating future lightning NO_x emissions. The traditional cloud-top height scheme of parametrising lightning shows a strong increase in lightning with global warming, while other parametrisations show either negative or weaker responses. An analysis of the meteorological changes driving the negative global lightning response simulated by the ice flux approach are consistent with current understanding of potential large-scale changes in tropical stability (Section 5.3.3). There is still much uncertainty underlying the future changes in meteorological variables relevant to lightning generation. However, the changes in several of these meteorological variables are not captured by the cloud-top height approach, which gives false confidence in the projected lightning NO_x increase by the scheme. The ice flux approach offers a physically based alternative the cloud-top height approach, but further studies should look to develop the definition of the sampling pressure level as well as quantify its uncertainty.

The impacts of lightning NO_x emission on tropospheric ozone chemistry are shown to depend on the climate in which changes in lightning NO_x emissions occur. A consistent response with the cloud-top height approach and the ice flux approach is that net ozone production efficiency decreases in the future climate compared to present-day. This is despite an increase in the gross ozone production efficiency, thereby suggesting that the loss of ozone changes by more than the production of ozone. This is likely due to the greater availability of water vapour to react with O(1D), a key loss reaction described in Chapter 1.

Toumi *et al.* (1996) proposed that lightning represented a positive feedback through the radiative warming caused through production of ozone. However, Wild *et al.* (2001) showed using a pulse lightning NO_x experiment that there could be net radiative cooling in the long-term through the reduction in methane. In this

thesis, the radiative forcing in a future climate resulting from the simulated change in lightning activity has been calculated for ozone and methane. As discussed above, the results show that the radiative warming of ozone is mostly offset by the radiative cooling of methane. However, there is a small positive feedback identified with the cloud-top height approach which is not evident in the ice flux approach. This is mainly because the ozone radiative forcing component from the cloud-top height approach is slightly larger than the ozone forcing simulated by the ice flux approach. The consequence is that the ozone forcing is not balanced by the methane forcing. Given the demonstrated bias of lightning and ozone in the tropics using the cloud-top height scheme, and the large radiative forcing efficiency of tropical ozone, the lightning-climate feedback suggested by the cloud-top height approach result is also likely biased.

6.3 Limitations

Using meteorological variables from a reanalysis dataset to develop a lightning parametrisation has its benefits and drawbacks. As acknowledged in Section 2.2.1, evaluations of the reanalysis data in the literature have highlighted biases in some meteorological variables, for example in precipitation over the tropical Pacific. The above biases are known biases, but there are also unknown biases relating to a lack of sufficient observations to either analyse or evaluate some variables, such as updraught mass flux. However, the reanalysis data do provide the best available, spatially and temporally complete, physically consistent dataset based on observations. Further work with the ice flux parametrisation should involve evaluation on a smaller scale, using direct measurements of meteorological variables in thunderstorms. Evaluation against other reanalysis datasets would also improve the robustness of the conclusions in Chapter 1.

Determination of the ozone production efficiency of lightning NO_x was performed in Chapter 4 using a statistical regression approach across six CCMs. Six CCMs was sufficient in Chapter 4 to give a significant result but the statistical regression method would benefit from an increase in the number of CCMs used. Not only would more CCMs improve the robustness of the ozone production efficiency estimate but it would offer more CCMs from which to explore the drivers of the differences in ozone production efficiency. Future model intercomparison studies should consider the above suggestion since the regression method used in Chapter 4 can be directly applied in order to establish how CCMs are developing between intercomparison projects.

The research in Chapter 4 was able to illustrate the potential for relationships between the simulated ozone production efficiency from lightning NO_x and the vertical distribution method of the lightning parametrisation. There also appeared to be a link to the abundance of NMVOCs. However, there was an insufficient number of CCMs available in this study to conclusively determine the source of variation in the ozone production efficiency from lightning NO_x emissions. An alternative study would use a single CCM (as in Chapter 3) but vary parameters in different simulations, such as the vertical distribution of lightning NO_x or NMVOC emissions, along with other possible controls on ozone production efficiency. Further understanding of the ozone production efficiency of lightning NO_x emissions, and why it varies substantially across models, is important given that lightning NO_x has a much larger ozone production efficiency than surface NO_x sources.

Throughout the thesis, study of ozone production has been based on simulations where lightning NO_x is spread throughout the grid cell. In reality, lightning NO_x is concentrated within a "plume" on a much smaller scale than the resolution of a CCM. Gressent *et al.* (2016) has recently demonstrated the potential for a sub-grid plume parametrisation for lightning NO_x. Further studies of LNO_x should

attempt to use such a plume parametrisation since plumes represent a different chemical environment to that of the diluted grid cell environment.

The final research chapter of this thesis, Chapter 5, presents one of the most comprehensive studies to connect: the effect of climate change on lightning, related meteorological processes, atmospheric composition, and radiative forcing. However, there remains scope to improve the robustness of these conclusions. For example, a single CCM has been used to explore the climate change effects. It is possible that other CCMs would project different responses of cloud ice and convective activity. Such differences between CCMs do not represent a flaw in the ice flux approach but offer an opportunity to determine the uncertainty in future lightning activity, based on uncertainty in the underlying meteorology. Furthermore, as the understanding and simulation of microphysical and convective processes improves within CCMs, the simulated lightning using the ice flux approach should improve. Improved representation of microphysical processes may also allow for greater level complexity to input variables of lightning parametrisation through incorporating graupel fluxes for example, a component of the non-inductive charging mechanism (Section 1.2) not included in the ice flux approach presented in this thesis.

Transient simulations of lightning flash rate require a parametrisation that is applicable as the climate changes. In Section 5.7, a sensitivity experiment was described, where the sampling pressure level was adjusted to be appropriate for the future climate of Chapter 5. Whilst this was all that was required for the time-slice experiments used in Chapter 5, for transient experiments the adjustment of the sampling level would need to be an interactive component of the lightning parametrisation. Further studies are required to build upon the generalisation presented in Section 5.7. A key aspect for further studies to determine is the frequency of re-calculating the sampling level, i.e. whether re-calculation should occur during every simulation time step, or whether it should occur on a monthly

or annual basis. Evaluation of any new scheme against lightning observations is necessary to ensure it is appropriate in the present-day climate.

6.4 Future work

The detailed investigation of flash rate frequency distributions using different lightning schemes in this thesis has been informative. Frequency distributions provide a useful metric to transition from evaluations on the larger scale to smaller scale with regards to temporal and spatial characteristics. Individual measurements made by satellites or ground-based networks can be used to produce frequency distributions to evaluate parametrisations over a range of scales and regions. Then storm-scale measurement campaigns can place results from the individual storms within the larger scale context of these observed frequency distributions.

In Chapter 3, the simulated annual cycle of lightning was evaluated against a satellite climatology over a number of regions to offer some direction to future measurement campaigns. South America in particular was identified as a region where focussed measurements would be useful to improve understanding of lightning processes. Biases in lightning over the northern part of South America were found to lead to biases in upper tropospheric ozone compared to ozone sonde measurements. Future research campaigns in the region could provide new information that would benefit the global-scale modelling of lightning.

Over the coming decade, one of the most promising resources for large-scale lightning research will be the use of lightning detectors on geostationary satellites. First, in the second half of 2016 there is a planned launch for the new generation GOES satellite, which will observe over North and South America and measure lightning with the Geostationary Lightning Mapper (GLM). Second, within a few

years the third generation of Meteosat will be launched to observe over Europe and Africa, and will also operate with a lightning detector. These satellites will introduce continuous measurement of lightning over a large proportion of the world.

With these new observations from geostationary satellites, there will be many possible avenues of research. There will be much greater overlap of satellite measurements with ground-based lightning measurements than occurred with low-earth orbit satellite measurements. The low-earth orbit satellites were not constantly measuring over regions with high-accuracy detector networks, as will be the case with the new geostationary satellites. Greater overlap of measurements will allow for a more robust analysis of the uncertainties associated with the different measurement techniques. Furthermore, overlapping measurements allow the study of multiple aspects of lightning in the same storms, since different detection methods measure different components of lightning flashes. In addition, the lightning measurements from the different geostationary satellites may be combined to provide much more data to understand differences in storms between land and ocean, between Africa and South America, and between the tropics and extratropics. Hence, these new measurements represent a promising resource to develop lightning parametrisations in CCMs and potentially reduce biases in lightning flash rate.

As well as offering opportunities to understand lightning processes, the geostationary satellites introduce greater opportunity to study the chemical processes associated with lightning. There will be many more coincident measurements of lightning by satellite and atmospheric composition by sondes and aircraft campaigns. By studying cases when storms occur near ozone sonde sites, there is scope to improve understanding of the ozone production resulting from storms. Finally, lightning measurements will be continuously measured along with cloud imagery,

overlapping measurements of atmospheric composition, and ground weather station measurements. This offers a raft of evaluation datasets to evaluate CCMs nudged by reanalysis data, providing an opportunity to improve understanding and reduce the uncertainty associated with global lightning parametrisation.

Measurements of lightning during recent El Nino events provide an observational record of the response of lightning to an atmospheric warming. Whilst, the response of the atmosphere to El Nino events may not be the same as the response to climate change (Lu *et al.*, 2008), examining the processes driving the response of lightning may provide new insight regarding the processes that could drive the response of lightning to climate change. Several studies have already proposed changes in lightning activity and lightning NO_x in response to El Nino and La Nina events (Doherty *et al.*, 2006; Satori *et al.*, 2009; Dowdy, 2016). Through the use of a CCM, scenarios of both greenhouse gas forcing and El Nino events can be studied, and their meteorological and atmospheric composition responses compared in detail. Furthermore, the response of lightning to recent El Nino events provides an opportunity to evaluate simulated lightning and atmospheric composition against observations.

In summary, this thesis has established a link between large-scale parametrisation of lightning and theory which has described the generation of lightning as a result of vertical fluxes of cloud ice in storms. From this reference point, many important aspects of lightning relevant to atmospheric chemistry modelling have been explored and put in the context of the simulated underlying meteorological processes. I hope the suggestions above inspire further research as there remains an array of fascinating research paths which can build upon this thesis to understand the global lightning activity, and its consequences in the field of atmospheric chemistry.

Chapter 7

Appendix

7.1 A lightning "forecast" over the UK for 1st July 2015

The thesis title page photo, "Lightning over the Forth", was taken on the night of 1st July 2015. This thunderstorm was sufficiently exciting to be reported upon by local media, although I personally managed to miss it by being asleep in Glasgow. Figure 7.1 shows the total lightning stroke measurements made with a ground-based network (Section 1.3), the Arrival Time Difference (ATD) UK lightning network, over the period 01/07/2015 12:00 – 02/07/2015 06:00. Alongside this are forecasts made, for the same period, with the ice flux parametrisation used within this thesis. The two ice flux approach forecasts either apply: the land and ocean equations from Section 2.4, or the land equation everywhere. I refer to the results as a forecast because forecast data from ERA-Interim is used, identical to the method described in Section 2.2.1.

The ATD measurements and the forecast with the ice flux approach are not

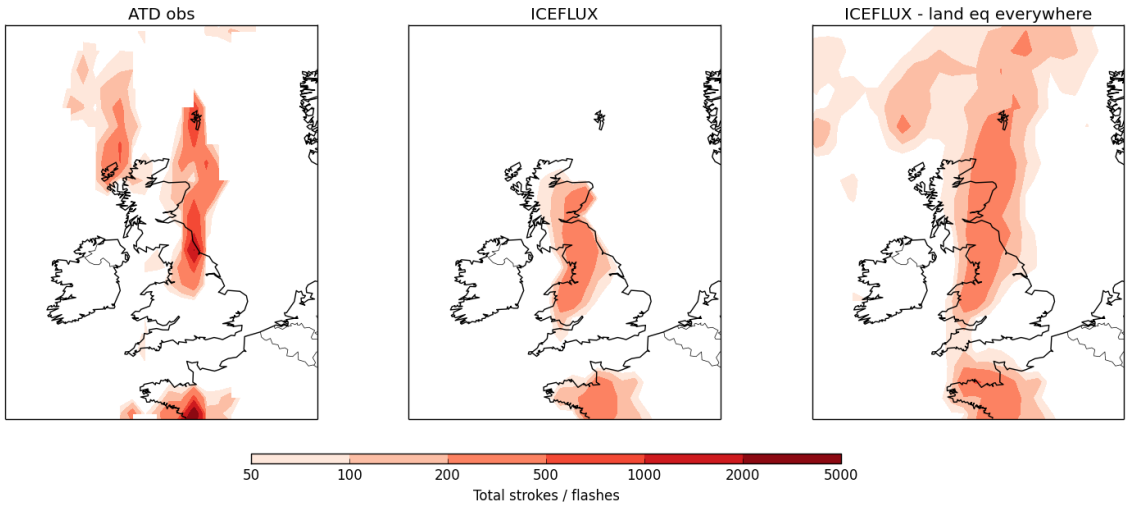

Figure 7.1: ATD measurements and ERA-Interim forecast using the ice flux approach, for lightning over the UK during the period 01/07/2015 12:00 – 02/07/2015 06:00.

directly comparable. The ATD network measures lightning strokes, principally cloud-to-ground strokes (Anderson and Klugmann, 2014). On the other hand, the ice flux approach estimates the total number of flashes, including intra-cloud flashes. To complicate matters further, multiple strokes can be measured for the same lightning flash. Without more detailed consideration, the two cannot be quantitatively compared. Nonetheless, the general locations forecast to receive lightning with the ice flux approach are close to those measured to have received lightning, if shifted to the southwest (Figure 7.1). Some differences are to be expected due to potential inaccuracies in the forecast meteorology.

The two versions of the ice flux approach used highlight that near to coasts it may be more appropriate to use the land equation. However, with locations further from the UK mainland than the Shetlands, the land equation of the ice flux approach does appear to overestimate lightning. The Shetlands are approximately 200 km from mainland UK, which suggests that over this kind of range from coasts the land equation should be applied, and beyond should be the ocean equation.

Such a variation is already used by some models implementing the cloud-top height approach (e.g. Murray *et al.* (2012), who apply the land equation in any grid cells with greater than 50 % land coverage).

It is promising to see the ice flux approach work successfully on an individual storm basis. It has captured the storm that passed over the Forth reasonably well, when the land equation is applied around the coast. It has also captured a storm occurring over western France, during the same time period, reasonably well (Figure 7.1). As stated in the thesis conclusions, more comprehensive testing along these lines in future work would be beneficial, and may highlight the potential for use of the ice flux approach in lightning forecasting.

References

Ahlgrimm, M. and Köhler, M. (2010). Evaluation of trade cumulus in the ECMWF model with observations from CALIPSO. *Monthly Weather Review*, **138**, 3071–3083.

Albrecht, R.I., Goodman, S.J., Petersen, W.A., Buechler, D.E., Bruning, E.C., Blakeslee, R.J. and Christian, H.J. (2011). The 13 years of TRMM Lightning Imaging Sensor : From individual flash characteristics to decadal tendencies The 13 years of TRMM Lightning Imaging Sensor : From individual flash characteristics to decadal tendencies. In *XIV International Conference on Atmospheric Electricity*, Rio de Janeiro, Brazil.

Albrecht, R.I., Goodman, S.J., Buechler, D.E., Blakeslee, R.J. and Christian, H.J. (2016). Where are the lightning hotspots on Earth? *Bulletin of the American Meteorological Society*.

Allen, D.J. and Pickering, K.E. (2002). Evaluation of lightning flash rate parameterizations for use in a global chemical transport model. *Journal of Geophysical Research: Atmospheres*, **107**, ACH 15–1–ACH 15–21.

Altaratz, O., Koren, I., Yair, Y. and Price, C. (2010). Lightning response to smoke from Amazonian fires. *Geophysical Research Letters*, **37**, L07801.

Anderson, G. and Klugmann, D. (2014). A European lightning density analysis using 5 years of ATDnet data. *Natural Hazards and Earth System Science*, **14**, 815–829.

Apel, E.C., Hornbrook, R.S., Hills, A.J., Blake, N.J., Barth, M.C., Weinheimer, A., Cantrell, C., Rutledge, S.A., Basarab, B., Crawford, J., Diskin, G., Homeyer, C.R., Campos, T., Flocke, F., Fried, A., Blake, D.R., Brune, W., Pollack, I., Peischl, J., Ryerson, T., Wennberg, P.O., Crounse, J.D., Wisthaler, A., Mikoviny, T., Huey, G., Heikes, B., Sullivan, D.O. and Riemer, D.D. (2015). Upper tropospheric ozone production from lightning NOx-impacted convection: Smoke ingestion case study from the DC3 campaign. *Journal of Geophysical Research: Atmospheres*, **120**.

Ávila, E.E., Lighezzolo, R.A., Castellano, N.E., Pereyra, R.G. and Bürgesser, R.E. (2013). Laboratory measurements of charge separation in low liquid water content conditions and low impact velocity. *Journal of Geophysical Research: Atmospheres*, **118**, 6680–6687.

Banerjee, A., Archibald, A.T., Maycock, A.C., Telford, P., Abraham, N.L., Yang, X., Braesicke, P. and Pyle, J.A. (2014). Lightning NOx, a key chemistry-climate interaction: Impacts of future climate change and consequences for tropospheric oxidising capacity. *Atmospheric Chemistry and Physics*, **14**, 9871–9881.

Barth, M.C., Lee, J., Hodzic, A., Pfister, G., Skamarock, W.C., Worden, J., Wong, J. and Noone, D. (2012). Thunderstorms and upper troposphere chemistry during the early stages of the 2006 North American Monsoon. *Atmospheric Chemistry and Physics*, **12**, 11003–11026.

Barthe, C. and Pinty, J.P. (2007). Simulation of electrified storms with comparison of the charge structure and lightning efficiency. *Journal of Geophysical Research*, **112**, D19204.

Barthe, C., Deierling, W. and Barth, M.C. (2010). Estimation of total lightning from various storm parameters: A cloud-resolving model study. *Journal of Geophysical Research*, **115**, D24202.

Basarab, B.M., Rutledge, S.A. and Fuchs, B.R. (2015). An improved lightning flash rate parameterization developed from Colorado DC3 thunderstorm data for use in cloud-resolving chemical transport models. *Journal of Geophysical Research*, **120**.

Beirle, S., Huntrieser, H. and Wagner, T. (2010). Direct satellite observation of lightning-produced NOx. *Atmospheric Chemistry and Physics*, **10**, 10965–10986.

Beirle, S., Koshak, W., Blakeslee, R. and Wagner, T. (2014). Global patterns of lightning properties derived by OTD and LIS. *Natural Hazards and Earth System Sciences Discussions*, **2**, 2765–2787.

Bitzer, P.M., Burchfield, J.C. and Christian, H.J. (2016). A Bayesian Approach to Assess the Performance of Lightning Detection Systems. *Journal of Atmospheric and Oceanic Technology*, **33**, 563–578.

Blyth, A.M., Christian Jr, H.J., Driscoll, K., Gadian, A.M. and Latham, J. (2001). Determination of ice precipitation rates and thunderstorm anvil ice contents from satellite observations of lightning. *Atmospheric Research*, **59-60**, 217–229.

Boccippio, D.J. (2001). Lightning Scaling Relations Revisited. *Journal of Atmospheric Sciences*, **59**, 1086–1105.

Boccippio, D.J., Koshak, W.J. and Blakeslee, R.J. (2002). Performance assessment of the Optical Transient Detector and Lightning Imaging Sensor. Part I: Predicted diurnal variability. *Journal of Atmospheric and Oceanic Technology*, **19**, 1318–1332.

Boersma, K.F., Eskes, H.J., Meijer, E.W. and Kelder, H.M. (2005). Estimates of lightning NOx production from GOME satellite observations. *Atmospheric Chemistry and Physics*, **5**, 2311–2331.

Bolker, B.M., Brooks, M.E., Clark, C.J., Geange, S.W., Poulsen, J.R., Stevens, M.H.H. and White, J.S.S. (2008). Generalized linear mixed models: A practical guide for ecology and evolution. *Trends in ecology and evolution*, **24**, 127–135.

Bond, D.W., Steiger, S., Zhang, R., Tie, X. and Orville, R.E. (2002). The importance of NOx production by lightning in the tropics. *Atmospheric Environment*, **36**, 1509–1519.

Brooks, H.E. (2013). Severe thunderstorms and climate change. *Atmospheric Research*, **123**, 129–138.

Bucsela, E.J., Pickering, K.E., Huntemann, T.L., Cohen, R.C., Perring, A., Gleason, J.F., Blakeslee, R.J., Albrecht, R.I., Holzworth, R., Cipriani, J.P., Vargas-Navarro, D., Mora-Segura, I., Pacheco-Hernández, A. and Laporte-Molina, S. (2010). Lightning-generated NOx seen by the Ozone Monitoring Instrument during NASA's Tropical Composition, Cloud and Climate Coupling Experiment (TC4). *Journal of Geophysical Research*, **115**, D00J10.

Burnham, K.P. and Anderson, D.R. (2002). *Model selection and multimodel inference: A practical information-theoretic approach*. Springer.

Bushell, A.C., Wilson, D.R. and Gregory, D. (2003). A description of cloud production by non-uniformly distributed processes. *Quarterly Journal of the Royal Meteorological Society*, **129**, 1435–1455.

Cecil, D.J., Buechler, D.E. and Blakeslee, R.J. (2014). Gridded lightning climatology from TRMM-LIS and OTD: Dataset description. *Atmospheric Research*, **135-136**, 404–414.

Cecil, D.J., Buechler, D.E. and Blakeslee, R.J. (2015). TRMM LIS climatology of thunderstorm occurrence and conditional lightning flash rates. *Journal of Climate*, **28**, 6536–6547.

Chameides, W.L. (1986). The Role of Lightning in the Chemistry of the Atmosphere. In *The Earth's Electrical Environment*, 70–77.

Changnon, S.A. and Changnon, D. (2001). Long-Term Fluctuations in Thunderstorm Activity in the United States. *Climate Change*, **50**, 489–503.

Chaudhuri, S. and Middey, A. (2013). Disparity in the characteristic of thunderstorms and associated lightning activities over dissimilar terrains. *Meteorology and Atmospheric Physics*, **119**, 151–161.

Chou, C. and Chen, C.A. (2010). Depth of convection and the weakening of tropical circulation in Global Warming. *Journal of Climate*, **23**, 3019–3030.

Christian, H.J., Blakeslee, R.J., Boccippio, D.J., Boeck, W.L., Buechler, D.E., Driscoll, K.T., Goodman, S.J., Hall, J.M., Koshak, W.J., Mach, D.M. and Stewart, M.F. (2003). Global frequency and distribution of lightning as observed from space by the Optical Transient Detector. *Journal of Geophysical Research*, **108**, 4005.

Collins, M., Knutti, R., Arblaster, J., Dufresne, J.L., Fichefet, T., Friedlingstein, P., Gao, X., Gutowski, W.J., Johns, T., Krinner, G., Shongwe, M., Tebaldi, C., Weaver, A.J. and Wehner, M. (2013). Long-term Climate Change: Projections, Commitments and Irreversibility, In: Climate Change 2013: The Physical Science Basis. Contribution of Working Group I to the Fifth Assessment Report of the Intergovernmental Panel on Climate Change [Stocker, T.F., D. Qin, G.-K. Plattner, M. Tignor, S.K. Allen, J. Boschung, A. Nauels, Y. Xia, V. Bex and P.M. Midgley (eds.)]. Tech. rep., Cambridge University Press, Cambridge, UK and New York, USA.

Cooray, V., Rahman, M. and Rakov, V. (2009). On the NOx production by laboratory electrical discharges and lightning. *Journal of Atmospheric and Solar-Terrestrial Physics*, **71**, 1877–1889.

Dahlmann, K., Grewe, V., Ponater, M. and Matthes, S. (2011). Quantifying the contributions of individual NOx sources to the trend in ozone radiative forcing. *Atmospheric Environment*, **45**, 2860–2868.

Dash, J.G., Mason, B.L. and Wettlaufer, J.S. (2001). Theory of charge and mass transfer in ice-ice collision. *Journal of Geophysical Research*, **106**, 20395–20402.

DeCaria, A.J., Pickering, K.E., Stenchikov, G.L. and Ott, L.E. (2005). Lightning-generated NOx and its impact on tropospheric ozone production: A three-dimensional modeling study of a Stratosphere-Troposphere Experiment: Radiation, Aerosols and Ozone (STERAO-A) thunderstorm. *Journal of Geophysical Research*, **110**, D14303.

Dee, D.P., Uppala, S.M., Simmons, A.J., Berrisford, P., Poli, P., Kobayashi, S., Andrae, U., Balmaseda, M.A., Balsamo, G., Bauer, P., Bechtold, P., Beljaars, A.C.M., van de Berg, L., Bidlot, J., Bormann, N., Delsol, C., Dragani, R., Fuentes, M., Geer, A.J., Haimberger, L., Healy, S.B., Hersbach, H., Holm, E.V., Isaksen, L., Kallberg, P., Kohler, M., Matricardi, M., McNally, A.P., Monge-Sanz, B.M., Morcrette, J.J., Park, B.K., Peubey, C., de Rosnay, P.,

Tavolato, C., Thépaut, J.N. and Vitart, F. (2011). The ERA-Interim reanalysis: configuration and performance of the data assimilation system. *Quarterly Journal of the Royal Meteorological Society*, **137**, 553–597.

Deierling, W., Petersen, W.A., Latham, J., Ellis, S. and Christian, H.J. (2008). The relationship between lightning activity and ice fluxes in thunderstorms. *Journal of Geophysical Research*, **113**, D15210.

Delanoë, J., Hogan, R.J., Forbes, R.M., Bodas-Salcedo, A. and Stein, T.H.M. (2011). Evaluation of ice cloud representation in the ECMWF and UK Met Office models using CloudSat and CALIPSO data. *Quarterly Journal of the Royal Meteorological Society*, **137**, 2064–2078.

Doherty, R.M., Stevenson, D.S., Johnson, C.E., Collins, W.J. and Sanderson, M.G. (2006). Tropospheric ozone and El Niño-Southern Oscillation: Influence of atmospheric dynamics, biomass burning emissions, and future climate change. *Journal of Geophysical Research*, **111**, D19304.

Doherty, R.M., Wild, O., Shindell, D.T., Zeng, G., MacKenzie, I.A., Collins, W.J., Fiore, A.M., Stevenson, D.S., Dentener, F.J., Schultz, M.G., Hess, P., Derwent, R.G. and Keating, T.J. (2013). Impacts of climate change on surface ozone and intercontinental ozone pollution: A multi-model study. *Journal of Geophysical Research: Atmospheres*, **118**, 1–20.

Dowdy, A.J. (2016). Seasonal forecasting of lightning and thunderstorm activity in tropical and temperate regions of the world. *Scientific Reports*, **6**, 20874.

Emmons, L.K., Walters, S., Hess, P.G., Lamarque, J.F., Pfister, G.G., Fillmore, D., Granier, C., Guenther, A., Kinnison, D., Laepple, T., Orlando, J., Tie, X., Tyndall, G., Wiedinmyer, C., Baughcum, S.L. and Kloster, S. (2010). Description and evaluation of the Model for Ozone and Related chemical Tracers, version 4 (MOZART-4). *Geoscientific Model Development*, **3**, 43–67.

Finney, D.L., Doherty, R.M., Wild, O., Huntrieser, H., Pumphrey, H.C. and Blyth, A.M. (2014). Using cloud ice flux to parametrise large-scale lightning. *Atmospheric Chemistry and Physics*, **14**, 12665–12682.

Fiore, A.M., Naik, V., Spracklen, D.V., Steiner, A., Unger, N., Prather, M., Bergmann, D., Cameron-Smith, P.J., Cionni, I., Collins, W.J., Dalsøren, S., Eyring, V., Folberth, G.a., Ginoux, P., Horowitz, L.W., Josse, B., Lamarque, J.F., MacKenzie, I.A., Nagashima, T., O'Connor, F.M., Righi, M., Rumbold, S.T., Shindell, D.T., Skeie, R.B., Sudo, K., Szopa, S., Takemura, T. and Zeng, G. (2012). Global air quality and climate. *Chemical Society Reviews*, **41**, 6663–6683.

Fritsch, J.M. and Chappell, C.F. (1980). Numerical Prediction of Convectively Driven Mesoscale Pressure Systems. Part I: Convective Parameterization. *Journal of the Atmospheric Sciences*, **37**, 1722–1733.

Fullerkrug, M., Price, C., Yair, Y. and Williams, E.R. (2002). Intense oceanic lightning. *Annales Geophysicae*, **20**, 133–137.

Goldenbaum, G.C. and Dickerson, R.R. (1993). Nitric oxide production by lightning discharges. *Journal of Geophysical Research*, **98**, 18333–18338.

Goodman, S.J., Blakeslee, R.J., Koshak, W.J., Mach, D., Bailey, J., Buechler, D., Carey, L., Schultz, C., Bateman, M., McCaul, E. and Stano, G. (2013). The GOES-R Geostationary Lightning Mapper (GLM). *Atmospheric Research*, **125-126**, 34–49.

Gressent, A., Sauvage, B., Cariolle, D., Evans, M., Leriche, M., Mari, C. and Thouret, V. (2016). Modeling lightning-NOx chemistry at sub-grid scale in a global chemical transport model. *Atmospheric Chemistry and Physics*, **16**, 5867?5889.

Grewe, V. (2007). Impact of climate variability on tropospheric ozone. *Science of the Total Environment*, **374**, 167–181.

Grewe, V., Brunner, D., Dameris, M., Grenfell, J., Hein, R., Shindell, D. and Staehelin, J. (2001). Origin and variability of upper tropospheric nitrogen oxides and ozone at northern mid-latitudes. *Atmospheric Environment*, **35**, 3421–3433.

Grewe, V., Reithmeier, C. and Shindell, D.T. (2002). Dynamic-chemical coupling of the upper troposphere and lower stratosphere region. *Chemosphere*, **47**, 851–861.

Gurevich, A.V. and Karashtin, A.N. (2013). Runaway Breakdown and Hydrometeors in Lightning Initiation. *Physical Review Letters*, **110**, 185005.

Hardiman, S.C., Boutle, I.A., Bushell, A.C., Butchart, N., Cullen, M.J.P., Field, P.R., Furtado, K., Manners, J.C., Milton, S.F., Morcrette, C., O'Connor, F.M., Shipway, B.J., Smith, C., Walters, D.N., Willett, M.R., Williams, K.D., Wood, N., Lukeabraham, N., Keeble, J., Maycock, A.C., Thuburn, J. and Woodhouse, M.T. (2015). Processes controlling tropical tropopause temperature and stratospheric water vapor in climate models. *Journal of Climate*, **28**, 6516–6535.

Held, I.M. and Soden, B.J. (2006). Robust Responses of the Hydrological Cycle to Global Warming. *Journal of Climate*, **19**, 5686–5699.

Hoerling, M.P., Schaack, T.K. and Lenzen, A.J. (1993). A global analysis of stratospherictropospheric exchange during northern winter. *Monthly Weather Review*, **121**, 162–172.

Huntrieser, H., Schumann, U., Schlager, H., Höller, H., Giez, A., Betz, H.D., Brunner, D., Forster, C., Pinto, O. and Calheiros, R. (2008). Lightning activity in Brazilian thunderstorms during TROCCINOX: implications for NOx production. *Atmospheric Chemistry and Physics*, **8**, 921–953.

Huntrieser, H., Schlager, H., Lichtenstern, M., Roiger, A., Stock, P., Minikin, A., Höller, H., Schmidt, K., Betz, H.D., Allen, G., Viciani, S., Ulanovsky, A., Ravegnani, F. and Brunner, D. (2009). NOx production by lightning in Hector: first airborne measurements during SCOUT-O3/ACTIVE. *Atmospheric Chemistry and Physics Discussions*, **9**, 14361–14451.

Huntrieser, H., Schlager, H., Lichtenstern, M., Stock, P., Hamburger, T., Höller, H., Schmidt, K., Betz, H.D., Ulanovsky, A. and Ravegnani, F. (2011). Mesoscale convective systems observed during AMMA and their impact on the NOx and O3 budget over West Africa. *Atmospheric Chemistry and Physics*, **11**, 2503–2536.

Huntrieser, H., Lichtenstern, M., Scheibe, M., Aufmhoff, H., Schlager, H., Pucik, T., Minikin, A., Weinzierl, B., Heimerl, K., Pollack, I.B., Peischl, J., Ryerson, T.B., Weinheimer, A.J., Honomichl, S., Ridley, B.A., Biggerstaff, M.I., Betten, D.P., Hair, J.W., Butler, C.F., Schwartz, M.J. and Barth, M.C. (2016). Injection of lightning-produced NOx, water vapor, wildfire emissions, and stratospheric air to the UT/LS as observed from DC3 measurements. *Journal of Geophysical Research: Atmospheres*, **121**.

Hutchins, M.L., Holzworth, R.H., Brundell, J.B. and Rodger, C.J. (2012). Relative detection efficiency of the World Wide Lightning Location Network. *Radio Science*, **47**, RS6005.

Hutchins, M.L., Holzworth, R.H., Virts, K.S., Wallace, J.M. and Heckman, S. (2013). Radiated VLF energy differences of land and oceanic lightning. *Geophysical Research Letters*, **40**, 2390–2394.

Jacob, D.J. and Winner, D.A. (2009). Effect of climate change on air quality. *Atmospheric Environment*, **43**, 51–63.

Jacobson, M.Z. and Streets, D.G. (2009). Influence of future anthropogenic emissions on climate, natural emissions, and air quality. *Journal of Geophysical Research*, **114**, D08118.

Jayaratne, E.R., Saunders, C.P.R. and Hallett, J. (1983). Laboratory studies of the charging of soft hail during ice crystal interactions. *Quarterly Journal of the Royal Meteorological Society*, **109**, 609–630.

Jiang, H. and Liao, H. (2013). Projected changes in NOx emissions from lightning as a result of 2000-2050 climate change. *Atmospheric and Oceanic Science Letters*, **6**, 284–289.

Johnson, P.C. (2014). Extension of Nakagawa & Schielzeth's R2 GLMM to random slopes models. *Methods in Ecology and Evolution*, **5**, 944–946.

Jourdain, L. and Hauglustaine, D.A. (2001). The global distribution of lightning NOx eimulated on-line in a general circulation model. *Physics and Chemistry of the Earth, Part C: Solar, Terrestrial and Planetary Science*, **26**, 585–591.

Kim, P.S., Jacob, D.J., Liu, X., Warner, J.X., Yang, K., Chance, K., Thouret, V. and Nedelec, P. (2013). Global ozoneCO correlations from OMI and AIRS: constraints on tropospheric ozone sources. *Atmospheric Chemistry and Physics*, **13**, 9321–9335.

Klein, S.A., Zhang, Y., Zelinka, M.D., Pincus, R., Boyle, J. and Gleckler, P.J. (2013). Are climate model simulations of clouds improving? An evaluation using the ISCCP simulator. *Journal of Geophysical Research Atmospheres*, **118**, 1329–1342.

Knutson, T.R. and Manabe, S. (1995). Time-Mean Response over the Tropical Pacific to Increased C02 in a Coupled Ocean-Atmosphere Model. *Journal of Climate*, **8**, 2181–2199.

Kumar, P.R. and Kamra, A. (2012). Variability of lightning activity in South/Southeast Asia during 1997-98 and 2002-03 El Nino/La Nina events. *Atmospheric Research*, **118**, 84–102.

Labrador, L.J., von Kuhlmann, R. and Lawrence, M.G. (2005). The effects of lightning-produced NOx and its vertical distribution on atmospheric chemistry : sensitivity simulations with MATCH-MPIC. *Atmospheric Chemistry and Physics*, **5**, 1815–1834.

Lacis, A.A., Wuebbles, D.J. and Logan, J.A. (1990). Radiative forcing of climate by changes in the vertical distribution of ozone. *Journal of Geophysical Research*, **95**, 9971–9981.

Lamarque, J.F., Emmons, L.K., Hess, P.G., Kinnison, D.E., Tilmes, S., Vitt, F., Heald, C.L., Holland, E.A., Lauritzen, P.H., Neu, J., Orlando, J.J., Rasch, P.J. and Tyndall, G.K. (2012). CAM-chem: Description and evaluation of interactive atmospheric chemistry in the Community Earth System Model. *Geoscientific Model Development*, **5**, 369–411.

Lamarque, J.F., Shindell, D.T., Josse, B., Young, P.J., Cionni, I., Eyring, V., Bergmann, D., Cameron-Smith, P., Collins, W.J., Doherty, R., Dalsoren, S., Faluvegi, G., Folberth, G., Ghan, S.J., Horowitz, L.W., Lee, Y.H., MacKenzie,

I.A., Nagashima, T., Naik, V., Plummer, D., Righi, M., Rumbold, S.T., Schulz, M., Skeie, R.B., Stevenson, D.S., Strode, S., Sudo, K., Szopa, S., Voulgarakis, A. and Zeng, G. (2013). The Atmospheric Chemistry and Climate Model Intercomparison Project (ACCMIP): Overview and description of models, simulations and climate diagnostics. *Geoscientific Model Development*, **6**, 179–206.

Latham, J., Blyth, A.M., Christian, H.J., Deierling, W. and Gadian, A.M. (2004). Determination of precipitation rates and yields from lightning measurements. *Journal of Hydrology*, **288**, 13–19.

Levy II, H., Moxim, W.J. and Kasibhatla, P.S. (1996). A global three-dimensional time-dependent lightning source of tropospheric NOx. *Journal of Geophysical Research*, **101**, 22911–22922.

Li, J.L., Jiang, J.H., Waliser, D.E. and Tompkins, A.M. (2007). Assessing consistency between EOS MLS and ECMWF analyzed and forecast estimates of cloud ice. *Geophysical Research Letters*, **34**, L08701.

Liaskos, C.E., Allen, D.J. and Pickering, K.E. (2015). Sensitivity of tropical tropospheric composition to lightning NOx production as determined by the NASA GEOS-Replay model. *Journal of Geophysical Research: Atmospheres*, **120**, 8512–8534.

Lin, R., Zhou, T. and Qian, Y. (2014). Evaluation of global monsoon precipitation changes based on five reanalysis datasets. *Journal of Climate*, **27**, 1271–1289.

Liu, C., Cecil, D.J., Zipser, E.J., Kronfeld, K. and Robertson, R. (2012). Relationships between lightning flash rates and radar reflectivity vertical structures in thunderstorms over the tropics and subtropics. *Journal of Geophysical Research*, **117**, D06212.

Logan, J.A. (1999). An analysis of ozonesonde data for the troposphere: Recommendations for testing 3-D models and development of a gridded climatology for tropospheric ozone. *Journal of Geophysical Research*, **104**, 16115–16149.

Lu, J., Chen, G. and Frierson, D.M.W. (2008). Response of the zonal mean atmospheric circulation to El Niño versus global warming. *Journal of Climate*, **21**, 5835–5851.

Martin, R.V., Sauvage, B., Folkins, I., Sioris, C.E., Boone, C., Bernath, P. and Ziemke, J. (2007). Space-based constraints on the production of nitric oxide by lightning. *Journal of Geophysical Research*, **112**, D09309.

Meijer, E., van Velthoven, P., Brunner, D., Huntrieser, H. and Kelder, H. (2001). Improvement and evaluation of the parameterisation of nitrogen oxide

production by lightning. *Physics and Chemistry of the Earth, Part C: Solar, Terrestrial and Planetary Science*, **26**, 577–583.

Miyazaki, K., Eskes, H.J., Sudo, K. and Zhang, C. (2014). Global lightning NOx production estimated by an assimilation of multiple satellite datasets. *Atmospheric Chemistry and Physics*, **14**, 3277–3305.

Morcrette, C.J. (2012). Improvements to a prognostic cloud scheme through changes to its cloud erosion parametrization. *Atmospheric Science Letters*, **13**, 95–102.

Morgenstern, O., Braesicke, P., O'Connor, F.M., Bushell, A.C., Johnson, C.E., Osprey, S.M. and Pyle, J.A. (2009). Evaluation of the new UKCA climate-composition model Part 1: The stratosphere. *Geoscientific Model Development*, **2**, 43–57.

Murray, L.T. (2016). Lightning NOx and Impacts on Air Quality. *Current Pollution Reports*.

Murray, L.T., Jacob, D.J., Logan, J.A., Hudman, R.C. and Koshak, W.J. (2012). Optimized regional and interannual variability of lightning in a global chemical transport model constrained by LIS/OTD satellite data. *Journal of Geophysical Research*, **117**, D20307.

Murray, L.T., Logan, J.A. and Jacob, D.J. (2013). Interannual variability in tropical tropospheric ozone and OH: The role of lightning. *Journal of Geophysical Research: Atmospheres*, **118**, 11,468–11,480.

Myhre, G., Highwood, E.J., Shine, K.P. and Stordal, F. (1998). New estimates of radiative forcing due to well mixed greenhouse gases. *Geophysical Research Letters*, **25**, 2715–2718.

Myhre, G., Shindell, D., Bréon, F.M., Collins, W., Fuglestvedt, J., Huang, J., Koch, D., Lamarque, J.F., Lee, D., Mendoza, B., Nakajima, T., Robock, A., Stephens, G., Takemura, T. and Zhan, H. (2013). Anthropogenic and Natural Radiative Forcing, In: Climate Change 2013: The Physical Science Basis. Contribution of Working Group I to the Fifth Assessment Report of the Intergovernmental Panel on Climate Change [Stocker, T.F., D. Qin, G.-K. Plattner, M. Tignor, S.K. Allen, J. Boschung, A. Nauels, Y. Xia, V. Bex and P.M. Midgley (eds.)]. Tech. rep., Cambridge University Press, Cambridge, UK and New York, USA.

Nag, A., Murphy, M.J., Schulz, W. and Cummins, K.L. (2015). Lightning locating systems: Characteristics and validation techniques. *Earth and Space Science*, **2**, 65–93.

Nakagawa, S. and Schielzeth, H. (2013). A general and simple method for obtaining R2 from generalized linear mixed-effects models. *Methods in Ecology and Evolution*, **4**, 133–142.

O'Connor, F.M., Johnson, C.E., Morgenstern, O., Abraham, N.L., Braesicke, P., Dalvi, M., Folberth, G.A., Sanderson, M.G., Telford, P.J., Voulgarakis, A., Young, P.J., Zeng, G., Collins, W.J. and Pyle, J.A. (2014). Evaluation of the new UKCA climate-composition model Part 2: The Troposphere. *Geoscientific Model Development*, **7**, 41–91.

Ott, L.E., Pickering, K.E., Stenchikov, G.L., Allen, D.J., DeCaria, A.J., Ridley, B., Lin, R.F., Lang, S. and Tao, W.K. (2010). Production of lightning NOx and its vertical distribution calculated from three-dimensional cloud-scale chemical transport model simulations. *Journal of Geophysical Research*, **115**, D04301.

Owens, M.J., Scott, C.J., Lockwood, M., Barnard, L., Harrison, R.G., Nicoll, K., Watt, C. and Bennett, A.J. (2014). Modulation of UK lightning by heliospheric magnetic field polarity. *Environmental Research Letters*, **9**, 115009.

Pan, L.L., Homeyer, C.R., Honomichl, S., Ridley, B.A., Weisman, M., Barth, M.C., Hair, J.W., Fenn, M.A., Butler, C., Diskin, G.S., Crawford, J.H., Ryerson, T.B., Pollack, I., Peischl, J. and Huntrieser, H. (2014). Thunderstorms enhance tropospheric ozone by wrapping and shedding stratospheric air. *Geophysical Research Letters*, **41**, 7785–7790.

Pawar, V., Pawar, S.D., Beig, G. and Sahu, S.K. (2012). Effect of lightning activity on surface NOx and O3 over a tropical station during premonsoon and monsoon seasons. *Journal of Geophysical Research*, **117**, D05310.

Peña-Arancibia, J.L., van Dijk, A.I.J.M., Renzullo, L.J. and Mulligan, M. (2013). Evaluation of precipitation estimation accuracy in reanalyses, satellite products, and an ensemble method for regions in Australia and south and east Asia. *Journal of Hydrometeorology*, **14**, 1323–1333.

Penki, R.K. and Kamra, A.K. (2013). The lightning activity associated with the dry and moist convections in the Himalayan Regions. *Journal of Geophysical Research: Atmospheres*, **118**, 6246–6258.

Petersen, W.A., Chistian, H.J. and Rutledge, S.A. (2005). TRMM observations of the global relationship between ice water content and lightning. *Geophysical Research Letters*, **32**, L14819.

Peterson, M. and Liu, C. (2013). Characteristics of lightning flashes with exceptional illuminated areas, durations, and optical powers and surrounding storm properties in the tropics and inner subtropics. *Journal of Geophysical Research: Atmospheres*, **118**, 11,727–11,740.

Pfeifroth, U., Mueller, R. and Ahrens, B. (2013). Evaluation of satellite-based and reanalysis precipitation data in the tropical Pacific. *Journal of Applied Meteorology and Climatology*, **52**, 634–644.

Pickering, K.E., Wang, Y., Tao, W.K., Price, C. and Muller, J.F. (1998). Vertical distributions of lightning NOx for use in regional and global chemical transport models. *Journal of Geophysical Research*, **103**, 31203–31216.

Pinheiro, J.C. and Bates, D.M. (2000). *Mixed-Effects Models in S and S-PLUS*. Springer.

Pinto, O., Pinto, I.R.C.A. and Ferro, M.A.S. (2013). A study of the long-term variability of thunderstorm days in southeast Brazil. *Journal of Geophysical Research: Atmospheres*, **118**, 5231–5246.

Planton, S. (2013). Annex III: Glossary, In: Climate Change 2013: The Physical Science Basis. Contribution of Working Group I to the Fifth Assessment Report of the Intergovernmental Panel on Climate Change [Stocker, T.F., D. Qin, G.-K. Plattner, M. Tignor, S.K. Allen, J. Boschung, A. Nauels, Y. Xia, V. Bex and P.M. Midgley (eds.)]. Tech. rep., Cambridge University Press, Cambridge, UK and New York, USA.

Pollack, I.B., Homeyer, C.R., Ryerson, T.B., Aikin, K.C., Peischl, J., Apel, E.C., Campos, T., Flocke, F., Hornbrook, R.S., Knapp, D.J., Montzka, D.D., Weinheimer, A.J., Riemer, D., Diskin, G., Sachse, G., Mikoviny, T., Wisthaler, A., Bruning, E., MacGorman, D., Cummings, K.A., Pickering, K.E., Huntrieser, H., Lichtenstern, M., Schlager, H. and Barth, M.C. (2016). Airborne quantification of upper tropospheric NO x production from lightning in deep convective storms over the United States Great Plains. *Journal of Geophysical Research: Atmospheres*, **121**, 2002–2028.

Pöschl, U., von Kuhlmann, R., Poisson, N. and Crutzen, P.J. (2000). Development and Intercomparison of Condensed Isoprene Oxidation Mechanisms for Global Atmospheric Modeling. *J. Atmos. Chem*, **37**, 29–52.

Prather, M.J., Ehhalt, D., Dentener, F., Derwent, R., Dlugokencky, E., Holland, E., Isaksen, I., Katima, J., Kirchoff, V., Matson, P., Midgley, P. and Wang, M. (2001). Atmospheric chemistry and greenhouse gases, in: Climate Change 2001: The Scientific Basis, Contribution of Working Group I to the Third Assessment Report of the Intergovernmental Panel on Climate Change, Edited by Houghton, J. T., Ding, Y., Griggs, D. J. Tech. rep., Cambridge University Press, Cambridge, UK.

Prather, M.J., Holmes, C.D. and Hsu, J. (2012). Reactive greenhouse gas scenarios: Systematic exploration of uncertainties and the role of atmospheric chemistry. *Geophysical Research Letters*, **39**, 6–10.

Price, C. and Rind, D. (1992). A simple lightning parameterization for calculating global lightning distributions. *Journal of Geophysical Research*, **97**, 9919–9933.

Price, C. and Rind, D. (1993). What determines the cloud-to-ground lightning fraction in thunderstorms? *Geophysical Research Letters*, **20**, 463–466.

Price, C. and Rind, D. (1994). Modeling global lightning distributions in a general circulation model. *Monthly Weather Review*, **122**, 1930–1939.

Price, C., Penner, J. and Prather, M. (1997). NOx from lightning 1. Global distribution based on lightning physics. *Journal of Geophysical Research*, **102**, 5929–5941.

Rakov, V.A. (2013). Electromagnetic Methods of Lightning Detection. *Surveys in Geophysics*, **34**, 731–753.

Reynolds, R.W., Smith, T.M., Liu, C., Chelton, D.B., Casey, K.S. and Schlax, M.G. (2007). Daily high-resolution-blended analyses for sea surface temperature. *Journal of Climate*, **20**, 5473–5496.

Reynolds, S.E., Brook, M. and Gourley, M.F. (1957). Thunderstorm charge separation. *Journal of Meteorology*, **14**, 426–436.

Ridley, B., Pickering, K. and Dye, J. (2005). Comments on the parameterization of lightning-produced NO in global chemistry-transport models. *Atmospheric Environment*, **39**, 6184–6187.

Romps, D.M., Seeley, J.T., Vollaro, D. and Molinari, J. (2014). Projected increase in lightning strikes in the United States due to global warming. *Science*, **346**, 851–854.

Rosenfeld, D. and Woodley, W.L. (2000). Deep convective clouds with sustained supercooled liquid water down to -37.5C. *Nature*, **405**, 440–442.

Rossow, W.B., Walker, A.W., Beuschel, D.E. and Roiter, M.D. (1996). International Satellite Cloud Climatology Project (ISCCP) documentation of new cloud data sets. Tech. Rep. January, World Meteorological Organisation, Geneva.

Said, R.K., Cohen, M.B. and Inan, U.S. (2013). Highly intense lightning over the oceans: Estimated peak currents from global GLD360 observations. *Journal of Geophysical Research: Atmospheres*, **118**, 6905–6915.

Satori, G., Williams, E. and Lemperger, I. (2009). Variability of global lightning activity on the ENSO time scale. *Atmospheric Research*, **91**, 500–507.

Saunders, C. (2008). Charge Separation Mechanisms in Clouds. *Space Science Reviews*, **137**, 335–353.

Schreier, M.M., Kahn, B.H., Sušelj, K., Karlsson, J., Ou, S.C., Yue, Q. and Nasiri, S.L. (2014). Atmospheric parameters in a subtropical cloud regime transition derived by AIRS and MODIS: observed statistical variability compared to ERA-Interim. *Atmospheric Chemistry and Physics*, **14**, 3573–3587.

Schumann, U. and Huntrieser, H. (2007). The global lightning-induced nitrogen oxides source. *Atmospheric Chemistry and Physics*, **7**, 3823–3907.

Solomon, R., Schroeder, V. and Baker, M.B. (2001). Lightning initiation conventional and runaway-breakdown hypotheses. *Quarterly Journal of the Royal Meteorological Society*, **127**, 2683–2704.

Squire, O.J., Archibald, A.T., Griffiths, P.T., Jenkin, M.E., Smith, D. and Pyle, J.A. (2015). Influence of isoprene chemical mechanism on modelled changes in tropospheric ozone due to climate and land use over the 21st century. *Atmos. Chem. Phys*, **15**, 5123–5143.

Stevenson, D., Doherty, R., Sanderson, M., Johnson, C., Collins, B. and Derwent, D. (2005). Impacts of climate change and variability on tropospheric ozone and its precursors. *Faraday Discussions*, **130**, 41–57.

Stevenson, D.S., Dentener, F.J., Schultz, M.G., Ellingsen, K., van Noije, T.P.C., Wild, O., Zeng, G., Amann, M., Atherton, C.S., Bell, N., Bergmann, D.J., Bey, I., Butler, T., Cofala, J., Collins, W.J., Derwent, R.G., Doherty, R.M., Drevet, J., Eskes, H.J., Fiore, A.M., Gauss, M., Hauglustaine, D.A., Horowitz, L.W., Isaksen, I.S.A., Krol, M.C., Lamarque, J.F., Lawrence, M.G., Montanaro, V., Müller, J.F., Pitari, G., Prather, M.J., Pyle, J.A., Rast, S., Rodriguez, J.M., Sanderson, M.G., Savage, N.H., Shindell, D.T., Strahan, S.E., Sudo, K. and Szopa, S. (2006). Multimodel ensemble simulations of present-day and near-future tropospheric ozone. *Journal of Geophysical Research*, **111**, D08301.

Stevenson, D.S., Young, P.J., Naik, V., Lamarque, J.F., Shindell, D.T., Voulgarakis, A., Skeie, R.B., Dalsoren, S.B., Myhre, G., Berntsen, T.K., Folberth, G.A., Rumbold, S.T., Collins, W.J., MacKenzie, I.A., Doherty, R.M., Zeng, G., van Noije, T.P.C., Strunk, A., Bergmann, D., Cameron-Smith, P., Plummer, D.A., Strode, S.a., Horowitz, L., Lee, Y.H., Szopa, S., Sudo, K., Nagashima, T., Josse, B., Cionni, I., Righi, M., Eyring, V., Conley, A., Bowman, K.W., Wild, O. and Archibald, A. (2013). Tropospheric ozone changes, radiative forcing and attribution to emissions in the Atmospheric Chemistry and Climate Model Intercomparison Project (ACCMIP). *Atmospheric Chemistry and Physics*, **13**, 3063–3085.

Stith, J.L., Avallone, L., Bansemer, A., Basarab, B., Dorsi, S.W., Fuchs, B., Lawson, R.P., Rogers, D.C., Rutledge, S. and Toohey, D.W. (2014). Ice particles in the upper anvil regions of midlatitude continental thunderstorms: the case for frozen-drop aggregates. *Atmospheric Chemistry and Physics*, **14**, 1973–1985.

Stockwell, D.Z., Giannakopoulos, C., Plantevin, P.H., Carver, G.D., Chipperfield, M.P., Law, K.S., Pyle, J.A., Shallcross, D.E. and Wang, K.Y. (1999). Modelling NOx from lightning and its impact on global chemical fields. *Atmospheric Environment*, **33**, 4477–4493.

Thompson, A.M. (2003). Southern Hemisphere Additional Ozonesondes (SHADOZ) 19982000 tropical ozone climatology 2. Tropospheric variability and the zonal wave-one. *Journal of Geophysical Research*, **108**, 8241.

Tiedtke, M. (1989). A comprehensive mass flux scheme for cumulus parameterization in large-scale models. *Monthly Weather Review*, **117**, 1779–1800.

Tiedtke, M. (1993). Representation of clouds in large-scale models. *Monthly Weather Review*, **121**, 3040–3061.

Tompkins, A.M., Gierens, K. and Rädel, G. (2007). Ice supersaturation in the ECMWF integrated forecast. *Quarterly Journal of the Royal Meteorological Society*, **133**, 53–63.

Tost, H., Jöckel, P. and Lelieveld, J. (2007). Lightning and convection parameterisations - uncertainties in global modelling. *Atmospheric Chemistry and Physics*, **7**, 4553–4568.

Toumi, R., Haigh, J.D. and Law, K.S. (1996). A tropospheric ozone-lightning climate feedback. *Geophysical Research Letters*, **23**, 1037–1040.

Ushio, T., Heckman, S.J., Boccippio, D.J., Christian, H.J. and Kawasaki, Z.I. (2001). A survey of thunderstorm flash rates compared to cloud top height using TRMM satellite data. *Journal of Geophysical Research: Atmospheres*, **106**, 24089–24095.

Virts, K.S., Wallace, J.M., Hutchins, M.L. and Holzworth, R.H. (2013). Highlights of a new ground-based, hourly global lightning climatology. *Bulletin of the American Meteorological Society*, **94**, 1381–1391.

Vonnegut, B. (1963). Some facts and speculations concerning the origin and role of thunderstorm electricity. *Meteorology Monograph*, **5**, 224–241.

Voulgarakis, A., Naik, V., Lamarque, J.F., Shindell, D.T., Young, P.J., Prather, M.J., Wild, O., Field, R.D., Bergmann, D., Cameron-Smith, P., Cionni, I., Collins, W.J., Dalsøren, S.B., Doherty, R.M., Eyring, V., Faluvegi, G., Folberth, G.A., Horowitz, L.W., Josse, B., MacKenzie, I.A., Nagashima, T., Plummer, D.A., Righi, M., Rumbold, S.T., Stevenson, D.S., Strode, S.A., Sudo, K., Szopa, S., Zeng, G., McKenzie, I.A., Nagashima, T., Plummer, D.A., Righi, M., Rumbold, S.T., Stevenson, D.S., Strode, S.A., Sudo, K., Szopa, S. and Zeng, G. (2013). Analysis of present day and future OH and methane

lifetime in the ACCMIP simulations. *Atmospheric Chemistry and Physics*, **12**, 22945–23005.

Waliser, D.E., Li, J.L.F., Woods, C.P., Austin, R.T., Bacmeister, J., Chern, J., Del Genio, A., Jiang, J.H., Kuang, Z., Meng, H., Minnis, P., Platnick, S., Rossow, W.B., Stephens, G.L., Sun-Mack, S., Tao, W.K., Tompkins, A.M., Vane, D.G., Walker, C. and Wu, D. (2009). Cloud ice: A climate model challenge with signs and expectations of progress. *Journal of Geophysical Research*, **114**, D00A21.

Walters, D.N., Williams, K.D., Boutle, I.A., Bushell, A.C., Edwards, J.M., Field, P.R., Lock, A.P., Morcrette, C.J., Stratton, R.A., Wilkinson, J.M., Willett, M.R., Bellouin, N., Bodas-Salcedo, A., Brooks, M.E., Copsey, D., Earnshaw, P.D., Hardiman, S.C., Harris, C.M., Levine, R.C., MacLachlan, C., Manners, J.C., Martin, G.M., Milton, S.F., Palmer, M.D., Roberts, M.J., Rodríguez, J.M., Tennant, W.J. and Vidale, P.L. (2014). The Met Office Unified Model Global Atmosphere 4.0 and JULES Global Land 4.0 configurations. *Geoscientific Model Development*, **7**, 361–386.

Wild, O. (2007). Modelling the global tropospheric ozone budget: Exploring the variability in current models. *Atmospheric Chemistry and Physics*, **7**, 2643–2660.

Wild, O., Prather, M.J. and Akimoto, H. (2001). Indirect long-term global radiative cooling from NO x Emissions. *Geophysical Research Letters*, **28**, 1719–1722.

Wild, O., Fiore, A.M., Shindell, D.T., Doherty, R.M., Collins, W.J., Dentener, F.J., Schultz, M.G., Gong, S., MacKenzie, I.A., Zeng, G., Hess, P., Duncan, B.N., Bergmann, D.J., Szopa, S., Jonson, J.E., Keating, T.J. and Zuber, A. (2012). Modelling future changes in surface ozone: a parameterized approach. *Atmospheric Chemistry and Physics*, **12**, 2037–2054.

Williams, E. (2005). Lightning and climate: A review. *Atmospheric Research*, **76**, 272–287.

Williams, E. and Sátori, G. (2004). Lightning, thermodynamic and hydrological comparison of the two tropical continental chimneys. *Journal of Atmospheric and Solar-Terrestrial Physics*, **66**, 1213–1231.

Williams, E.R. (1985). Large-scale charge separation in thunderclouds. *Journal of Geophysical Research*, **90**, 6013–6025.

Williams, E.R. (1989). The tripole structure of thunderstorms. *Journal of Geophysical Research*, **94**, 13151–13167.

Wilson, D.R., Bushell, A.C., Kerr-Munslow, A.M., Price, J.D. and Morcrette, C.J. (2008a). PC2: A prognostic cloud fraction and condensation scheme. I: Scheme description. *Quarterly Journal of the Royal Meteorological Society*, **134**, 2093–2107.

Wilson, D.R., Bushell, A.C., Kerr-Munslow, A.M., Price, J.D., Morcrette, C.J. and Bodas-Salcedob, A. (2008b). PC2: A prognostic cloud fraction and condensation scheme. II: Climate model simulations. *Quarterly Journal of the Royal Meteorological Society*, **134**, 2109–2125.

Wong, J., Barth, M.C. and Noone, D. (2013). Evaluating a lightning parameterization based on cloud-top height for mesoscale numerical model simulations. *Geoscientific Model Development*, **6**, 429–443.

Wu, D.L., Austin, R.T., Deng, M., Durden, S.L., Heymsfield, A.J., Jiang, J.H., Lambert, A., Li, J., Livesey, N.J., McFarquhar, G.M., Pittman, J.V., Stephens, G.L., Tanelli, S., Vane, D.G. and Waliser, D.E. (2009). Comparisons of global cloud ice from MLS, CloudSat, and correlative data sets. *Journal of Geophysical Research*, **114**, D00A24.

Wu, S., Mickley, L.J., Jacob, D.J., Logan, J.A., Yantosca, R.M. and Rind, D. (2007). Why are there large differences between models in global budgets of tropospheric ozone? *Journal of Geophysical Research*, **112**, D05302.

Xu, W. and Zipser, E.J. (2012). Properties of deep convection in tropical continental, monsoon, and oceanic rainfall regimes. *Geophysical Research Letters*, **39**, L07802.

Yoshida, S., Morimoto, T., Ushio, T. and Kawasaki, Z. (2009). A fifth-power relationship for lightning activity from Tropical Rainfall Measuring Mission satellite observations. *Journal of Geophysical Research*, **114**, D09104.

Young, P.J., Archibald, A.T., Bowman, K.W., Lamarque, J.F., Naik, V., Stevenson, D.S., Tilmes, S., Voulgarakis, A., Wild, O., Bergmann, D., Cameron-Smith, P., Cionni, I., Collins, W.J., Dalsøren, S.B., Doherty, R.M., Eyring, V., Faluvegi, G., Horowitz, L.W., Josse, B., Lee, Y.H., MacKenzie, I.A., Nagashima, T., Plummer, D.A., Righi, M., Rumbold, S.T., Skeie, R.B., Shindell, D.T., Strode, S.A., Sudo, K., Szopa, S. and Zeng, G. (2013). Pre-industrial to end 21st century projections of tropospheric ozone from the Atmospheric Chemistry and Climate Model Intercomparison Project (ACCMIP). *Atmospheric Chemistry and Physics*, **13**, 2063–2090.

Zeng, G., Pyle, J.A. and Young, P.J. (2008). Impact of climate change on tropospheric ozone and its global budgets. *Atmospheric Chemistry and Physics*, **8**, 369–387.

Zhang, Q., Körnich, H. and Holmgren, K. (2013). How well do reanalyses represent the southern African precipitation? *Climate Dynamics*, **40**, 951–962.

Ziemke, J.R., Chandra, S., Labow, G.J., Bhartia, P.K., Froidevaux, L. and Witte, J.C. (2011). A global climatology of tropospheric and stratospheric ozone derived from Aura OMI and MLS measurements. *Atmospheric Chemistry and Physics*, **11**, 9237–9251.